STRUCTURAL BEHAVIOR OF REINFORCED CONCRETE BEAM COLUMN JOINTS UNDER CYCLIC LOADING

Submitted by

Ahmed Farhan Ahnaf Siddique

A thesis submitted to the Department of Civil Engineering, Bangladesh University of Engineering and Technology in partial fulfillment of the requirements for the degree of

Master of Science in Civil and Structural Engineering

Department of Civil Engineering

Bangladesh University of Engineering and Technology

September 2021

The thesis titled "Structural Behavior of Reinforced Concrete Beam Column Joints Under Cyclic Loading", submitted by Ahmed Farhan Ahnaf Siddique, Student ID: 1018042306P (Session: October, 2018) has been accepted as satisfactory in partial fulfillment of the requirement for the degree of Master of Science in Civil and Structural Engineering on September 26, 2021.

BOARD OF EXAMINERS

Dr. Raquib Ahsan
Professor
Department of Civil Engineering
BUET, Dhaka-1000

Chairman
(Supervisor)

Dr. Md. Delwar Hossain
Professor and Head
Department of Civil Engineering
BUET, Dhaka-1000

Member
(Ex-Officio)

Dr. Tahsin Reza Hossain
Professor
Department of Civil Engineering
BUET, Dhaka-1000

Member

Lt Col Md Jahidul Islam, PhD
Associate Professor
Department of Civil Engineering,
Military Institute of Science and Technology
(MIST), Dhaka-1216.

Member
(External)

DECLARATION

It is thereby declared that except for the contents where specific references have been made to the work of others, the study contained in this thesis is the result of investigations carried out by the author under the supervision of Dr. Raquib Ahsan, Professor, Department of Civil Engineering, Bangladesh University of Engineering and Technology.

No part of this thesis has been submitted to any other university or educational establishment for a degree, diploma or other qualification (except for publication).

_____

Ahmed Farhan Ahnaf Siddique

i

ACKNOWLEDGEMENT

ABSTRACT

Reinforced concrete frame structure is the most common building form in Bangladesh at present. It is commonly found in the construction industry that the different components of the frame is cast with concrete mixes made with different coarse aggregates, mainly brickbats and crushed stone. This practice has an impact on the joint region where the different concrete mixes come together. These joint regions are the most susceptible zone under earthquakes in a reinforced concrete frame structure which requires immediate attention with the alarmingly increasing number of earthquake occurrences. However, there is no study found in literature which focuses on the seismic performance of these structures where dissimilar coarse aggregate concrete mixes are used in same frame.

The present study focuses on the structural behavior of reinforced concrete joints designed and detailed according to BNBC 2020 cast with dissimilar coarse aggregate concrete under the action of cyclic loading. Eight exterior beam-column joint specimens were prepared in order to determine their behavior with respect to cracking and failure characteristics, hysteresis response, stiffness degradation, ductility, and energy dissipation capacity. Along with conventional aggregates, the performance of wastes such as steel slag and recycled concrete aggregate in the joints has also been studied in this research to suggest a sustainable alternative.

Ductility of specimens cast with dissimilar coarse aggregate concrete mixes was 9.8% to 23.3% lower as compared to the specimens cast with uniform coarse aggregate concrete mixes; while the energy dissipation capacity was also 14.8% to 22.1% lower. The cracks appeared earlier in lower displacements for specimens with dissimilar coarse aggregates although the strength and elasticity of the concrete mixes were similar. Thus, the present study suggests that beam-column joints with dissimilar coarse aggregate concrete must be carefully analyzed and designed in terms of the seismic requirements of the structure before their use.

The energy dissipation capacity was 11.4% to 25.7% higher for specimens in which crushed stone aggregates were replaced by steel slag aggregates. Ductility was 3.7% to 11.4% higher while the energy dissipation capacity was 4.3% to 32.5% higher for specimens cast with recycled aggregate concrete compared to those cast with brick aggregate. The results establish that, steel slag and recycled concrete aggregate can be excellent alternative coarse aggregate choices in reinforced concrete frame structures.

TABLE OF CONTENTS

LIST OF TABLES

LIST OF FIGURES

NOTATION AND ABBREVIATIONS

Symbols	Description
BNBC	Bangladesh National Building Code
ACI	American Concrete Institute
ASCE	American Society of Civil Engineers
ASTM	American Society for Testing and Materials
FEMA	Federal Emergency Management Agency
SDC	Seismic Design Category
IMF	Intermediate Moment Frame
OMF	Ordinary Moment Frame
SMF	Special Moment Frame
f_c'	Compressive Strength of Concrete
f_y	Yield Strength of Steel
FRP	Fiber Reinforced Polymer
RCC	Reinforced Cement Concrete
PC	Prestressed Concrete
UHPC	Ultra High Performance Concrete
GFRP	Glass Fiber Reinforced Polymer
OPC	Ordinary Portland Cement
BS	British Standard
BOF	Basic Oxygen Furnace
EAF	Electric Arc Furnace
ACV	Aggregate Crushing Value
FM	Fineness Modulus
Δ	Displacement
θ	Rotation
μ	Displacement Ductility
LVDT	Linear Variable Differential Transformer

CHAPTER 1
INTRODUCTION

1.1 Background

Reinforced concrete frame structures are the most common building form at present all over the world including Bangladesh (Meyer 2009; Saiada 2014). Reinforced concrete structures started its journey back in 1854 when the first reinforced concrete home was constructed (Giatec Scientific 2017). With the increasing number of occurrences of earthquakes in Bangladesh, it has become essential to ensure the safety and sustainability of the reinforced concrete buildings against earthquakes (Siddique and Hossain 2020).

Before 1970s, reinforced concrete buildings were designed only considering gravity loads and hence the seismic performances of those reinforced concrete buildings were very poor. One of the main reasons behind the poor seismic performance of such old buildings is the weaknesses possessed by the beam-column joints (Pampanin et al. 2002; Bai et al. 2003; Genesio et al. 2010; Kibria et al. 2020).

Many quasi static cyclic load tests on beam-column joints have been performed as joints are the most vulnerable part of the frame structure susceptible to earthquakes. Many researchers studied the influence of proper detailing within the joints as well as the use of high performance materials in improving the performance of reinforced concrete frame structures. The effect of a more rigorous shear reinforcement detailing as well as retrofitting have also been studied.

The seismic behavior of beam-column joints constructed with different combinations of coarse aggregates (brickbats, stone chips, recycled concrete aggregates, and steel slags) is hardly found in literature. However, it is more or less being practiced in the construction industry of Bangladesh where brickbat aggregates are used in concrete mix of beams and crushed stone aggregates are used in concrete mix of columns. Therefore, beam-column joints designed as per the detailing provisions of Bangladesh National Building Code (BNBC) and cast with dissimilar coarse aggregate concrete mixes in its frame components require thorough investigation. Hence, it was deemed necessary to address the research gap in the present state of the art.

1.2   Objectives of the Research

The main objectives of this thesis are summarized below:

i.   To evaluate the structural behavior of reinforced concrete exterior beam-column joints cast with different coarse aggregates under cyclic excitation in terms of failure and cracking characteristics, hysteresis behavior, stiffness degradation, displacement ductility, and energy dissipation capacity.

ii.   To compare the seismic performance of beam-column joints cast with dissimilar coarse aggregate concrete mixes in its components to those cast with uniform coarse aggregate concrete mix.

iii.   To study the structural behavior of beam-column joints made with electric arc furnace steel slags as a replacement of crushed stone aggregates in concrete mix of columns and joints of reinforced concrete frames subjected to seismic forces.

iv.   To assess the structural behavior of beam-column joints made with recycled concrete aggregate as a replacement of brickbat aggregates in concrete mix of beams and joints of reinforced concrete frames subjected to seismic forces.

1.3   Outline of the Methodology

To investigate the structural behavior of reinforced concrete beam-column joints under cyclic loadings, one-third scale T-shaped subassemblies have been selected to represent the essential components of beam-column joint. The joints have been designed and detailed in accordance with BNBC 2020 so that the specimens fail due to flexure in hinges formed in beams. The specimens have been cast with adequate quality control and cured appropriately up to 28 days.

The beam-column joints have been loaded axially to simulate gravity loading in columns and laterally in a direction perpendicular to the beam longitudinal axis for cyclic loading using hydraulic jacks. A displacement controlled loading protocol have been applied where deflection dial gauges were used to measure displacements.

The cracking characteristics and failure patterns have been observed simultaneously during the tests. Load-displacement responses, moment-rotation responses, stiffness degradations, ductility, and energy dissipation capacity have been determined in order to make a quantitative comparison among the performance of the specimens.

A total of eight beam-column joint subassemblies have been tested in terms of different coarse aggregate concrete combinations as described below:

i. Two control specimens cast with uniform coarse aggregate concrete mix in all its components. The first one was cast with crushed stone aggregate concrete while the second one was cast with brick aggregate concrete.

ii. Two specimens cast with crushed stone aggregate concrete in columns and brickbat aggregate concrete in beams.

iii. Two specimens cast with steel slag aggregate concrete in columns and brickbat aggregate concrete in beams.

iv. Two specimens cast with crushed stone aggregate concrete in columns and recycled aggregate concrete in beams.

1.4 Scope of the Study

This study considered one-third scale reinforced concrete exterior beam-column joints designed and detailed according to BNBC 2020. The reinforcements used in this research are grade 500 AWR 6 mm bars and grade 500 DWR 8 mm bars. Ordinary portland cement and locally available sand is used in all the specimens. The coarse aggregates used in this research are brickbats, stone chips, steel slag, and recycled concrete. The specimens were subjected to quasi-static incremental reversed cyclic loading. The loads were applied with manually operated hydraulic jacks and the displacement were measured with deflection dial gauges capable of measuring displacements as small as 0.01 mm.

1.5 Organization of the Thesis

This thesis has been divided into five chapters to properly present the study in a sequential manner.

Chapter One describes the background of the research along with the objectives and scope of the study.

Chapter Two contains the literature review where relevant theories, Codes, and concepts are described. Previous researches on structural behavior of reinforced concrete beam-column joints are also presented in this chapter. The research gap in the present state of the art is determined by analyzing the past researches.

Chapter Three explains the experimental methodology which is followed in this research. The properties of the used materials are summarized in this chapter. The process of preparation of specimens is described in detail. The experimental test setup is explained with necessary figures and the data acquisition techniques are described.

Chapter Four presents the test results with proper illustrations, images, graphs, tables, and charts. The test results of each specimen are summarized. On the basis of these results, a comprehensive comparison is made among the specimens with appropriate analysis. The analyses are discussed with possible interpretations.

Chapter Five concludes the thesis with major findings and observations of the present study. In the end, recommendations and suggestions are provided to future researchers of relevant field who may extend the present study.

CHAPTER 2
LITERATURE REVIEW

2.1 Introduction

Concrete is by far the most common building materials used for construction all over the world at present as properly designed and produced concrete provides excellent mechanical and durability properties (Meyer 2009). Around 18 billion metric tons of concrete are produced each year worldwide (Mohammed et al. 2016). In recent times, moment resisting reinforced concrete frame are the most built structural form of buildings in Bangladesh as well as most parts of the world (Saiada 2014).

However, Bangladesh lies in a seismically active region and is situated very close to the northwestern end of the Indo-Australian plate which has been subjected to the long term process of subduction between the plate margins of Indo-Australian and Eurasian plates (Siddique 2018; Siddique and Hossain 2020; Indian Institute of Technology, Kanpur 2002). With the alarming increase in the occurrence rate of earthquakes, structural engineers and building designers have been forced to ensure safety to the buildings under such hazard events.

Prior to 1970, reinforced concrete buildings were designed for gravity loads only due to the lack of proper building Codes. Therefore, the buildings did not show adequate seismic performances. The poor seismic performance of the structures were mainly due to the weaknesses possessed by the beam-column joints (Pampanin et al. 2002; Bai et al. 2003; Genesio et al. 2010; Kibria et al. 2020).

Several guidelines have been developed since then to overcome these deficiencies the first of them being published in United States in 1976 (ACI 352R-76). Many buildings constructed prior to 1976 may have significant weaknesses in the joint regions (Pampanin et al. 2002; Bai et al. 2003; Khan 2014). Due to poor design and detailing of the beam-column joints of these buildings, they may lead to a total or partial collapse due to an earthquake (Prota et al. 2004; Khan 2014). A number of international Codes and guidelines have been developed since then and have also been revised periodically (ACI 318-11, ASCE 31-03, ASCE 41-17, BNBC 2020).

This chapter describes the history of reinforced concrete construction as well as the influence of the constituents of concrete on the characteristics of the latter. The

guidelines for earthquake resistant structures and reinforced concrete moment resisting frames are discussed. Furthermore, types of joints and the forces acting on exterior joint under seismic condition along with the shear resisting mechanism in an exterior joint are explained. This chapter also extracted the specifications from ACI and BNBC on seismic detailing of reinforced concrete buildings especially the beam-column joint. Finally, previous researches on structural behavior of reinforced concrete beam-column joints under cyclic loading are reviewed and summarized. Research gap in existing state of the art has been identified from the detail literature review which will be addressed through the present research work.

2.2 Reinforced Concrete Construction

Reinforced concrete is becoming more and more popular worldwide as a choice of construction materials. The demand for concrete is projected to increase by 8.3% every year (Mohammed et al. 2016). The volume of cement demand globally has doubled from 1.8 billion tons in 2002 to 3.7 billion ton in 2012 and it is still increasing (Armstrong 2013). With the increasing demand of reinforced concrete construction, safety under seismic hazard events of such structures are becoming more concerning for the civil engineering society.

2.2.1 Present Scenario of Reinforced Concrete Construction

Construction of reinforced concrete structures are increasing rapidly in all the major cities of Bangladesh due to the necessity of development of a large number of infrastructures as well as the growth of real estate business. To meet the huge demand of cement for making concrete structures, more than 60 cement companies are producing cement and supplying it to the market in Bangladesh currently (Mohammed et al. 2012).

Cement industry in Bangladesh is the 40th largest market in the world which produces over 25 million metric tons per year, whereas the global production is about 4000 million metric tons per year. The rate of consumption of cement at present is about 110kg per capita per year in Bangladesh and the rate increases by 20-25% every year (Mohammed et al. 2016).

The demand for aggregates is also increasing simultaneously at a very high rate as aggregates make up the majority volume in concrete. In 2013, the global demand for

aggregates was more than 20 billion metric tons and this demand increases by 2.9% every year. The projected demand will be increased in much faster rate in the Asia-Pacific region and so there might be a crisis of virgin aggregates. Therefore, it is high time that a sustainable solution is found to continue the pace of development in the construction industry (Mohammed et al. 2016).

2.2.2   Variation of Reinforced Concrete Constituents in Construction

Reinforced concrete frames are constructed by adding steel reinforcement with concrete. These steel reinforcements varies in size and strength from structure to structure. In Bangladesh, up to 500 grade steel is produced by various steel reinforcement manufacturers. Nevertheless, steel is mostly homogeneous as a construction material. On the other hand, the constituents of concrete varies greatly in constructions. Concrete is chiefly composed by mixing cement, fine aggregate, coarse aggregate, water, and occasionally special admixtures to enhance certain properties (Nilson et al. 2010).

These constituents of concrete are available in a number of variations. Cement is available in a number of types of Ordinary Portland Cement and Portland Composite Cement. Sand is used as fine aggregates in almost all concretes although the gradation varies. However, many different materials are used as coarse aggregate.

Due to lack of availability of stones, brick chips are more popular choice of use as coarse aggregate in Bangladesh for making concrete. Stone chips are also used but the quality varies greatly. Round shaped stone commonly called shingles are also used in construction as coarse aggregates for its better workability. Jhama brick chips are also found in the market but it is rarely used (Uddin 2013).

2.3   Influence of Coarse Aggregates on Reinforced Concrete Behavior

Different choice of coarse aggregate in concrete significantly influence the mechanical properties of concrete. Kalra and Mehmood (2018) concluded that the compressive strength of concrete is affected by the type of aggregate for high strength concrete. They further added that stiffer aggregates produce stiffer concrete mix. The modulus of elasticity of concrete is mainly dependent on the mortar aggregate interface. However, the tensile strength of aggregate is independent of its type and is significantly affected by its surface characteristic.

The type of coarse aggregate significantly affects the strength, modulus of elasticity, and steel corrosion resistance of concrete (Ahmad and Alghamdi 2012). The strength, stiffness, and fracture energy of concrete is highly affected by the type of aggregate, especially for high-strength concrete (Özturan and Çeçen 1997; Wu et al. 2001).

Concrete strength increases with the increase in size of coarse aggregate up to 25mm and decreases as the aggregate size increases beyond 25mm (Hossain et al. 2015). The quality of coarse aggregate significantly influences the mechanical properties of concrete (Beshr et al. 2003). However, dormant aggregate has no adverse impact on concrete strength and quality of structural components if the procured aggregates are totally free from clay and silt contents (Ogunbayo et al. 2018).

Uddin (2013) carried out a study to compare the properties of concrete made with different aggregates. The findings are summarized in Table 2.1 and Figures 2.1-2.2.

Table 2.1: Properties of Aggregates Investigated (Uddin 2013)

Type of Aggregates	Notations	FM	Bulk unit weight (kg/m^3)	Water content (%)	% of Wear
Brick Chips	NB-SSD		2000	11.5*	26.3
	NB-AD		1961	7.6	
	NB-CAD		1939	5.4	
	NB-OD	6.69	1885	0	
	NB-SW		2040	15.5	
Crushed Stone	CS		2650	0.8*	25
Shingles	SG		2800	2*	20.78
Jhama Brick	JB		1500	12.2*	37.16

*Absorption Capacity
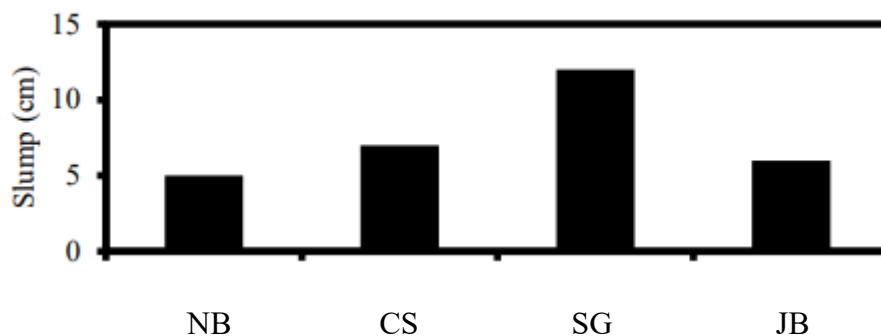
Figure 2.1: Workability of concrete made with different aggregates (W/C=0.55) (Uddin 2013)
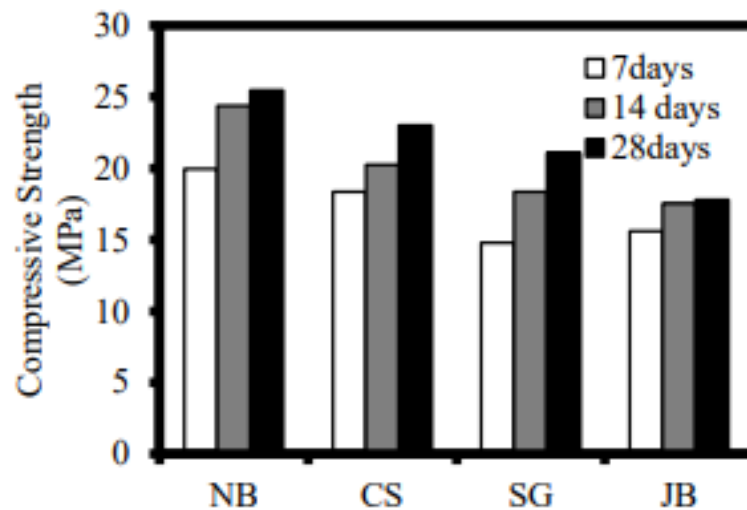
Figure 2.2: Compressive strength of concrete made with different aggregate (Uddin 2013)

2.3.1 Stone Chips Aggregate

Crushed stone is the most common type of coarse aggregate used in concrete globally. Although there is a scarcity of natural stones in Bangladesh, huge amount of stones are being withdrawn every day, especially from Sylhet (Rezaul et al. 2017). Despite the limitations, crushed stone aggregate is widely used in concrete construction.

2.3.2 Brickbat Aggregate

Although natural stones are most commonly used globally, brick chips or brickbats are used as a very common artificial aggregate in Bangladesh. Brickbat aggregates are easily available in Bangladesh and much cheaper than crushed stone (Hossain et al. 2015). Although brickbats are referred to as weaker compared to stone chips, weaker aggregates in fact produces more ductile concrete than stronger aggregates (Beshr et al. 2003). It is suggested that high-strength concrete with lower brittleness can be made by selecting high-strength aggregate with low brittleness (Wu et al. 2001). Considering the facts, brickbats have grown to be an excellent alternate choice of artificial coarse aggregate in concrete structures.

2.3.3 Recycled Concrete Aggregate

The common choices of coarse aggregates in Bangladesh, namely stone chips and brickbats, have their limitations as well. As a result of natural stone extraction, reserve of stones are being depleted which poses a great threat to us in the near future while

9

brick production is associated with a lot of negative environmental impacts (Rezaul et al. 2017). As an alternative choice of aggregate, recycled concrete can be used which is low cost and has less negative environmental impact.

The replacement of natural aggregates by recycled concrete aggregates for concrete is possible although the mechanical and durability properties of concretes produced with recycled concrete aggregates are found to be inferior to those of concretes produced with natural aggregates (Berredjem et al. 2020). However, different types of recycled concrete aggregates show different results compared to the corresponding natural aggregates (Zhou and Chen 2017).

2.3.4 Steel Slag Aggregate

Another alternate choice of coarse aggregate in concrete can be steel slags which is an industrial waste available in abundant quantity in Bangladesh. Steel slag is the waste product of steel manufacturing industry which is produced while molten steel is separated from impurities in steel furnace. It is obtained in liquid state as a complex solution of oxides and silicates which solidifies when cooled (Elahi 2021). The American Society for Testing and Materials (ASTM) defines steel slag as a non-metallic product consisting calcium silicates and ferrites combined with fused oxides of iron, aluminium, manganese, calcium, and magnesium that are produced simultaneously with steel in furnaces (Rezaul et al. 2017).

It is estimated that, 100 to 150 kg of slag is generated for production of 1 ton steel (Lee et al. 2019). This huge amount of steel slag requires proper utilization in various possible sectors which can reduce the volume of steel slag to be disposed. However, there is no specific guidelines regarding their proper disposal and feasible utilization in Bangladesh. Around 8 million tons of steel is manufactured annually in the country which produces around 120000 to 160000 tons of slag every year, which is a significantly huge amount (Hoque and Hossen 2019).

Rezaul et al. (2017) found that the compressive strength of concrete made with steel slag aggregate ranged from 3288 to 3699 psi and the splitting tensile strength was 183 to 294 psi which indicates good possibility of the use steel slag in concrete construction. Beshr et al. (2003) also reported that concrete produced with steel slag aggregates shows high compressive strength and split tensile strength. Considering the facts, it can be said that steel slag can be an excellent choice of coarse aggregate in concrete.

2.4 Earthquake Resistant Structures and Moment Resisting Frames

According to Bolt (2021), earthquake is defined as any sudden shaking of the ground caused by the passage of seismic waves through earth's rocks. The earth's crust has a huge amount of energy stored and seismic waves are produced whenever some form of this energy is suddenly released. Earthquakes generally occur along geologic fault lines as a result of the tectonic plate movements (Nilson et al. 2010).

Every year, around 50000 earthquakes occur over the entire earth that are large enough to be noticed without the aid of instruments. Approximately 100 of these are of significant size which can produce substantial damage to human lives if their epicenters are near areas of habitation. Immensely large earthquakes occur about once per year on average which have been responsible for an enormous number of deaths and an innumerable amount of damage to property over the centuries (Bolt 2021).

To minimize the damages caused by earthquakes, many building Codes and guidelines have been developed over the years. The purpose of these Codes are to ensure that the structures are earthquake resistant. Earthquake resistant structures are structures that is designed to prevent total collapse, preserve life, and minimize damage during a seismic hazard event (Britannica 2011). Earthquakes exert forces laterally that a properly designed earthquake resistant structure absorb and dissipate.

The purpose of earthquake resistant design provisions according to BNBC 2020 is to provide guidelines for the design and construction of new structures which are subjected to earthquake ground motions. The focus is to minimize the risk for all structures, to increase the expected performance of higher occupancy structures as compared to ordinary structures, and to improve the capability of essential structures to function after an earthquake. Nevertheless, it is not economically feasible to design and construct structures without any damage for a major earthquake event and so the intent is to allow inelastic deformation and structural damage at favorable locations in the structure without risking structural integrity and to prevent structural collapse during a major earthquake (BNBC 2020).

However, these guidelines are regularly revised and updated to meet the changes of modern era. The concept of earthquake resistant structure design developed in the past may be revised in near future to meet modern social and economic requirements and sustainable development goals. Seismic design philosophy for structures can be

changed from life safety to business continuity for modern and resilient societies. To ensure that, structures have to be designed in such way that it can be rapidly restored to full operation with least disruption and cost after a large earthquake (Takagi and Wada 2018).

There is a vital distinction between the design of a structure and the construction methods used to fabricate that structure. The construction of a structure that is capable to withstand the sudden ground shaking caused by earthquakes is essential. Construction methods vary radically throughout the world, so the engineers must be aware of local construction methods and resource availability before deciding whether a certain earthquake resistant design will be practical and realistic for the region (Cofer 2015). Nevertheless, all buildings does not possess the same seismic risk. The factors that affect a structure's seismic risk according to FEMA P749-10 are:

   i.   The intensity of ground shaking and other earthquake effects the structure is likely to experience and

   ii. The structure's use including consideration of the number of people who would be affected by the structure's failure and the need to use the structure for its intended purpose after an earthquake.

The aforementioned Codes use the Seismic Design Category (SDC) concept to classify structures according to their possible seismic risk. Structures are allocated to a seismic design category depending on the severity of ground shaking, the nature of the structure's occupancy and use, and other seismic effects that the structure may experience during its service life (FEMA P749-10).

There are six seismic design categories categorized from A to F with structures posing lowest seismic risk assigned to seismic design category A and structures posing the highest seismic risk assigned to seismic design category F according to the provisions of ACI, ASCE, and FEMA. The Codes therefore require increasingly more rigorous seismic design, detailing requirements, construction practice, and higher cost of providing seismic resistance at higher seismic design category to ensure that all buildings provide an acceptable risk. BNBC 2020 only recognizes seismic design categories B, C, and D as the other seismic design categories are nonexistent. Seismic design categories among B, C, or D are assigned based on seismic zone, local site conditions, and importance class of building as shown in Table 2.2.

Table 2.2: Seismic Design Category of Buildings (BNBC 2020)

Site Class	Occupancy Category I, II and III				Occupancy Category IV			
	Zone 1	Zone 2	Zone 3	Zone 4	Zone 1	Zone 2	Zone 3	Zone 4
SA	B	C	C	D	C	D	D	D
SB	B	C	D	D	C	D	D	D
SC	B	C	D	D	C	D	D	D
SD	C	D	D	D	D	D	D	D
SE, S_1, S_2	D	D	D	D	D	D	D	D

In Bangladesh, the most common building system is reinforced concrete moment frames. The structural safety of such frames under an earthquake event is of the highest concern and various Codes (ACI 318-11, ASCE/SEI 7-10, ASCE 31-03, ASCE 41-17, BNBC 2020 etcetera) have specific guidelines for moment frames. Various researchers have emphasized on earthquake resistant design of moment resisting frames (Syed et al. 2017; Saravanan et al. 2021). Moment frames are defined as a frame in which members and joints are capable of resisting forces primarily by flexure (ASCE/SEI 7-10; BNBC 2020). The earthquake loading to be considered for design on such frames is extensively specified in ASCE/SEI 7-10, BNBC 2020, and various other international Codes. Moment frames are categorized as intermediate moment frames (IMF), ordinary moment frames (OMF), and special moment frames (SMF).

2.4.1 Ordinary Moment Frames

Ordinary moment frames are those moment resisting frames that does not meet special detailing requirements for ductile behavior. Ordinary moment frames are anticipated to withstand small inelastic deformations in their members and joints when subjected to lateral seismic forces resulting from the ground motions of the design earthquake (BNBC 2020).

2.4.2 Intermediate Moment Frames

Intermediate moment frames are expected to resist seismic forces for structures designed in seismic design category C (BNBC 2020 part VI chapter 8). The performance objectives of intermediate moment frames are to avoid shear failures of its members and to provide enough ductility in order to ensure plastic hinge development in beams and columns (FEMA P-751 2012).

2.4.3 Special Moment Frames

Special moment frames are expected to resist seismic forces for structures designed in seismic design category D (BNBC 2020 part VI chapter 8). The performance objective of special moment frames are to avoid story mechanism by providing strong columns, provide sufficient ductility to ensure hinge development by confining concrete core and preventing rebar buckling, and to provide sufficient shear strength of members and joints to prevent any sort of shear failures (FEMA P-751 2012).

2.5 Beam-Column Joint

According to Nilson et al. (2010), a beam-column joint is defined as the portion of a column within the depth of the beams that frame into it. In the earlier days, the design of joints was limited to providing adequate anchorage for the reinforcement. With the increasing use of high strength concrete and material development, member cross sections have become smaller and the use of larger diameter and higher strength reinforcing bars have increased. Therefore, greater attention is required to be given to joint design and detailing. ACI 352R-02 (2002) has provided a detailed guideline for the design of beam-column joints in both ordinary structures and structures required to resist heavy cyclic loading into the inelastic range.

A beam-column joint in a frame transfers the loads and moments at the ends of the beams into the columns (Wight and Macgregor 2012). However, these joints are poor sources of energy dissipation and so inelastic deformations due to joint shear forces or bond deterioration has to be minimized (Paulay and Priestley 1992). The functional requirement of such joints is to enable the adjoining beams and column to develop and sustain their full capacity (Kibria 2014; Khan 2014; Jahan 2016).

However, beam-column joints are recognized as one of the most critical regions in reinforced concrete frames subjected to severe seismic attacks. Moment reversals occur across the joint in both beams and columns and the joint region is subjected to horizontal and vertical shear forces that has magnitude many times higher than that in adjacent beams and columns (Paulay and Priestley 1992). As a result, joint shear failure is an alarming possibility during earthquake events. Shear failure is always brittle in nature which is totally unacceptable structural performance, especially during seismic

events (Uma and Prasad 2006). Therefore, joint capacity and its failure mechanism is of great concern in modern structures.

2.5.1 Classification of Beam-Column Joints

ACI 352R-02 (2002) broadly classifies beam-column joints into two groups depending on the deformations of the joints.

i. Type 1 joints are those which connects members in an ordinary structure designed on the basis of strength. The structures with type 1 joints, referred to as non-seismic structures, are intended to resist gravity and normal wind load.

ii. Type 2 joints are those which connects members designed to accommodate large inelastic deformations. The structures with type 2 joints, referred to as seismic structures, are designed for earthquake motions, very high winds, or blast effects.

In moment resisting frames, three types of joints are identified (Uma and Prasad 2006).

i. Interior joint: when four beams frame into the vertical faces of a column.

ii. Exterior joint: when one beam frames into a vertical face of the column and two other beams frame from perpendicular directions into the joint

iii. Corner joint: when a beam each frames into two adjacent vertical faces of a column, then the joint is called as a corner joint.

These three types of joints are shown in Figures 2.3 to 2.5
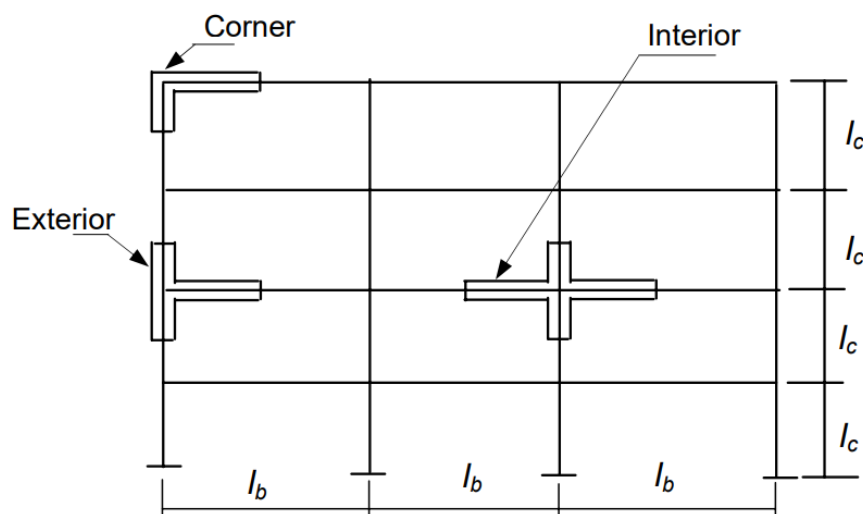
Figure 2.3: Types of beam-column joints (Uma and Prasad 2006; Kibria 2014; Khan 2014; Jahan 2016)

(a) Interior   (b) Exterior   (c) Corner
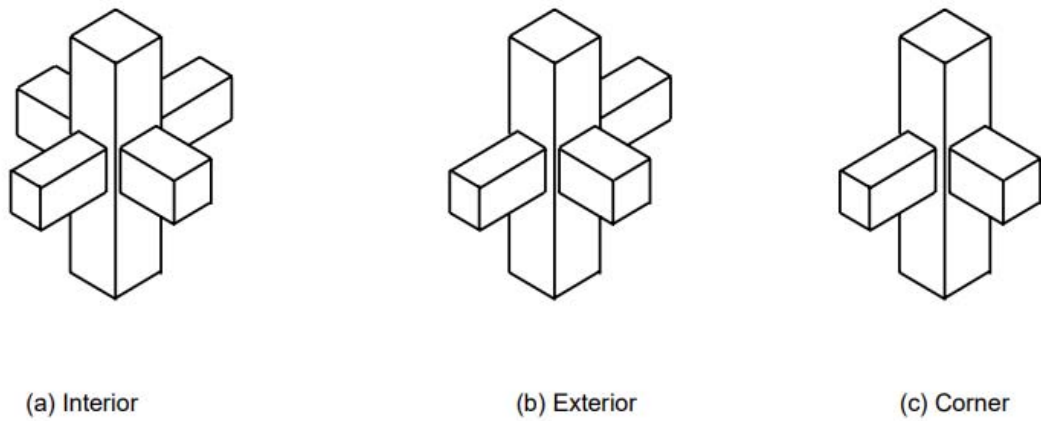
Figure 2.4: Types of beam-column joints – isometric view (Uma and Prasad 2006; Kibria 2014; Khan 2014; Jahan 2016)
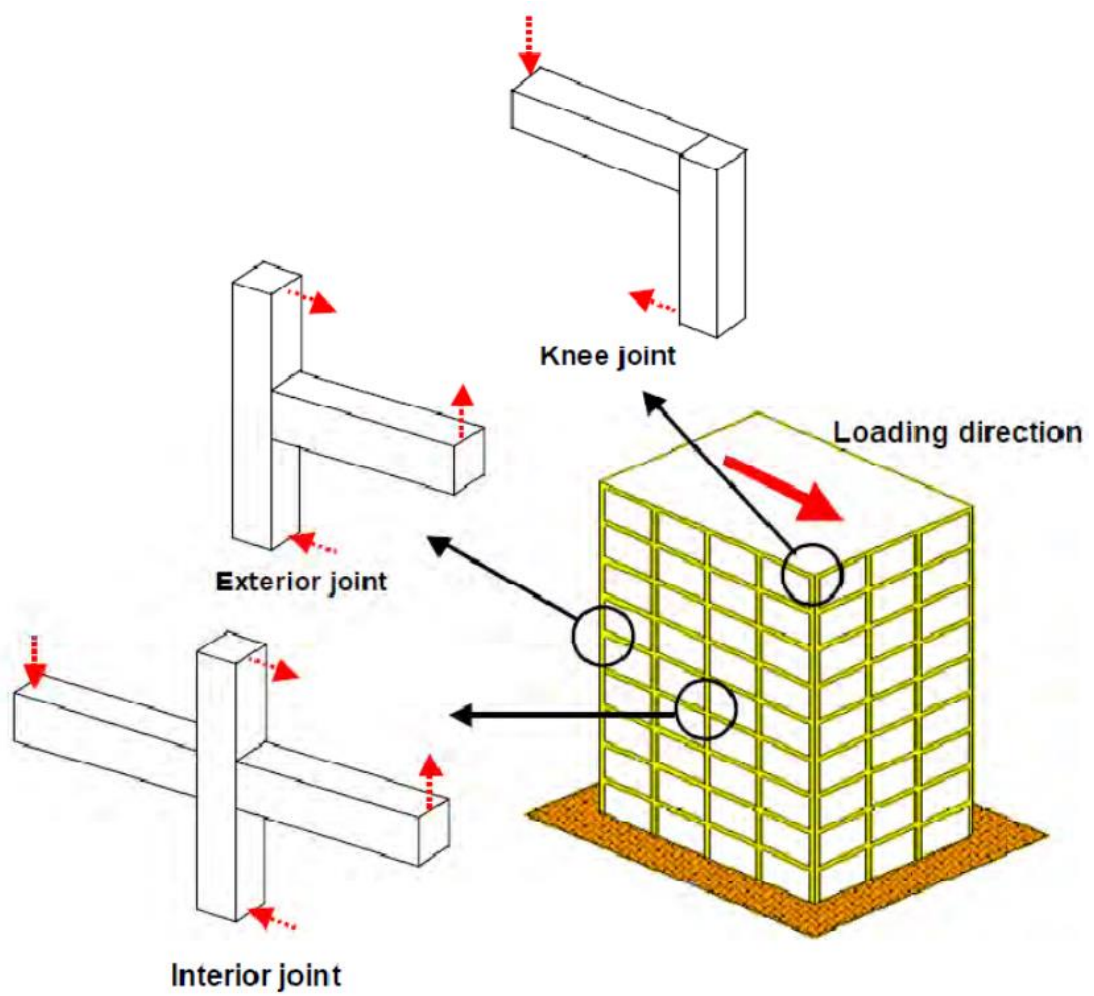
Figure 2.5: Types of beam-column joints – 3D view (Kim et al. 2007; Khan 2014)

2.5.2 Exterior Beam-Column Joints

In this research, exterior beam-column joints are extensively studied. Figure 2.6 shows various geometric configurations of exterior joints. Some of these joints occur in plane frame as illustrated in (a) and (c), while some occur in two way or space frames as illustrated in (b) and (d). Exterior joints have the configurations of (a) or (b) if they occur at the top floor while they have the configurations of (c) or (d) if they occur at intermediate floors (Paulay and Priestley 1992).
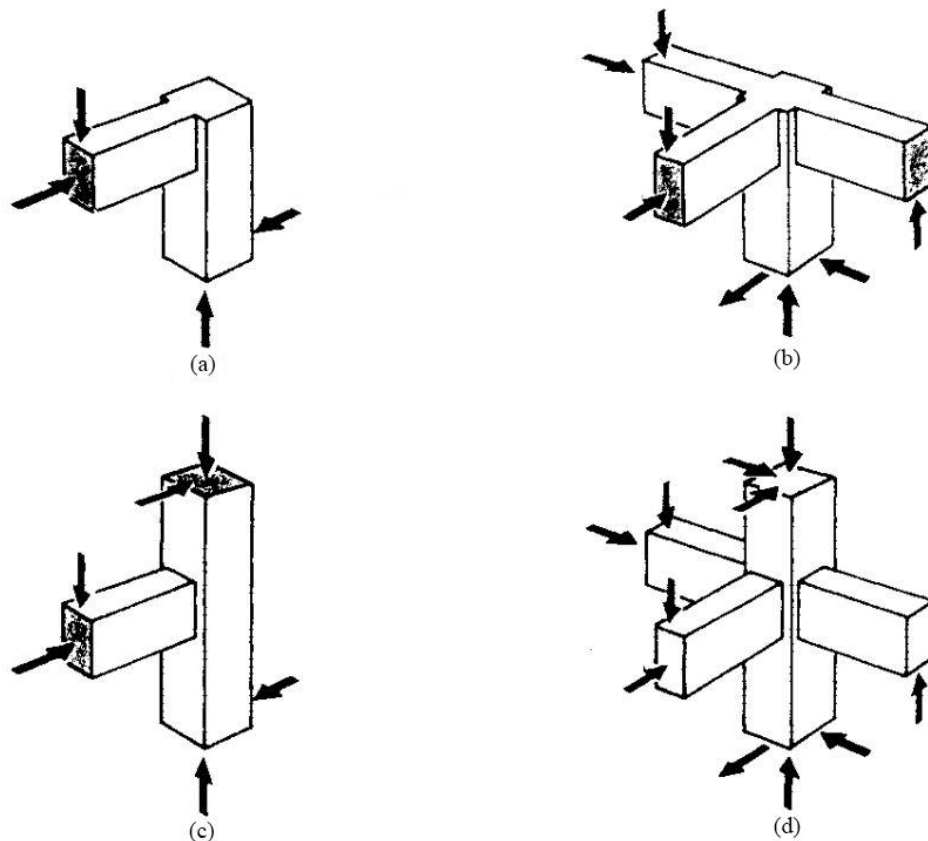
Figure 2.6: Exterior beam-column joints (Paulay and Priestley 1992)

2.6 Forces Acting on Exterior Joints

The failure in moment resisting reinforced concrete structures must not be at the column region which leads to a catastrophic failure. The joints must have adequate strength to allow the members to utilize their maximum capacity. The failure should occur at the plastic hinges. (Paulay and Priestley 1992; Khan 2014). Therefore, the mechanics of joints under gravity and lateral loads must be properly understood.

The effects of loads on joints are discussed in this section with reference to stresses and the associated crack patterns developed in the joints. The forces on a typical joint subjected to gravity loading is shown in Figure 2.7(a). The tension and compression from the beam ends and axial loads from the columns can be transmitted directly through the joint. For seismic loading, the equilibrating forces from beams and columns is shown in Figure 2.7(b). It is observed that, the equilibrating forces develop diagonal tensile and compressive stresses within the joint as the cracks begin to develop perpendicular to the tension diagonal in the joint and at the faces of the joint where the beams frame into the joint. As concrete is weak in tension, transverse reinforcements should be provided in such a way that they cross the plane of failure in order to resist the diagonal tensile forces (Uma and Prasad 2006; Kibria 2014; Khan 2014).

a. Gravity loading   b. Seismic loading
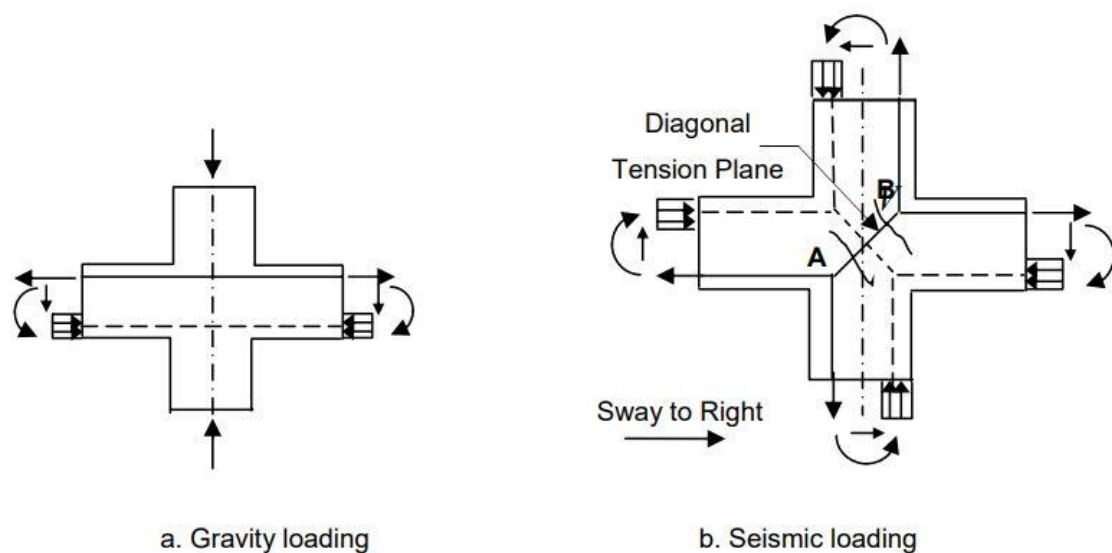
Figure 2.7: Forces acting on a typical beam-column joint (Uma and Prasad 2006; Khan 2014; Kibria 2014)

At an exterior joint, only one beam frames into a column and so the forces acting on an exterior joint will be a bit different as shown in Figure 2.8(a). The shear force in the joint gives rise to diagonal cracks thus requiring reinforcement of the joint. Some of the detailing patterns for exterior joints are shown in Figures 2.8(b) and 2.8(c). The bars bent away from the joint core result in efficiencies of 25-40 % while those passing through and anchored in the joint core show 85- 100% efficiency. However, the stirrups have to be provided to confine the concrete core within the joint (Uma and Prasad 2006; Jahan 2016).
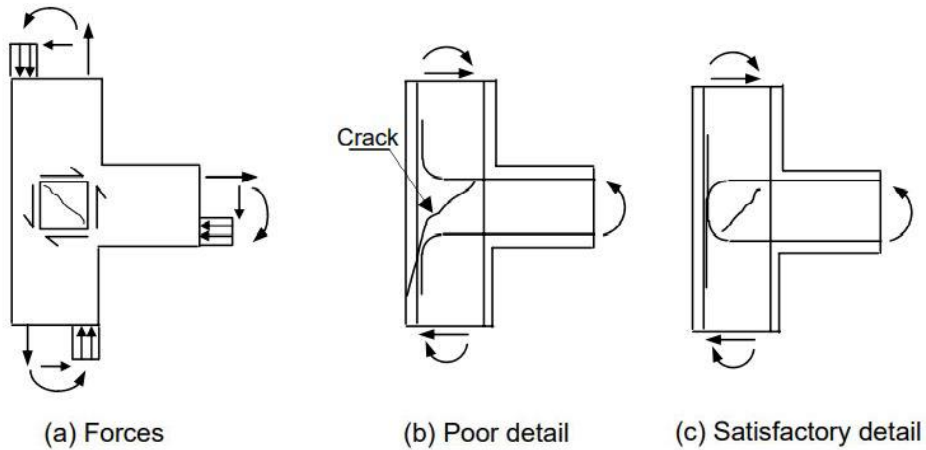
Figure 2.8: Forces acting on exterior joints (Uma and Prasad 2006; Jahan 2016)

The stress resultants from the framing members are transferred into the joint through bond forces along the longitudinal reinforcement bars passing through the joint and through flexural compression forces acting on the joint face. The joints should have enough strength to resist the induced stresses and sufficient stiffness to control undue deformations (Uma and Prasad 2006).

2.6.1 Behavior of Exterior Beam-Column Joints under Cyclic Loading

Cheung et al. (1993) extensively discussed the behavior of beam column joints of reinforced concrete frames. According to Jahan (2016), moment resisting frames are anticipated to obtain ductility and energy dissipating capacity from the flexural yield mechanism occurring at plastic hinges. According to Uma and Prasad (2006), the inelastic rotations spread over definite regions in reinforced concrete members which are called plastic hinges. The material properties are beyond elastic limits during inelastic deformations and hence damages in these regions are evident. The plastic hinges are estimated locations of structural members where the structural damage can be allowed to take place due to inelastic actions related to large deformations.

In seismic design, the plastic hinges are accepted to be formed in beams but not in columns. This mechanism with beam yielding is the characteristic of strong column-weak beam behavior where the inelastic rotational demands can be reasonably achieved through proper reinforcement detailing of beams. On the other hand, the imposed inelastic rotational demands are very high if plastic hinges are allowed to form in columns which is very challenging to be satisfied with any possible detailing. This mechanism is called column yielding or story mechanism (Uma and Prasad 2006).

It has to be ensured in design that the columns above and below the joint have adequate flexural strength when the adjacent beams develop flexural over-strength through their plastic hinges. This flexural strength ratio of column to beam is a key factor to safeguard that possible plastic hinging occurs in beams rather than in columns.

The joint behavior shows a complex interaction between bond and shear as the bond performance of the reinforcements anchored in a joint affects the shear resisting mechanism of the joint to a significant extent (Khan 2014). Beam-column joint behavior is controlled by this bond and shear failure mechanisms, which are weak sources for energy dissipation (Uma and Prasad 2006).

The performance criteria for joints under seismic actions are summarized by Uma and Prasad (2006) as well as Jahan (2016) which are as follows:

i.   The joint should have sufficient strength to enable the maximum capacities to be mobilized in the adjoining flexural members.

ii.   The degradation of joints should be so limited such that the capacity of the column is not affected in carrying its design loads.

iii.   The joint deformation should not result in increased story drift.

2.6.2   Bond Requirements of Exterior Joints

The ACI Committee 352 along with supporting ACI Codes have clearly specified the bond and shear requirements of beam-column joints. These specifications have been extensively explained by many authors (Paulay and Priestley 1992; Nilson et al. 2010; Wight and Macgregor 2012; Uma and Prasad 2006; Khan 2014; Kibria 2014; Jahan 2016). The bond and shear forces developed in exterior joints elaborated by these authors are summarized in this section.

The flexural forces from the members adjoined in joints cause tension or compression forces in the longitudinal reinforcing bars passing through the joint. Large tensile forces are transferred through bond during plastic hinge formation. Splitting cracks are formed along the longitudinal bars at the face of the joint when the bars are stressed beyond yield. Taking this into consideration, adequate development length for the reinforcements must be ensured within the joint. Therefore, the bond requirement has a directly affected by the geometric sizes of the beams and columns framing into the joint. The bond distribution along the longitudinal bars is shown in Figure 2.9.
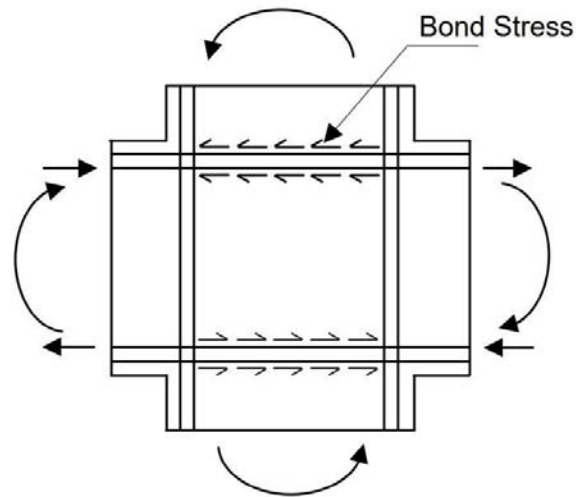
Figure 2.9: Bond stress on longitudinal bars in joints (Uma and Prasad 2006)

The beam longitudinal reinforcement that frames into the column ends within the joint core in exterior joints. After a few cycles of inelastic loading, the deterioration of bond initiated at the column face progresses towards the joint core. Repeated loading aggravates the situation and a complete loss of bond may take place up to the beginning of the bent portion of the bar. As a result, the longitudinal bars will get pulled out due to progressive loss of bond and the pull out failure results in complete loss of flexural strength which is unacceptable at any stage. The pull out failure of reinforcements in exterior joints can be prevented to a great extent by the provision of hooks or by some positive anchorage as shown in Figure 2.10.
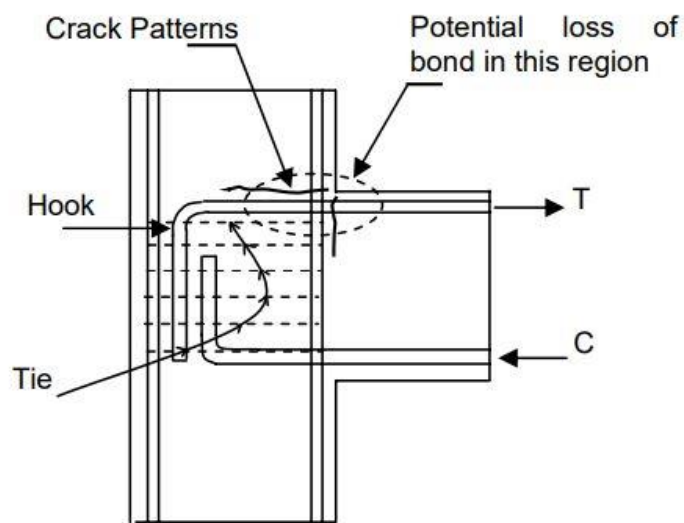
Figure 2.10: Detailing to improve bond mechanism at exterior joints
(Uma and Prasad 2006; Jahan 2016)

For type 2 joints, the development length of beam reinforcement terminating in a standard 90° hook, is given by ACI 318-11 Code section 21.7.5 which is shown in Equation 2.1.

Development length, $l_{dh} = \dfrac{f_y d_b}{65\lambda\sqrt{f'_c}}$ (2.1)

The value of λ is 1.0 for normal weight and 0.75 for lightweight concrete. The minimum value for l_{dh} shall be at least $8d_b$ or 6 inches (150 mm) for normal weight concrete and at least $10d_b$ and 7.5 inches for lightweight concrete (ACI 318-11; Nilson et al. 2010; Wight and Macgregor 2012).

However, when the reinforcement is subjected to compression, the hooks shown in Figure 2.10 is not that much helpful to cater the requirements of development length in compression. In such cases, the horizontal ties in the form of transverse reinforcement provide effective restraints against the hook in the joint when the longitudinal bar is in compression.

The factors influencing bond performance of the longitudinal bars are confinement, clear distance between the bars, and nature of the surface of the bar. Joint horizontal shear reinforcements improve anchorage of reinforcing bars (Ichinose 1991). Better bond performance is achieved when the clear distance between the reinforcements is less than 5 times the diameter of the bar (Eligehausen et al. 1983). Deformed bars give better performance in bond as well as the behavior of the reinforcements in bond also depends on the quality of concrete around it (Uma and Prasad 2006; Jahan 2016).

2.6.3   Shear Requirements of Exterior Joints

The external forces acting on joint face develop high shear stresses at the joint. This shear stress give rise to diagonal stresses which causes diagonal cracks as the tensile stresses in concrete exceeds its tensile strength. Extensive cracking also occur at the joint under load reversals which affects its strength and stiffness. Therefore, the joint becomes flexible to undergo large shear deformations. Although, the shear force determination in both vertical and horizontal direction is usually essential, it is sufficient to determine the shear force demand in only the horizontal direction since Code procedures aim at the beam hinging mechanism (Kibria 2014).

Figure 2.11 shows the shear forces in an exterior beam column joint. Based on equilibrium principles as shown in the free body diagram, the column shear force and the horizontal shear force in the joint can be evaluated with the following equations.

Column shear force, $V_{col} = \dfrac{T_b z_b + V_b \frac{h_c}{2}}{l_c}$ (2.2)

Horizontal shear across the joint, $V_{jh} = V_{col}\left(\dfrac{l_c}{z_b} - 1\right) - V_b\left(\dfrac{h_c}{2z_b}\right)$ (2.3)

It has to be kept in mind that, when the beam and slab are monolithically cast, the slab reinforcement participates significantly towards the negative flexural strength of the beam. The beam flexural over-strength should be determined by considering the beam as a T-beam or L-beam with appropriate flange width (Uma and Prasad 2006).
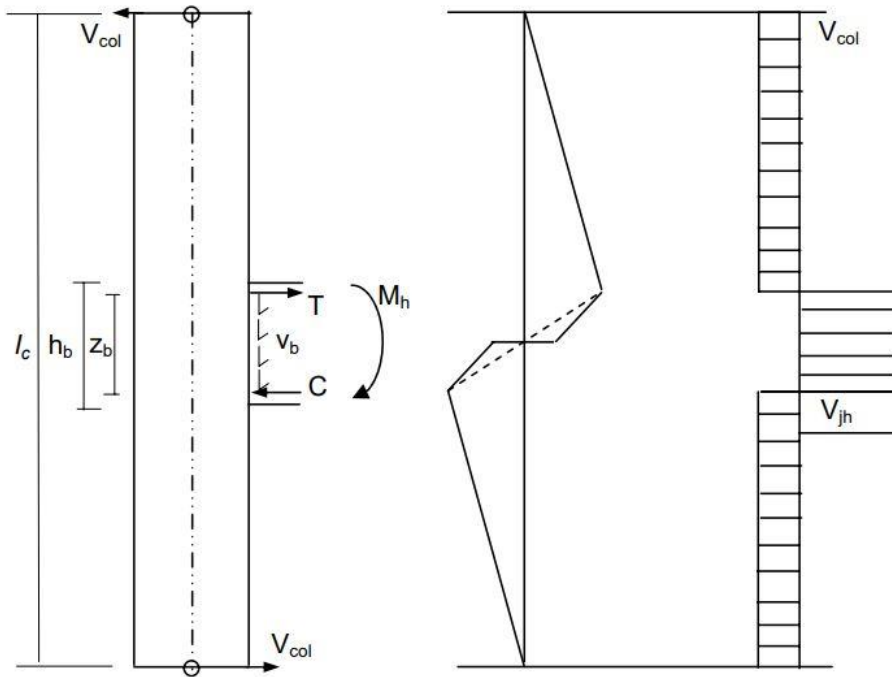
Figure 2.11: Shear force in exterior joint (Uma and Prasad 2006; Jahan 2016)

However, the Equations 2.2 and 2.3 are rigorous and involve the vertical shear developed by the end moments of the beam. A larger column width, h_c, and higher vertical beam shear V_b, reduce the shear force in the joint as seen from the equations. Nevertheless, for engineering designs, a simpler approach is followed to estimate the joint shear force that is assumed to act on a horizontal plane passing through the joint as given in Equations 2.4 and 2.5. Figure 2.12 shows a schematic representation of joint shear equilibrium in exterior joints.

(a) Exterior column-beam joint.

(b) Top half of
exterior joint.
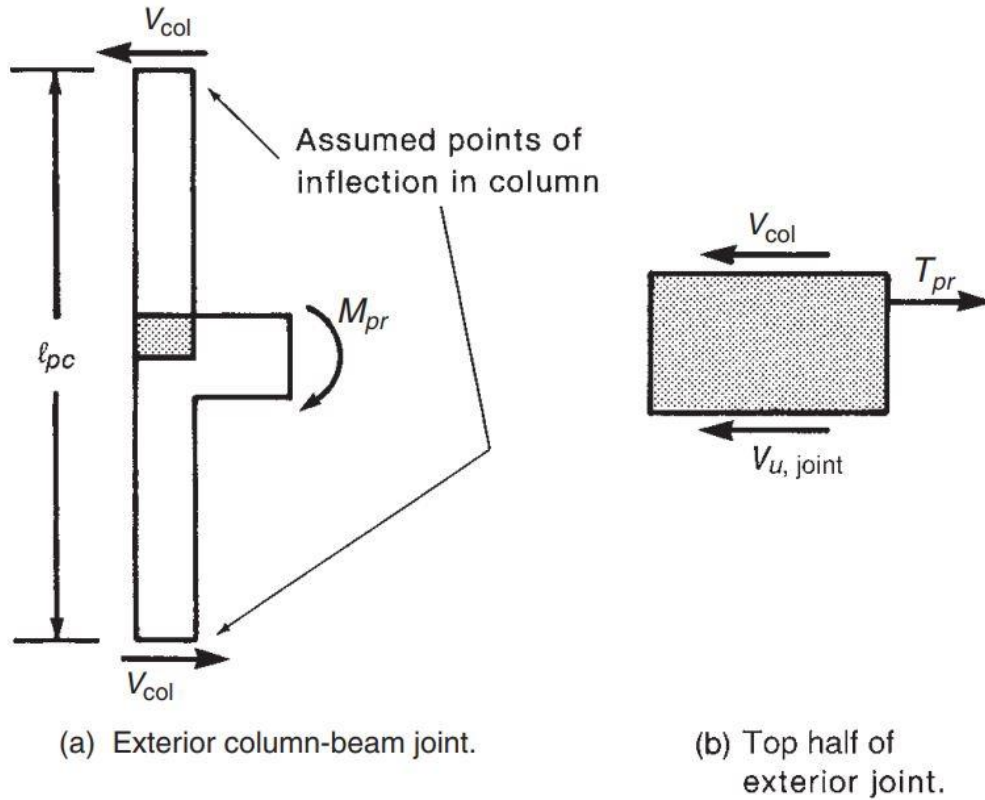
Figure 2.12: Joint shear equilibrium in exterior joints (Wight and Macgregor 2012)

Column shear force, $V_{col} = \dfrac{M_{pr}}{l_c}$ (2.4)

Horizontal shear across the joint, $V_{u,joint}$ or, $V_{jh} = T_{pr} - V_{col}$ (2.5)

Equations 2.4 and 2.5 give higher values of joint shear forces than those given by Equations 2.2 and 2.3.

Here, T_{pr} is the tensile force in the reinforcement in the beam at its probable capacity which is given by Equation 2.6.

Tensile force in beam reinforcement, $T_{pr} = \alpha A_s f_y$ (2.6)

The factor α in the above equation is intended to account for the actual yield strength of a bar which is in fact larger than the specified strength and that at higher deformations the bar could possibly be strained into the strain-hardening range of behavior. This factor α is taken at least 1.0 for type-1 frames where ductility requirement is limited, and at least 1.25 for type-2 frames which requires a sufficient amount of ductility (Wight and Macgregor 2012).

2.7   Seismic Shear Resistance of Beam-Column Joints

Lima et al. (2012) extensively overviewed several proposed theoretical and empirical models for evaluating shear strength of beam-column joints. Kim et al. (2007) developed an experimental database to determine joint shear strengths under lateral earthquake loading. The joint region can be assumed as a two dimensional plane subjected to the internal forces of beam and column consisting of compressive, tensile and shear forces acting on the joint face. Shear forces in the joint region results in diagonal compressive and tensile forces within the joint core which forms a diagonal failure plane. The shear resisting mechanism involves a diagonal concrete strut action and a truss action as shown in Figure 2.13.
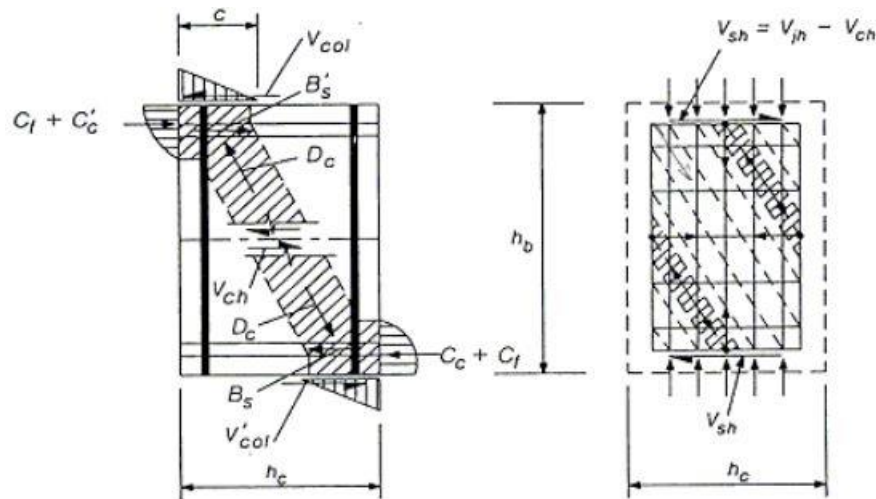
Figure 2.13: Shear resisting mechanism of joints (Uma and Prasad 2006)

The diagonal concrete strut mechanism is formed by diagonal concrete compression force in the joint which is produced by compressive and shear stresses on concrete at critical sections of the beam and the column. On the other hand, the truss mechanism is formed by a combination of the bond stress transfer along the longitudinal reinforcements of beam and column, the tensile resistance of lateral ties, and the compressive resistance of uniform diagonal concrete struts in the joint (Uma and Prasad 2006).

During an earthquake event, the concrete strut is gradually weakened by the reversed cyclic loading while the concrete compressive strength is reduced by the tensile strain which is increasing at a direction perpendicular to the main strut. These two phenomenon results in shear compression failure of the concrete strut.

On a horizontal plane, the shear strength at the mid-height of a beam-column joint is given by Equation 2.7.

Nominal shear strength of joint, $V_n = \gamma \sqrt{f_c'} A_j$ (2.7)

Here, γ refers to a set of constants given in Table 2.3 which is related to the configuration and confinement of the joint specified by ACI 318-11 Code section 21.7.4.1 and A_j is the effective joint area which is the product of effective joint width, b_j defined in Equation 2.8, and the depth of the column, h. However, A_j cannot exceed the area of the column (Wight and Macgregor 2012).

Effective joint width, $b_j = b + h \leq b + 2x$ (2.8)

The definition of effective joint width, b_j, for seismic design is illustrated in Figure 2.14 as specified by ACI 318-11 Commentary section R21.7.4.

Table 2.3: Values of γ for beam-column joints (Nilson et al. 2010)

	Continuous Columns		Discontinuous Columns	
Joint	Gravity Frames (Type 1)	Moment Frames (Type 2)	Gravity Frames (Type 1)	Moment Frames (Type 2)
Interior	24	20	20	15
Exterior	20	15	15	12
Column	15	12	12	8
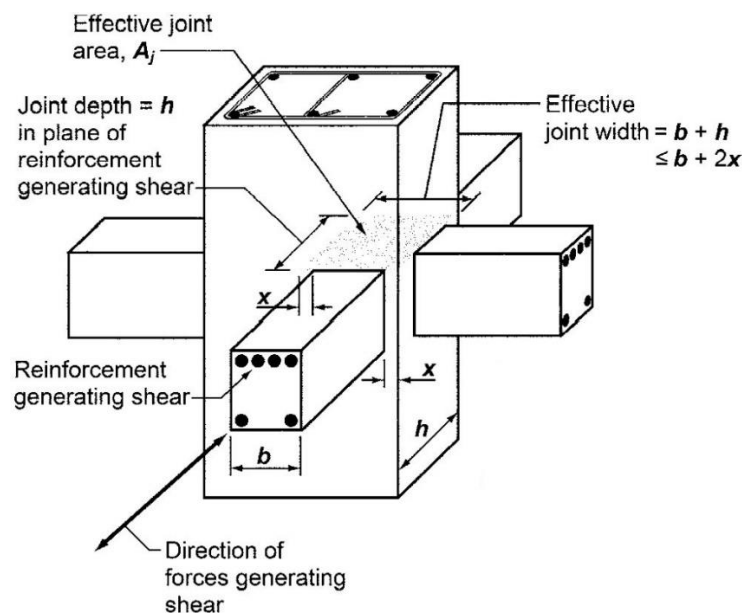
Figure 2.14: Effective joint width of type 2 beam-column joint (ACI 318-11)

2.8 Code Requirements of Reinforced Concrete Beam-Column Joints

Rahman et al. (2018) performed a comparison of seismic performance of reinforced concrete buildings designed following the Code provisions in Bangladesh, India, and United States of America. Beam-column joints with non-ductile reinforcement detailing show brittle failure modes under cyclic excitation (Ghobarah and El-Amoury 2005). Improving the joint reinforcement detailing enhances the hysteretic response and cracking mainly localizes in the beam creating a distinct flexural hinge (Chalioris et al. 2008). Joints designed only for gravity loads are extremely vulnerable to seismic action (Pampanin et al. 2002). These researches indicate the importance of proper seismic design and detailing of joints. The guidelines for such design and detailing provisions are specified by Codes (ACI 352R-02; BNBC 2020) which are discussed in this section.

2.8.1 Column Longitudinal Reinforcement Spacing

Longitudinal bars of the column passing through the joint should be distributed around the perimeter. The center to center spacing between adjacent bars should not exceed the larger of 8 inches (200 mm) and one-third of the column cross-section dimension. The spacing should not exceed 12 inches (300 mm) in any case (ACI 352R-02).

2.8.2 Joint Transverse Reinforcement

The transmission of column axial load through the joint and the shear demand from members into the joint require adequate lateral concrete confinement in the joint. If spiral transverse reinforcement is used, the volumetric ratio ρ_s should not be less than the value determined from Equations 2.9 and 2.10 (ACI 352R-02; BNBC 2020).

$$\rho_s = 0.12 \frac{f_c'}{f_{yh}} \tag{2.9}$$

$$\rho_s = 0.45 \left(\frac{A_g}{A_c} - 1 \right) \frac{f_c'}{f_{yh}} \tag{2.10}$$

On the other hand, if rectangular hoop and crosstie horizontal transverse reinforcement are used, the total cross-sectional area of a single hoop, overlapping hoops, or hoops with crossties of the same size in each direction, A_{sh} should be at least equal to the value determined from Equations 2.11 and 2.12 (ACI 352R-02; BNBC 2020). The detailing provision is illustrated in Figure 2.15.

$$A_{sh} = 0.3 \frac{s_h b_c'' f_c'}{f_{yh}} \left(\frac{A_g}{A_c} - 1 \right)$$
(2.11)

$$A_{sh} = 0.09 \frac{s_h b_c'' f_c'}{f_{yh}}$$
(2.12)

Here,

A_{sh} = total cross-sectional area of all legs of hoop reinforcement, including crossties, crossing a section;

s_h = center to center spacing of hoops or hoops plus crossties;

b_c'' = core dimension of tied column defined as outside to outside edge of transverse reinforcement bars perpendicular to the transverse reinforcement area being designed;

A_g = gross area of column section;

A_c = area of the concrete core (to the outside of the stirrups);

f_c' = specified compressive strength of concrete in the connection;

f_{yh} = specified yield strength of hoop and crosstie reinforcement, but is no more than 60000 psi (420 MPa).
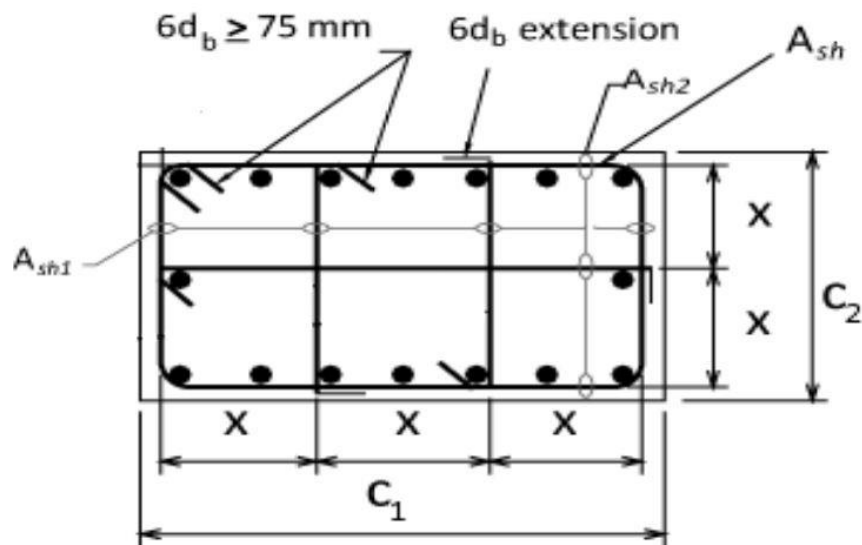
Figure 2.15: Transverse reinforcement details in joint region (BNBC 2020)

The center to center spacing between each layer of horizontal transverse reinforcement, s_h, should not exceed the smallest of one-fourth of the minimum column dimension, six times the diameter of column longitudinal bars to be restrained, and 6 inches (150 mm). The lateral center to center spacing between legs of overlapping hoops or crossties should not be higher than 12 inches (300 mm), and each end of a crosstie should engage a peripheral longitudinal reinforcing bar (ACI 352R-02; BNBC 2020).

a) Closed Hoop

b) Single Leg Cross Tie

Figure 2.16: Required dimensions of transverse reinforcement (ACI 352R-02)

Hoops and single leg crossties should be as shown in Figure 2.16. Hoops should be closed with seismic hooks. The 90 degree ends should be alternated on opposite faces of the column for adjacent single leg crossties, except for exterior and corner connections where 135 degree crosstie bends always should be used.

General requirements and transverse reinforcement requirements for joints are illustrated in Figures 2.17 and 2.18.

Figure 2.17: General requirements and transverse reinforcement requirements for joints not confined by structural member (BNBC 2020)

Figure 2.18: Transverse reinforcement requirements for joints confined by structural member (BNBC 2020)

2.8.3   Shear and Flexural Strength Requirements

The shear strength of beam-column joints have been described in section 2.7. For type 2 connections, the sum of the nominal flexural strengths of the column sections (ΣM_c) above and below the joint, calculated using the factored axial load that results in the minimum column-flexural strength, should not be less than 1.2 times the sum of the nominal flexural strengths of the beam sections (ΣM_g) at the joint as shown in Equation 2.13 (ACI 352R-02; BNBC 2020). Joints with beams framing in from two directions, this provision should be checked independently in each direction.

$$\Sigma M_c \geq 1.2 \Sigma M_g \tag{2.13}$$

2.8.4 Development Length of Reinforcements

The minimum development length l_{dh} is defined in Equation 2.1 in section 2.6.2. The hook tail extensions should project towards the joint mid-height. For type 2 connections with columns wider than beams, all straight bars passing through the joint should be selected such that Equations 2.14 and 2.15 as specified in ACI 352R-02 section 4.5.5 are satisfied (ACI 352R-02; BNBC 2020).

$$\frac{h_{(column)}}{d_{b\,(beam\,bars)}} \geq 20\frac{f_y(psi)}{60000} \geq 20 \qquad\qquad (2.14)$$

$$\frac{h_{(beam)}}{d_{b\,(column\,bars)}} \geq 20\frac{f_y(psi)}{60000} \geq 20 \qquad\qquad (2.15)$$

2.9 Previous Studies on Structural Behavior of Beam-Column Joints

Numerous studies have been carried out from the realization of the importance of beam-column joints in moment frames under seismic loading. A few of the recent literature of studies associated to the structural behavior of beam-column joints under cyclic loading is stated in this section.

A number of researches have been conducted by studying the impact of material development in cyclic behavior of joints. The effect of prestressing, using glass fiber reinforced polymer reinforcing bars instead of steel reinforcements, partially replacing cement with some other binding materials, using ultra-high performance concrete etcetera on the seismic performance of joints have been studied by many authors.

Hamahara et al. (2007) compared the structural behavior under reversed cyclic loading of exterior beam-column joints prepared with prestressed and non-prestressed reinforced concrete. Tests were conducted on eight prestressed and two non-prestressed full scale joint assemblies. The results concluded that prestressing force does not differ significantly on the ultimate shear strength of beam-column joints. The design shear force acting on a joint core should be calculated using the average shear force determined from the moment at the beam-column interfaces and not by the horizontal input shear force. The authors developed design equations to estimate design shear forces and ultimate shear capacities of prestressed concrete joints which were compared and validated with 51 beam-column joint assemblies test data that failed in shear in the joint cores.

Mady et al. (2011) reflected on the seismic behavior of concrete joints reinforced with glass fiber reinforced polymer bars and stirrups. Two full scale exterior beam-column joint specimens, one reinforced with glass fiber reinforced polymer while the other reinforced with steel, were constructed and tested. The experimental results revealed that the glass fiber reinforced polymer reinforced joint can withstand up to 4.0% drift ratio and can recover its deformation without any major residual strains. This designates the viability of using glass fiber reinforced polymer bars and stirrups as reinforcement in joints subjected to seismic loading.

Gil-Martin et al. (2019) experimented with three half scaled specimens which included a control specimen made of traditional concrete and another two specimens in which the joint were cast with epoxy resin and ground rubber respectively as partial replacement of cement. The effect of the two aforementioned polymer cement concretes on the overall structural behavior of the reinforced concrete joints was studied in terms of strength degradation, load carrying capacity, stiffness degradation, ductility, energy dissipation capacity, pinching width ratio, joint damage level, and equivalent viscous damping ratio. The outcomes revealed that the epoxy resin concrete showed better structural behavior while the results corresponding to ground tire rubber concrete exhibited poor structural behavior.

Khan et al. (2018) studied the seismic performance of shear deficient beam-column joints which were strengthened by ultra-high performance fiber reinforced concrete. The research conducted an experimental program with four one-third scale exterior beam-column joints without any transverse reinforcement in their joint core. Normal concrete joints with deficiencies in resisting seismic action were cast and strengthened with a layer of ultra-high performance fiber reinforced concrete and tested under reversed cyclic loading. The strengthening of specimens were done in two methods; firstly, by sandblasting the normal concrete substrate surface of joints and in-situ casting of a 30 mm thick ultra-high performance fiber reinforced concrete jacket, and secondly, by bonding 30 mm thick prefabricated ultra-high performance fiber reinforced concrete plates to the joints using epoxy resins and special fillers. The results indicated that the first method was highly effective in terms of joint shear capacity, deformation capacity, stiffness characteristics, and energy dissipation capacity compared to the second method.

Zhang et al. (2020) studied the application of ultra-high performance concrete in reinforced concrete joints. Ultra-high performance concrete shows significantly higher shear resistance and bond strength compared to normal concrete due to its greater compressive and tensile strengths which helps reducing the amount of ties and anchorage length of the longitudinal reinforcement in the joint zone. Four full scale interior precast composite beam-column joints were tested to quantitatively evaluate the effect of replacing the normal concrete by ultra-high performance concrete in the joint region. The main focus of this research were anchorage lengths, anchorage methods, and stirrup ratios in the joint zone. The results demonstrate that stirrups are not required in the ultra-high performance concrete joint zone. The anchorage length of beam straight and headed reinforcements can be reduced to $16d_b$ and $8.1d_b$ respectively. The application of ultra-high performance concrete in beam-column joints can ease the fabrication process.

Various other researchers also found the importance of shear reinforcement detailing as a significant factor of seismic performance of reinforced concrete beam-column joints. Shear reinforcements have been replaced by geogrid materials, discontinuous ties and stirrups have been replaced with continuous spirals, the angle of the shear reinforcements have been made at an inclined angle, and many variations of shear reinforcements in joints were studied. The effect of yielding of hoops on the seismic performance of joints is another important parameter studied by researchers.

Saha and Meesaraganda (2019) presented an experimental research on continuous rectangular spiral reinforced beam-column subassemblies cast with self-compacting concrete subjected to cyclic loading. Three sets of one-third scale exterior beam-column joints for different flexural strength ratio (1.3, 1.5, and 2.0 respectively), with continuous rectangular spiral reinforcement and individual closed stirrups as reference specimen, were considered in the investigation. Three different inclinations of stirrups angles (75°, 80°, and 85°) were considered for the spiral reinforcements. The study focused on the seismic behavior of the beam-column joint in terms of hysteresis behavior, load displacement pattern, failure pattern, and energy dissipation. The findings showed that continuous spiral stirrups outperformed the conventional stirrups in terms of ultimate strength, ductility factor, stiffness degradation, and cumulative energy dissipation which provides a feasible, suitable, and efficient upgrading technique for structural joints.

33

Azimi et al. (2020) designed six full scale exterior beam-column joints for low and high ductility modules as per Eurocode CEN-EC8. The study converted the conventional discontinuous shear reinforcement system into a continuous system introducing a new shear reinforcement joint mechanism naming it the twisted opposing rectangular spiral. Both numerical and experimental investigations were carried out and the proposed reinforcement was found to intersect shear cracks at a more favorable angle as well as it considerably eliminated slip at the hooks which occurs for conventional stirrups. The proposed connection showed improvement of its capacity to dissipate energy, lateral strength, and ductility.

Majumder and Saha (2020) investigated the efficacy of geogrid material on enhancing the cyclic performance of non-ductile joints by experimental and numerical study. Three one-third scale exterior joints were tested where two control specimens were cast with and without seismic detailing while the other one was cast with geogrid reinforced non-seismic detailing. Nonlinear finite element analyses of the joint confined with geogrid were also carried out. The cyclic performance were explored on the basis of failure patterns, load displacement behavior, and ductility. The test results and the finite element simulation confirmed that geogrid confinement is effective for improving the load carrying capacity and ductility.

Sasmal and Ramanjaneyulu (2012) evaluated the strength hierarchy of three different types of exterior joints (gravity load designed, non-ductile and ductile) based on Eurocode and Indian Standards. Six full scale exterior joints were designed and detailed for three different stages and tested under cyclic loads. Strength hierarchy, ultimate strength, and critical failure modes were analytically estimated which correlated with the experimental results of the specimens. It was identified that the predominant mode of failure was joint shear failure for both "Non Ductile" and "Ductile" specimens. On the other hand, the "Gravity Load Design" specimen failed to perform satisfactorily against reversed loading due to its poor anchorage details. The authors emphasized on the fact that the existing strength hierarchy is not optimum even for the "Ductile" specimens and the final failure is controlled by joint shear strength.

Choudhury and Laskar (2020) carried out experiments on four one-third scaled exterior beam-column subassemblies with flexural strength ratio 1.4 which were designed and detailed following provisions of Indian Standard Code of Practice. The study focused

on the damaged joint core as yielded hoop reinforcements remain inside the joint core after rehabilitation due to practical difficulties. The results showed that peak load, ductility, and energy dissipation were reduced by 12–23%, 31–49% and 24–55%, respectively, for specimens with pre-yielded hoops compared to the control specimen. Also, the degradation of stiffness and damage index were greater in specimens with pre-yielded hoops. The authors concluded that only replacement of damaged concrete with suitable alternative material may not enhance the seismic performance of rehabilitated joints up to its undamaged state.

Many researches have been carried out proposing new detailing in joints. Shen et al. (2021) proposed a novel reinforcement detail for reinforced concrete beam-column joints in the form of unbonded diagonal bars which were mechanically anchored at beam ends. A large number of ties are needed in joint cores of reinforced concrete moment resisting frames subjected to high seismic forces which causes reinforcement congestion leading to construction difficulty and insufficient concrete compaction resulting in poor seismic performance. The proposed detail alleviates the reinforcement congestion through partially replacing horizontal ties by plastic hinge relocation and input shear force reduction mechanisms. Experiments were conducted on four two-thirds scale interior joint specimens under quasi-static cyclic load, including three specimens adopting the proposed reinforcement detail and one designed with the Code. Results showed that the proposed detail is capable of relocating the plastic hinges away from the beam-joint interfaces as well as it improves the loading capacity, stiffness, energy dissipation capacity, and bonding condition of beam longitudinal bars within the joint cores. The proposed reinforcement detail also enhances cracking resistance and reduces the joint distortion while additional amount of ties results in marginal improvement. The authors also proposed an analytical model considering plastic hinge relocation and input joint shear force reduction for joints with the novel reinforcement detail that can adequately predict the loading capacity and the failure mode.

Cosgun et al. (2019) ran two series of tests with exterior beam-column joints. The first series of tests included four two-third scale specimens while the second series of tests were conducted on two additional specimens with the same details but strengthened using fiber reinforced polymer sheets. The study was based on the concept that the use of low strength concrete, plain reinforcing bars, problematic anchorage details, and inadequate transverse reinforcement in joints are the factors increasing the failure risk

during earthquakes. The objective was to investigate the effects of the anchorage details of longitudinal beam reinforcements on the joint performance and quantifying the contribution of retrofitting the joints using fiber reinforced polymer sheets. The longitudinal reinforcement of the beam were anchored with 90-degree hooks, 180-degree hooks and straight bar (no hook) within the joint in the test program. Problematic anchorage details had a substantial adverse effect on the seismic performance of the joints while fiber reinforced polymer retrofitting caused a significant increase in peak loads and sustained ductility.

Various other researchers also studied the impact of retrofitting on the cyclic behavior of joints. Mukherjee and Joshi (2005) investigated the performance of retrofitted and rehabilitated beam-column joints under cyclic loading. Two sets of one-third scale interior joints were cast for experimental verification of which one set of joints had sufficient steel reinforcements with appropriate detailing of reinforcements while the other set had deficient bond lengths of the beam reinforcements at the connections with the columns. Glass and carbon fiber reinforced polymer sheets and strips were applied on the joints in different arrangements. The control specimens were further reused after testing as damaged specimens for rehabilitation. The rehabilitation were carried out using fiber reinforced polymer, the performance of which were compared with that of the undamaged specimens. Results show that both glass and carbon composites can be efficiently used for retrofitting and rehabilitation of beam-column joints. However, specimens strengthened with carbon fiber reinforced polymer show stiffer behavior than glass fiber reinforced polymer strengthened specimens. Results also suggest that along with restoration of its original strength, fiber reinforced polymer considerably enhances the joints yield load, initial stiffness, and energy dissipation capacity.

Realfonzo et al. (2014) also conducted an experimental campaign with the aim to investigate the seismic performance of joints retrofitted with fiber reinforced polymer systems. Test matrix included eight full scale exterior beam-column subassemblies without adequate seismic detailing. Two of these were control specimens while the other six were strengthened by using different fiber reinforced polymer systems. Some specimens were repaired with fiber reinforced polymer systems and re-tested once it was damaged. The results have allowed to identify the most suitable FRP configurations for retrofitting.

Dang and Dinh (2017) fabricated four half scale exterior beam-column joints and tested them under cyclic loading. One control specimen was designed to fail in joint shear while the other three were retrofitted by steel jacketing and haunch retrofit solutions. The structural performance of the specimens were examined in terms of load-drift relationship, damage and failure, ductility, energy dissipation capacity, and strain profiles of longitudinal bars. The test results established that the proposed retrofit methods enhance the seismic capacity in terms of the strength, energy dissipation capacity, and deformation capacity.

Ghobarah and El-Amoury (2005) studied the behavior of rehabilitated reinforced concrete joints and compared it with the performance of existing joints designed following pre-seismic Codes to assess the proposed rehabilitation techniques. Six full scale exterior beam-column joint subassemblies with non-ductile detailing were tested under quasi-static load that simulates earthquake forces. Three of these specimens had inadequate anchorage length of the bottom beam reinforcements of which two were strengthened using carbon fiber reinforced polymer sheets by attaching it to the bottom beam face. Other three specimens had no reinforcing ties installed in the joint region in addition to inadequate anchorage length of the beam reinforcements of which two were strengthened using glass fiber reinforced polymer jackets on the joint region. Results indicated that both rehabilitation techniques were effective in eliminating brittle joint shear and steel bar bond-slip failure modes as ductile beam hinging occurred instead.

As seen from the aforementioned researches, cyclic load tests have been carried out on different sizes of specimens ranging from full scale to one-third scale. Chung et al. (2004) assessed the dynamic effect and the similitude effect on reinforced concrete joints. Eight exterior beam-column joint subassemblies with scale ratios of 1, 1/2, and 1/4 were tested. It was established that the maximum strength of joints subjected to dynamic loading is about 20% higher than that of the static loading test while the energy dissipation capacity was about 15% greater for the dynamic tests than that for static tests. The stiffness of three different sizes of specimens tested were found to be within ±5% in the static loading rate test. ACI 374.1-05 (2014) allows scaling specimens up to one-third of full scaled specimens in order to ensure that scaled down specimens are large enough to be representative of the real material characteristics and load transfer mechanism of full scaled specimens which is followed in this thesis. A summary of the recent studies on beam-column joints are enlisted in Table 2.4

Table 2.4: Summary of the previous studies on structural behavior of reinforced concrete joints under cyclic loading

Authors	Material	Scale	Coarse Aggregates	Detailing	Location	Study Parameter
Hamahara et. al. (2007)	RCC and PC	1	X	X	Exterior	Joint shear capacity of RCC and PC
Mady et. al. (2011)	Concrete with GFRP	1	X	X	Exterior	GFRP reinforcements
Gil-Martin et. al. (2019)	RCC	1/2	X	X	Exterior	Partial cement replacement
Khan et. al. (2018)	UHPC	1/3	X	X	Exterior	Ultra-high performance fiber reinforced concrete
Zhang et. al. (2020)	UHPC	1	X	√	Interior	Ultra-high performance concrete and shear reinforcement detailing
Saha and Meesaraganda (2019)	RCC	1/3	X	√	Exterior	Continuous spiral reinforcements
Azimi et. al. (2020)	RCC	1	X	√	Exterior	Continuous spiral reinforcements
Majumder and Saha (2020)	RCC with Geogrid	1/3	X	√	Exterior	Geogrid as shear reinforcements
Sasmal and Ramanjaneyulu (2012)	RCC	1	X	√	Exterior	Gravity load design, seismic detailing, and ductile detailing
Choudhury and Laskar (2020)	RCC	1/3	X	X	Exterior	Effect of hoop reinforcement yielding
Shen et. al. (2021)	RCC	2/3	X	√	Interior	Novel detailing with diagonal anchor rods
Cosgun et. al. (2019)	RCC	2/3	X	√	Exterior	End hook anchorage details and retrofitting (FRP)
Mukherjee and Joshi (2005)	RCC with FRP	1/3	X	X	Interior	Retrofitting (FRP)
Realfonzo et. al. (2014)	RCC with FRP	1	X	X	Exterior	Retrofitting (FRP)
Dang and Dinh (2017)	RCC	1/2	X	X	Exterior	Retrofitting (Steel Jacketing and Haunch Element)
Chung et. al. (2004)	RCC	1; 1/2; 1/4	X	X	Exterior	Scale Effects

2.10 Summary

The evolution of reinforced concrete buildings and its proper design in Bangladesh based on specific guidelines according to building Codes are presented in this chapter. To make a reinforced concrete moment frame appropriately an earthquake resistant structure, the design guidelines must be followed. In Bangladesh, BNBC 2020 is the building Code followed and practiced for design which explains the details of earthquake resistant structures.

The most vital part of moment frames under an earthquake hazard event are the beam-column joints as it exhibits large shear forces under such events. Joint failure occurs to be the most catastrophic type of failure which must be avoided under any circumstances and so proper design and detailing of joints are of high priority. However, due to the poor understanding of importance of joint detailing in the construction industry and the construction difficulties owing to reinforcement congestion and concrete compaction in the joint region, beam-column joints are often seen to be a vulnerable zone of the structure especially under high seismic loads. Properly designed and detailed joints must have sufficient capacity to allow the adjoining beams and columns to develop their ultimate strengths and the failure should localize in a distinct plastic hinge in the beam away from the joint-beam interface.

Different constituent materials of concrete have significant impact on its characteristics which have been observed by many researchers. Recent studies covered a great number of parameters concerning the behavior of beam-column joints under cyclic loading. However, studies with joint performance based on the choice of coarse aggregate is hardly found in literature which establishes a research gap in the state of the art which this thesis aims to fill in.

CHAPTER 3
EXPERIMENTAL PROGRAM

3.1 Introduction

This research have been carried out to study the behavior of the reinforced concrete exterior beam-column joints designed according to BNBC 2020 with intermediate moment frame detailing provisions made with different coarse aggregates under reversed cyclic loading. The current construction practices of reinforced concrete structures in Bangladesh uses mainly brickbats and crushed stone as coarse aggregates in reinforced concrete. It is also found that, different choices of course aggregates are used in the different components of the same structural frame in order to ensure strong column-weak beam phenomenon. However, the seismic behavior of such frames made with different aggregates has not been studied yet. To capture the behavior of such frames correctly, material properties had to be determined appropriately and a proper experimental research was essential to be carried out in a methodological manner. In this study, eight exterior beam-column joint specimens were prepared which were subjected to constant axial load in columns and incremental reversed cyclic loading at the tip of the beams. The cracking characteristics, failure patterns, load-deflection response, moment-rotation response, energy dissipation capacity, stiffness degradation, and ductility were determined and analyzed to study the behavior of the specimens.

This chapter discusses the properties of the materials used in this research work, the details of the selected model, the description and preparation technique of the specimens, the details of experimental setup and instrumentation, as well as the data acquisition technique. The loading protocol applied to the specimens have also been defined in this chapter.

3.2 Material Properties

The main constituents of reinforced concrete are cement, fine aggregate, coarse aggregate, and steel reinforcement. Locally available sand have been used as fine aggregates while crushed bricks, stone chips, recycled concrete, and electric arc furnace steel slag have been used as coarse aggregates. The properties of these materials have been tested in laboratory or collected from the specification of the manufacturer which

are discussed in this section. The properties of concrete has also been tested in laboratory which is also outlined here.

3.2.1 Cement

Ordinary Portland Cement (OPC) type CEM-I 52.5 N conforming to the Standards of BDS EN 197-1:2003 have been used in this research. The chemical composition of this cement has been collected from the manufacturer while other properties have been determined in the concrete laboratory of Department of Civil Engineering, BUET.

Table 3.1: Properties of cement used in this study

Chemical properties	
Silicon dioxide, SiO_2 (%)	20.7
Aluminium oxide, Al_2O_3 (%)	4.90
Ferric oxide, Fe_2O_3 (%)	3.26
Calcium oxide, CaO (%)	63.8
Magnesium oxide, MgO (%)	1.56
Sulfur trioxide, SO_3 (%)	2.40
Insoluble residue, IR (%)	0.32
Loss on ignition, LOI (%)	1.26
Total alkali (Na_2O+ K_2O) (%)	0.46
Chloride content, Cl^- (%)	0.006
Physical properties	
Fineness (m^2/kg)	425
Specific gravity (gm/cc)	3.14
Cement mortar compressive strength	
3 days (MPa)	22.7
7 days (MPa)	34.7
28 days (MPa)	43.1
Others	
Water for normal consistency (%)	25
Initial setting time (minutes)	143
Final setting time (minutes)	350

The cement mortar compressive strength has been determined in accordance with ASTM C109-11b, the setting time has been determined in accordance with ASTM C191-08a, the normal consistency has been determined in accordance with ASTM C187-11, the fineness has been determined in accordance with ASTM C204-11, and the specific gravity has been determined in accordance with ASTM C188-09. All the properties of cement are shown in Table 3.1.

3.2.2 Fine Aggregates

Locally available sand have been used as fine aggregates for this research as shown in Figure 3.1. The specific gravity and water absorption of sand have been determined in the laboratory in accordance with ASTM C128-01. The bulk specific gravity have been found to be 2.59 (oven dry basis) and the water absorption capacity to be 0.93%. The sieve analysis was performed in accordance with ASTM C136. The fineness modulus of sand have been determined to be 2.92. The grain size distribution curve for sand is shown in Figure 3.2 and the sieve analysis data is shown in appendix A1.1.

Figure 3.1: Fine aggregate (locally available sand)
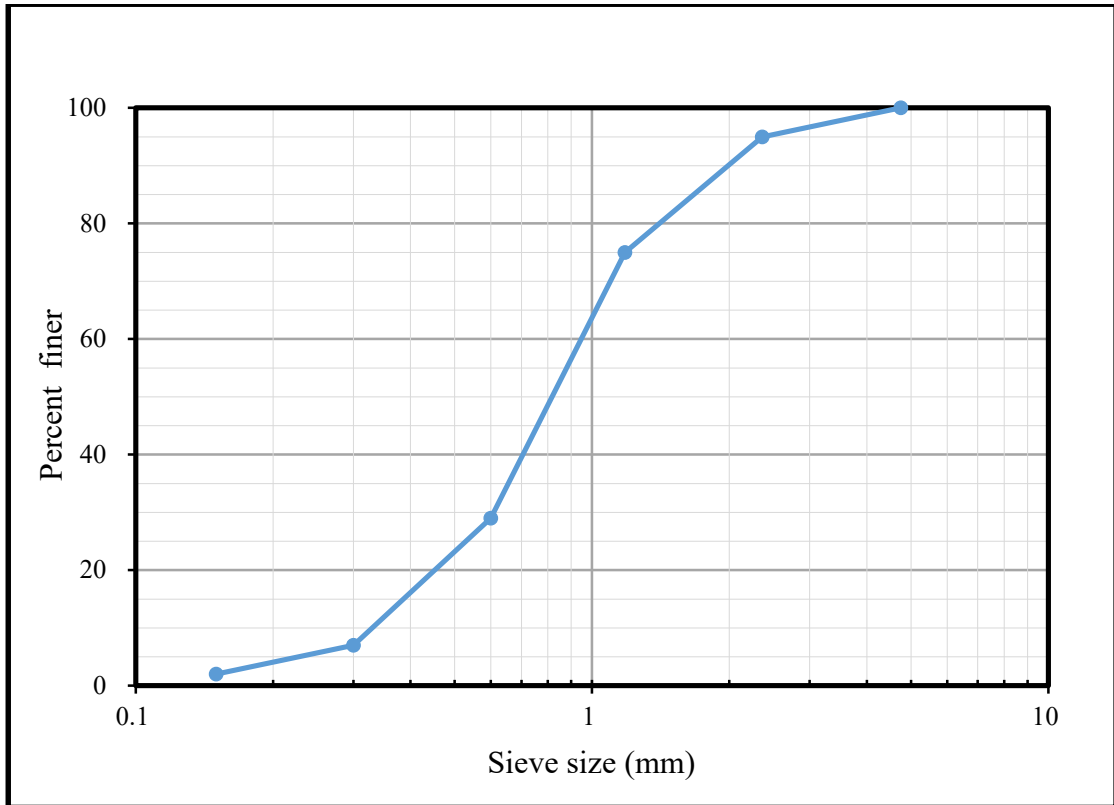
Figure 3.2: Grain size distribution of sand

3.2.3 Coarse Aggregates

Four types of coarse aggregates have been used in this study for the preparation if different concrete mixes. Properties of these aggregates have been determined in concrete laboratory and transportation laboratory of Department of Civil Engineering, BUET. Aggregate crushing value was determined in accordance with BS 812 while the specific gravity and water absorption of coarse aggregates have been determined in accordance with ASTM C127. Sieve analysis was performed in accordance with ASTM C136. The material properties for crushed stone, brickbats, steel slag aggregates, and recycled concrete aggregates are shown in this section.

i.   Crushed Stone:

10mm downgrade crushed stone have been used as one of the coarse aggregates for this research as shown in Figure 3.3. The aggregate crushing value of stone chips have been found to be 20%, the bulk specific gravity to be 2.60 (oven dry basis), and the water absorption capacity to be 1.50%. The fineness modulus have been found to be 5.95. The grain size distribution curve for stone chips is shown in Figure 3.4 and the sieve analysis data is shown in appendix A1.2.

43

Figure 3.3: Coarse aggregate (stone chips)
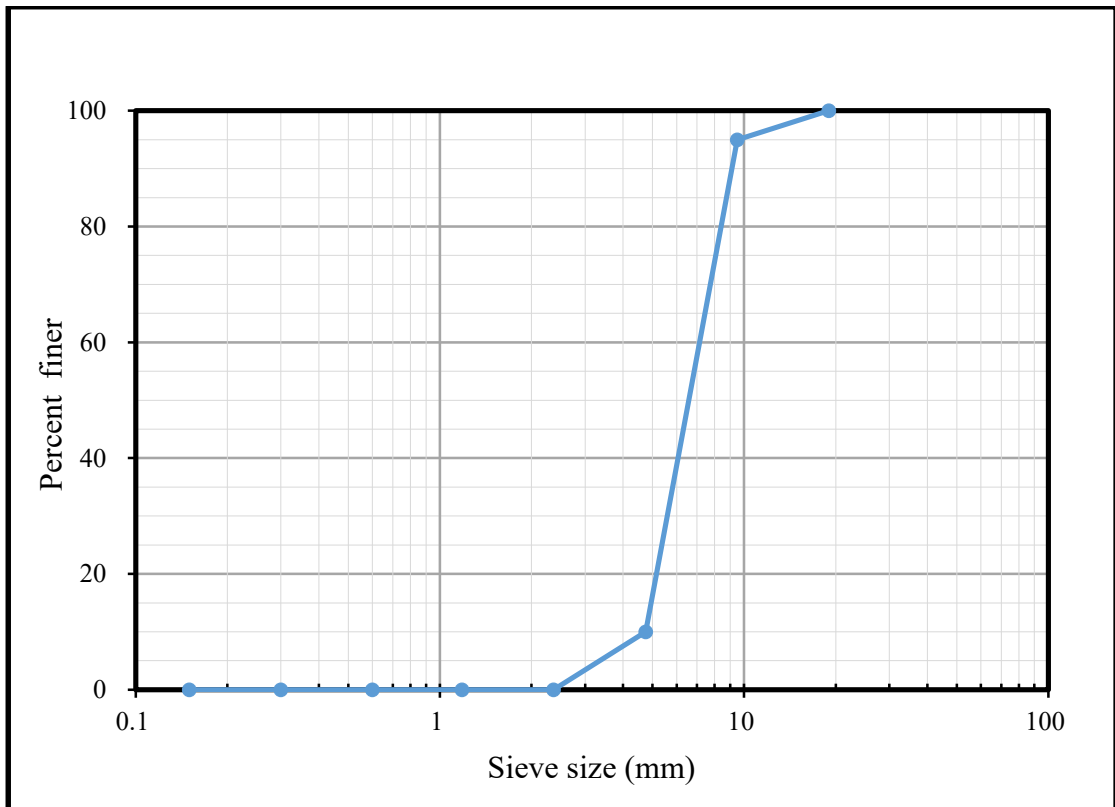
Figure 3.4: Grain size distribution of stone chips

ii. Brickbats:

Locally available picket bricks were crushed to 10mm downgrade size which has been used as another type of coarse aggregates for this research as shown in Figure 3.5. The aggregate crushing value of brickbats have been found to be 30%, the bulk specific gravity to be 1.79 (oven dry basis), and the water absorption capacity to be 14.7%. The fineness modulus have been found to be 6.01. The grain size distribution curve for brickbats is shown in Figure 3.6 and the sieve analysis data is shown in appendix A1.3.

Figure 3.5: Coarse aggregate prepared from picket bricks (brickbats)
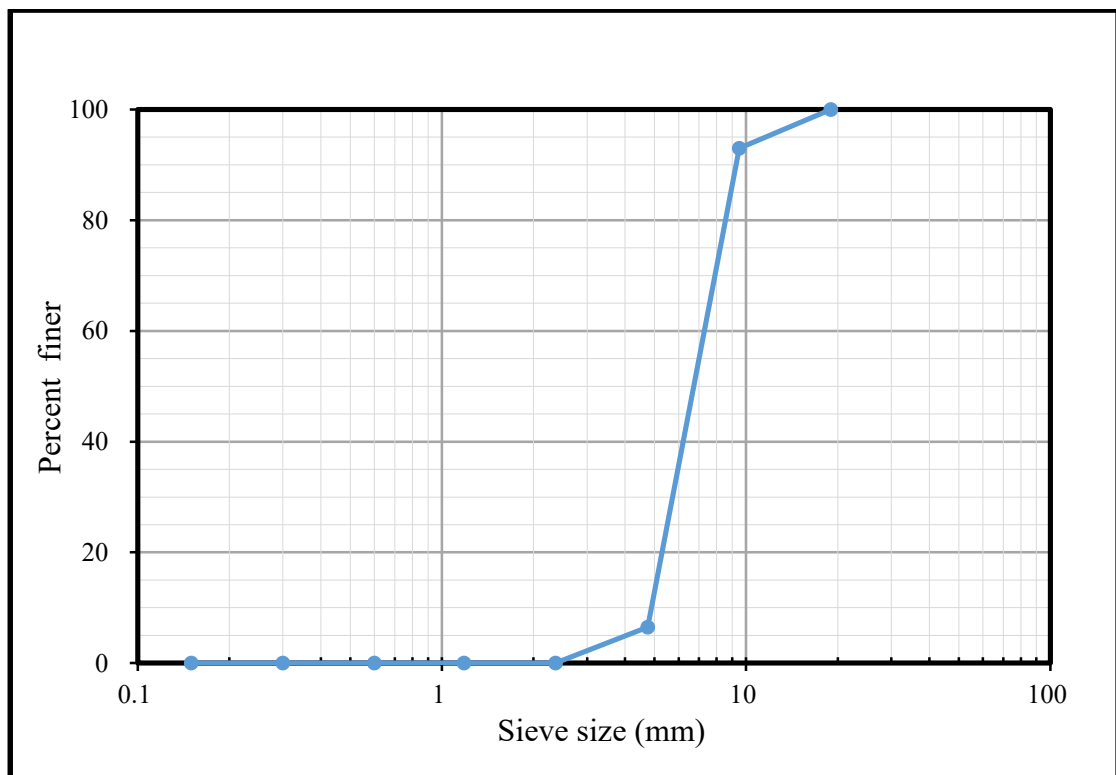
Figure 3.6: Grain size distribution of brickbats

45

iii. Steel Slags:

There are many of types of steel slag generated in many parts of the steel manufacturing process which can be classified into the following categories:

a. Blast Furnace Slag
b. Steel Furnace Slag
     i. Basic Oxygen Furnace (BOF) Slag
    ii. Electric Arc Furnace (EAF) Slag
   iii. Ladle Slag

Electric arc furnace (EAF) is one of the process of steel making and the slag generated from this process is defined as electric arc furnace slag. 10mm downgrade electric arc furnace steel slag has been used as another type of coarse aggregates for this research as shown in Figure 3.7. The aggregate crushing value of steel slag aggregate have been found to be 12%, the bulk specific gravity to be 3.35 (oven dry basis), and the water absorption capacity to be 1.60%. The fineness modulus have been found to be 6.01. The grain size distribution curve for steel slag aggregate is shown in Figure 3.8 and the sieve analysis data is shown in appendix A1.4.

Figure 3.7: Coarse aggregate acquired from EAF slag (steel slag)
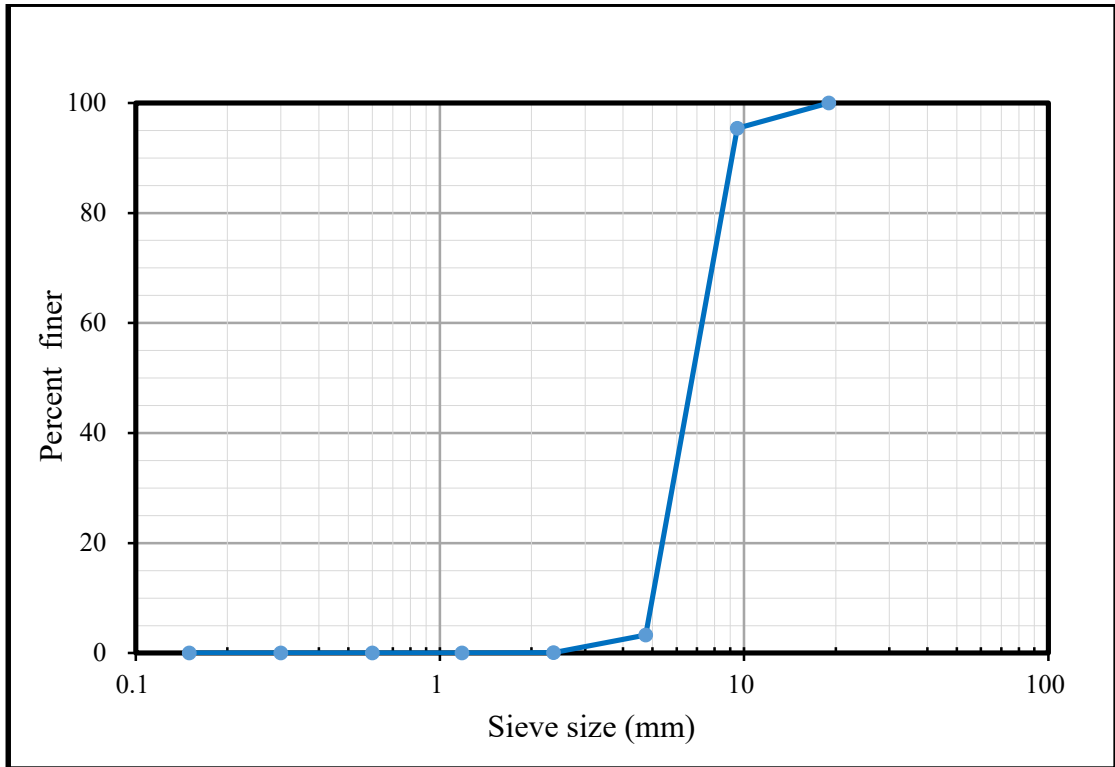
Figure 3.8: Grain size distribution of steel slag

iv. Recycled Concrete Aggregates:

Concrete compressive strength tests are performed on 100 mm diameter and 200 mm height concrete cylinders according to ASTM C39. A huge number of such samples are tested every day in concrete laboratory of Department of Civil Engineering, BUET. After testing, samples with natural stone aggregates with similar strengths have been collected and crushed to 10mm downgrade size which has been used as another type of coarse aggregates for this research as shown in Figure 3.9.

Figure 3.9: Coarse aggregate acquired from concrete cylinders (recycled concrete)

The aggregate crushing value of recycled concrete aggregates have been found to be 24%, the bulk specific gravity to be 2.28 (oven dry basis), and the water absorption capacity to be 6.60%. The fineness modulus have been found to be 5.88. The grain size distribution curve for recycled concrete aggregates is shown in Figure 3.10 and the sieve analysis data is shown in appendix A1.5.
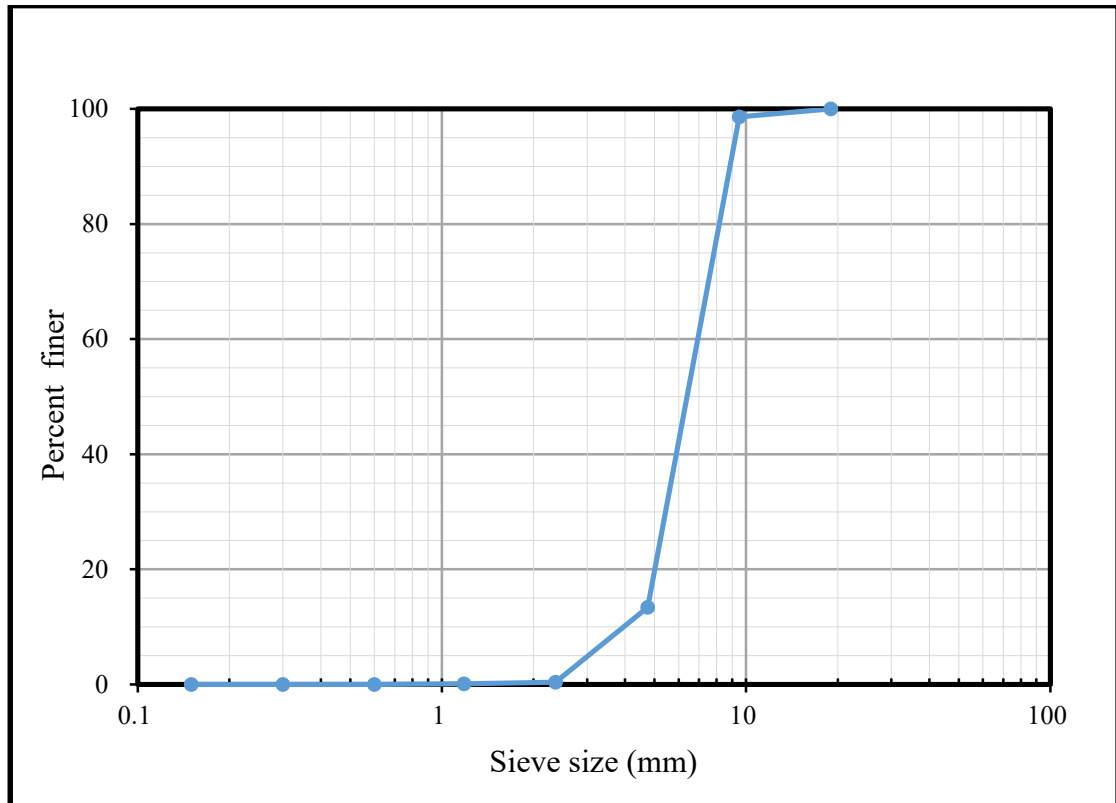
Figure 3.10: Grain size distribution of recycled concrete

The properties of various coarse aggregates used in this research work is summarized in Table 3.2.

Table 3.2: Properties of coarse aggregates used in this study

Parameter	Type of Coarse Aggregate			
	Stone Chips	Brickbats	Steel Slag	Recycled Concrete
ACV (%)	20	30	12	24
Bulk specific gravity	2.60	1.79	3.35	2.28
Water absorption capacity (%)	1.50	14.7	1.60	6.60
FM	5.95	6.01	6.01	5.88

3.2.4 Reinforcement

Two types of steel reinforcements have been used for longitudinal and transverse reinforcements in this research work. As the specimens have been reduced to one-third scale to accommodate the experimental setup, the reinforcing bars were also had to be scaled down accordingly to simulate real scale behavior as 6 mm and 8 mm bars have been used. The 6 mm bars were grade 500 AWR while the 8 mm bars were grade 500 DWR. Low ductility 6 mm bars had to be used in this study as higher grade 6 mm bars are not manufactured in Bangladesh. The tensile test results are shown in Table 3.3 and the stress versus strain plots for each bars are displayed in appendix A2. From the test results, it has been found that the yield strength of 6 mm bars were 654.5 MPa while that of 8 mm bars were 602.5 MPa.

Table 3.3: Properties of steel reinforcements used in this study

Sl. No.	Diameter (mm)	Weight (gm)	Length (cm)	Cross-Sectional Area (mm^2)	Yield Load (N)	Ultimate Load (N)	Ultimate Load/Yield Load	Yield Strength (MPa)	Average Yield Strength f_y (MPa)	Average Yield Strength f_y (ksi)	Elongation (%)
1	6	135	60.3	28.5	18670	19490	1.04	655.5			5
2	6	135	60	28.6	18630	19610	1.05	650.8	654.5	94.9	4
3	6	135	60	28.6	18800	19560	1.04	656.8			4
1	8	222	56.8	49.7	30710	37340	1.22	617.6			11
2	8	221	56.7	49.6	29490	36930	1.25	594.7	602.5	87.4	11
3	8	220	56.5	49.5	29500	36510	1.24	595.5			11

3.2.5 Concrete

Four different concrete mixes were prepared using ordinary portland cement, sand, and four different course aggregates as mentioned earlier in this chapter. All of the coarse aggregates were 10 mm downgrade. The concrete mix ratio was kept 1:1.5:3 by volume while the water-cement ratio was kept constant at 0.45 for all four mixes. Approximately 25 mm slump value were achieved to ensure sufficient workability of all of the concrete mixes. Compressive strength, modulus of elasticity, and stress versus strain relationship of concrete were determined through laboratory tests which is described in this section.

i. Compressive Strength of Concrete

The compressive strengths of concrete have been determined by performing compression tests in accordance with ASTM C39 on 100 mm diameter and 200 mm height concrete cylinders. The concrete cylinders were cured up to 28 days age in curing tanks after which they were tested in compression testing machine as shown in Figures 3.11 and 3.12. The compressive strength test results of the four concrete mixes are summarized in Table 3.4. It has been found that the compressive strength of concrete made with stone chips were 27.4 MPa, that made with brick chips were 28.3 MPa, that made with steel slag aggregates were 36.3 MPa, and that made with recycle concrete aggregates were 32 MPa.

Figure 3.11: Curing of concrete cylinders

Figure 3.12: Compressive strength test of concrete cylinders

Table 3.4: Compressive strength of concrete

Sl.	Coarse Aggregate	Specimen Area (sq. in)	Maximum Load (lb)	Crushing Strength (psi)	Average Crushing Strength	Mode of Failure
1	Stone Chips	12.7	49514	3908	**3980 psi**	Combined
2	Stone Chips	12.7	50640	3997	**27.4 MPa**	Combined
3	Stone Chips	12.7	51248	4045	**280 kg/cm²**	Combined
1	Brickbats	12.7	51023	4027	**4100 psi**	Combined
2	Brickbats	12.4	52145	4198	**28.3 MPa**	Combined
3	Brickbats	12.7	51696	4080	**288 kg/cm²**	Combined
1	Steel Slag	12.7	70536	5567	**5270 psi**	Combined
2	Steel Slag	12.6	64831	5166	**36.3 MPa**	Combined
3	Steel Slag	12.7	64256	5071	**371 kg/cm²**	Combined
1	Recycled Concrete	12.4	57527	4632	**4640 psi**	Combined
2	Recycled Concrete	12.7	58873	4647	**32 MPa**	Combined
3	Recycled Concrete	12.7	58649	4629	**326 kg/cm²**	Combined

ii. Modulus of Elasticity of Concrete

The modulus of elasticity of concrete have been determined according to test method ASTM C469. Similar concrete cylinders to those tested for compressive strength were prepared. The objective was to determine a stress versus strain relationship. The load was applied using a universal testing machine while the apparatus used for determining the longitudinal deformation is called a compressometer as shown in Figure 3.13. The stress versus strain graphs for four concrete mixes are shown in appendix A3. The modulus of elasticity is calculated using equation 3.1 which is suggested by Saha (2019).

Modulus of Elasticity, $E = \dfrac{S_2 - S_1}{\varepsilon_2 - 0.00005}$ (3.1)

Where,

E = Modulus of elasticity,

S_2 = Stress corresponding to 40% of ultimate load,

S_1 = Stress corresponding to a longitudinal strain of .00005,

ε_2 = Strain corresponding to stress S_2.

Figure 3.13: Stress versus strain test of concrete

The modulus of elasticity of four concrete mixes are presented in Table 3.5.

Table 3.5: Modulus of elasticity of concrete

Coarse Aggregate Type	Modulus of Elasticity (GPa)	Modulus of Elasticity (ksi)
Stone Chips	21.2	3079
Brickbats	20.9	3032
Steel Slag	35.6	5163
Recycled Concrete	23.7	3437

3.3 Selection of Model

The test models have been selected considering a full scale eight storied reinforced concrete intermediate moment frame building located in Dhaka as shown in Figures 3.14 to 3.16. The building has been analyzed as per the provisions of BNBC 2020. An exterior beam-column joint from story-5 of the building has been selected for the experimental program details of which are discussed in section 3.4.
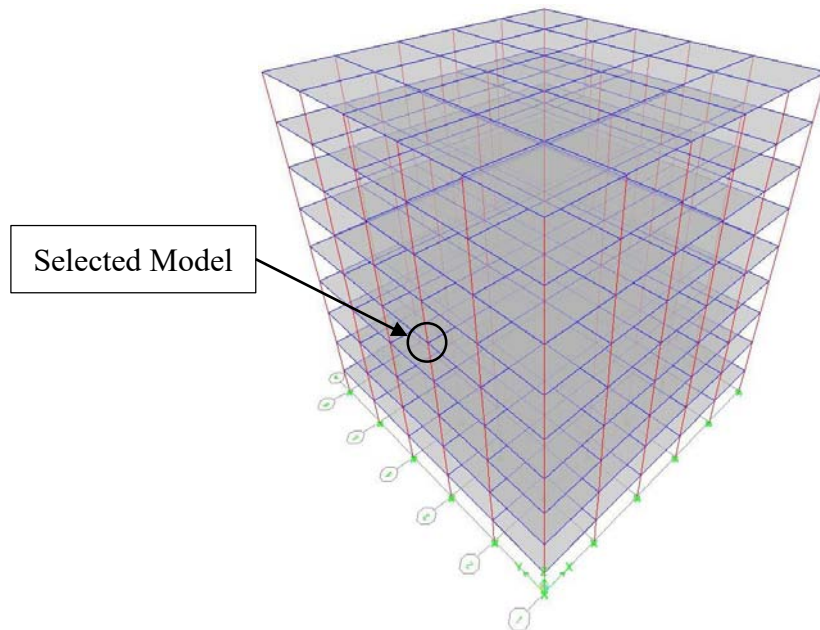
Figure 3.14: 3D view of the structure
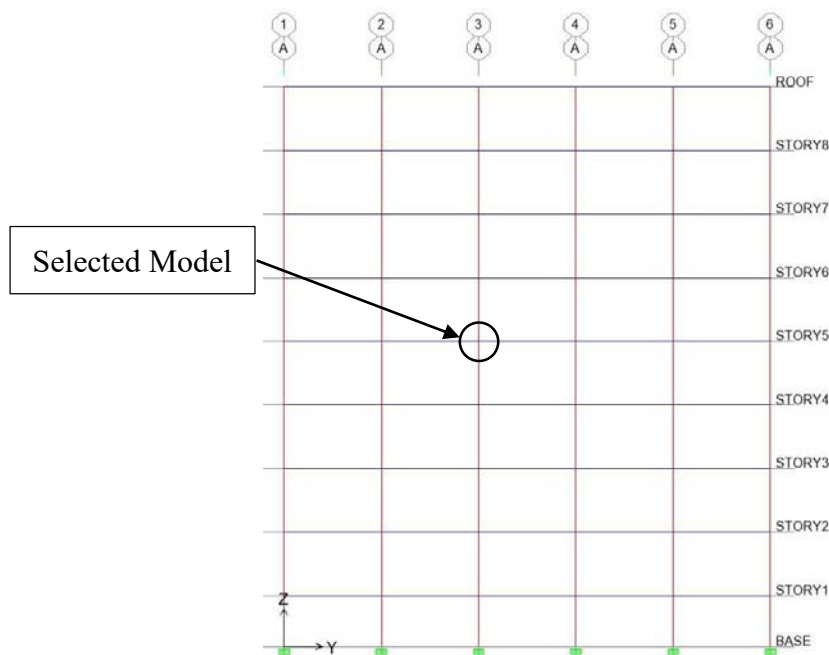
Figure 3.15: Elevation view of the structure
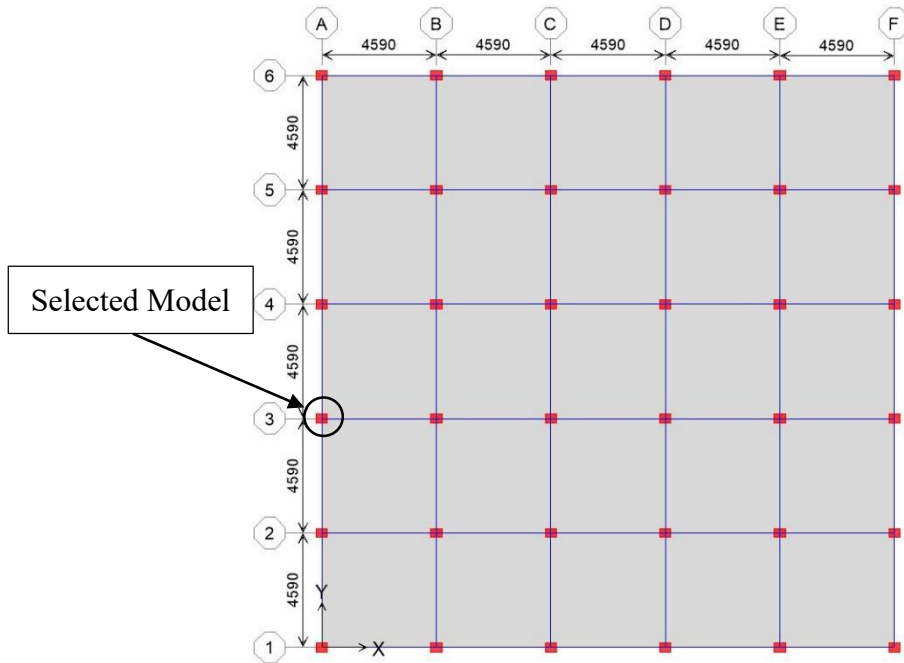
Figure 3.16: Plan view of the structure

3.4 Details of the Selected Model

Considering the existing laboratory setup, one-third scaled beam-column subassemblies have been chosen to analyze the structural behavior of such joints. ACI 374.1-05 allows test modules to be scaled down to one-third scale so that the modules are large enough to fully represent the behavior and complexities of the real materials and of the load transfer mechanisms in the full scale model.

The cross-sections of beams and columns of the specimens were 120 mm x 150 mm as they were reduced to one-third scale. The specimens were cast up to probable inflection point of the beams and columns. The length of the half span of beam was therefore 765 mm and the height of the column was 1400 mm. It has been assumed that, due to the partial fixity in the joint region of reinforced concrete frames, the inflection point in columns will be at 0.70 times of the full height of column.

The material sizes were also reduced to approximately one-third scale to reflect their effect on the scaled down specimens. In order to ensure that, 10 mm downgrade coarse aggregates were used along with 8 mm and 6 mm diameter steel reinforcing longitudinal and transverse bars. The reinforcement design and detailing have been done in accordance with intermediate moment frame detailing provisions of BNBC 2020. Dimensions and detailing of the specimens are shown in Figures 3.17 and 3.18.

Figure 3.17: Details of the test specimen

Figure 3.18: Details of beams and columns of the test specimen

55

The beam-column joints were also designed in accordance with BNBC 2020 in order to ensure that flexural failure occurs in beams through plastic hinge formation. The yield moment capacities of beams and columns as well as the joint shear demands and capacities have been determined which are shown in appendix B.

3.5   Description of the Test Specimens

Eight exterior beam-column joint specimens were constructed for the experiment out of which two were control specimens. The coarse aggregates in beams, columns, and joints were varied in the specimens keeping the same geometry and reinforcement details mentioned in the previous section. The first control specimen was cast with stone chips aggregate concrete in beam, column, and joint while the second control specimen was cast with brickbats aggregate concrete in beam, column, and joint. The six other specimens have been cast with different coarse aggregate concrete mixes in beams, columns, and joints. The specimens are designated according to the coarse aggregates in concrete mixes in the frame elements and joints which is shown in Table 3.6.

Table 3.6: Specimen designation of the test modules

Specimen Designation	Description	Mix Ratio	Coarse Aggregate (Beam)	Coarse Aggregate (Column)	Coarse Aggregate (Joint)
1-SS-C1	Control 1	1:1.5:3	Stone chips	Stone chips	Stone chips
2-BB-C2	Control 2	1:1.5:3	Brickbats	Brickbats	Brickbats
3-BS-B	Variations with stone chips and brickbats	1:1.5:3	Brickbats	Stone chips	Brickbats
4-BS-S		1:1.5:3	Brickbats	Stone chips	Stone chips
5-BSS-B	Variations with steel slag and brickbats	1:1.5:3	Brickbats	Steel slag	Brickbats
6-BSS-SS		1:1.5:3	Brickbats	Steel slag	Steel slag
7-RCS-RC	Variations with stone chips and recycled concrete	1:1.5:3	Recycled concrete	Stone chips	Recycled concrete
8-RCS-S		1:1.5:3	Recycled concrete	Stone chips	Stone chips

3.6 Preparation of the Test Specimens

The test samples have been prepared in the concrete laboratory of Department of Civil Engineering, BUET. Proper quality control have been ensured during the preparation of the samples which is discussed in this section.

3.6.1 Formwork Preparation

Formwork is required to control the shape and provide support to the fresh flowing concrete. The formwork must withstand all of the loads coming on it through the weight and pressure of the concrete while casting as well as any other loads imposed by materials, equipment, personnel, or environmental loads. Formwork supports the concrete structure until the concrete sets and hardens to gain sufficient strength to support itself and imposed loads. Formworks are generally made of timber and steel. In this research, timber formworks have been used as shown in Figure 3.19.

It has been ensured that the joints in the formwork were water tight against leakage. The formwork have been set accurately to the desired line and levels. It has also been ensured that the surface was plane.

Figure 3.19: Preparation of formworks

3.6.2 Reinforcement Preparation

After the preparation of farm work, reinforcements were bound according to the details shown in Figures 3.17 and 3.18. A clear cover of 12 mm had been ensured and the reinforcements where properly aligned. The ties and stirrups were properly hooked at the ends according to the provisions of BNBC 2020. The ties have been continued throughout the joint region for all specimens. After the reinforcements were prepared, they were placed inside the formworks providing proper clear covers using cement concrete blocks. The preparation of reinforcements are shown in Figure 3.20.

Figure 3.20: Preparation of reinforcements

3.6.3 Concrete Mix Preparation

Four separate concrete mixes have been prepared by varying the types of coarse aggregates in each mix. Appropriate quantities of cement, sand, coarse aggregate, and water have been added inside the motorized mixture machine which insured thorough and homogeneous mixing of concrete. Slump have been measured so that sufficient workability of concrete is achieved. The concrete mix preparation process is shown in Figure 3.21.

Figure 3.21: Preparation of concrete mix

3.6.4 Concrete Casting

After reinforcements were properly placed over the formwork, fresh concrete mix was carefully poured on it. The specimens which had different concrete mixes in beam, column, and joint; special arrangements inside the formwork was prepared to ensure the appropriate placement of each mix. The casting of all the specimens were completed at the same day within the final setting time. However, this may not always be practiced in the construction industry. Mechanical vibrator machine was used to compact the concrete so that no air void existed inside the concrete. The casting of concrete is shown in Figures 3.22 and 3.23.

Figure 3.22: Compaction of concrete using mechanical vibrator

Figure 3.23: Specimens after fresh concrete is cast

3.6.5 Curing

The hydration process of concrete significantly influences the quality of concrete. Proper curing ensures that the reaction process is completed sufficiently and concrete gains its required strength. Water curing method has been applied after the final setting of the specimens. Thick jute cloths were used to cover the specimens which absorbed the externally applied water for curing which is shown in Figure 3.24.

Figure 3.24: Curing of concrete

3.6.6 White Coloring

After 28 days of curing, formworks were removed and the specimens were for testing. However, for better visibility of cracks, fractures, and their exact locations, all the specimens have been colored with white paint. Figures 3.25 and 3.26 shows the specimens before and after white coloring is done.

Figure 3.25: Specimens before white coloring is done

Figure 3.26: Specimens after white coloring is done

3.6.7 Attachments to the Specimens for Load Application

The specimens were subjected to constant axial load on columns and cyclic loads transversely applied to the tip of the beams during the experiment. However, to ensure that the loads were applied smoothly, concentrically, and uniformly, the ends of the columns were capped using customized steel molds as shown in Figure 3.27 while the tip of the beam was attached to a customized steel collar as shown in 3.28. The push-pull hydraulic jack was attached to this color which applied cyclic load at the tip of the beam.

Figure 3.27: Customized steel capping at column ends

Figure 3.28: Customized steel collar at beam end

3.7 Experimental Test Setup

The experimental test setup was prepared in the concrete laboratory of department of civil engineering, BUET. The specimens where rotated 90° for the convenience of testing. The bottom of the specimen were supported by rollers which rested on customized steel boxes which were bolted to the strong floor. The hydraulic jack used for axial compression of column and the push-pull jack used for cyclic loading were attached to the reaction frames. The arrangement is shown in Figures 3.29 and 3.30.
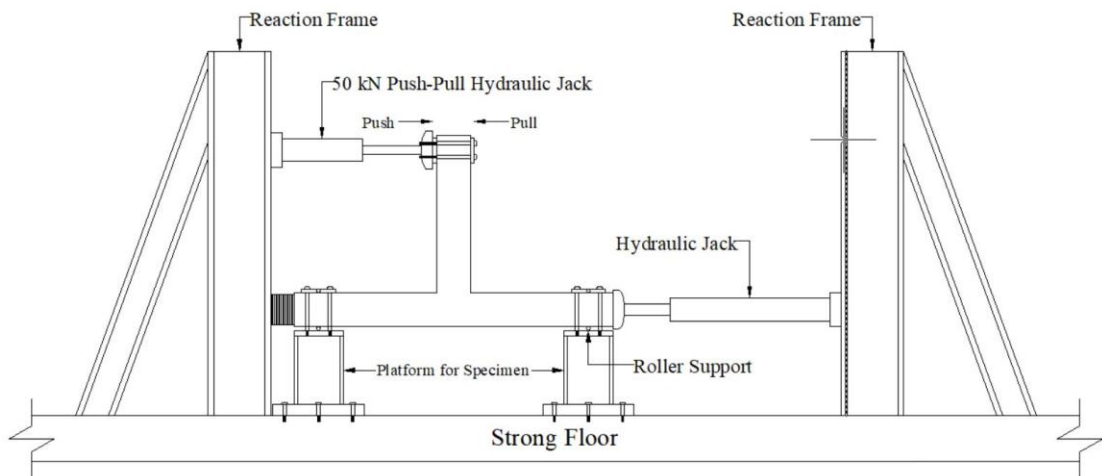
Figure 3.29: Schematic diagram of the experimental test setup

Figure 3.30: Actual experimental test setup

Deflection dial gauges were attached in order to measure displacements at three different positions of the specimens as shown in Figure 3.31.
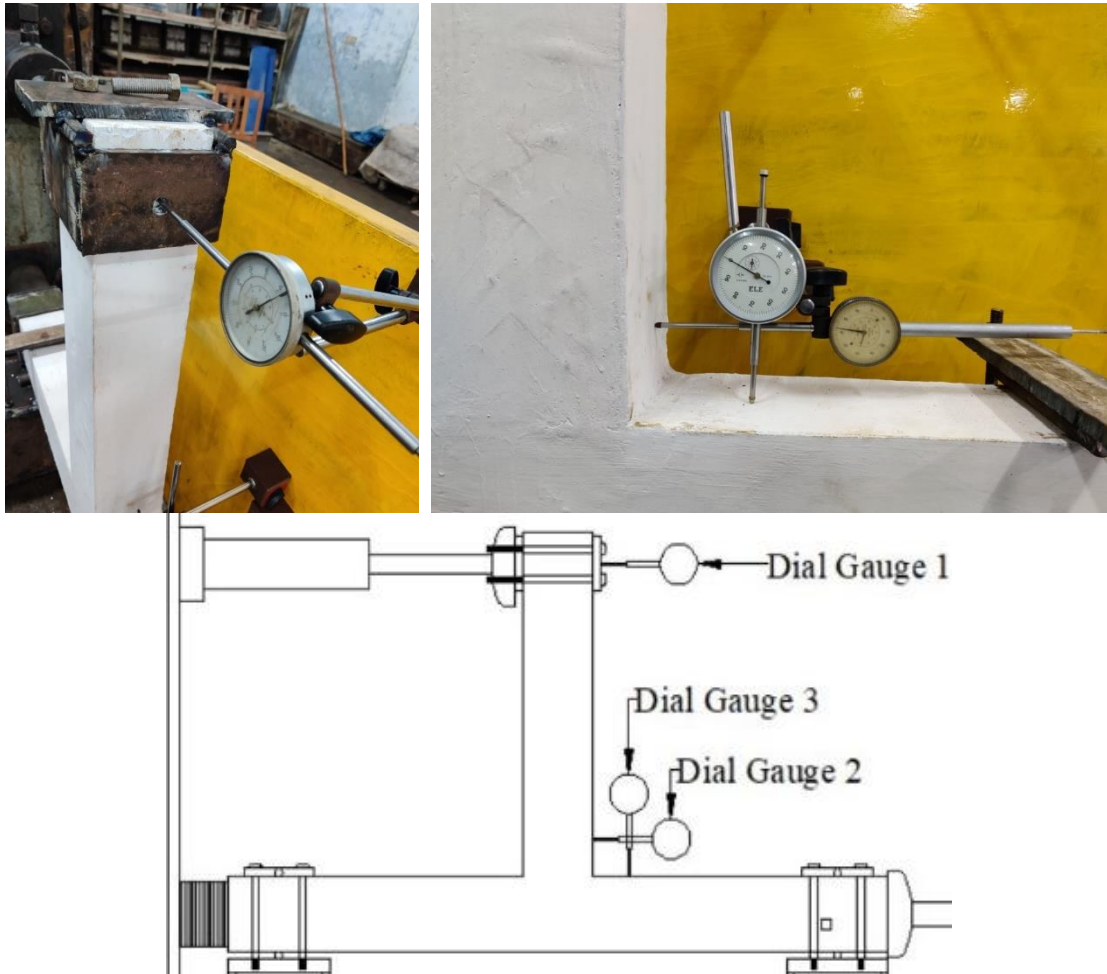
Figure 3.31: Locations of deflection dial gauges

3.8 Loadings

Quasi static reversed cyclic load have been applied to the specimens during the experiment. The loading protocol is defined in this section.

3.8.1 Axial Load on Column

The behavior of beam-column joints differs with the confinement of columns. Many researchers have kept a constant axial compressive load on column during the test. It is found in most of the literature that 10% of the compressive force carrying capacity of column is loaded to confine the column which is followed in this research (Zhang et. al. 2020; Gil-Martin et. al. 2019; Cosgun et. al. 2019; Choudhury and Laskar 2020). Table 3.7 shows the constant axial force applied on the eight specimens.

Table 3.7: Axial forces applied on columns of the test specimens

Specimen Designation	Coarse Aggregate in Column Concrete Mix	f_c' (Column) (Mpa)	Axial Force Applied on Column (0.1*f_c'*A_g) (kN)
1-SS-C1	Stone chips	27.4	49.3
2-BB-C2	Brickbats	28.3	50.9
3-BS-B	Stone chips	27.4	49.3
4-BS-S	Stone chips	27.4	49.3
5-BSS-B	Steel slag	36.3	65.3
6-BSS-SS	Steel slag	36.3	65.3
7-RCS-RC	Stone chips	27.4	49.3
8-RCS-S	Stone chips	27.4	49.3

3.8.2 Cyclic Load on Beam

Deflection control reversed cyclic load have been applied end the tip of the beam using a push-pull jack. The jack head was joined by bolts to the collar attached at the beam tip. The jack was fixed to the reaction frame as shown in the previous section.
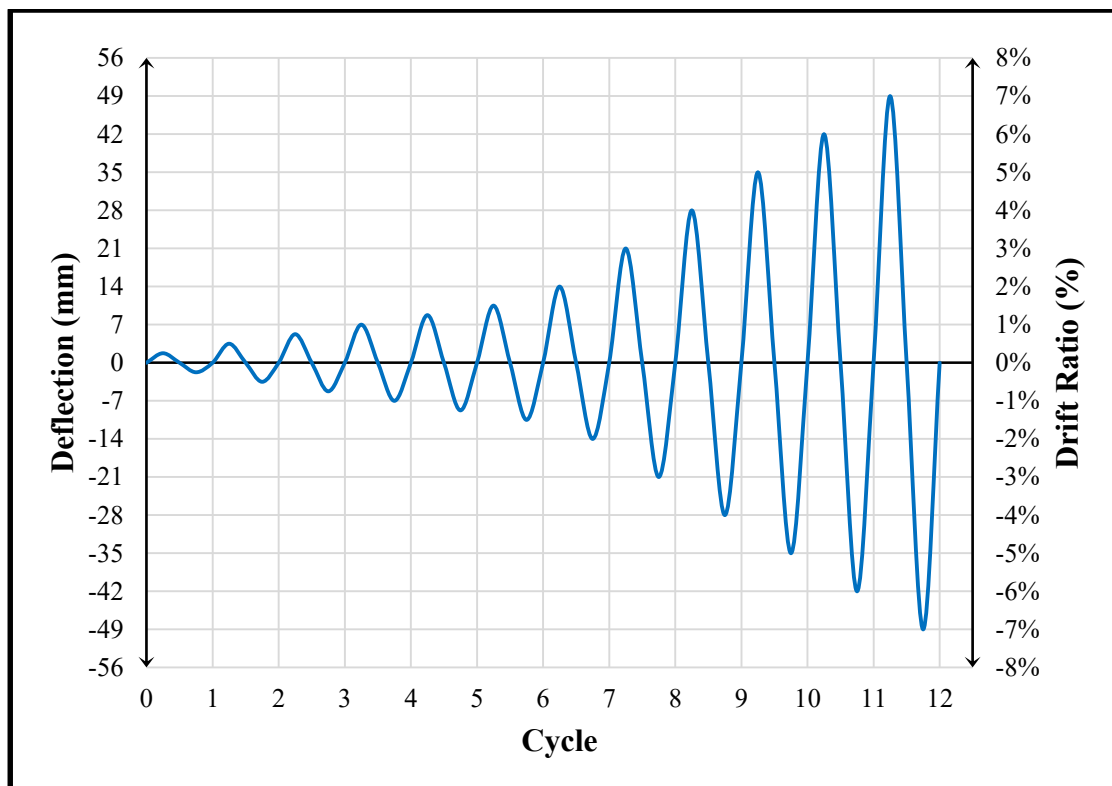
Figure 3.32: Loading protocol applied to the specimens

The structural behavior of beam-column joint is greatly influenced by the loading protocol applied to it. ASCE 41-17 has recommended that the loading protocol used must be well defined with proper descriptions of the displacements in each cycle. However, there is no fixed loading protocol for concrete structures specified by any design Codes or literature. ACI 374.1-05 has provided an example of test sequence of displacement controlled cycles for concrete structures. A similar loading protocol is followed in this research which is define in Figure 3.32. Although the loading protocol defines 12 cycles up to 49 mm displacement, all the test specimens failed on the 8th cycle.

3.9   Instrumentation and Data Acquisition

Both the jacks used to apply the loads on the specimens had been calibrated prior to the start of the tests. Standard load cell was used to calibrate the jacks. Deflection dial gauges have been used to measure the displacement at the point of load application as shown in Figure 3.31. The rotation of the joints were measured using trigonometry with the help of the dial gauge readings placed near the joint.

3.9.1   Cracking Characteristics and Failure Patterns

The formation of cracks have been marked with the help of a marker. The pattern of failure has also been observed and images of the specimens have been taken to further analyze the cracking characteristics and failure patterns.

3.9.2   Load versus Displacement Response

The applied loads on the tip of the beam have been recorded along with the corresponding displacements at the point of loading at every cycle. The loads have been plotted against corresponding displacements in order to further analyze the response of the specimens under cyclic loading. The failure envelopes have been defined by recording the peak loads and peak displacements at each cycle for each specimen.

3.9.3   Moment versus Rotation Response

The applied moment on joints have also been plotted against corresponding rotations of the joint. The failure envelopes have been defined by recording the peak moments and peak rotations at each cycle for each specimen.

3.9.4 Stiffness Degradation

The stiffness of a joint is determined at each cycle by calculating the secant stiffness joining the peak points at the forward and reverse half-cycles as shown in Figure 3.33 (Choudhury and Laskar 2020; Gil-Martin et. al. 2019; Khan et. al. 2018; Realfonzo et. al. 2014; Saha and Meesaraganda 2019; Shen et. al. 2021). The stiffness is recorded at each cycle for each specimen which is plotted to analyze the stiffness degradation patterns of the specimens.
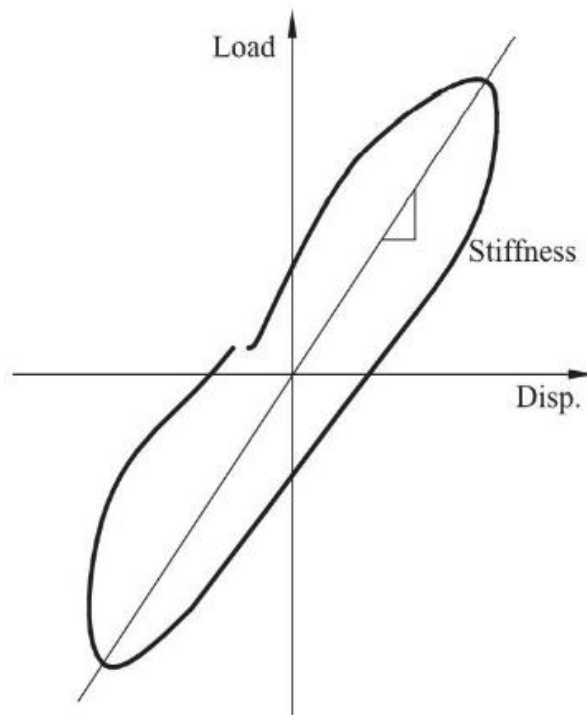
Figure 3.33: Definition of Stiffness (Li et. al. 2013)

3.9.5 Displacement Ductility

The ductility of a joint is defined as the ratio of ultimate displacement to yield displacement of the joint under cyclic loading (Park 1988; Choudhury and Laskar 2020; Li et. al. 2013). Displacement ductility of the joint is referred by the word ductility in this thesis. The yield displacement is determined by joining the origin with the point at 75% of the peak load on the load-displacement failure envelope curve and extrapolating it up to the maximum load as shown in Figure 3.34 (Park 1988; Choudhury and Laskar 2020; Li et. al. 2013). The ultimate displacement is determined at the point when the transverse or longitudinal reinforcing steel fractures or the longitudinal compression reinforcement buckles (Park 1988) as shown in Figure 3.34.
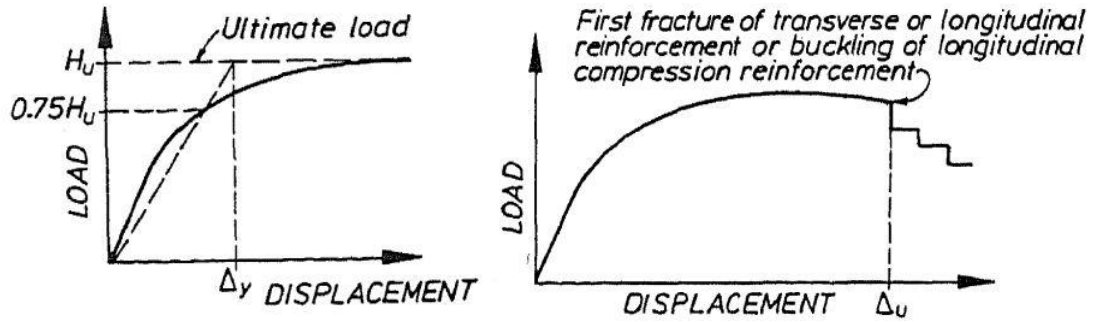
Figure 3.34: Determination of yield and ultimate displacement (Park 1988)

3.9.6 Energy Dissipation Capacity

Energy dissipation of a specimen in a certain cycle is determined by integrating the area of the load versus displacement hysteresis loop as shown in Figure 3.35. The cumulative energy dissipation capacity of a specimen is determined by adding the energy dissipation capacities of all cycles. The area of a loop have been determined using the trapezoidal rule in this research. The area of a segment is calculated using equation 3.2.

Area of a segment, $\Delta A = \frac{1}{2} * (y_{i+1} + y_i) * (x_{i+1} - x_i)$ (3.2)
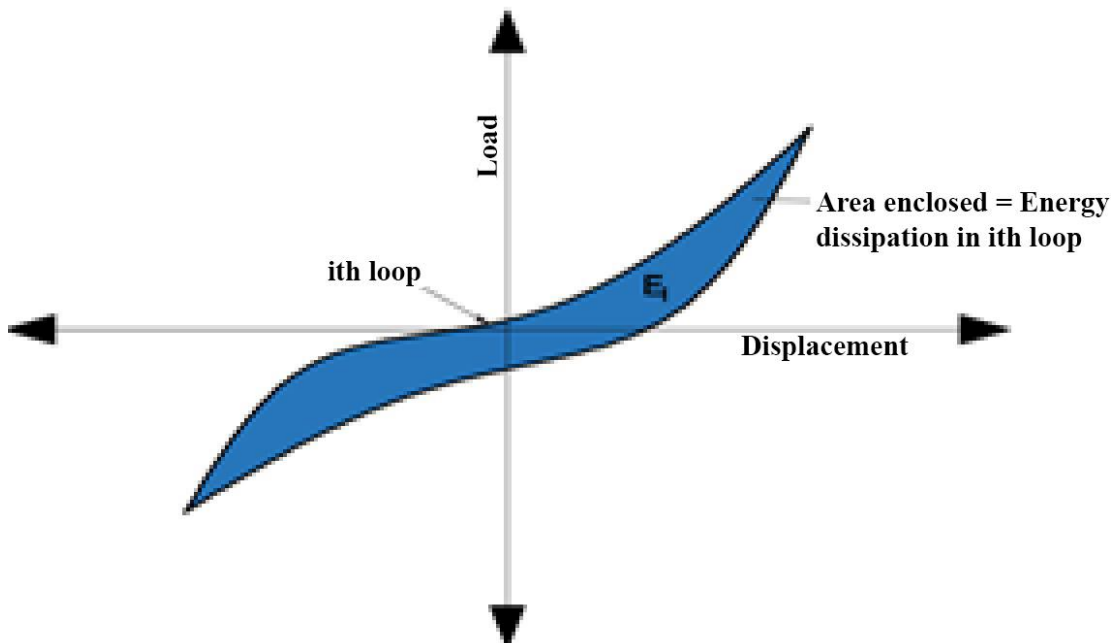
Figure 3.35: Determination of energy dissipation capacity of a cycle of a specimen (Khan et. al. 2018)

68

3.10 Summary

The methodology and the test scheme is presented in this chapter. The materials that were used to prepare the specimens have been tested and their properties have been described elaborately. The selection process of the model has been done rationally and the design and detailing of the specimens have been done in accordance with BNBC 2020. The reinforcement detailing and the geometry of the beam-column joint specimens have been described with proper illustrations. The preparation process of the test specimens have been presented sequentially. The experimental test setup has been illustrated schematically and with the help of real images. The application of loads to the specimen have been defined along with the description of the loading protocol. Finally, the instrumentation and data acquisition concepts have been described elaborately. The overall methodology is shown in a flowchart in Figure 3.36.
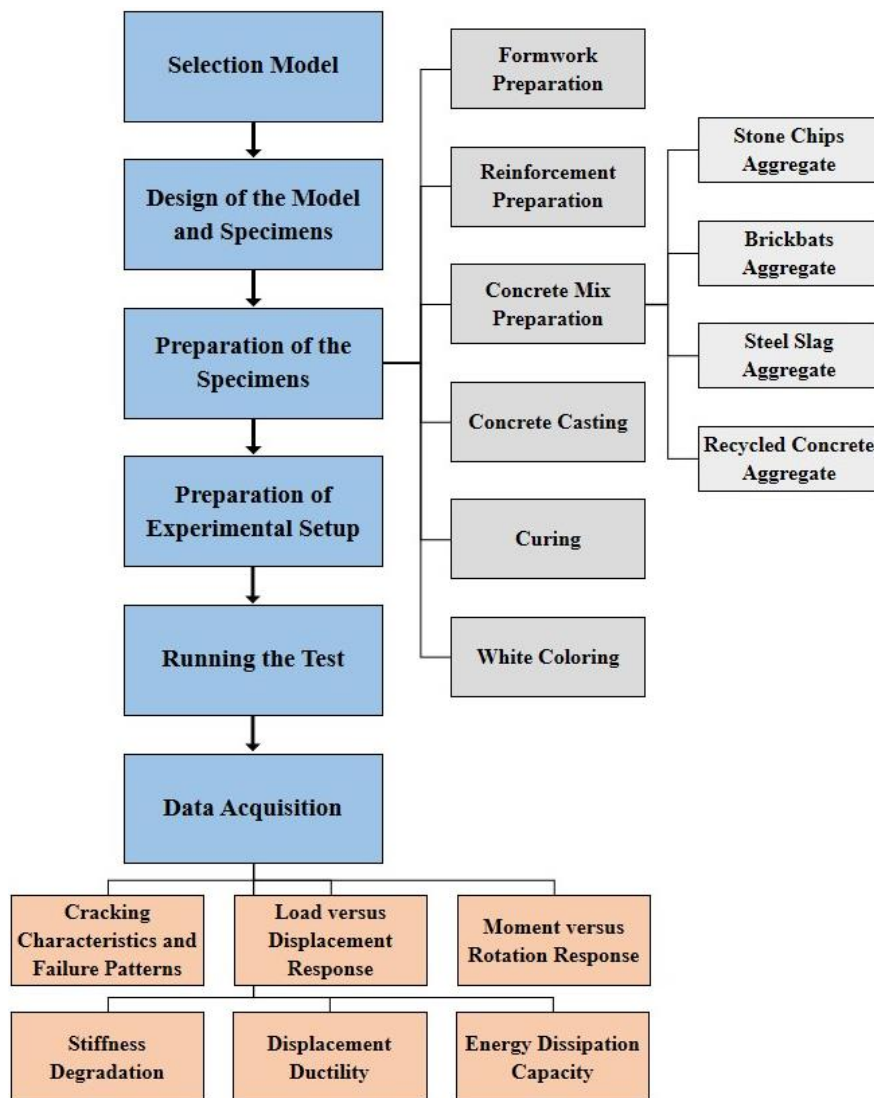
Figure 3.36: Outline of the methodology of this study

69

CHAPTER 4
RESULTS AND DISCUSSION

4.1 Introduction

The objective of this research is to evaluate the performance of beam-column joints made with different choices of coarse aggregates in concrete mixes. Results obtained from the reversed cyclic load tests on all the eight specimens are presented in this chapter. The effect of using different coarse aggregate concrete mixes in beams, columns, and joint regions are illustrated in the chapter along with relevant discussions and interpretations. The cracking and failure characteristics, load-displacement response, moment-rotation response, stiffness degradation, displacement ductility, and energy dissipation results are summarized in this chapter in order to analyze the comparative performance of the specimens under cyclic loading.

This chapter is divided into two major parts for a better understanding of the test results. Firstly, the results of each specimens are analyzed with proper graphs, charts, and illustrations. Afterwards, the analyzed results are interpreted and compared among specimens made with different coarse aggregates to identify the relative performances of the joints. The findings are summarized at the end of this chapter.

4.2 Cracking Characteristics and Failure Patterns

The cracks formed in the eight concrete specimens during the tests are shown in Figures 4.1a to 4.8a. The first crack initiated within the first four cycles which further propagated in the later stages as shown in Figures where the numbers indicate the cycle in which the cracks formed. The specimens failed due to flexure during cycle eight after which the test had been discontinued. The failure occurred at the hinge formed in the beam near the joint-beam interface which is shown in Figures 4.1b to 4.8b.

Figure 4.1: (a) Cracks in specimen 1-SS-C1 (b) Failure zone of specimen 1-SS-C1
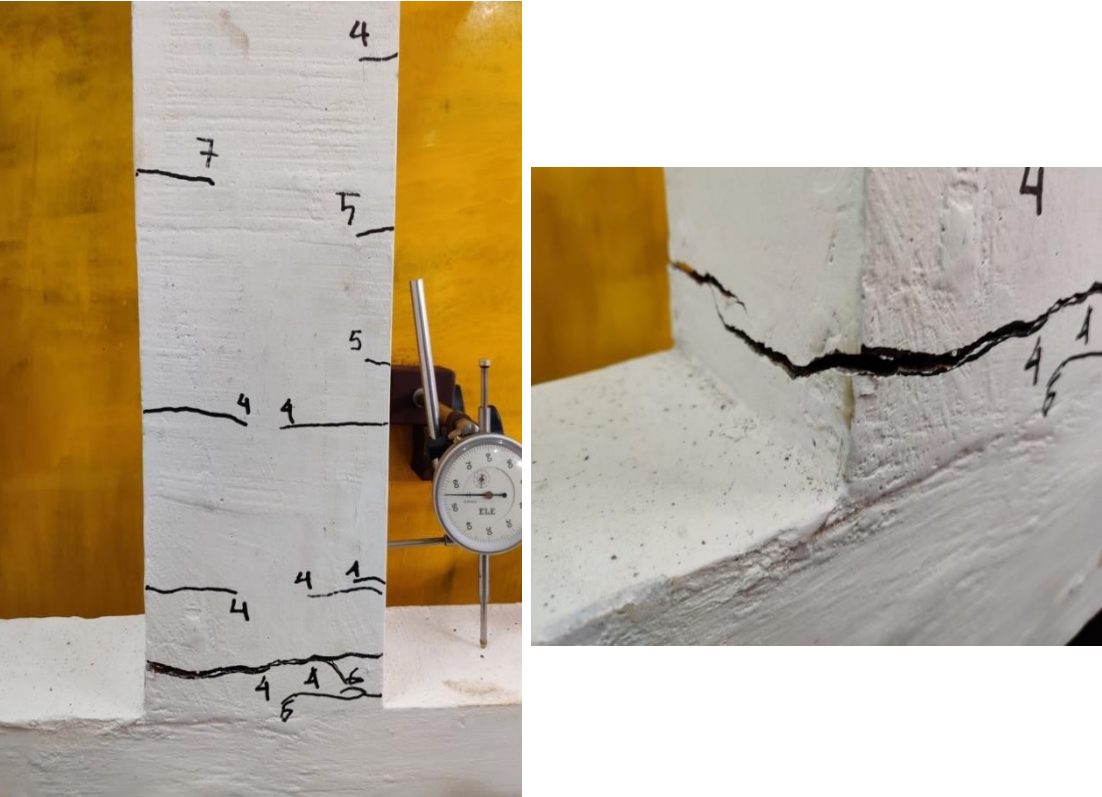
Figure 4.2: (a) Cracks in specimen 2-BB-C2 (b) Failure zone of specimen 2-BB-C2
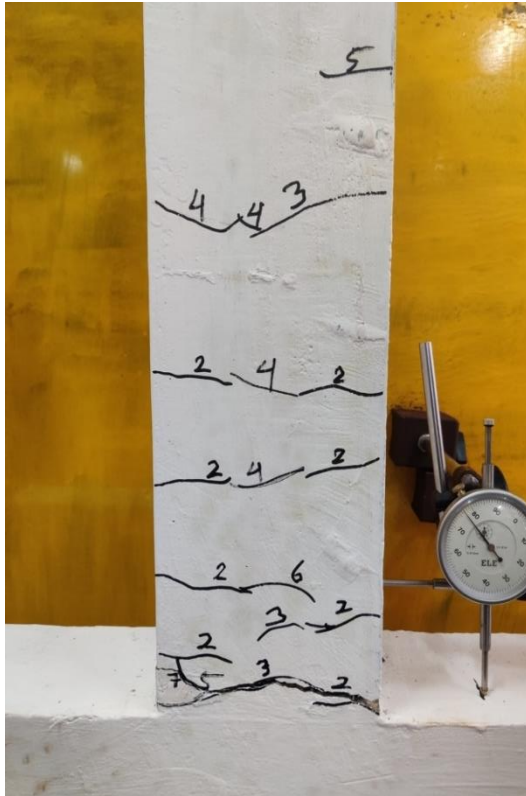
Figure 4.3: (a) Cracks in specimen 3-BS-B (b) Failure zone of specimen 3-BS-B
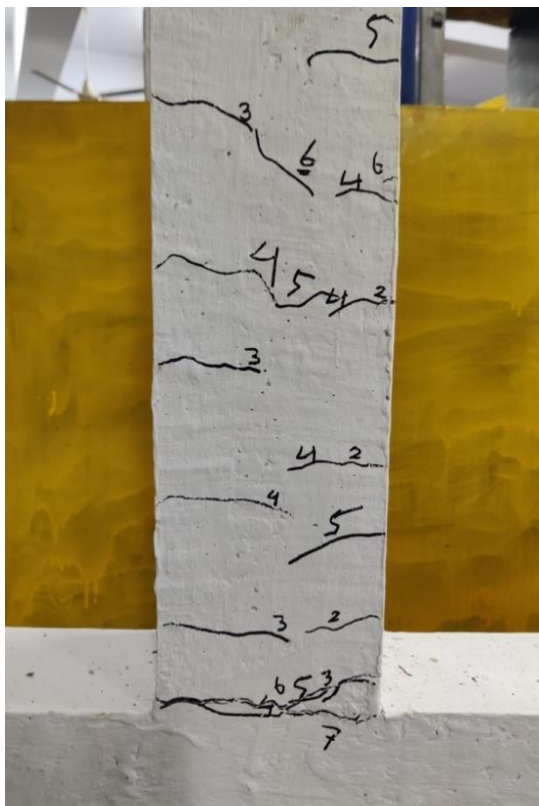
Figure 4.4: (a) Cracks in specimen 4-BS-S (b) Failure zone of specimen 4-BS-S

Figure 4.5: (a) Cracks in specimen 5-BSS-B (b) Failure zone of specimen 5-BSS-B
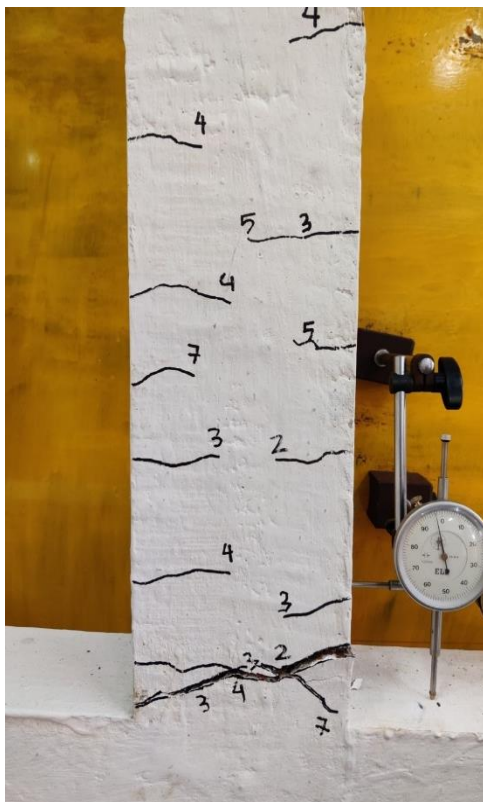
Figure 4.6: (a) Cracks in specimen 6-BSS-SS (b) Failure zone of specimen 6-BSS-SS
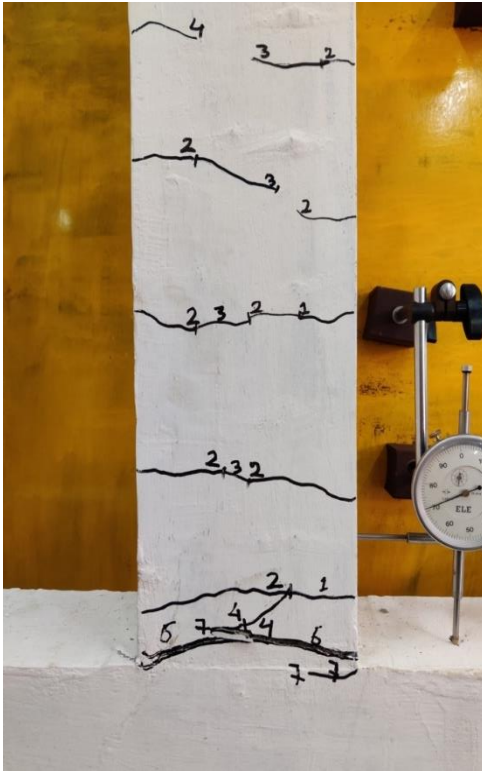
Figure 4.7: (a) Cracks in specimen 7-RCS-RC (b) Failure zone of specimen 7-RCS-RC
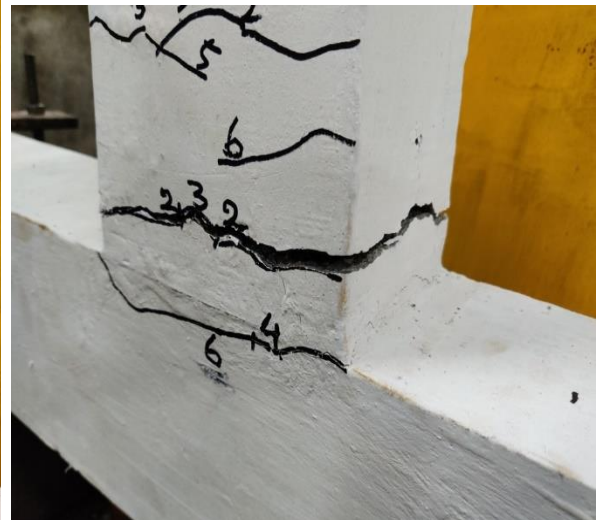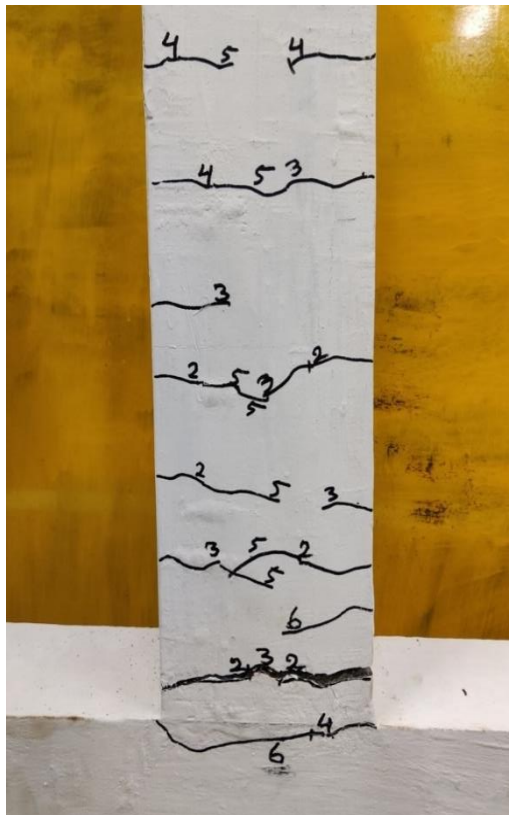
Figure 4.8: (a) Cracks in specimen 8-RCS-S (b) Failure zone of specimen 8-RCS-S

4.3   Load - Displacement Response

The applied load and corresponding displacements of the specimens in each cycle are plotted as shown in Figures 4.9 to 4.16. For a better understanding, the curves in each cycle have been colored differently. The load-displacement failure envelope is plotted by joining the peaks of the hysteresis curve as shown in Figures 4.17 to 4.24. The peak load versus displacement data for the specimens are provided in appendix C.
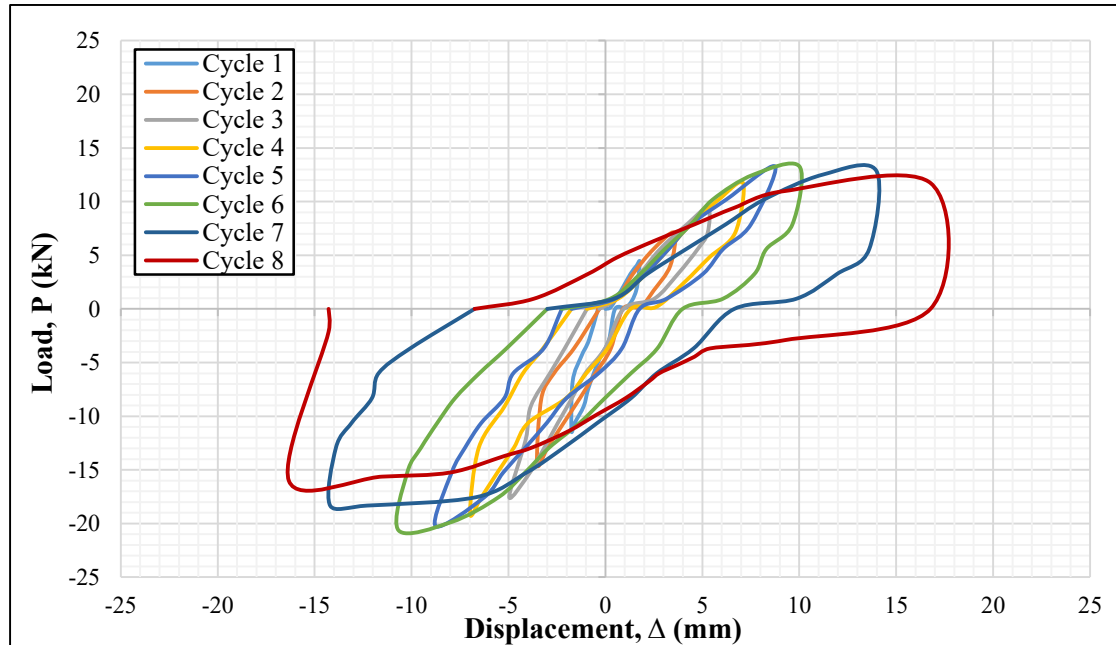
Figure 4.9: Load - displacement response of specimen 1-SS-C1
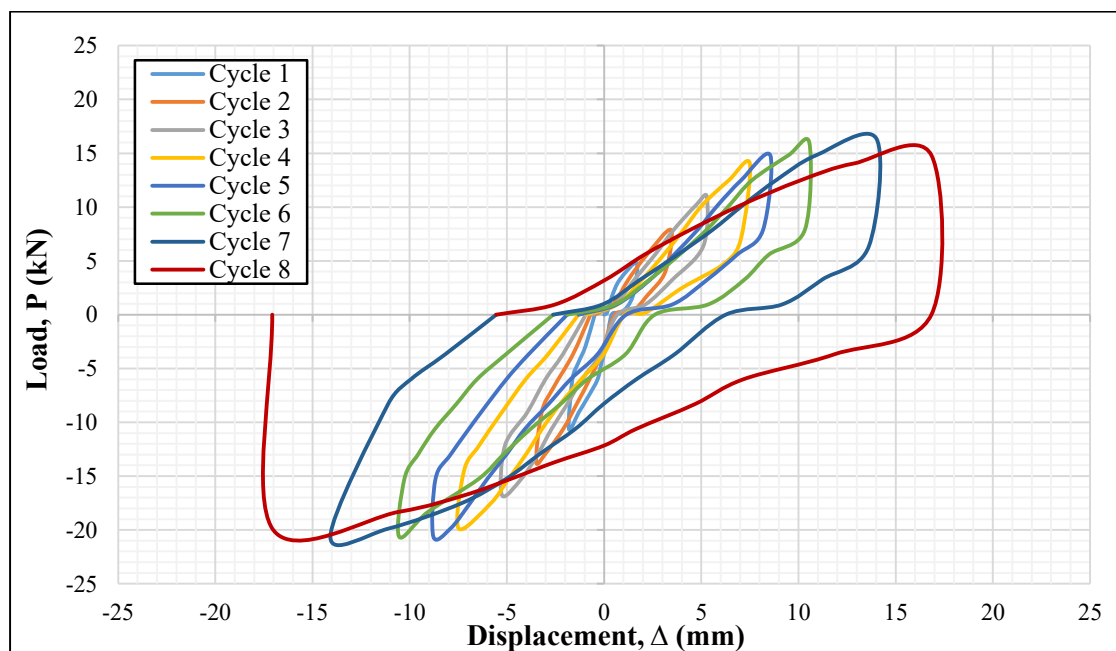
Figure 4.10: Load - displacement response of specimen 2-BB-C2

75
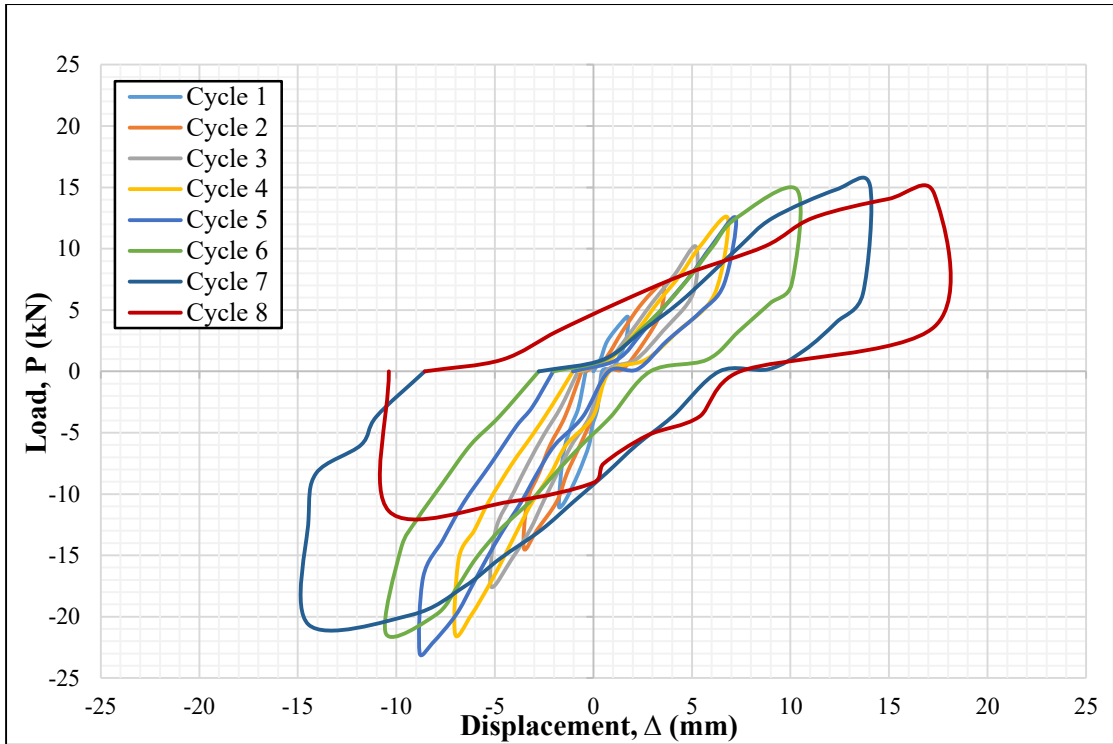
Figure 4.11: Load - displacement response of specimen 3-BS-B
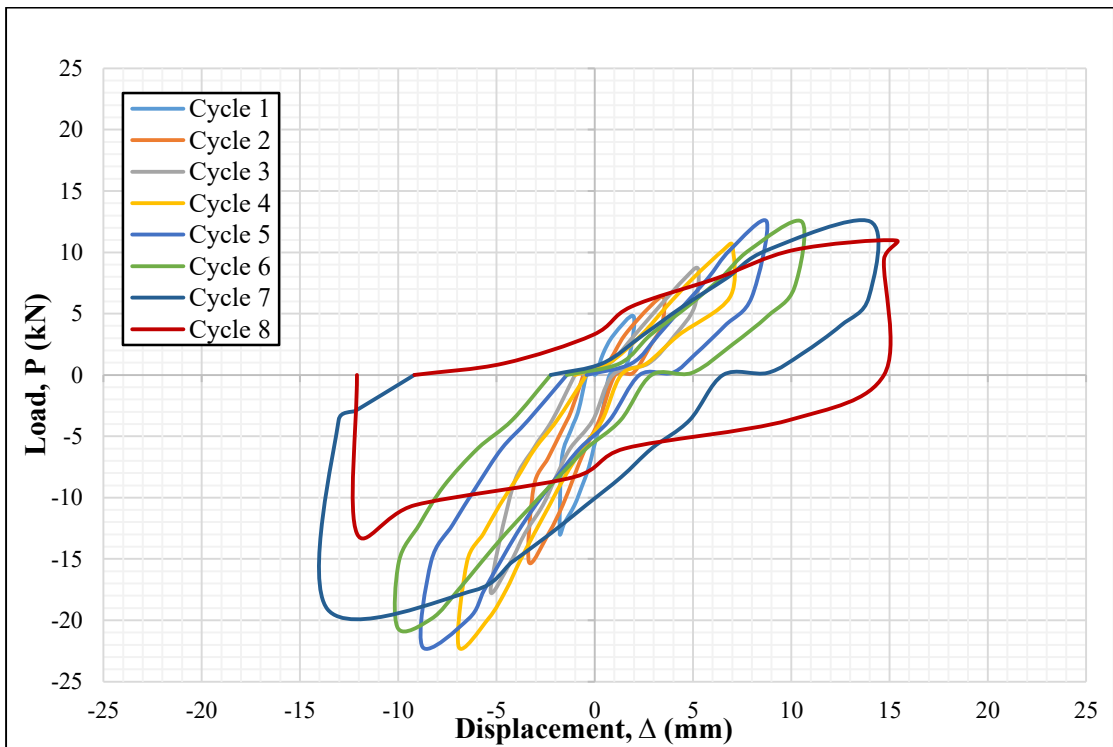
Figure 4.12: Load - displacement response of specimen 4-BS-S

76
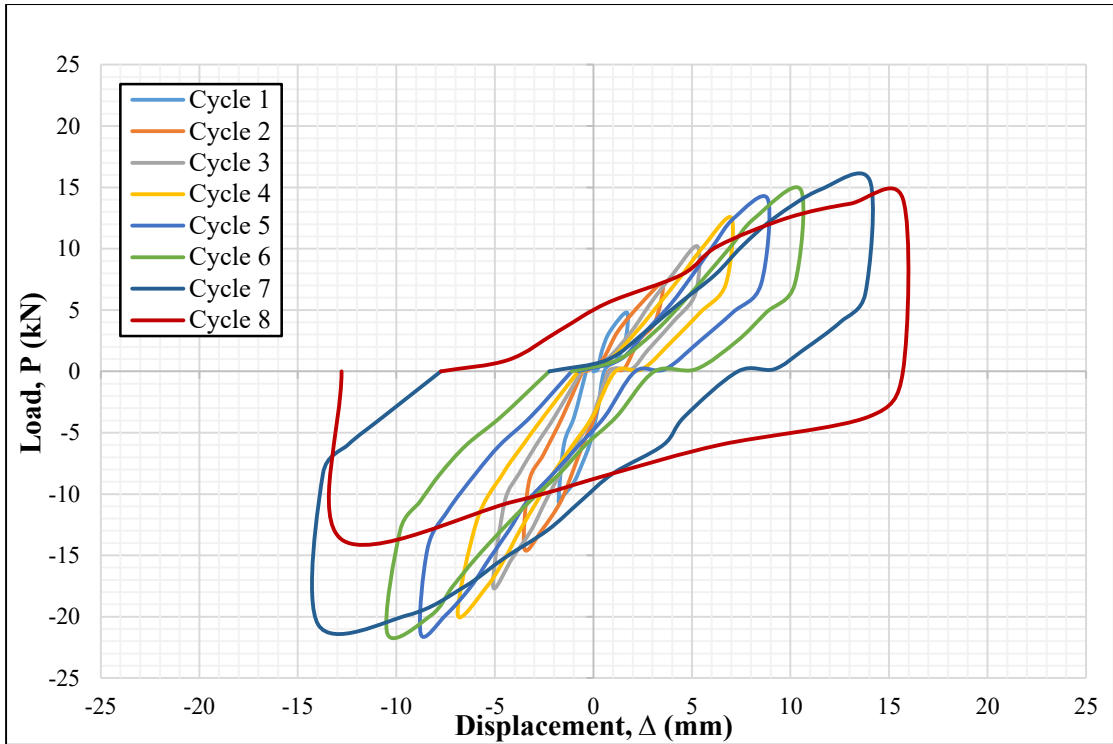
Figure 4.13: Load - displacement response of specimen 5-BSS-B
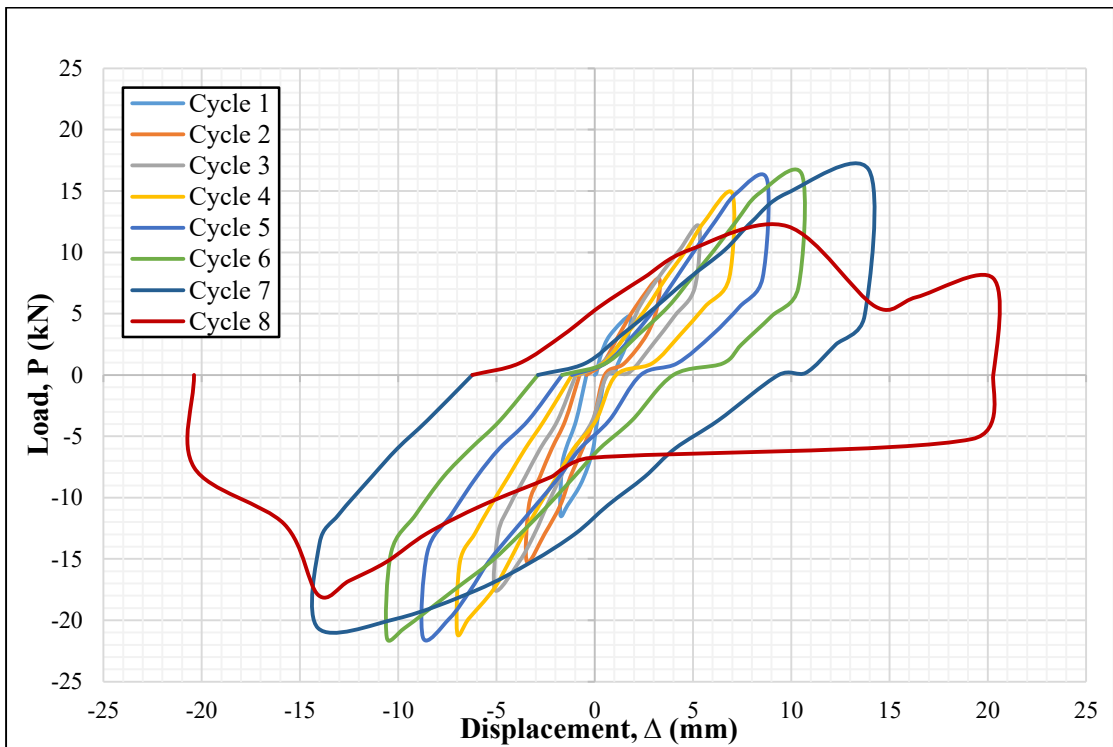
Figure 4.14: Load - displacement response of specimen 6-BSS-SS
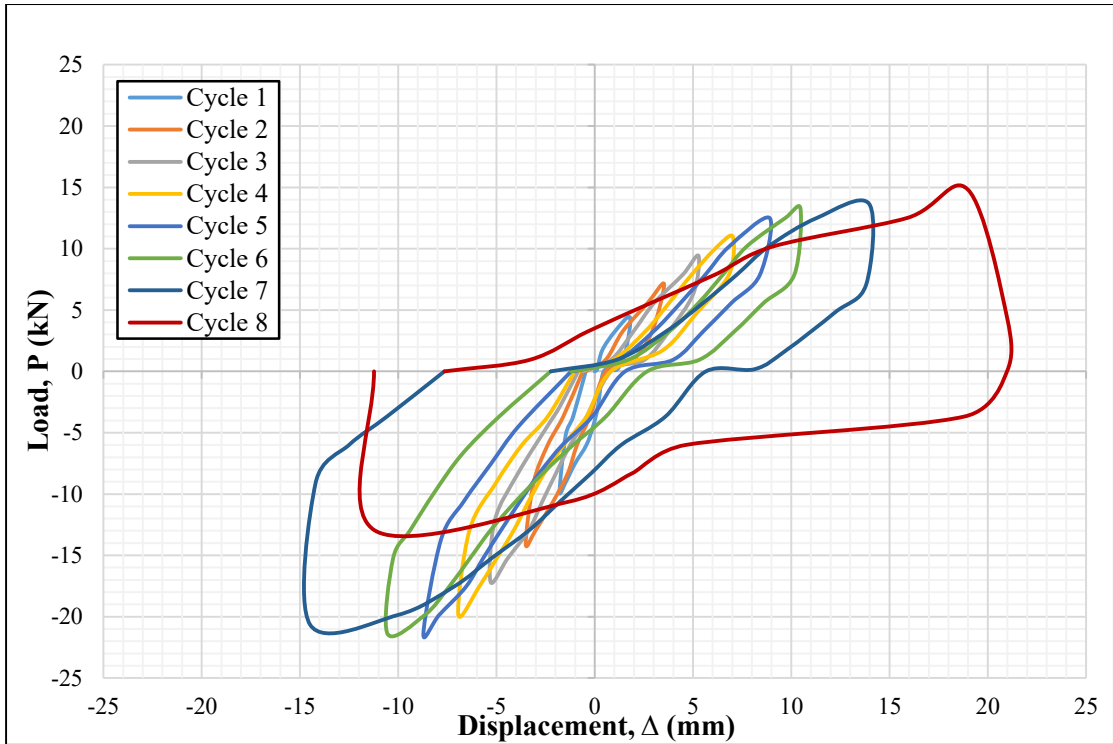
Figure 4.15: Load - displacement response of specimen 7-RCS-RC
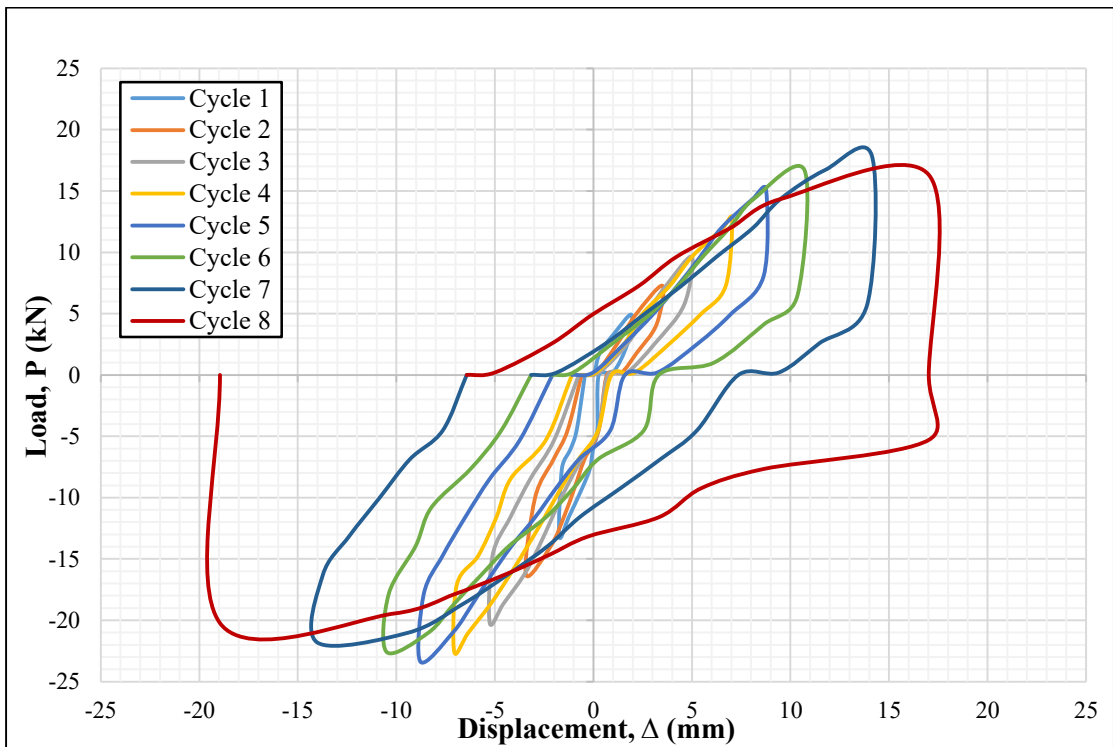
Figure 4.16: Load - displacement response of specimen 8-RCS-S
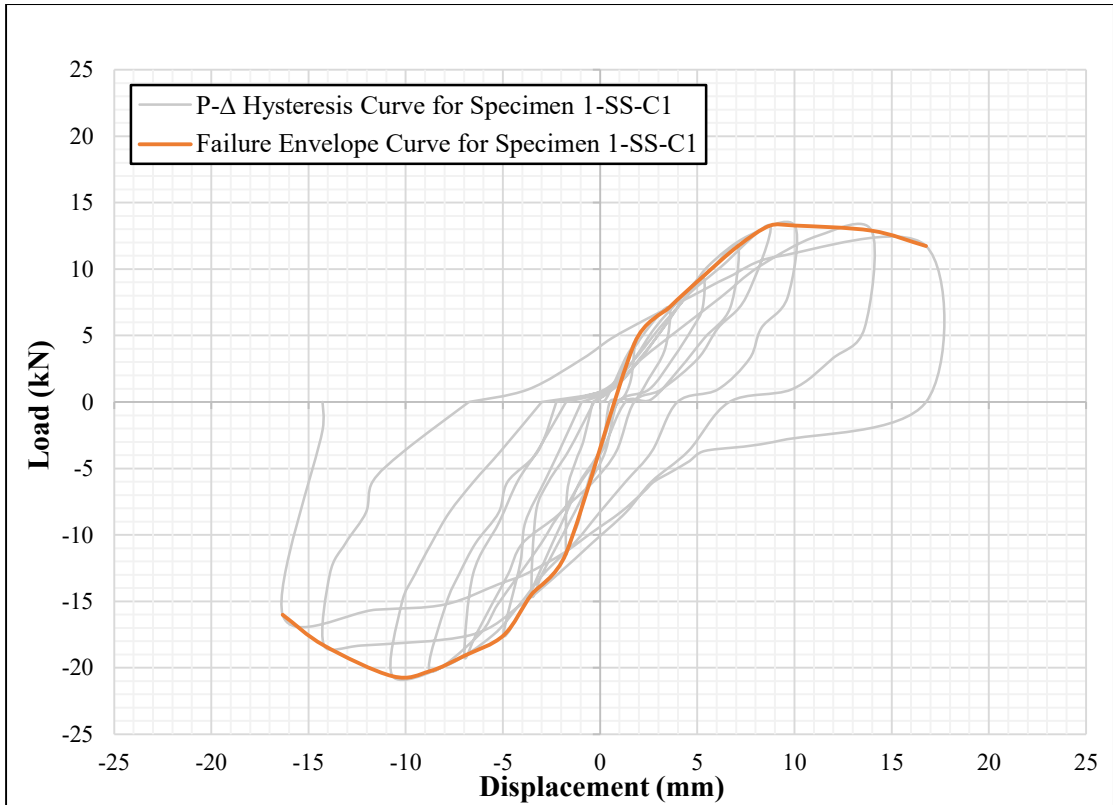
Figure 4.17: Load - displacement failure envelope of specimen 1-SS-C1
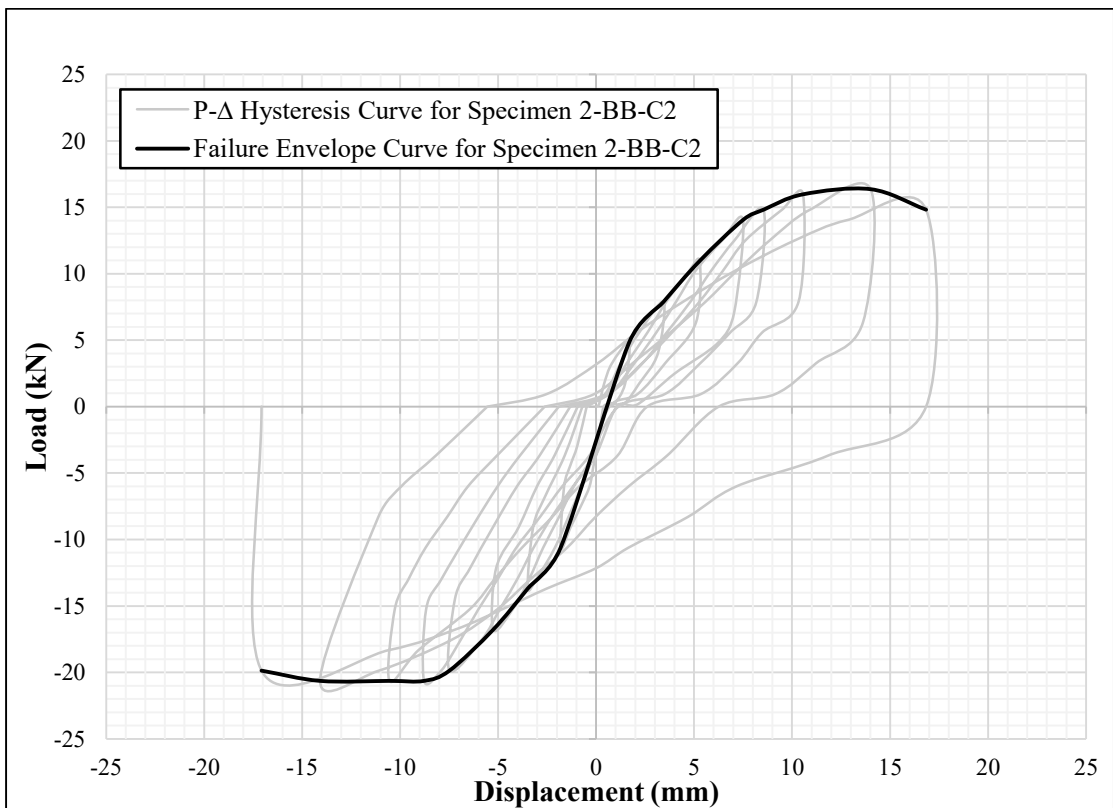
Figure 4.18: Load - displacement failure envelope of specimen 2-BB-C2
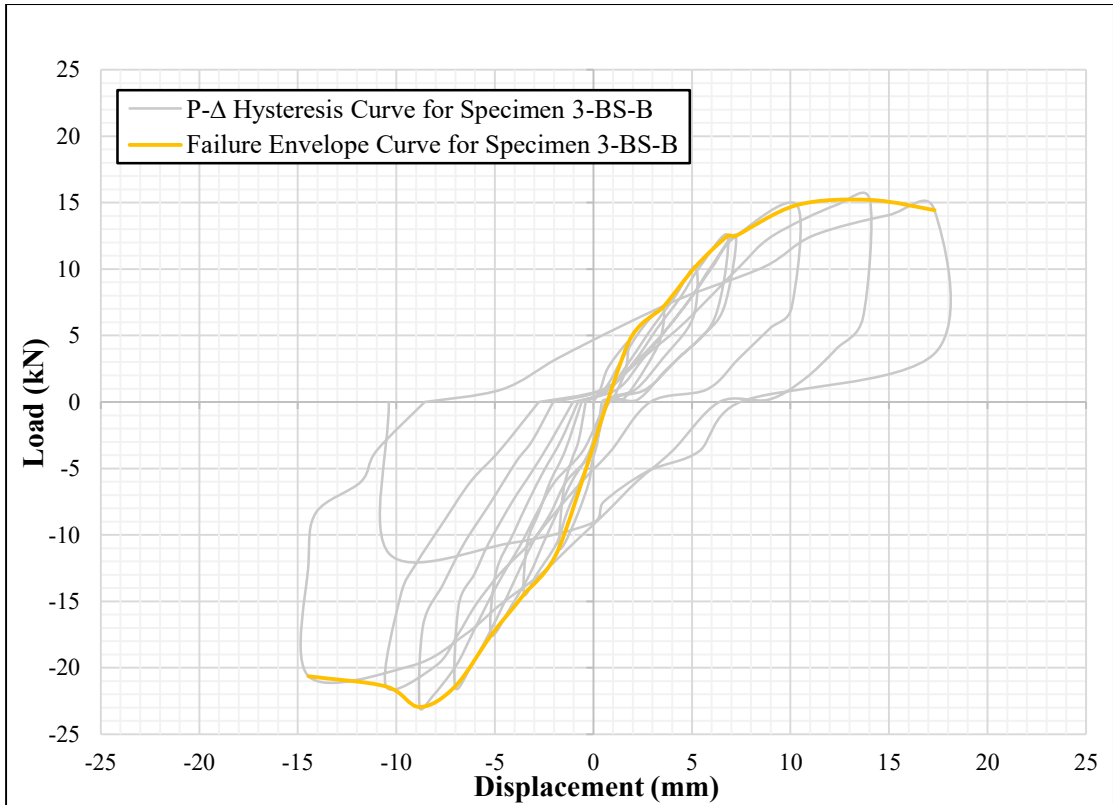
Figure 4.19: Load - displacement failure envelope of specimen 3-BS-B
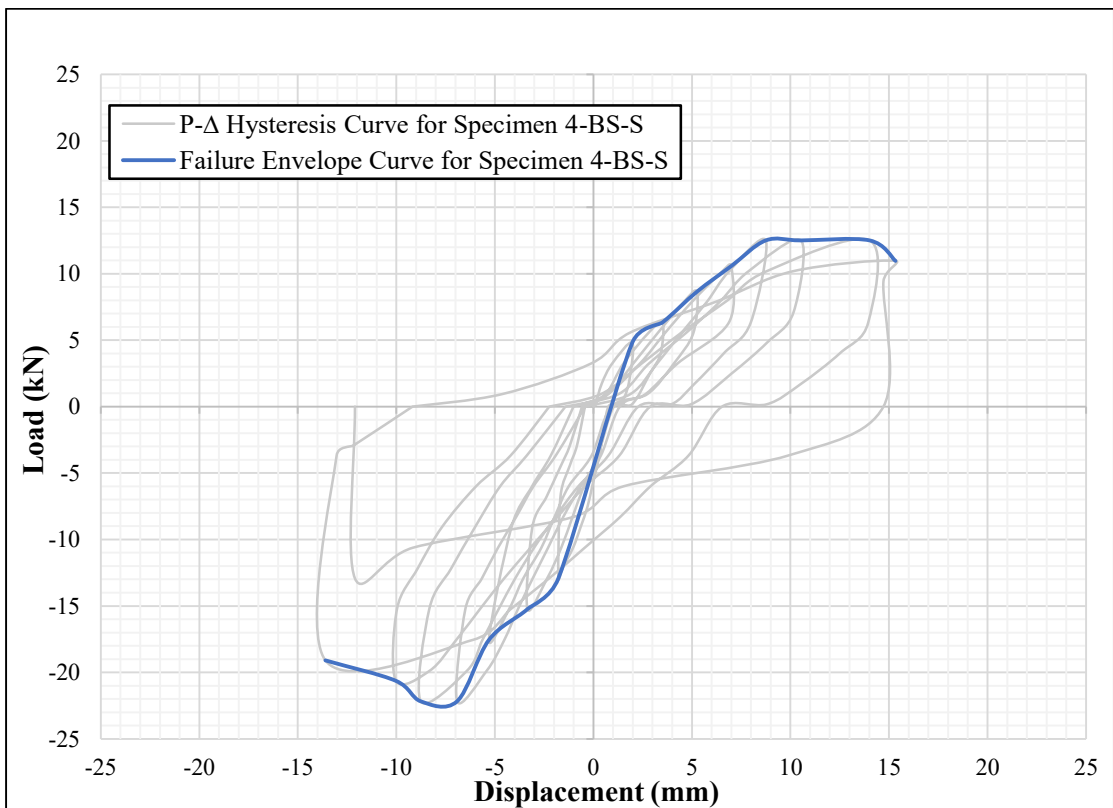
Figure 4.20: Load - displacement failure envelope of specimen 4-BS-S
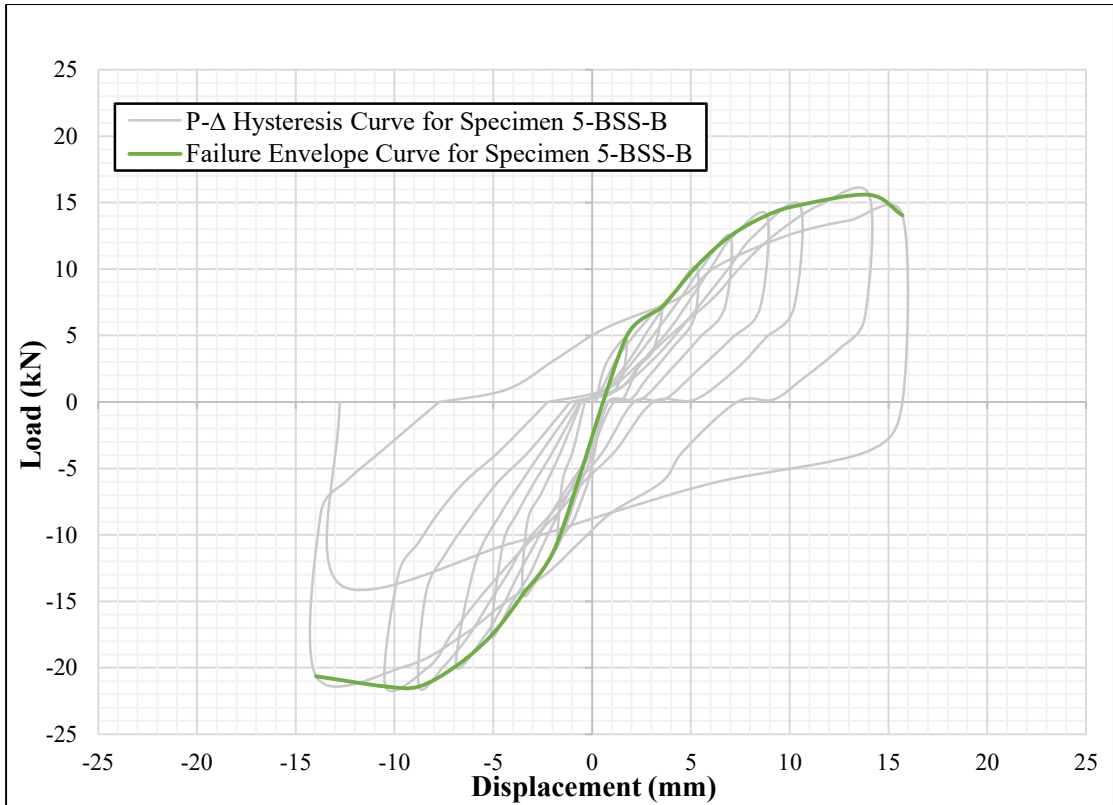
Figure 4.21: Load - displacement failure envelope of specimen 5-BSS-B
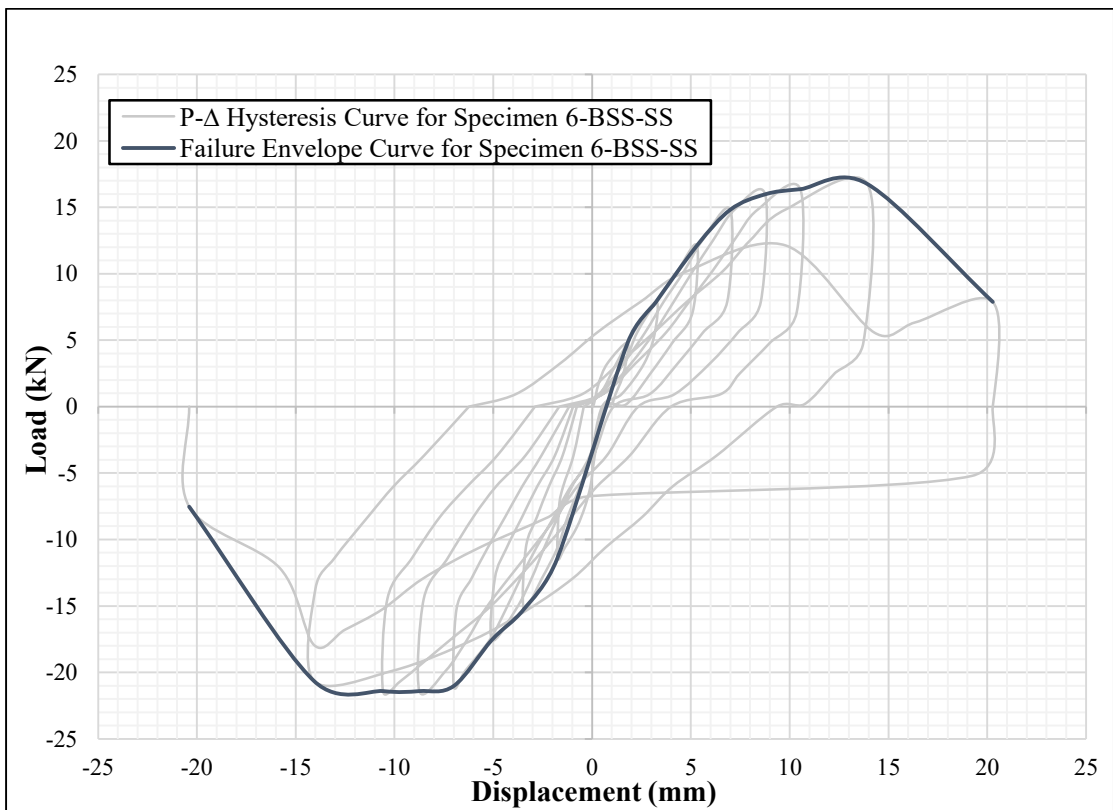
Figure 4.22: Load - displacement failure envelope of specimen 6-BSS-SS

81
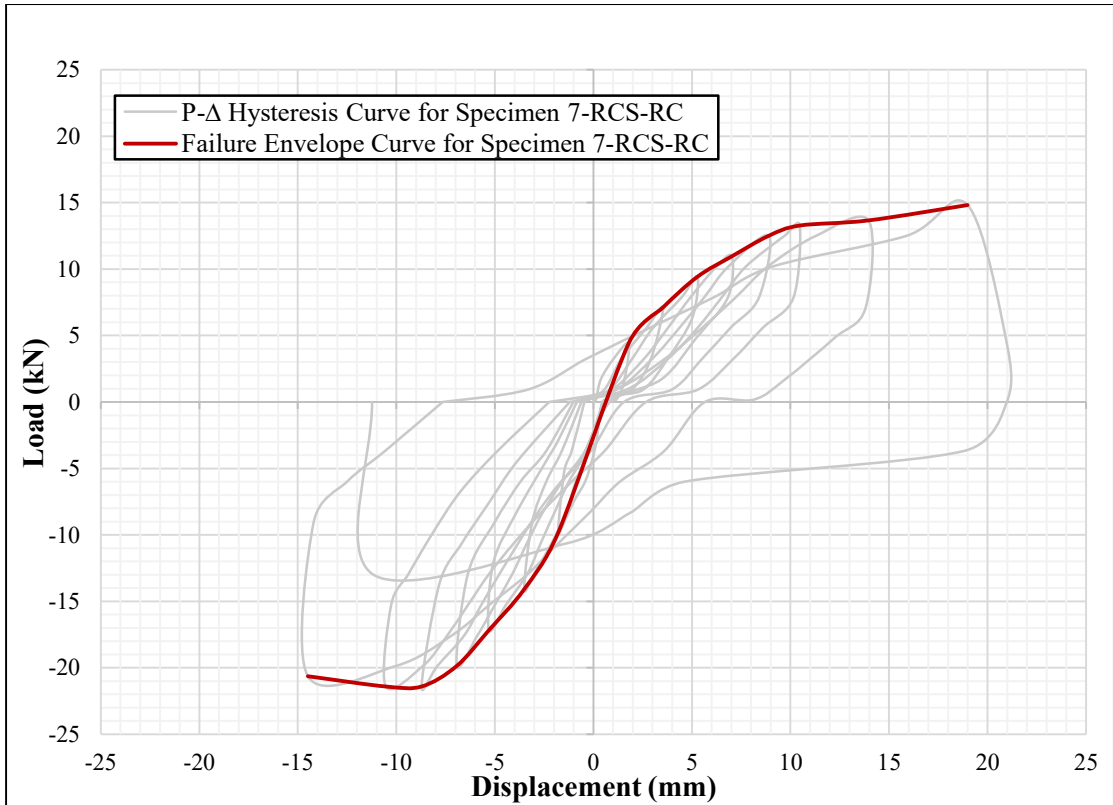
Figure 4.23: Load - displacement failure envelope of specimen 7-RCS-RC
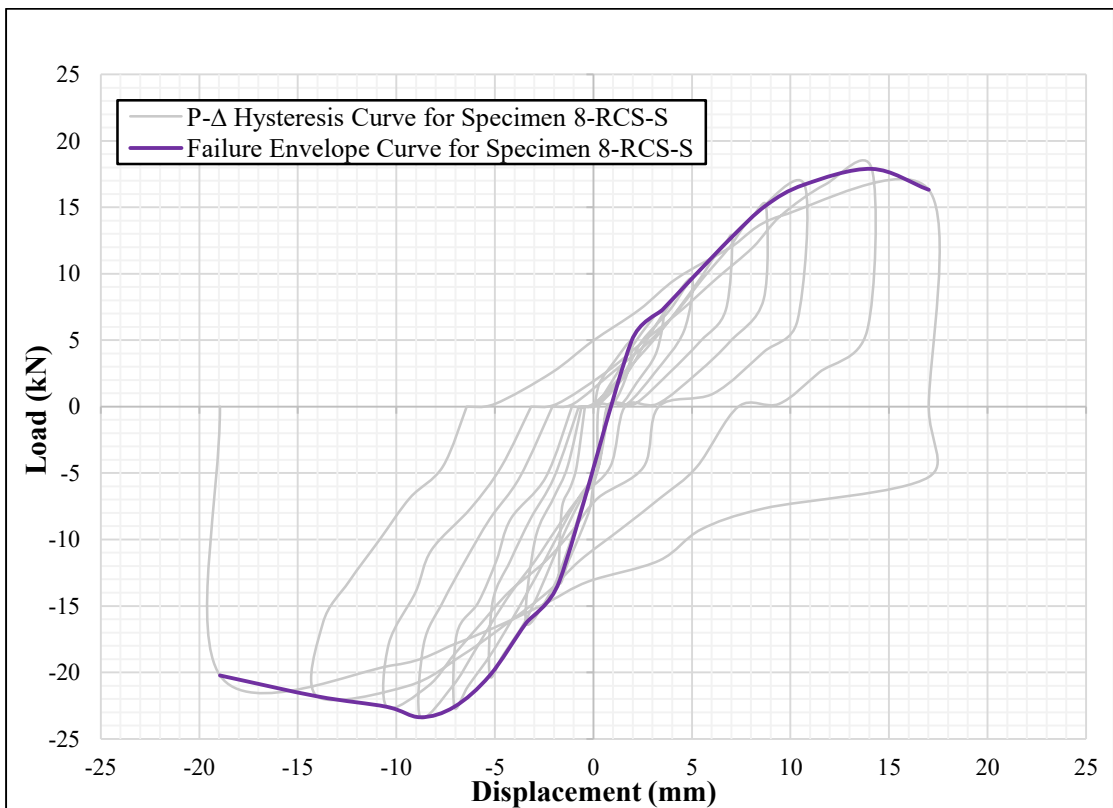
Figure 4.24: Load - displacement failure envelope of specimen 8-RCS-S

4.4 Moment - Rotation Response

The applied moment and corresponding beam-joint rotations of the specimens in each cycle are plotted as shown in Figures 4.25 to 4.32. For a better understanding, the curves in each cycle have been colored differently. The moment-rotation failure envelope is plotted by joining the peaks of the hysteresis curve as shown in Figures 4.33 to 4.40. The peak moment versus rotation data for the specimens are provided in appendix D.
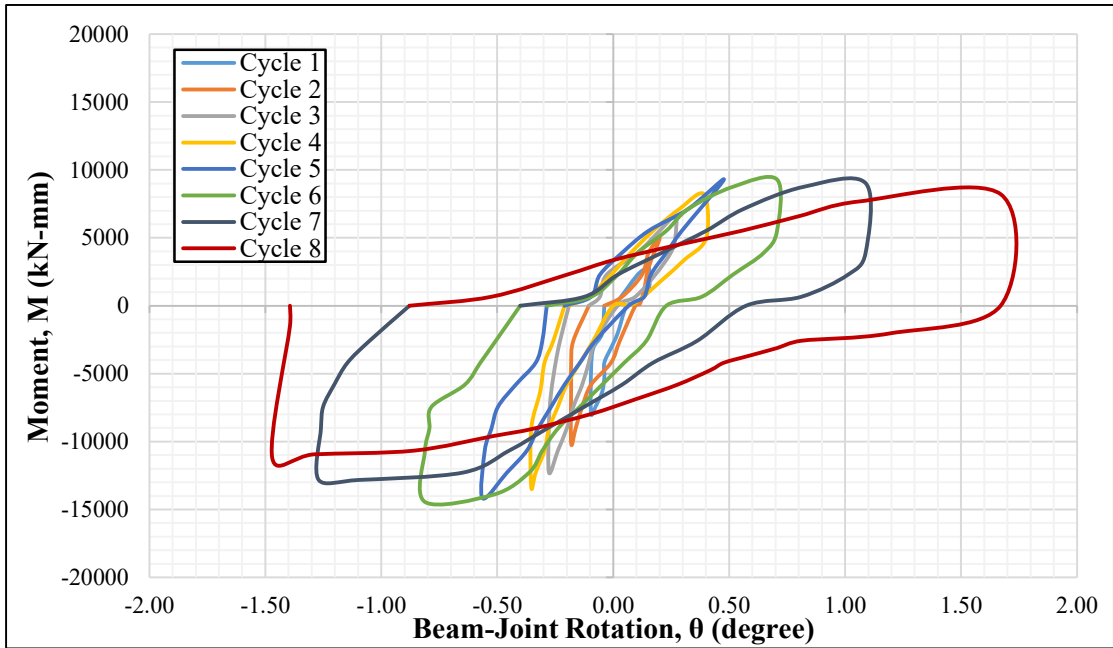
Figure 4.25: Moment - rotation response of specimen 1-SS-C1
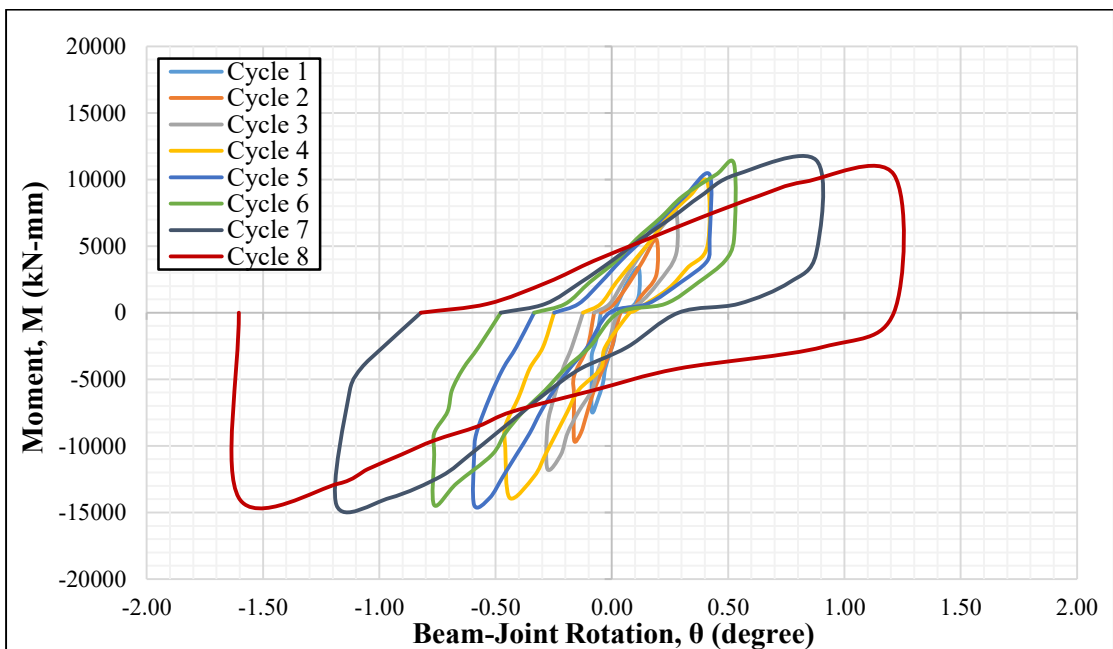
Figure 4.26: Moment - rotation response of specimen 2-BB-C2
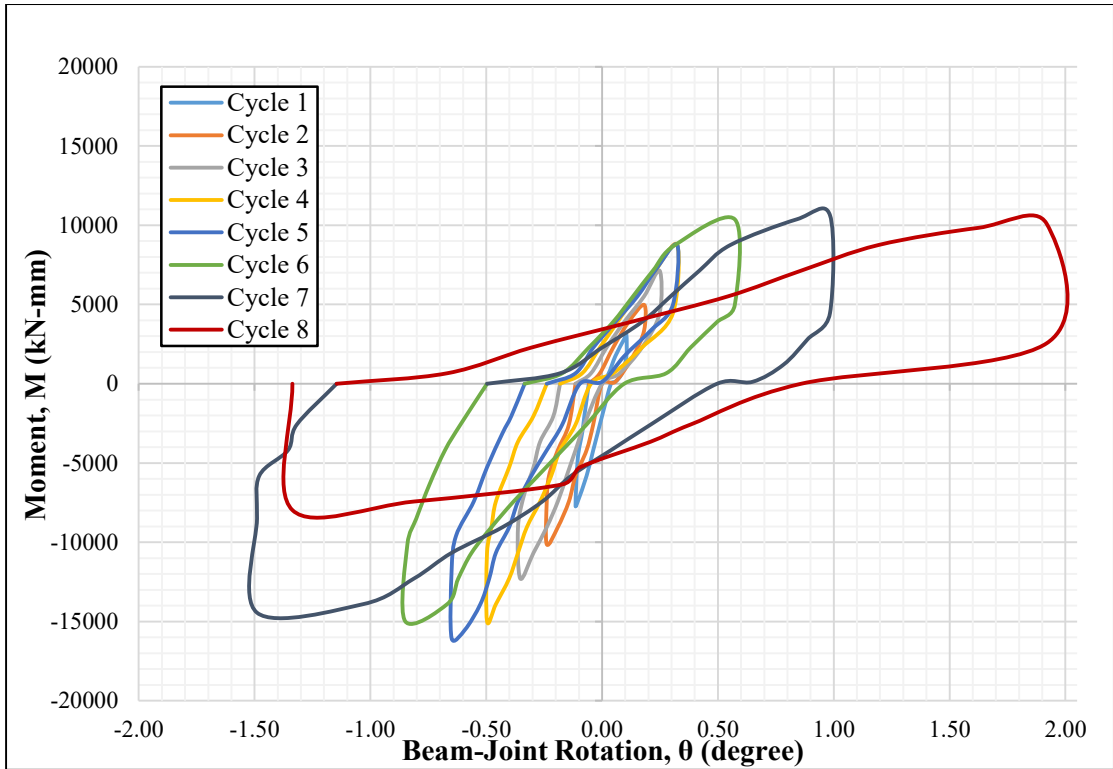
Figure 4.27: Moment - rotation response of specimen 3-BS-B
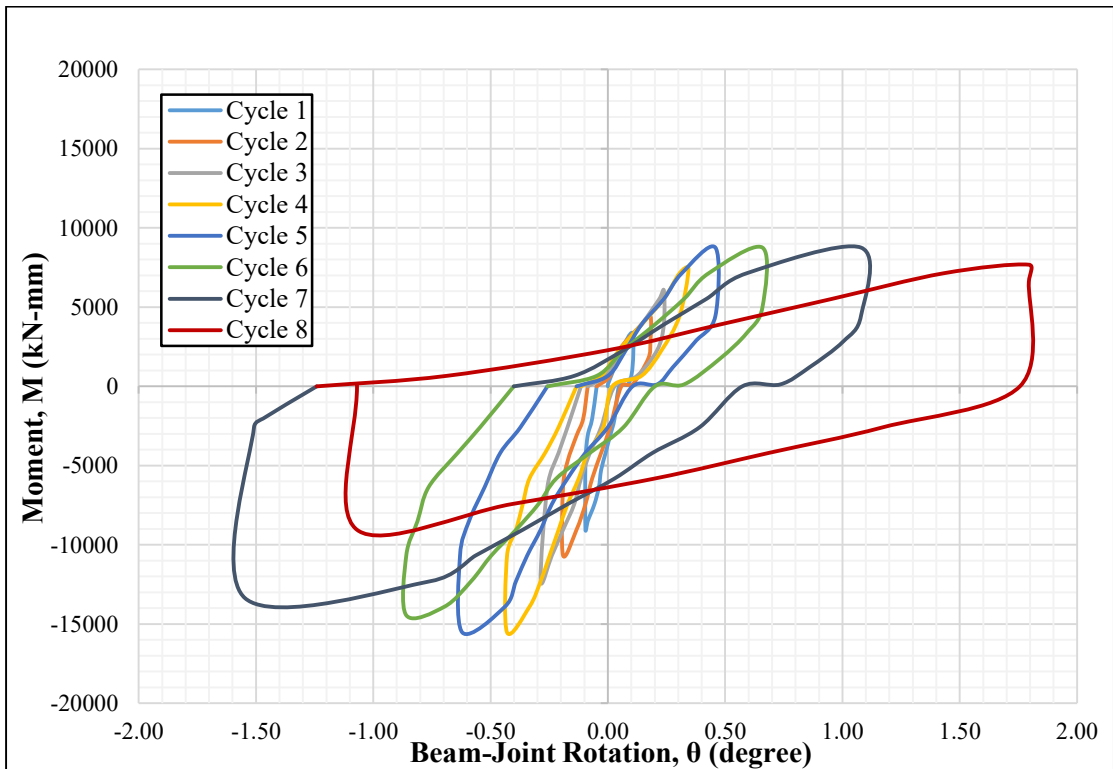
Figure 4.28: Moment - rotation response of specimen 4-BS-S
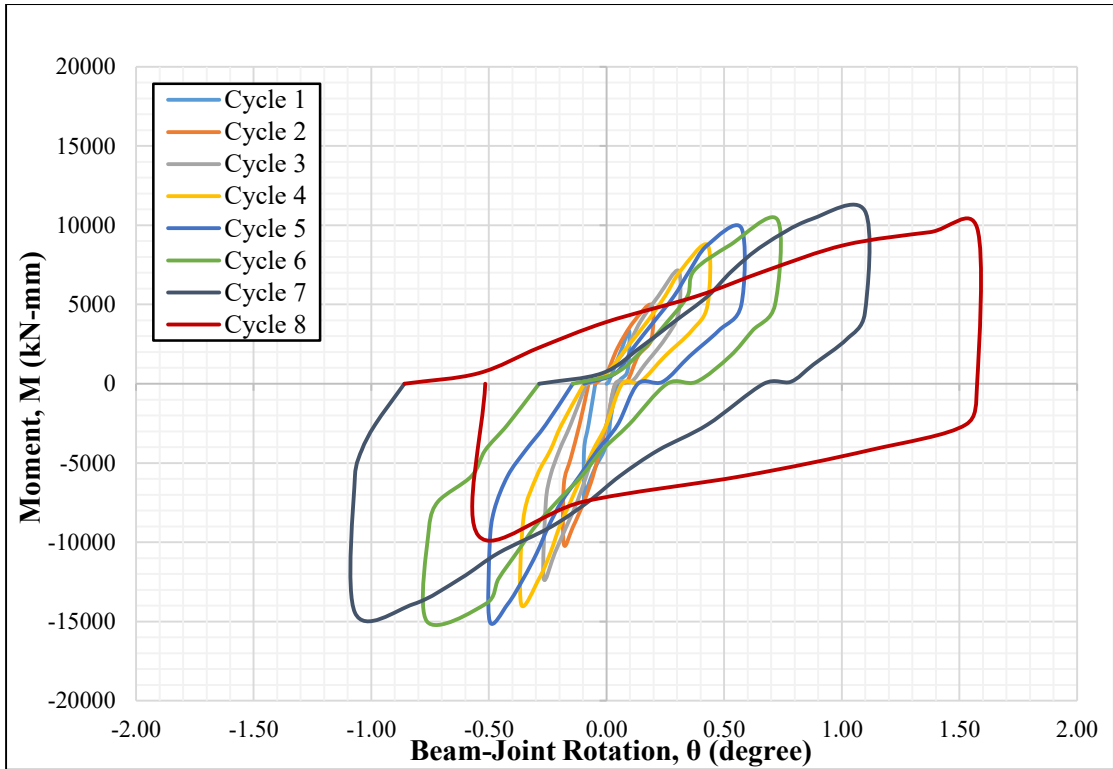
Figure 4.29: Moment - rotation response of specimen 5-BSS-B
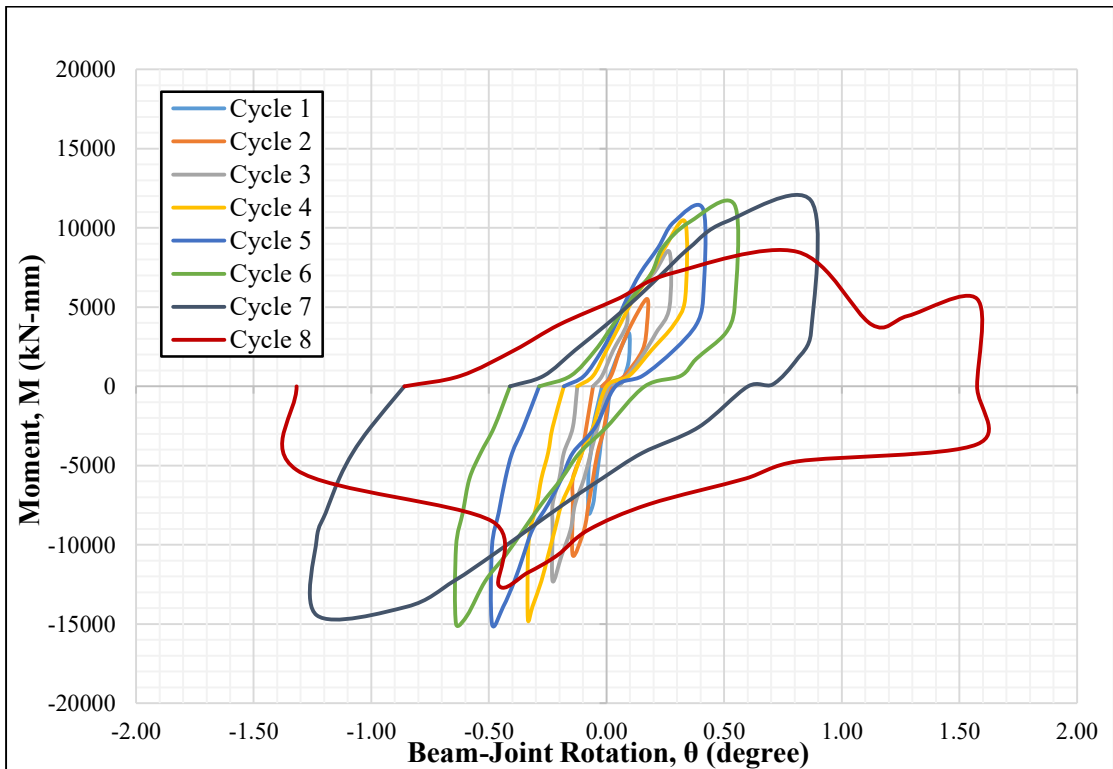
Figure 4.30: Moment - rotation response of specimen 6-BSS-SS
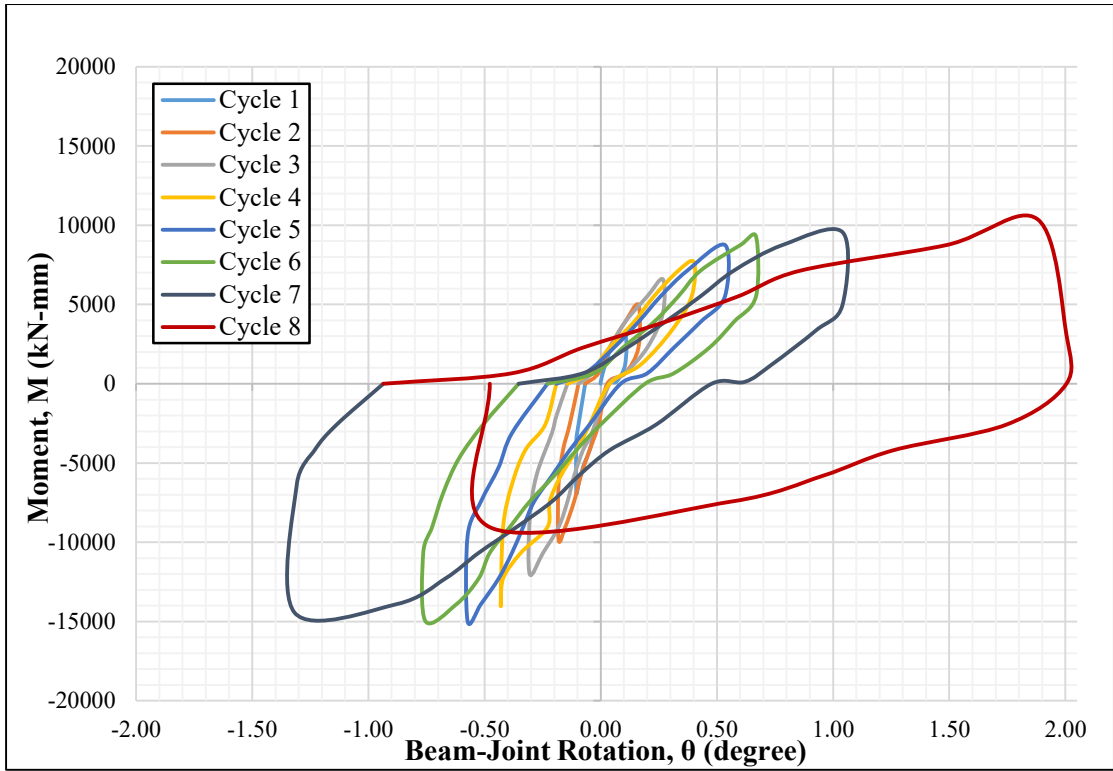
Figure 4.31: Moment - rotation response of specimen 7-RCS-RC
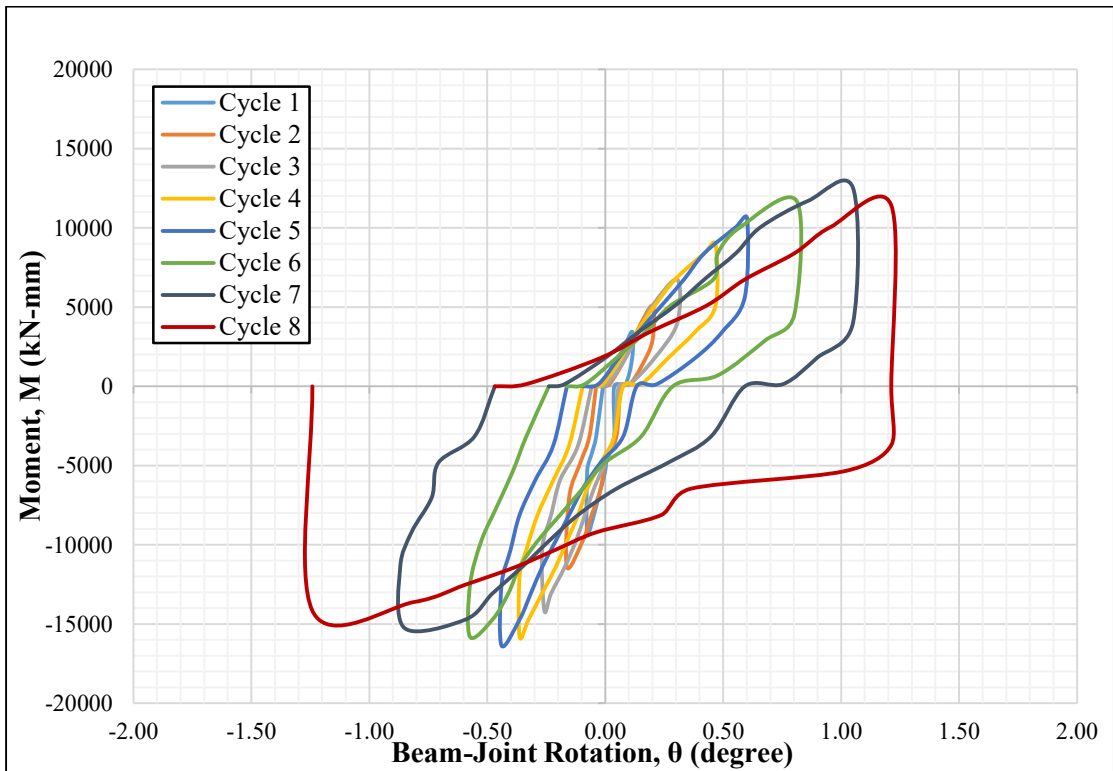
Figure 4.32: Moment - rotation response of specimen 8-RCS-S

86
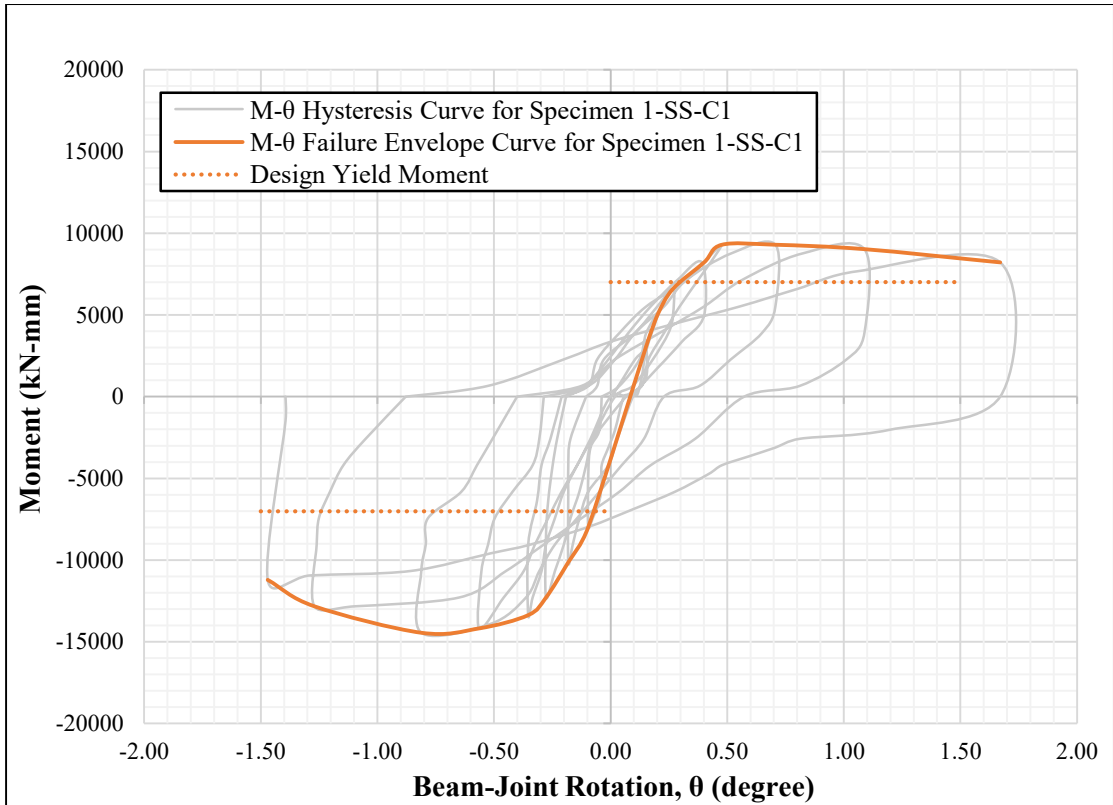
Figure 4.33: Moment - rotation failure envelope of specimen 1-SS-C1
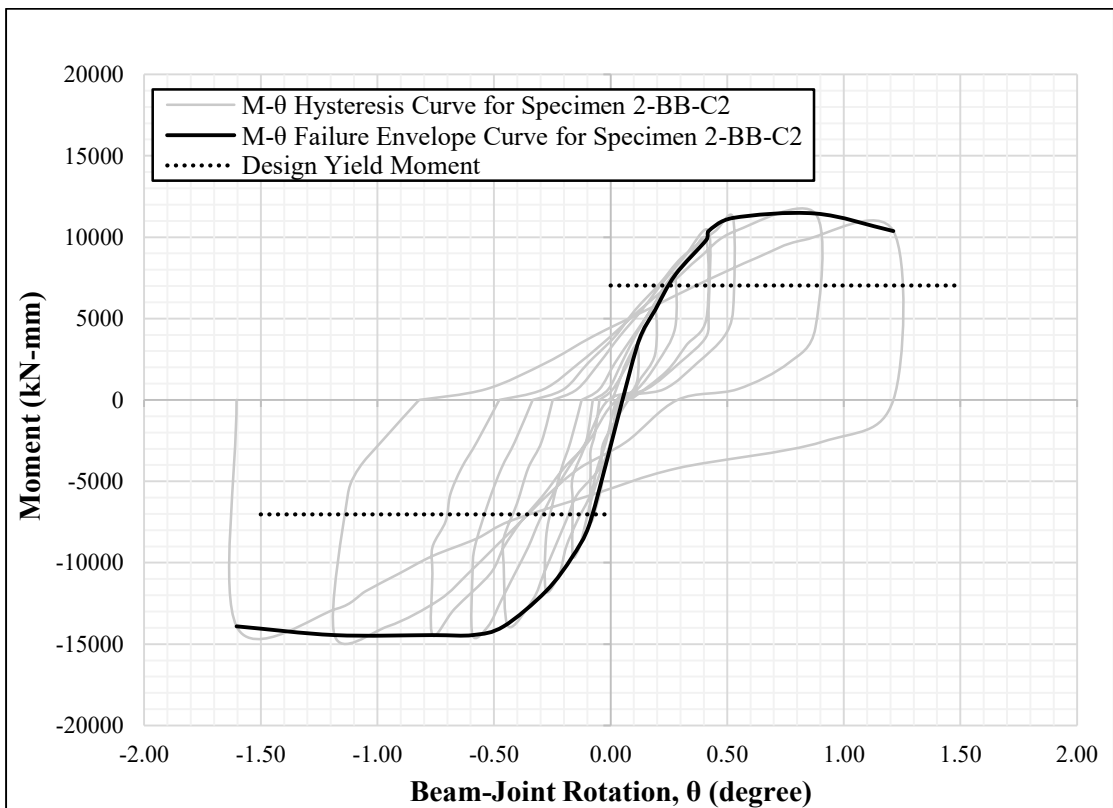
Figure 4.34: Moment - rotation failure envelope of specimen 2-BB-C2

87
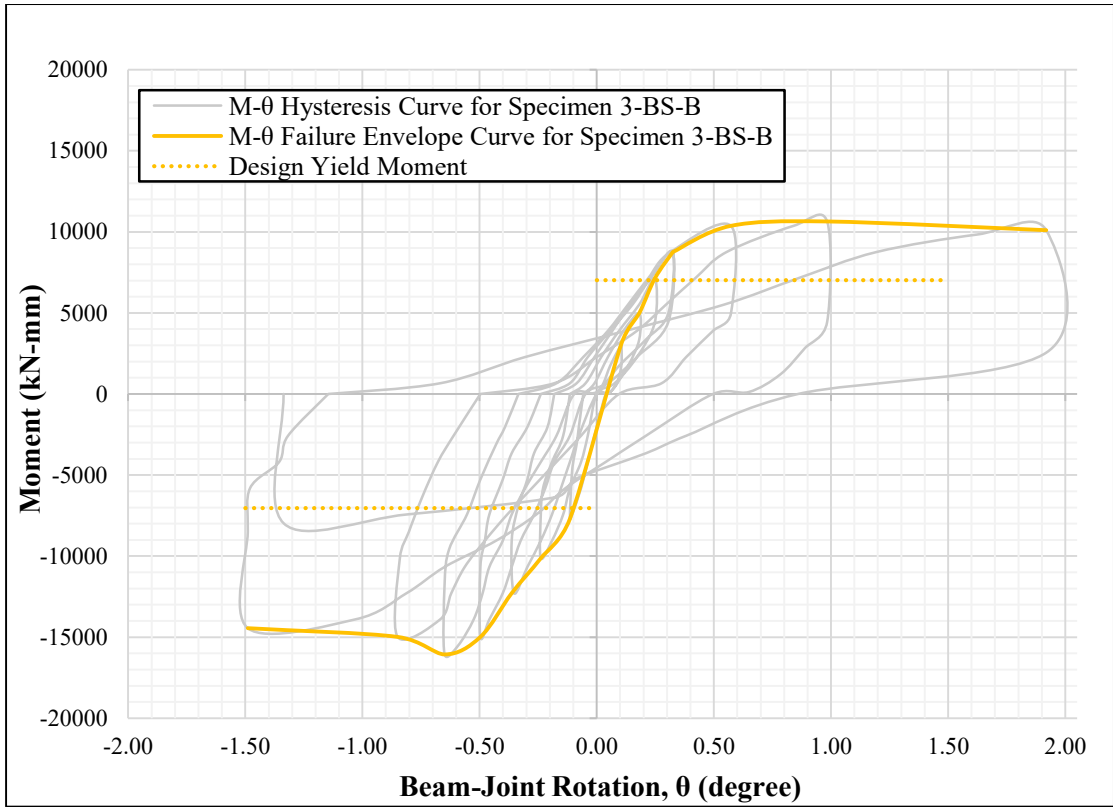
Figure 4.35: Moment - rotation failure envelope of specimen 3-BS-B
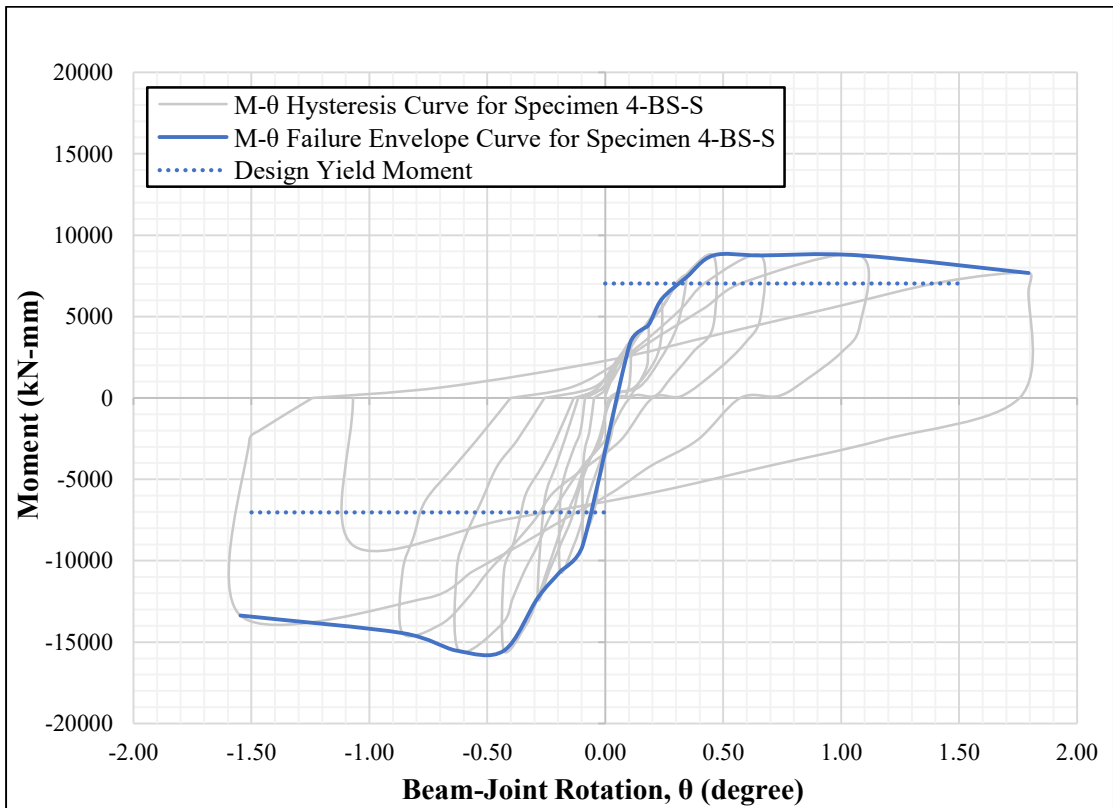
Figure 4.36: Moment - rotation failure envelope of specimen 4-BS-S
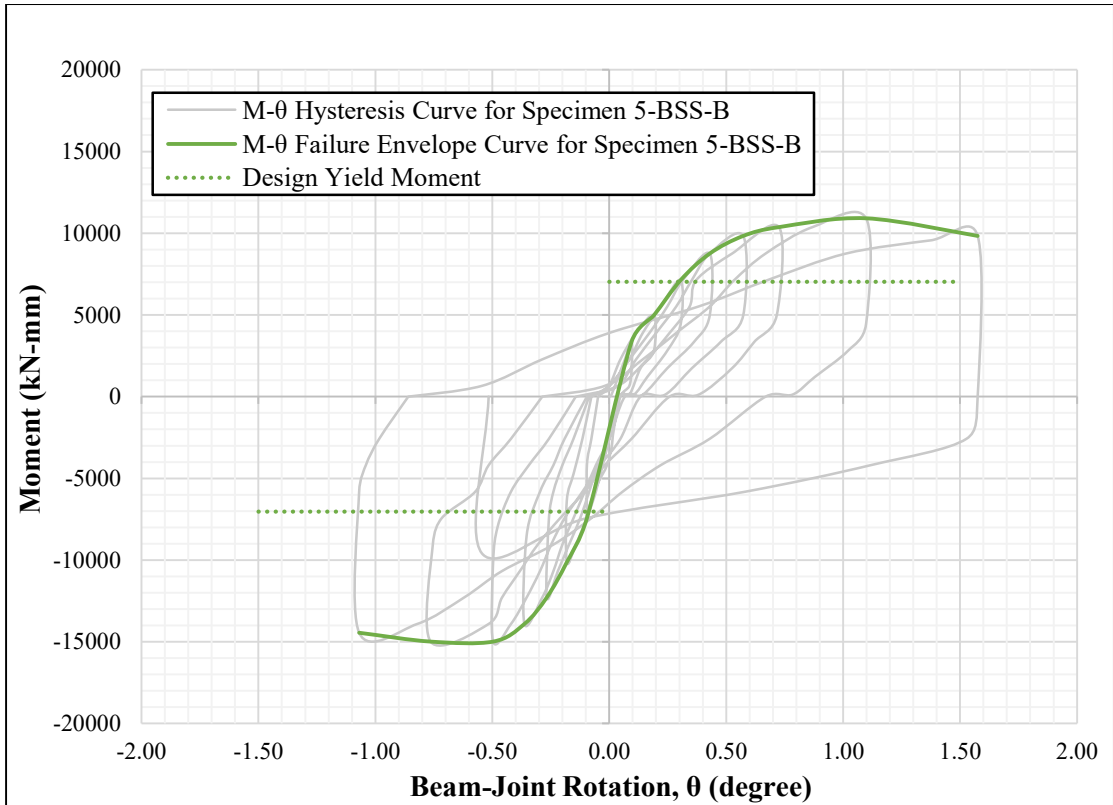
Figure 4.37: Moment - rotation failure envelope of specimen 5-BSS-B
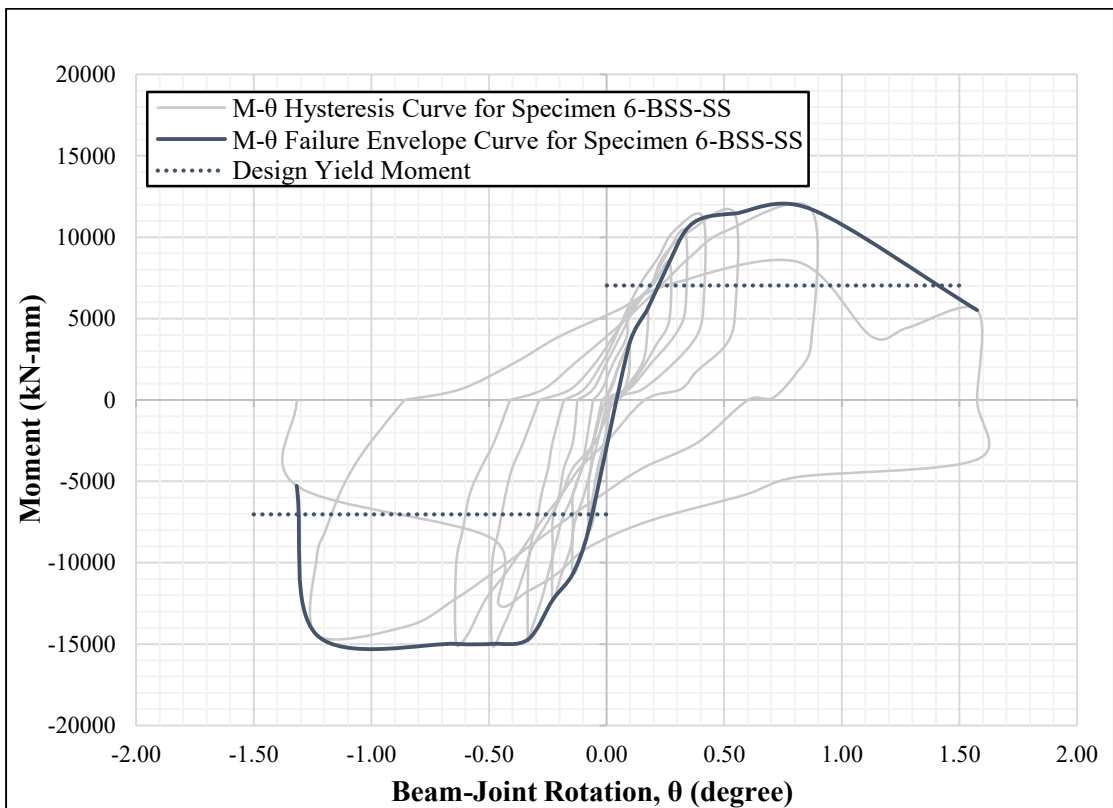
Figure 4.38: Moment - rotation failure envelope of specimen 6-BSS-SS
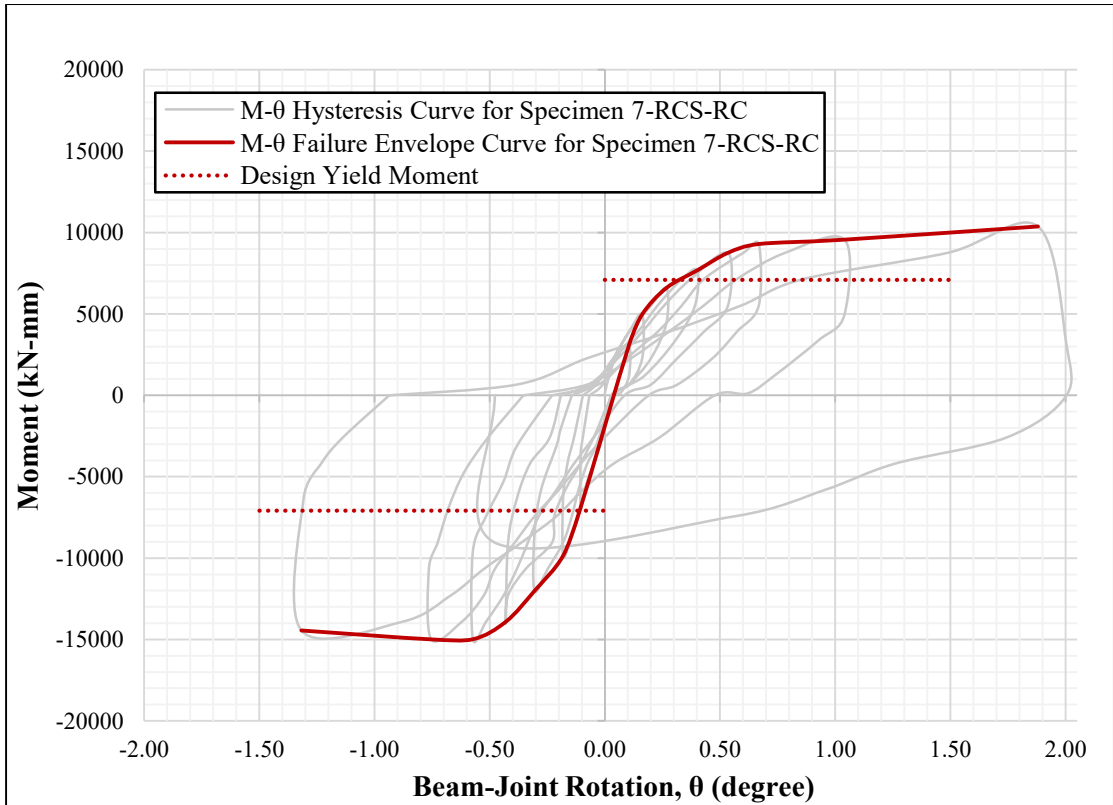
Figure 4.39: Moment - rotation failure envelope of specimen 7-RCS-RC
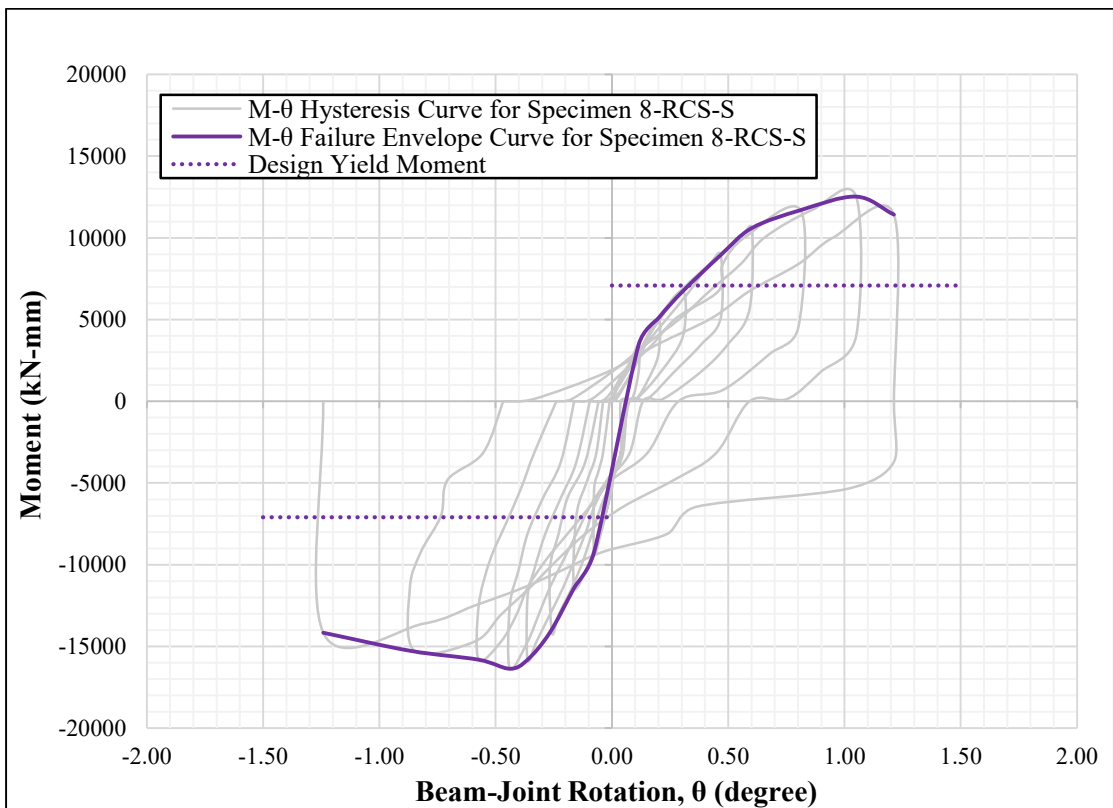
Figure 4.40: Moment - rotation failure envelope of specimen 8-RCS-S

90

4.5   Stiffness Degradation

The stiffness of the specimens are shown in Table 2.1. The stiffness degradation occurred in an exponential decay pattern as shown in Figures 4.41 to 4.48.

Table 4.1: Stiffness of the specimens

Specimen Designation	Stiffness in First Cycle (kN/mm)	Stiffness in Eighth Cycle (kN/mm)
1-SS-C1	4.49	0.86
2-BB-C2	4.42	1.02
3-BS-B	4.39	0.93
4-BS-S	4.73	0.87
5-BSS-B	4.44	0.97
6-BSS-SS	4.56	1.26
7-RCS-RC	3.98	0.92
8-RCS-S	4.94	1.02
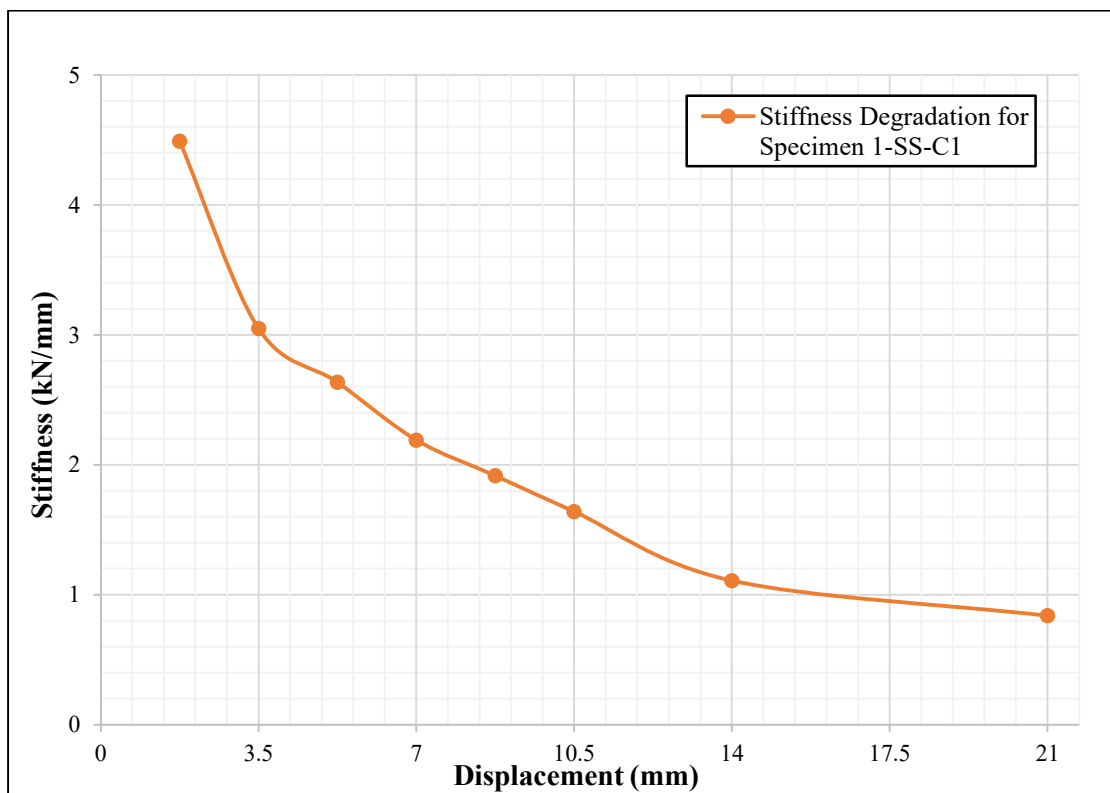
Figure 4.41: Stiffness degradation curve of specimen 1-SS-C1
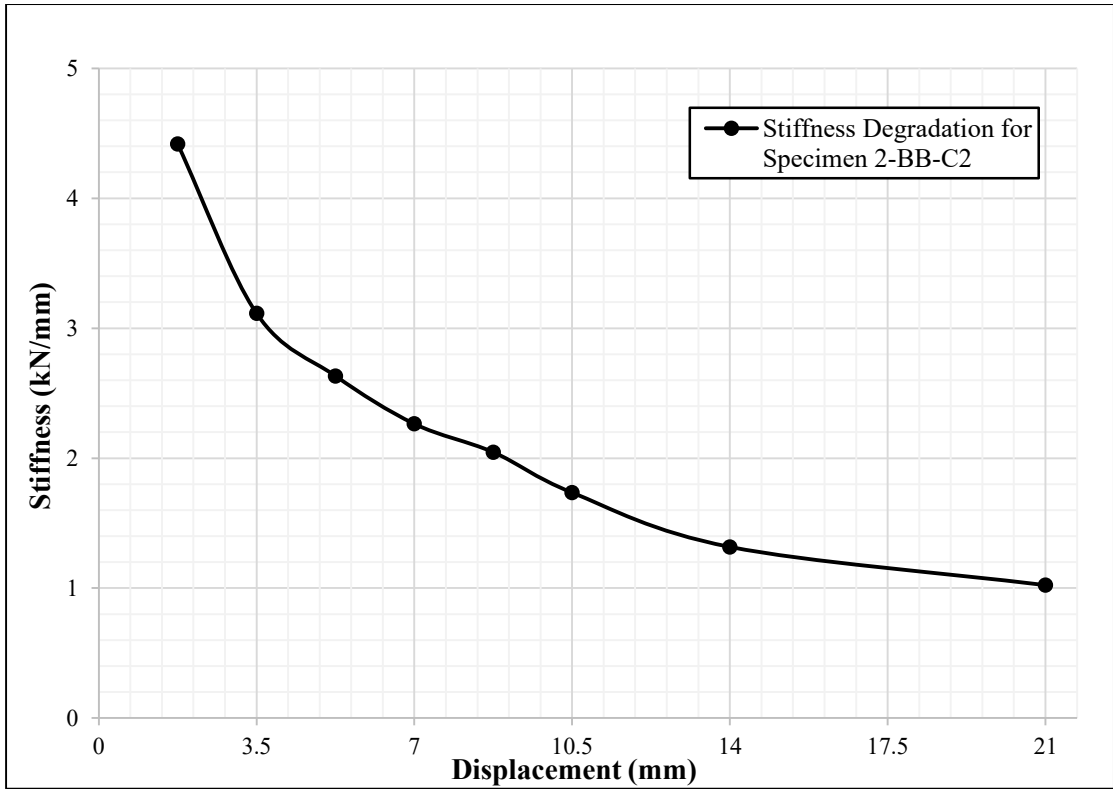
Figure 4.42: Stiffness degradation curve of specimen 2-BB-C2
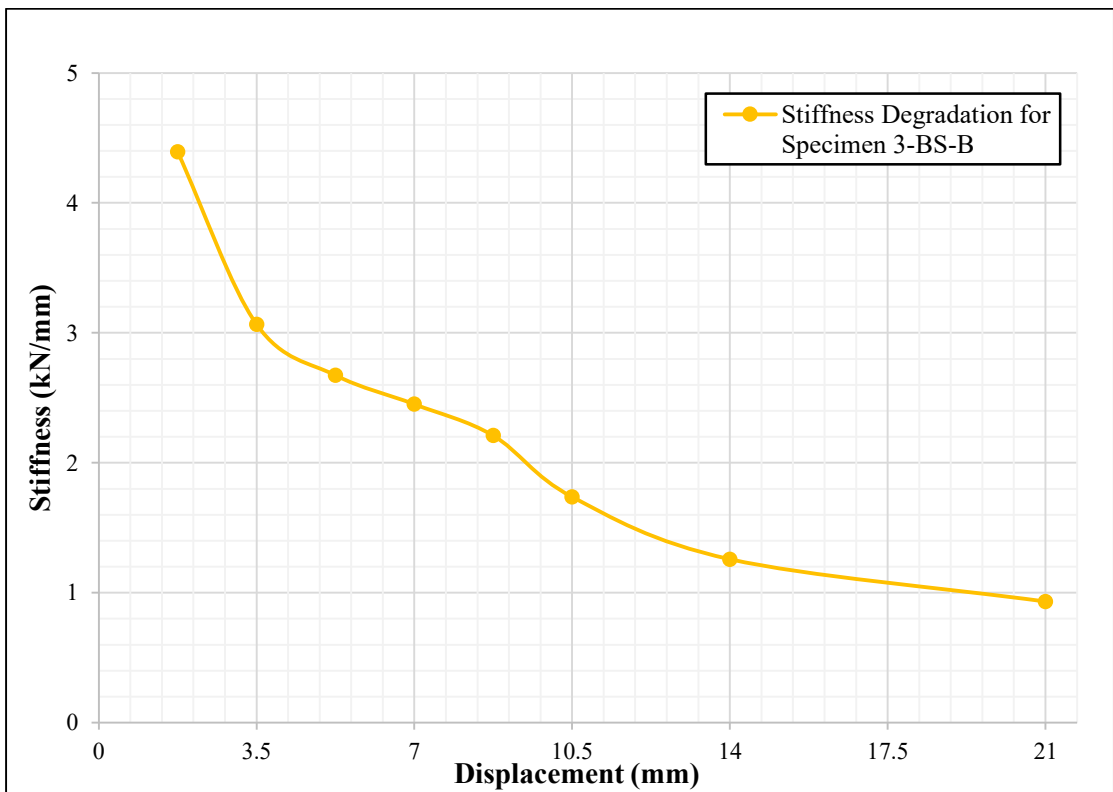
Figure 4.43: Stiffness degradation curve of specimen 3-BS-B
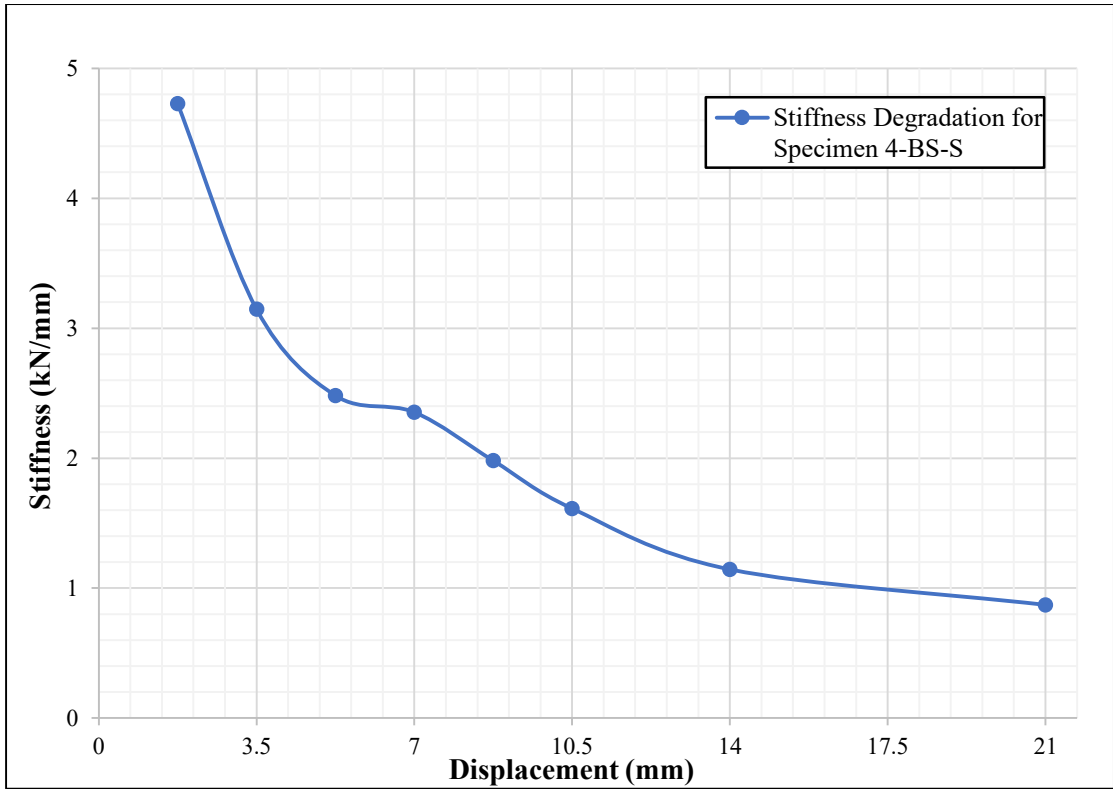
Figure 4.44: Stiffness degradation curve of specimen 4-BS-S
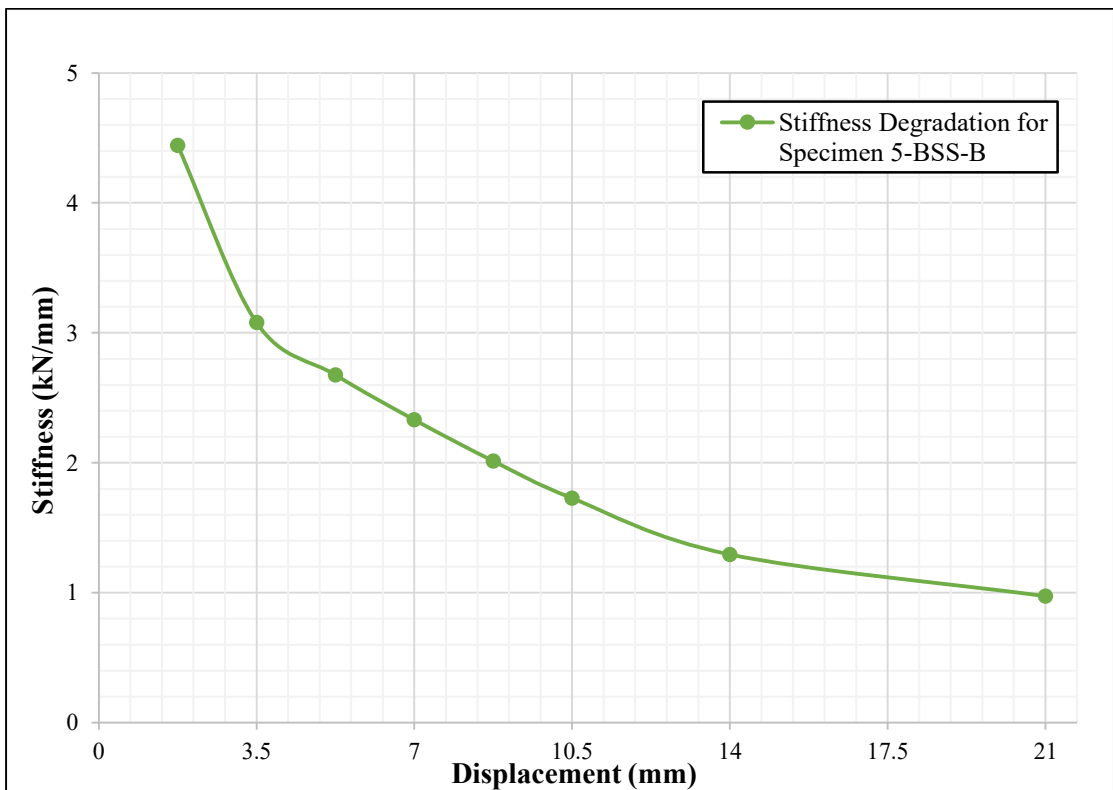
Figure 4.45: Stiffness degradation curve of specimen 5-BSS-B
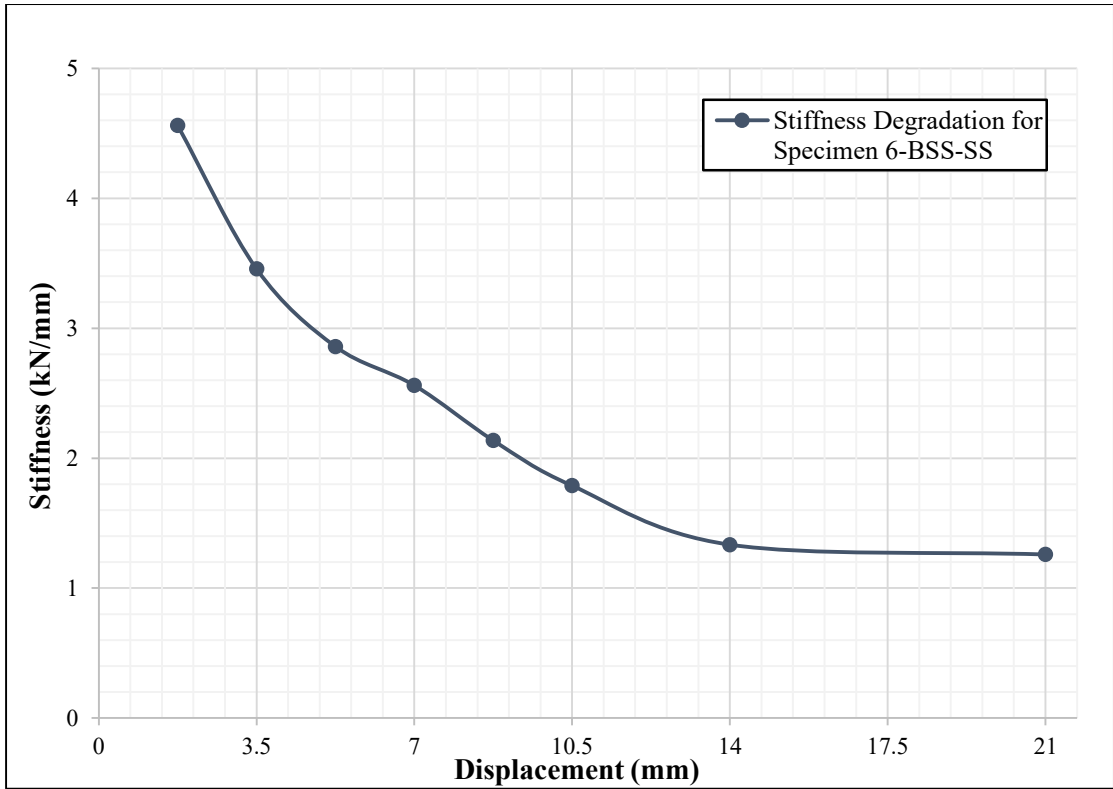
Figure 4.46: Stiffness degradation curve of specimen 6-BSS-SS
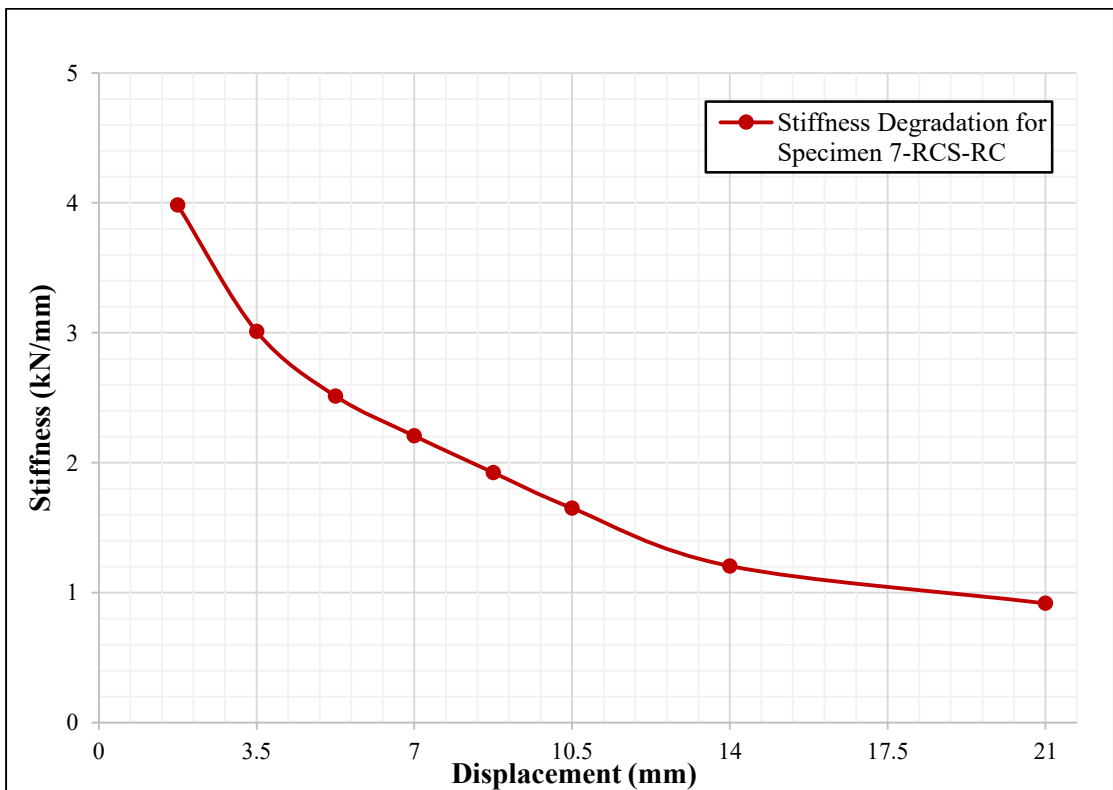
Figure 4.47: Stiffness degradation curve of specimen 7-RCS-RC

94
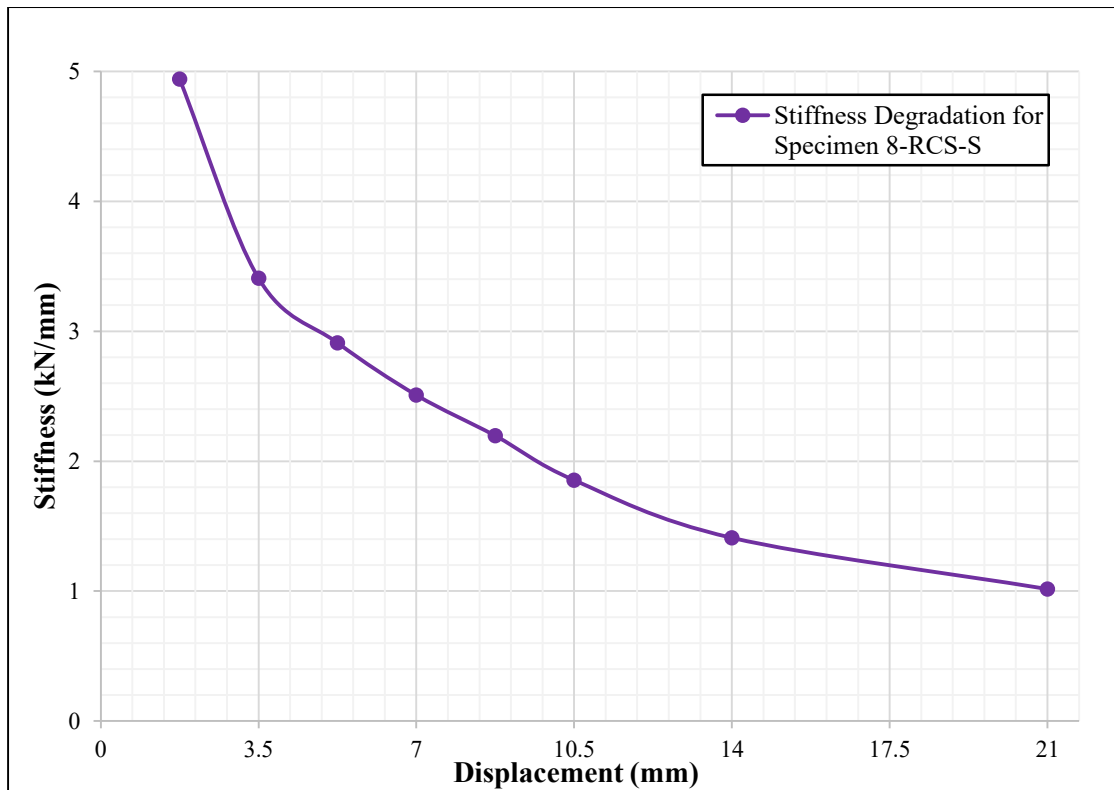
Figure 4.48: Stiffness degradation curve of specimen 8-RCS-S

4.6   Displacement Ductility

The yield displacements, ultimate displacements, and displacement ductilities of the specimens are shown in Table 4.2.

Table 4.2: Displacement ductility of the specimens

Specimen Designation	Yield Displacement (mm)	Ultimate Displacement (mm)	Ductility $\mu = \Delta u/\Delta y$
1-SS-C1	6.46	16.6	2.56
2-BB-C2	7.15	17.0	2.37
3-BS-B	7.36	15.9	2.16
4-BS-S	6.96	14.5	2.08
5-BSS-B	7.15	14.8	2.08
6-BSS-SS	6.40	20.3	3.18
7-RCS-RC	7.91	17.7	2.24
8-RCS-S	7.67	18.0	2.35

4.7 Energy Dissipation Capacity

The cumulative energy dissipation capacities of the specimens are plotted as shown in Figures 4.49 to 4.56. The cumulative energy dissipation occurred in an exponential growth pattern. The cumulative energy of the specimens after eight cycles are shown in Table 4.3.

Table 4.3: Cumulative energy dissipation capacity of the specimens

Specimen Designation	Cumulative Energy Dissipation Capacity (kN-mm)
1-SS-C1	1206
2-BB-C2	1281
3-BS-B	1050
4-BS-S	1049
5-BSS-B	1185
6-BSS-SS	1412
7-RCS-RC	1097
8-RCS-S	1555
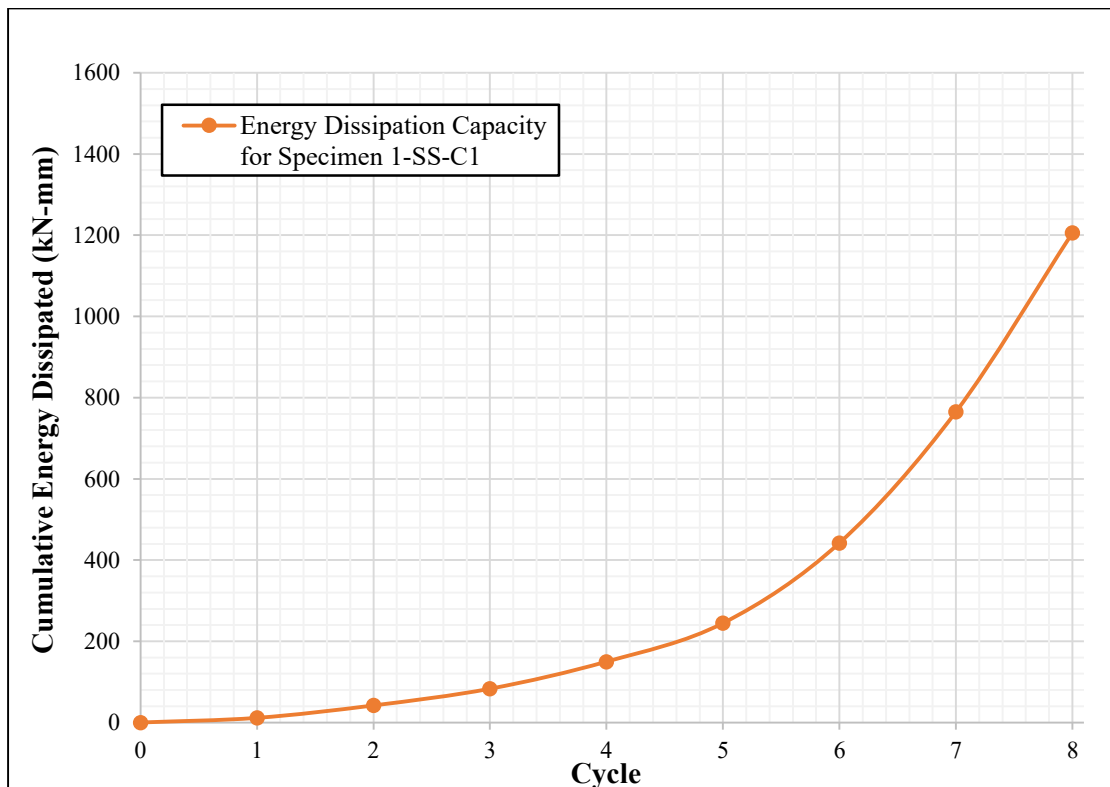
Figure 4.49: Cumulative energy dissipation capacity curve of specimen 1-SS-C1
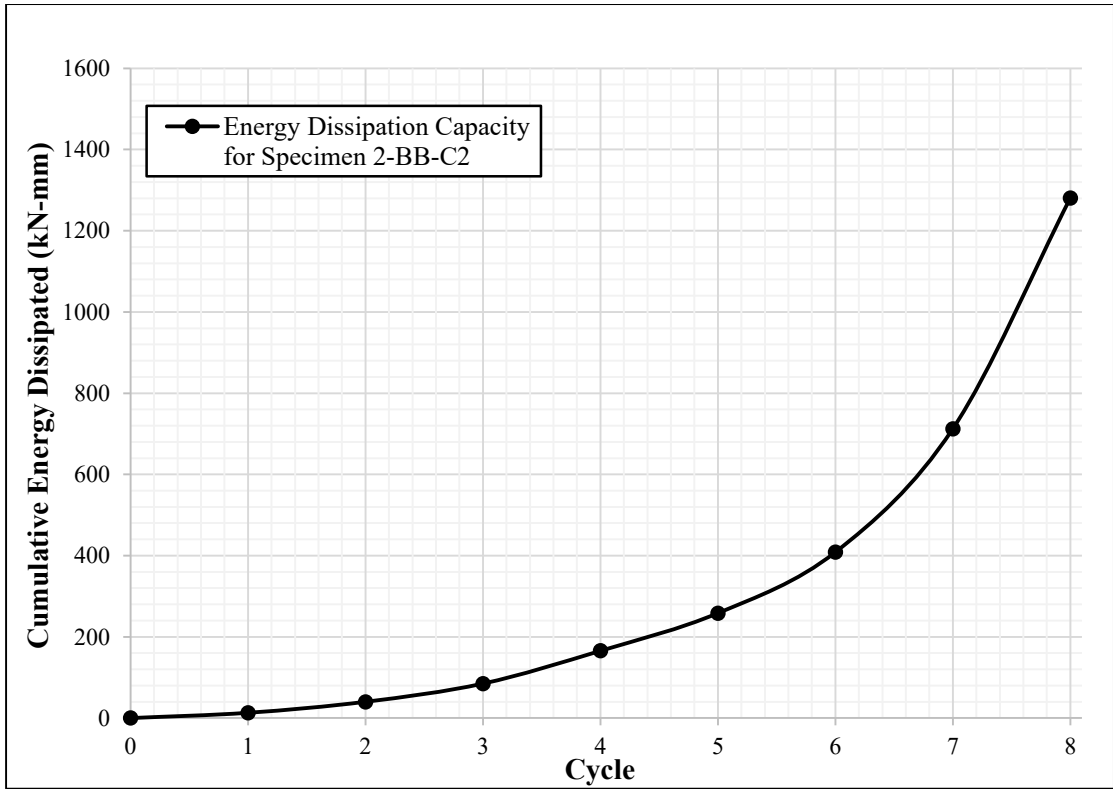
Figure 4.50: Cumulative energy dissipation capacity curve of specimen 2-BB-C2
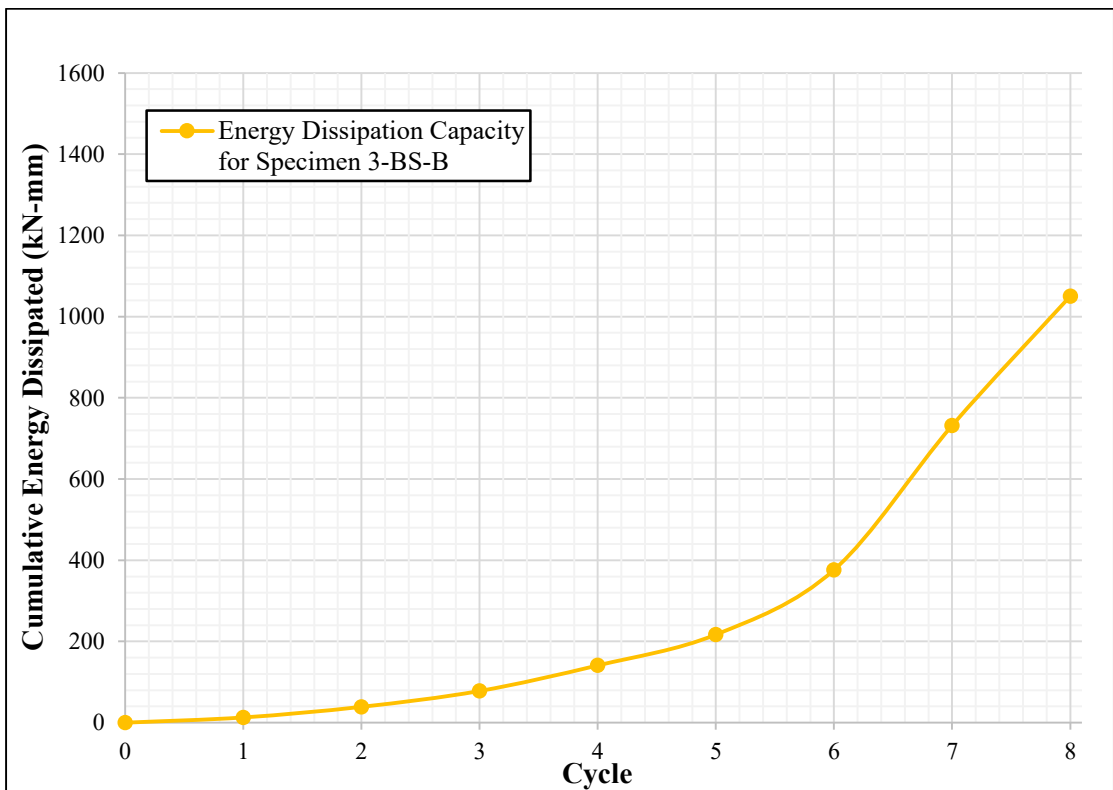
Figure 4.51: Cumulative energy dissipation capacity curve of specimen 3-BS-B

97
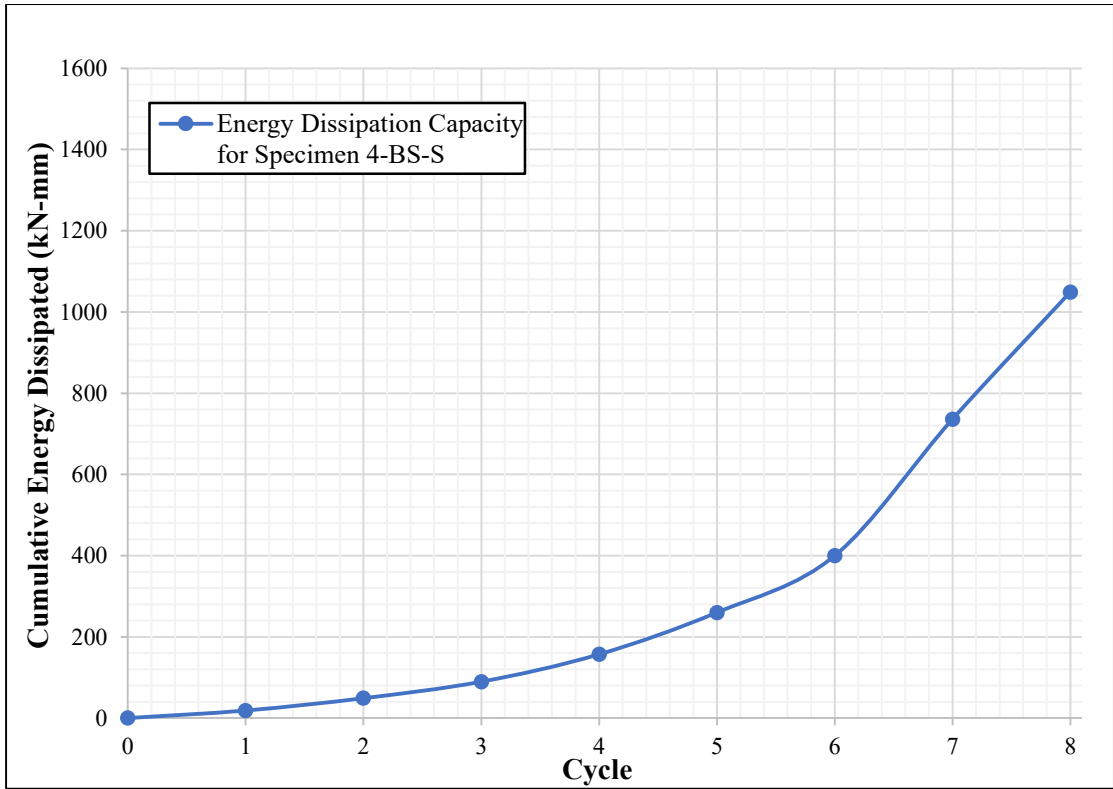
Figure 4.52: Cumulative energy dissipation capacity curve of specimen 4-BS-S
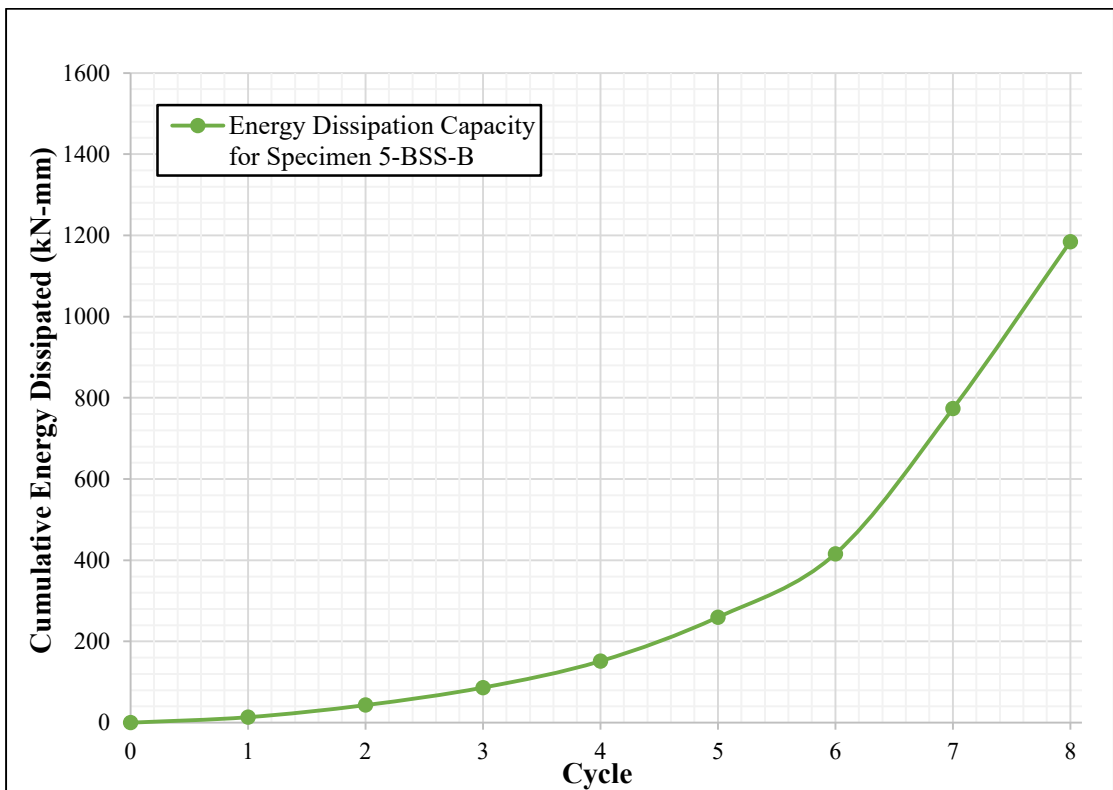
Figure 4.53: Cumulative energy dissipation capacity curve of specimen 5-BSS-B
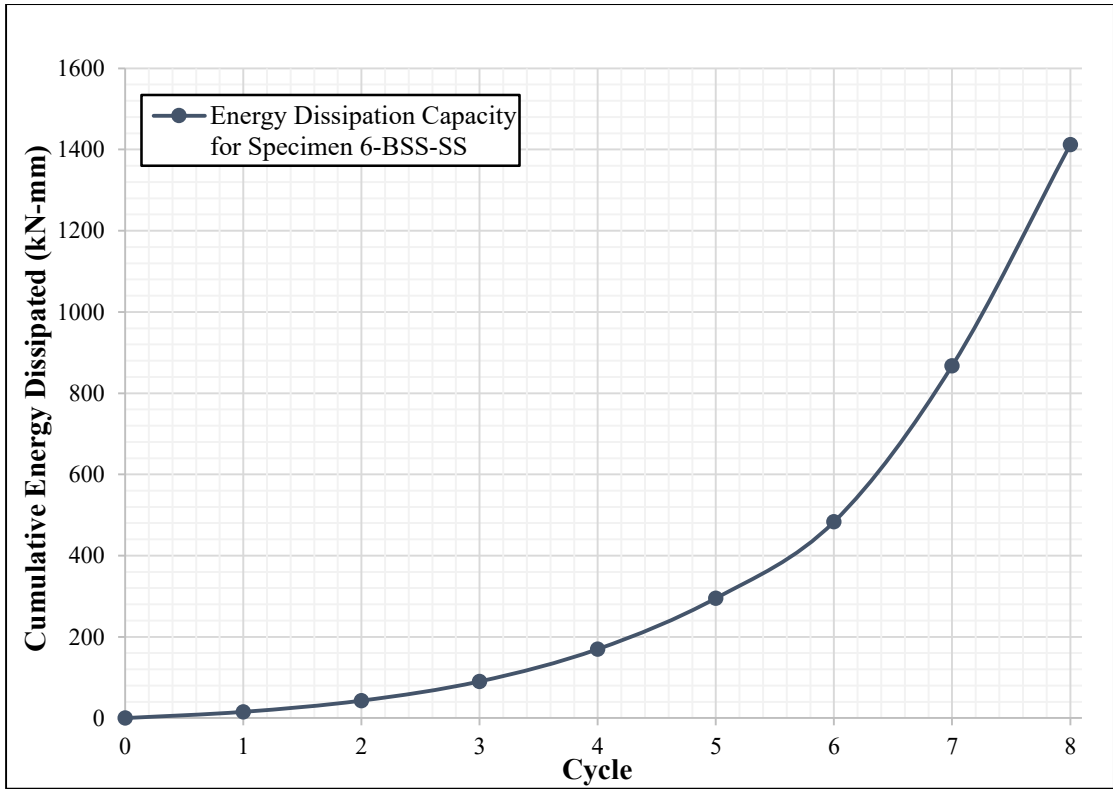
Figure 4.54: Cumulative energy dissipation capacity curve of specimen 6-BSS-SS
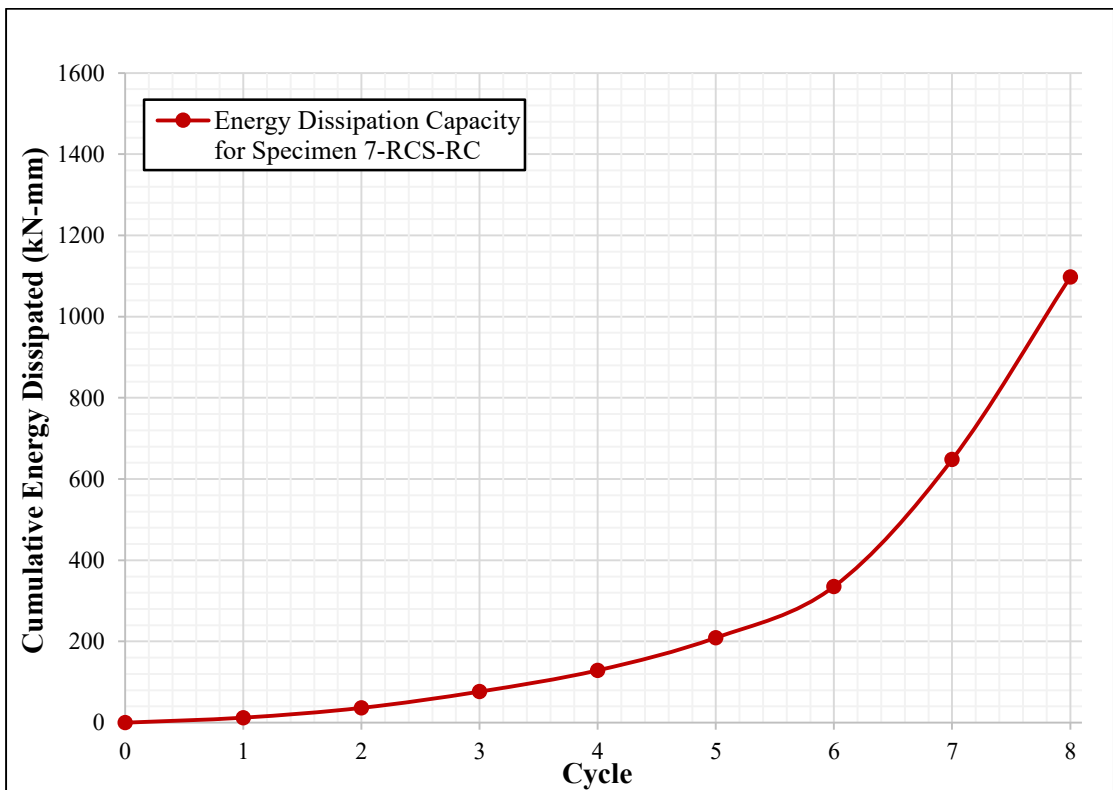
Figure 4.55: Cumulative energy dissipation capacity curve of specimen 7-RCS-RC
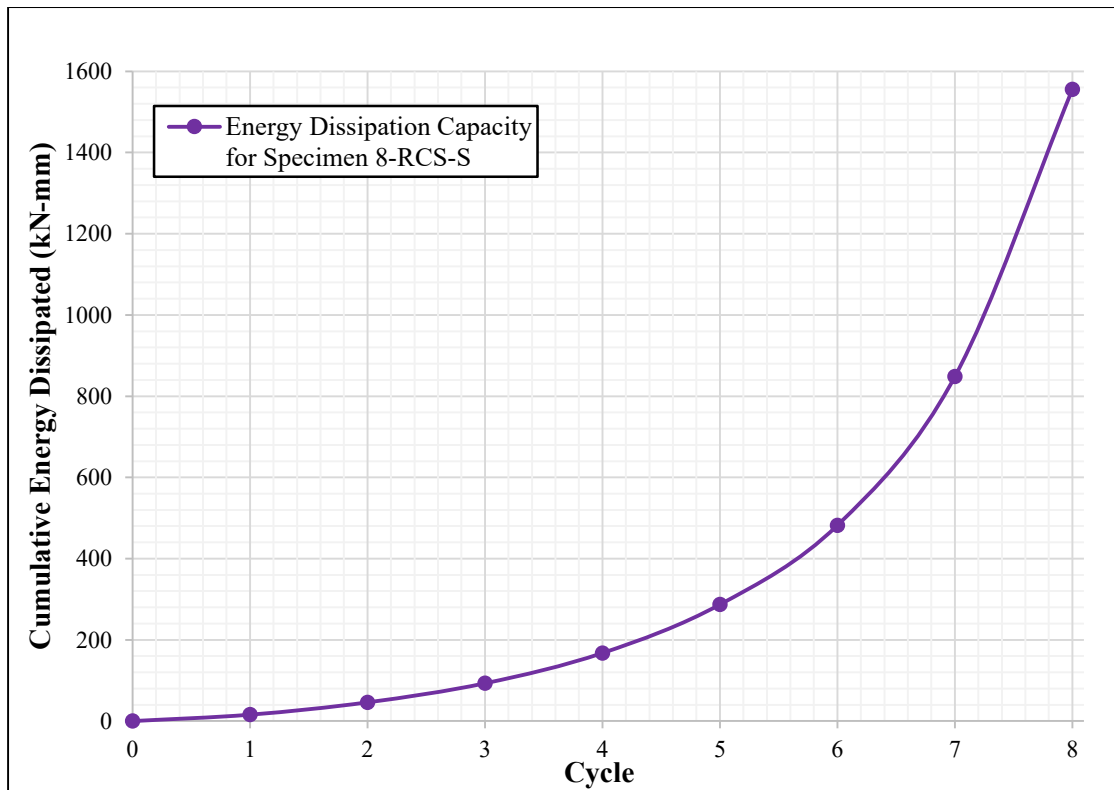
Figure 4.56: Cumulative energy dissipation capacity curve of specimen 8-RCS-S

4.8 Comparison between Uniform Coarse Aggregate Concrete and Dissimilar Coarse Aggregate Concrete Beam-Column Joints

On the basis of the test results discussed in the previous sections, a study to analyze the comparative performance of beam-column joints made with brickbat aggregate concrete and stone chips aggregate concrete have been carried out in this section. The objective is to determine whether the use of dissimilar concrete mixes in beams, columns, and joints in the same frame provide satisfactory seismic performance or not. The test results of 1-SS-C1, 2-BB-C2, 3-BS-B, and 4-BS-S have been compared on the basis of cracking characteristics, hysteresis behavior, stiffness degradation, displacement ductility, and energy dissipation capacity in the following subsections.

4.8.1 Comparison of Cracking Characteristic

The cracks formed in the specimens 1-SS-C1, 2-BB-C2, 3-BS-B, and 4-BS-S are shown in Figure 4.57. It can be seen that, the number of cracks were much higher in the specimens cast with dissimilar coarse aggregate concretes compared to that cast with uniform coarse aggregate concrete. Besides, the cracks appeared in earlier cycles in the
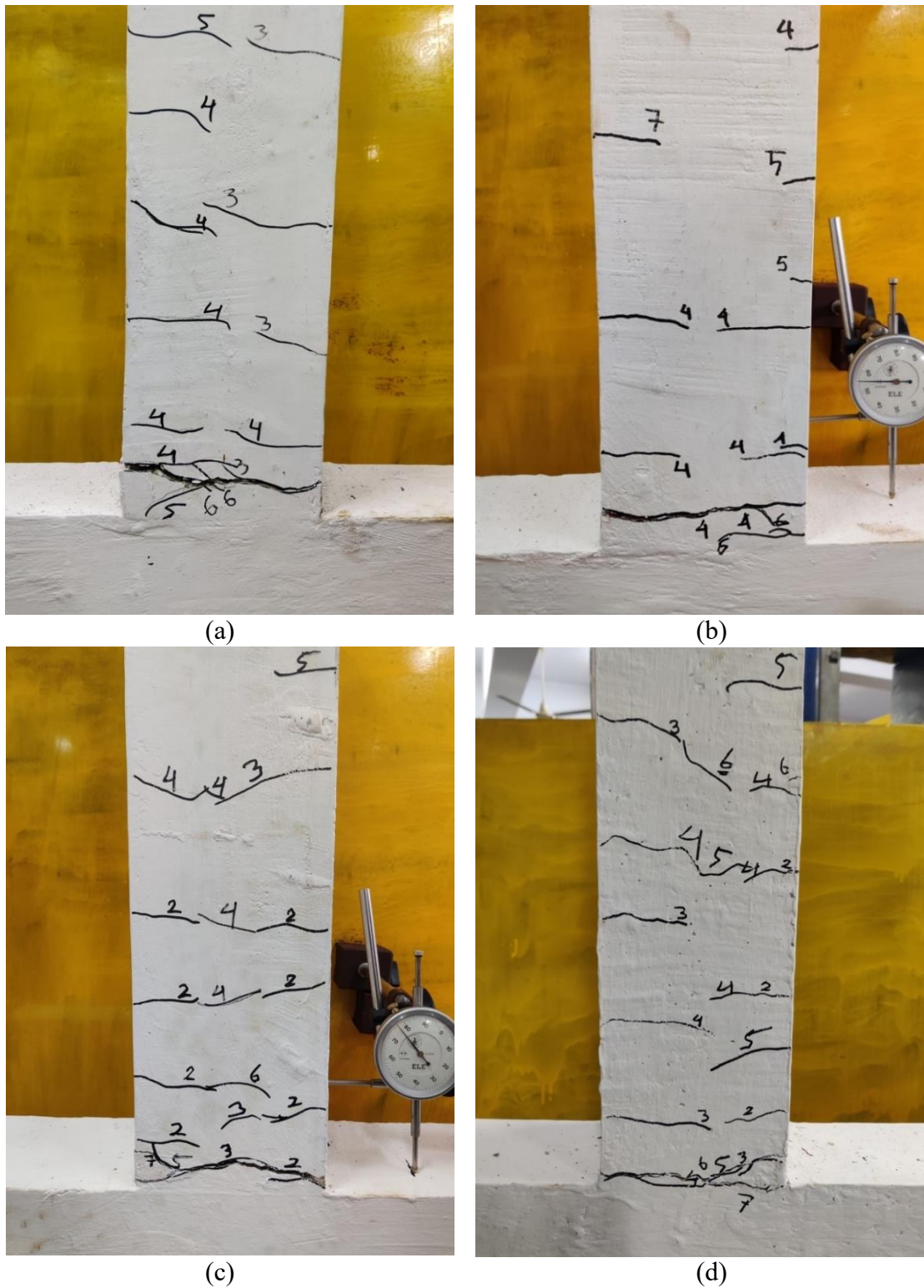
Figure 4.57: Cracks formed in specimen (a) 1-SS-C1, (b) 2-BB-C2, (c) 3-BS-B and (d) 4-BS-S

specimens cast with dissimilar coarse aggregate concretes compared to that cast with uniform coarse aggregate concrete. The displacements at which the formation of first crack in the specimens took place are listed in Table 4.4.

Table 4.4: Displacement in specimens 1-SS-C1, 2-BB-C2, 3-BS-B and 4-BS-S at the formation of first crack

Specimen Designation	Displacement at the Point of Applied Load (mm)	Cycle Number
1-SS-C1	4.96	3 (Reverse)
2-BB-C2	5.06	4 (Forward)
3-BS-B	3.52	2 (Forward)
4-BS-S	3.35	2 (Reverse)

It is also seen that the formation of first crack occurred in much lower displacements in specimens cast with dissimilar coarse aggregate concretes compared to that cast with uniform coarse aggregate concrete. The results reveal that the cracking characteristics of brickbat aggregate concrete is better than that of stone chips aggregate concrete for specimens cast with uniform coarse aggregate concrete. For specimens cast with dissimilar coarse aggregate concretes, the specimen with brickbat aggregate concrete in joint region performed better in terms of cracking characteristics.
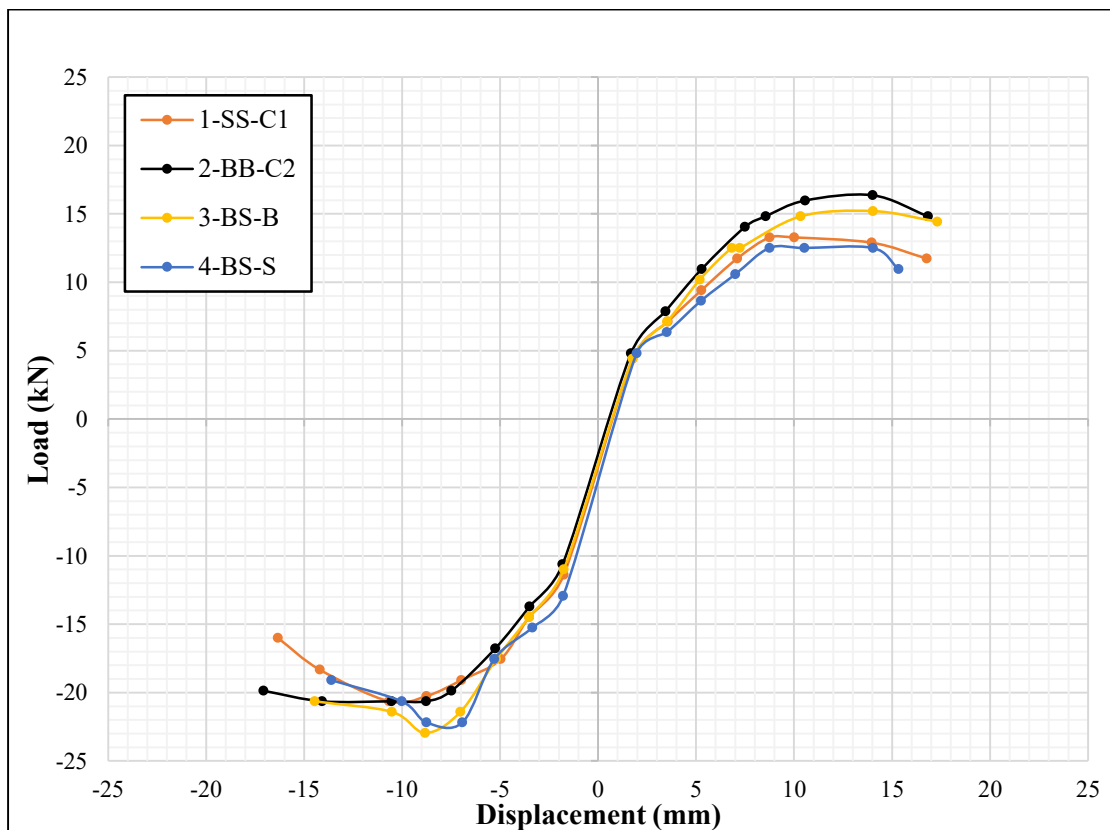
Figure 4.58: Failure envelopes of 1-SS-C1, 2-BB-C2, 3-BS-B, and 4-BS-S

4.8.2 Comparison of Failure Envelopes

The load versus displacement failure envelopes of the specimens 1-SS-C1, 2-BB-C2, 3-BS-B, and 4-BS-S are shown in Figure 4.58. Almost similar failure envelopes have been found in these specimens. However, the specimens cast with brickbat aggregate concrete performed better than stone chips aggregate concrete for uniform coarse aggregate concrete specimens. For specimens cast with dissimilar coarse aggregate concretes, the specimen with brickbat aggregate concrete in joint region performed better.

4.8.3 Comparison of Stiffness Degradations

The stiffness degradations of the specimens 1-SS-C1, 2-BB-C2, 3-BS-B, and 4-BS-S are shown in Figure 4.59. The stiffness degradation was almost similar and stiffness degraded exponentially for all the specimens. The stiffness degraded from 76.8% to 81.6% at the eighth cycle compared to the first cycle for these specimens.
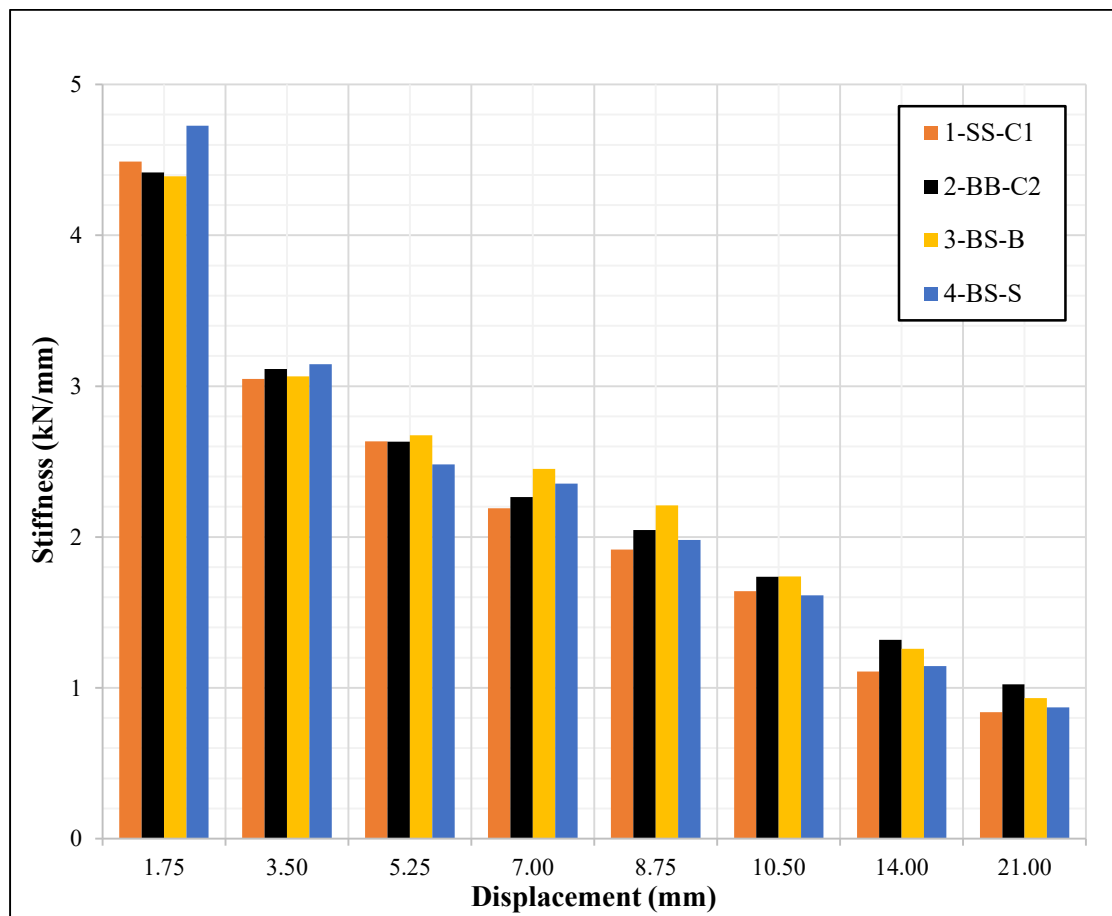
Figure 4.59: Stiffness degradations of 1-SS-C1, 2-BB-C2, 3-BS-B, and 4-BS-S

4.8.4 Comparison of Displacement Ductilities

The displacement ductilities of 1-SS-C1, 2-BB-C2, 3-BS-B, and 4-BS-S are listed in Table 4.5. For a better understanding, the ductility values are illustrated in Figure 4.60. It has been found that, the displacement ductilities of specimens cast with dissimilar coarse aggregate concretes were much lesser compared to that cast with uniform coarse aggregate concrete.

Table 4.5: Displacement ductilities of 1-SS-C1, 2-BB-C2, 3-BS-B and 4-BS-S

Specimen Designation	Yield Displacement (mm)	Ultimate Displacement (mm)	Displacement Ductility, μ
1-SS-C1	6.46	16.6	2.56
2-BB-C2	7.15	17.0	2.37
3-BS-B	7.36	15.9	2.16
4-BS-S	6.96	14.5	2.08
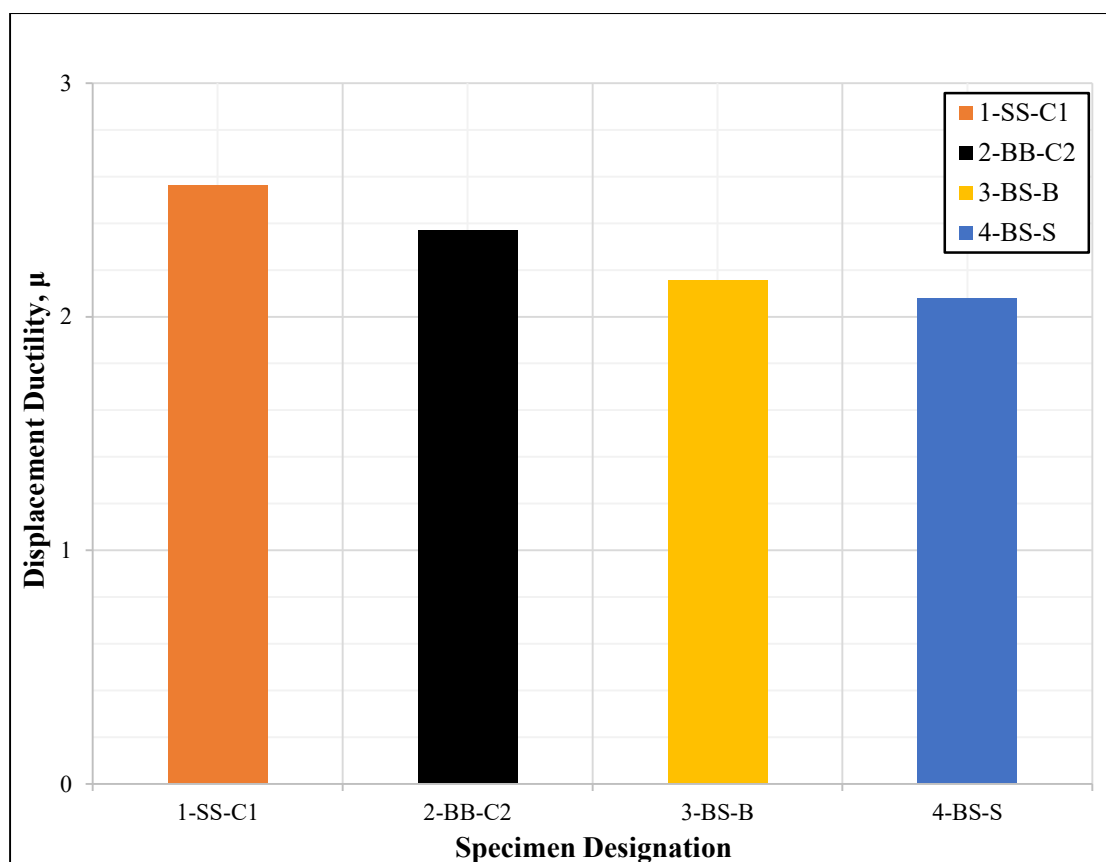
Figure 4.60: Displacement ductilities of 1-SS-C1, 2-BB-C2, 3-BS-B, and 4-BS-S

4.8.5 Comparison of Energy Dissipation Capacities

The energy dissipation capacities of 1-SS-C1, 2-BB-C2, 3-BS-B, and 4-BS-S are shown in Figure 4.61. It has been found that, the energy dissipation capacities of specimens cast with dissimilar coarse aggregate concretes were much lesser compared to that cast with uniform coarse aggregate concrete. However, the energy dissipation capacities of specimens cast with dissimilar coarse aggregate concretes were similar for joints cast with brickbat aggregate concrete and stone chips aggregate concrete.
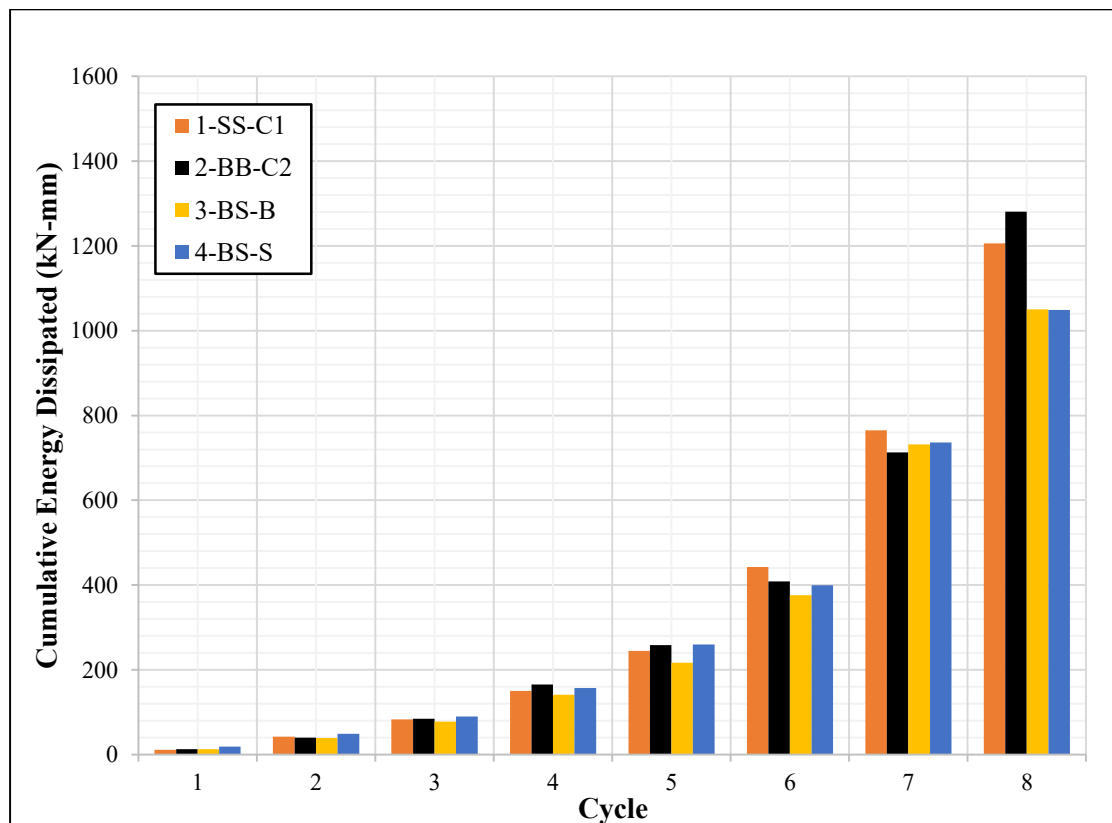
Figure 4.61: Energy dissipation capacities of specimens 1-SS-C1, 2-BB-C2, 3-BS-B, and 4-BS-S

4.8.6 Summary of the Comparison

The summary of comparison on the tests performed on specimen 1-SS-C1, 2-BB-C2, 3-BS-B, and 4-BS-S is provided below:

    i.   The cracks in concrete appear faster in lower displacements and the number of cracks formed are higher for dissimilar coarse aggregate concrete beam-column joints compared to uniform coarse aggregate concrete joints. This may be possible due to the fact that the adhesive force in uniform concrete mixes is

higher which tends to increase the potential of concrete to remain uncracked under tension for longer periods.

ii. Brickbat aggregate concrete performed better in terms of cracking characteristics than stone chips aggregate concrete in spite of having similar compressive strength and elasticity of concrete.

iii. The failure envelopes, yield displacements, and ultimate displacements of brickbat aggregate concrete have been found to be slightly better than that of stone chips aggregate concrete for the same reasoning.

iv. The stiffness degraded exponentially which have been found to be similar in the specimens.

v. Ductility has been found to be 9.8% to 23.3% higher for uniform coarse aggregate concrete than those for dissimilar coarse aggregate concretes. The energy dissipation capacity has also been found to be 14.8% to 22.1% higher for uniform coarse aggregate concrete. This may also be due to the fact that the adhesive force in uniform concrete mixes is higher. Moreover, a weaker zone in the joint is created at the interface where the dissimilar concrete mixes join.

vi. All the parameters between specimens 3-BS-B and 4-BS-S have been found to be almost same which suggests that the performance of beam-column joint is similar whether brickbat aggregate concrete or stone chips aggregate concrete is used in the joint region. This may be due to the fact that there is no significant correlation between the bond strength of reinforcing steel with brickbat aggregate concrete and stone chips aggregate concrete (Hoque et. al. 2020).

vii. The results lead to the conclusion that using different concrete mixes in different components of the same frame weakens the performance of the beam-column joint in terms of cracking behavior, ductility, and energy dissipation capacity under cyclic excitation even if the concrete mixes are of similar compressive strength and elasticity.

viii. It is highly recommended that, dissimilar coarse aggregate concrete joints must be carefully analyzed and designed in terms of the seismic requirements of the structure before their use in different components of the same frame.

4.9 Performance of Steel Slag Aggregate as a Replacement of Stone Chips Aggregate in Beam-Column Joints with Dissimilar Coarse Aggregate Concrete

On the basis of the test results discussed in the previous sections, a study to analyze the comparative performance of dissimilar coarse aggregate beam-column joints by replacing stone chips aggregate concrete with steel slag aggregate concrete in columns and joint regions have been carried out in this section. The objective is to determine whether the use of steel slag aggregate concrete mix in beam-column joints provide better seismic performance than that of stone chips aggregate concrete or not. The results of 3-BS-B, 4-BS-S, 5-BSS-B, and 6-BSS-SS have been compared on the basis of cracking characteristics, hysteresis behavior, stiffness degradation, displacement ductility, and energy dissipation capacity in the following subsections.

4.9.1 Comparison of Cracking Characteristic

The cracks formed in the specimens 3-BS-B, 4-BS-S, 5-BSS-B, and 6-BSS-SS are shown in Figure 4.62. It can be seen that, the number of cracks were almost similar in the specimens cast with steel slag aggregate concrete in columns and joints compared to that cast with stone chips aggregate concrete. The cracks appeared in second cycles in all the specimens. The displacements at which the formation of first crack in the specimens took place are listed in Table 4.6.

Table 4.6: Displacement in specimens 3-BS-B, 4-BS-S, 5-BSS-B, and 6-BSS-SS at the formation of first crack

Specimen Designation	Displacement at the Point of Applied Load (mm)	Cycle Number
3-BS-B	3.52	2 (Forward)
4-BS-S	3.35	2 (Reverse)
5-BSS-B	3.50	2 (Reverse)
6-BSS-SS	3.45	2 (Reverse)

It is also seen that the formation of first crack occurred in almost same displacements in the specimens. The results reveal that the cracking characteristics is mainly governed by the nature of concrete used in beam portion which is expected as flexural cracks developed in beams.
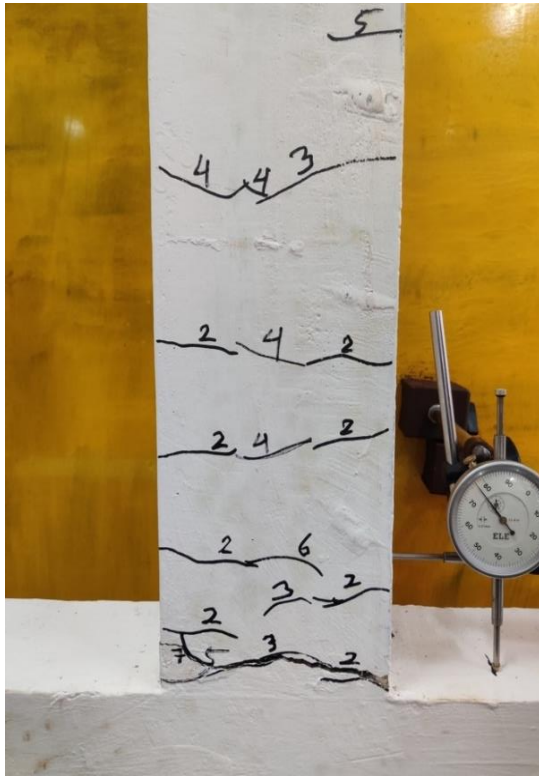
(a)
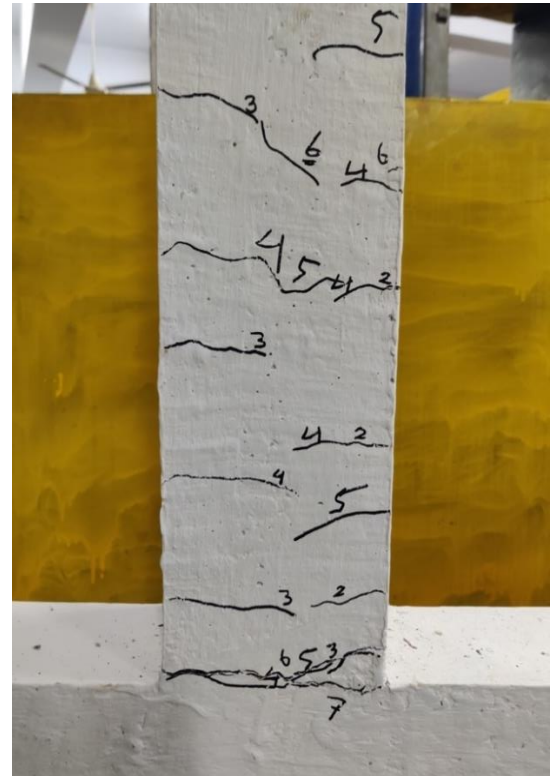
(b)

(c)
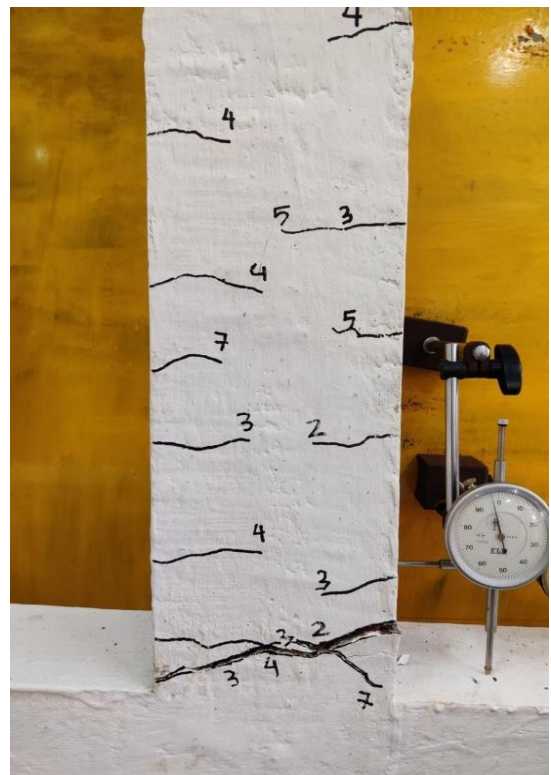
(d)

Figure 4.62: Cracks formed in specimen (a) 3-BS-B, (b) 4-BS-S, (c) 5-BSS-B, and (d) 6-BSS-SS

4.9.2 Comparison of Failure Envelopes

The load versus displacement failure envelopes of 3-BS-B, 4-BS-S, 5-BSS-B, and 6-BSS-SS are shown in Figure 4.63. Almost similar failure envelopes have been found in the specimens except for specimen 6-BSS-SS. The specimen cast with steel slag aggregate concrete in the joint region performed far better than those cast with stone chips or brickbat aggregate concrete.
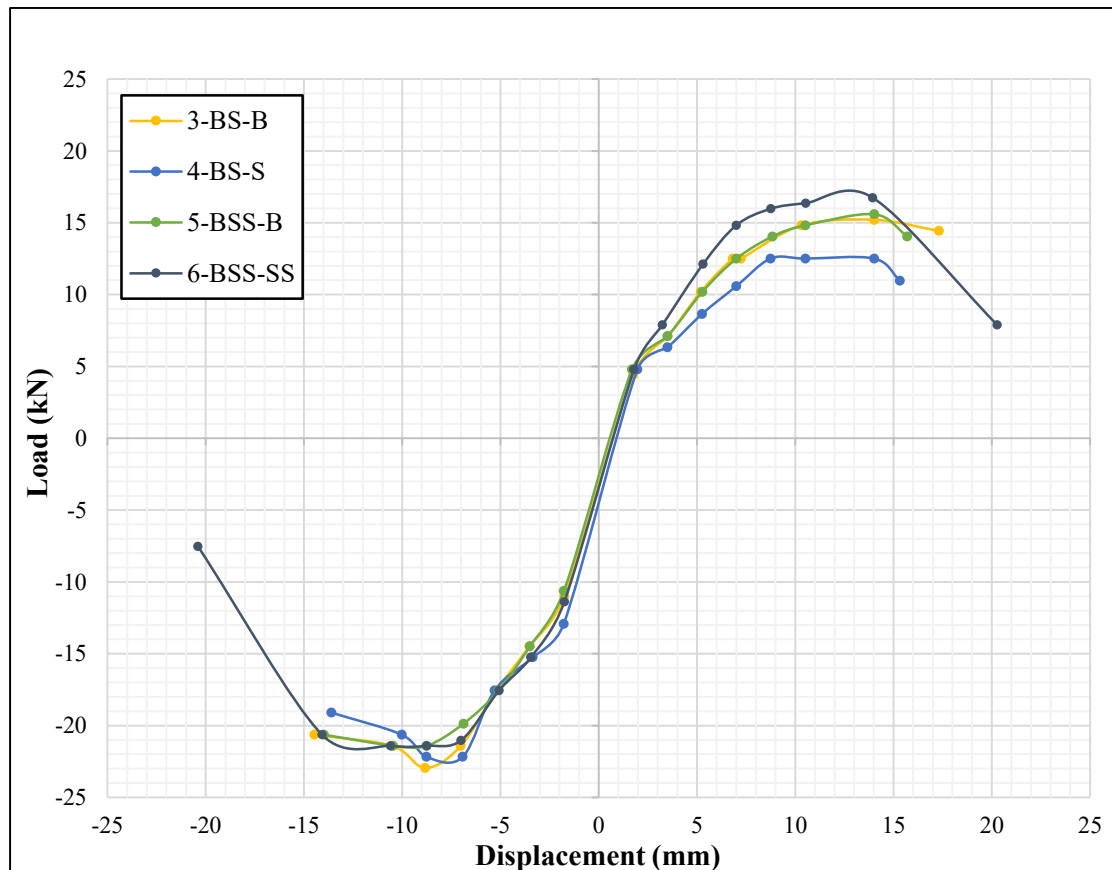
Figure 4.63: Failure envelopes of 3-BS-B, 4-BS-S, 5-BSS-B, and 6-BSS-SS

4.9.3 Comparison of Stiffness Degradations

The stiffness degradations of the specimens 3-BS-B, 4-BS-S, 5-BSS-B, and 6-BSS-SS are shown in Figure 4.64. The stiffness degradation was almost similar except for specimen 6-BSS-SS. The stiffness degraded exponentially for all the specimens. The stiffness degraded from 78.1% to 81.6% at the eighth cycle compared to the first cycle for the specimens 3-BS-B, 4-BS-S, and 5-BSS-B while that degraded 72.4% for specimen 6-BSS-SS.
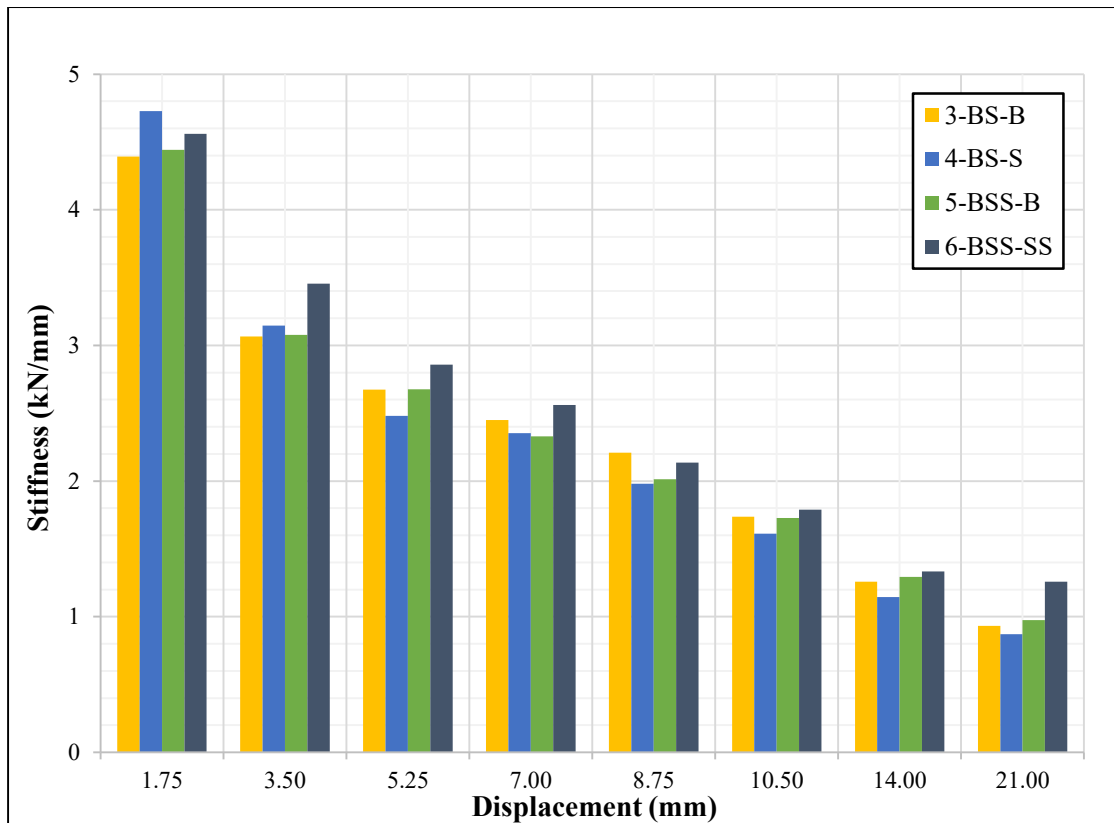
Figure 4.64: Stiffness degradations of 3-BS-B, 4-BS-S, 5-BSS-B, and 6-BSS-SS

4.9.4 Comparison of Displacement Ductilities

The displacement ductilities of 3-BS-B, 4-BS-S, 5-BSS-B, and 6-BSS-SS are listed in Table 4.7. For a better understanding, the ductility values are illustrated in Figure 4.65. It has been found that, the displacement ductility of specimen cast with steel slag aggregate concrete in the joint region was much higher compared to the other specimens.

Table 4.7: Displacement ductilities of 3-BS-B, 4-BS-S, 5-BSS-B, and 6-BSS-SS

Specimen Designation	Yield Displacement (mm)	Ultimate Displacement (mm)	Displacement Ductility, μ
3-BS-B	7.36	15.9	2.16
4-BS-S	6.96	14.5	2.08
5-BSS-B	7.15	14.8	2.08
6-BSS-SS	6.40	20.3	3.18
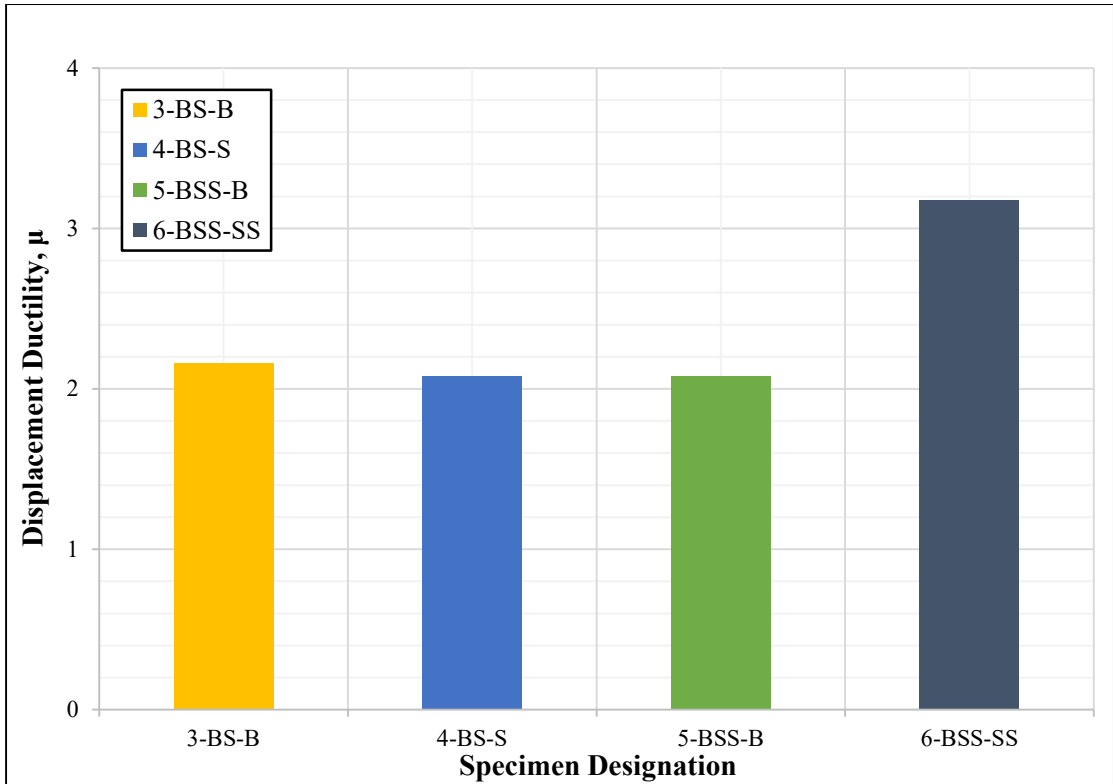
Figure 4.65: Displacement ductilities of 3-BS-B, 4-BS-S, 5-BSS-B, and 6-BSS-SS
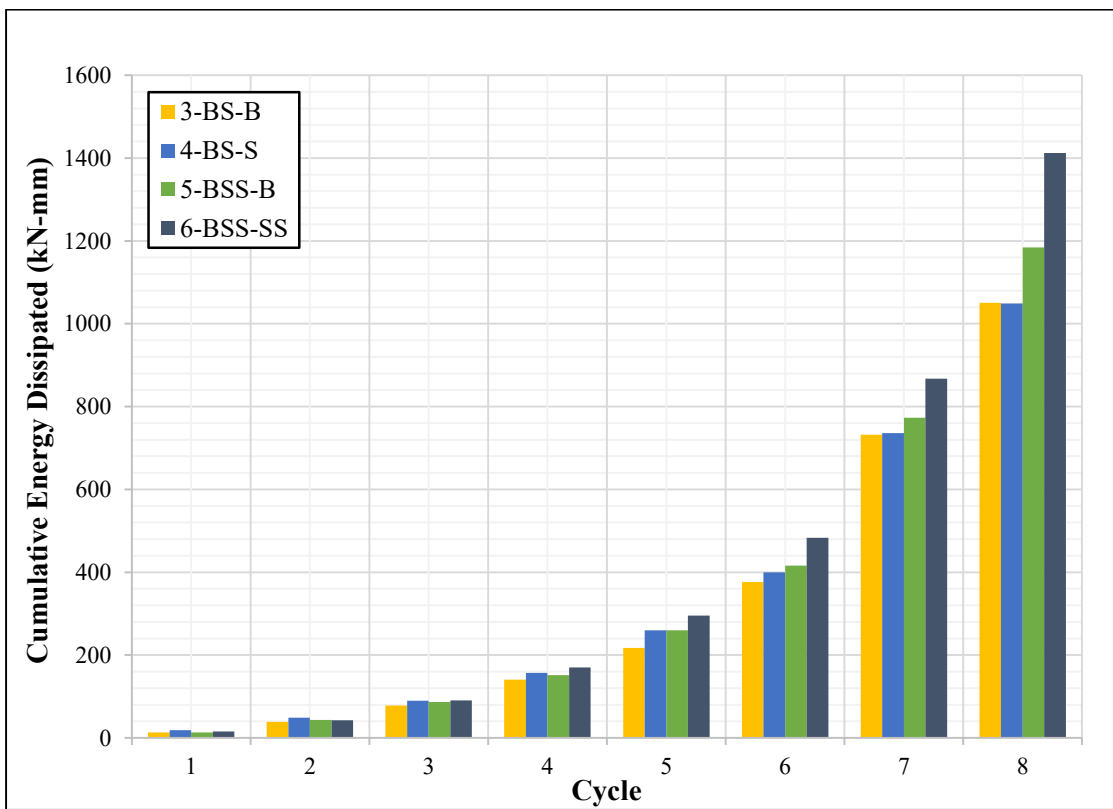
Figure 4.66: Energy dissipation capacities of specimens 3-BS-B, 4-BS-S, 5-BSS-B, and 6-BSS-SS

4.9.5 Comparison of Energy Dissipation Capacities

The energy dissipation capacities of 3-BS-B, 4-BS-S, 5-BSS-B, and 6-BSS-SS are shown in Figure 4.66. It has been found that, the energy dissipation capacities of specimens cast with steel slag aggregate concrete was much higher compared to that cast with stone chips aggregate concrete. Moreover, the energy dissipation capacity of specimen cast with steel slag aggregate concrete in joint region was much higher for joints cast with brickbat aggregate concrete and stone chips aggregate concrete.

4.9.6 Summary of the Comparison

The summary of comparison on the tests performed on 3-BS-B, 4-BS-S, 5-BSS-B, and 6-BSS-SS is provided below:

i.   The cracking characteristics have been found to be similar for 3-BS-B, 4-BS-S, 5-BSS-B, and 6-BSS-SS. This is due to the fact that flexural cracks have formed in all specimens which is mainly governed by the nature of concrete used in beam portion.

ii. The failure envelope of the specimen cast with steel slag aggregate concrete in joint portion have been found to be far better than that of the rest of the specimens. This is due to the fact that the bond performance of specimens made with steel slag aggregates are superior to that made with stone aggregates (Kim et. al. 2012).

iii. The stiffness degraded exponentially which have been found to be similar in the specimens.

iv. Ductility has been found to be almost same for specimens made with brickbat or stone chips aggregate concrete in joint region. However, the ductility has been found to be 34.6% higher for the specimen cast with steel slag aggregate concrete in the joint region compared that cast with stone chips aggregate concrete. This is due to the fact that the ductility capacity of electric arc furnace steel slag aggregate specimens is superior to that of natural stone chips aggregate specimens although their flexural strengths are similar (Kim et. al. 2014). Furthermore, steel slag aggregates had lower aggregate crushing value than stone chips which may result in steel slag aggregates to stay in its initial shape and size in higher loads.

v. The energy dissipation capacity has been found to be 11.4% to 25.7% higher for specimens made with steel slag aggregate concrete. This may be due to the fact that the bond performance of steel slag aggregate concrete is 8% to 20% higher than that of stone chips aggregate concrete (Lee et. al. 2020).

vi. The failure envelope, ductility, and energy dissipation capacity showed better results for 6-BSS-SS than those for 5-BSS-B. This suggests that, the bond strength between reinforcing steel and joint concrete mix plays a significant role in the overall seismic performance of the beam-column joint.

vii. The results lead to the conclusion that using steel slag aggregate as a replacement of stone chips aggregate in concrete greatly enhances the performance of the beam-column joint in terms of hysteresis behavior, ductility, and energy dissipation capacity under cyclic excitation. Thus, steel slag aggregate can be used as an excellent alternative choice of coarse aggregate in concrete used in framed structures. However, the steel slag aggregate concrete used in this study had superior compressive strength and elasticity compared to those of stone chips aggregate concrete. The performance of high strength stone chips aggregate concrete may show better seismic performance.

4.10 Performance of Recycled Concrete Aggregate as a Replacement of Brickbat Aggregate in Beam-Column Joints with Dissimilar Coarse Aggregate Concrete

On the basis of the test results discussed in the previous sections, a study to analyze the comparative performance of dissimilar coarse aggregate beam-column joints by replacing brickbat aggregate concrete with recycled aggregate concrete in beams and joint regions have been carried out in this section. The objective is to determine whether the use of recycled aggregate concrete mix in beam-column joints provide better seismic performance than that of brickbat aggregate concrete or not. The results of specimens 3-BS-B, 4-BS-S, 7-RCS-RC, and 8-RCS-S have been compared on the basis of cracking characteristics, hysteresis behavior, stiffness degradation, displacement ductility, and energy dissipation capacity in the following subsections.

### 4.10.1 Comparison of Cracking Characteristic

The cracks formed in the specimens 3-BS-B, 4-BS-S, 7-RCS-RC, and 8-RCS-S are shown in Figure 4.67. It can be seen that, the number of cracks were almost similar in
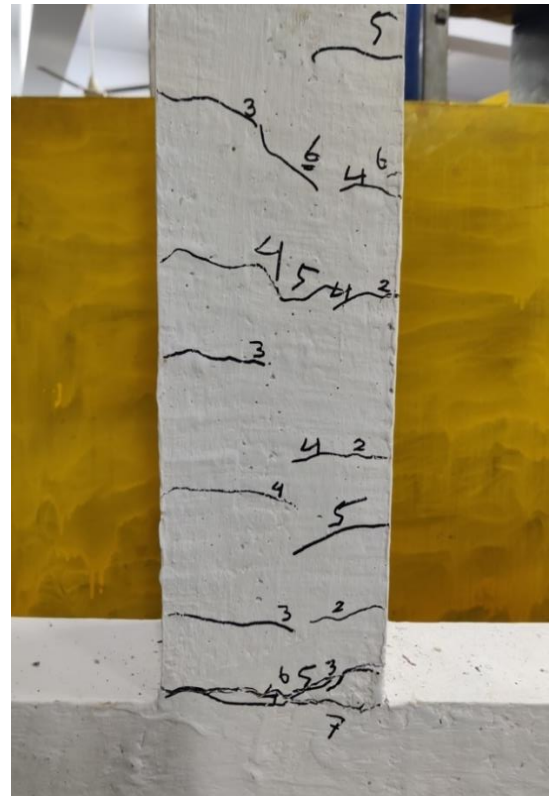
Figure 4.67: Cracks formed in specimen (a) 3-BS-B, (b) 4-BS-S, (c) 7-RCS-RC, and (d) 8-RCS-S

114

the specimens cast with recycled aggregate concrete in beams and joints compared to that cast with brickbat aggregate concrete. The cracks appeared in second cycles in all the specimens except 7-RCS-RC at which the first crack appeared in first cycle. The displacements at which the formation of first crack in the specimens took place are listed in Table 4.8.

Table 4.8: Displacement in specimens 3-BS-B, 4-BS-S, 7-RCS-RC, and 8-RCS-S at the formation of first crack

Specimen Designation	Displacement at the Point of Applied Load (mm)	Cycle Number
3-BS-B	3.52	2 (Forward)
4-BS-S	3.35	2 (Reverse)
7-RCS-RC	1.79	1 (Reverse)
8-RCS-S	2.15	2 (Forward)

It is seen that the formation of first crack occurred in lesser displacements in specimens cast with recycled aggregate concrete in beams and joints compared to that cast with brickbat aggregate concrete. The results suggest that the adhesive force in recycled aggregate concrete is lower than that of brickbat aggregate concrete.

4.10.2 Comparison of Failure Envelopes

The load versus displacement failure envelopes of 3-BS-B, 4-BS-S, 7-RCS-RC, and 8-RCS-S are shown in Figure 4.68. Almost similar failure envelopes have been found in the specimens except for specimen 8-RCS-S which showed better performance. The specimen cast with recycled aggregate concrete in the joint region performed worse than that cast with stone chips aggregate concrete.

4.10.3 Comparison of Stiffness Degradations

The stiffness degradations of 3-BS-B, 4-BS-S, 7-RCS-RC, and 8-RCS-S are shown in Figure 4.69. The stiffness degraded exponentially as the degradations have been found to be almost similar for all the specimens. The stiffness degraded from 76.9% to 81.6% at the eighth cycle compared to the first cycle for 3-BS-B, 4-BS-S, 7-RCS-RC, and 8-RCS-S.
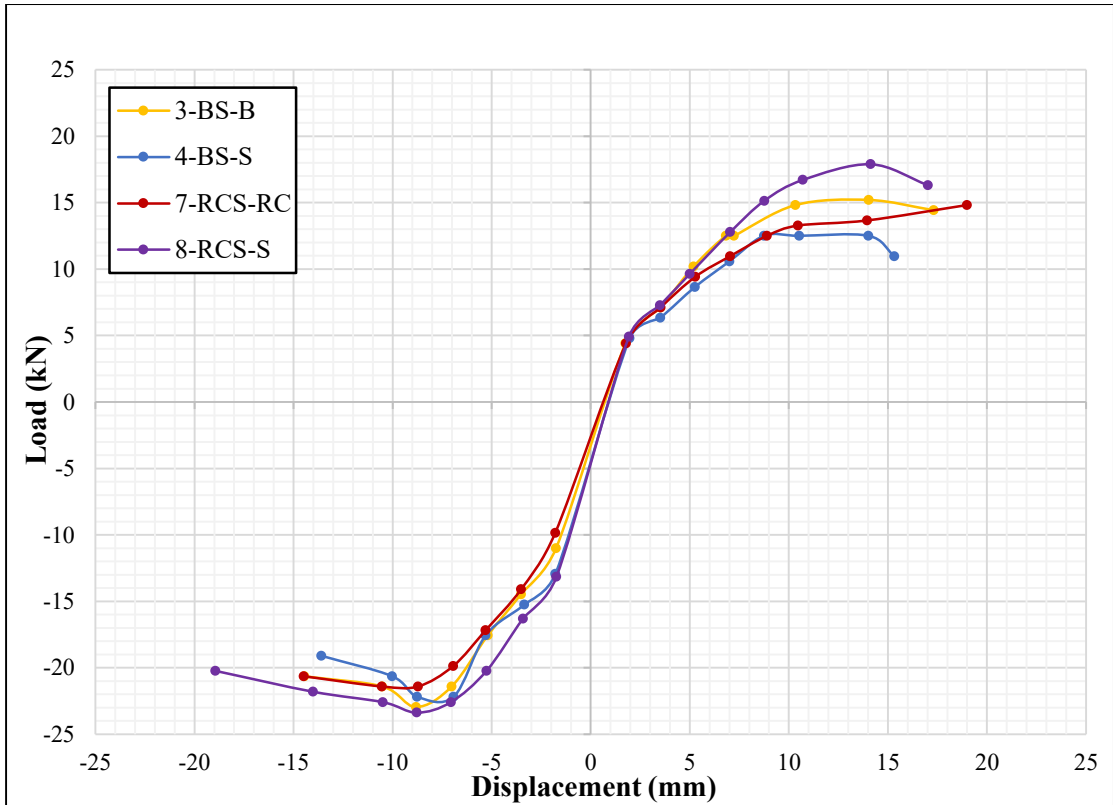
Figure 4.68: Failure envelopes of 3-BS-B, 4-BS-S, 7-RCS-RC, and 8-RCS-S
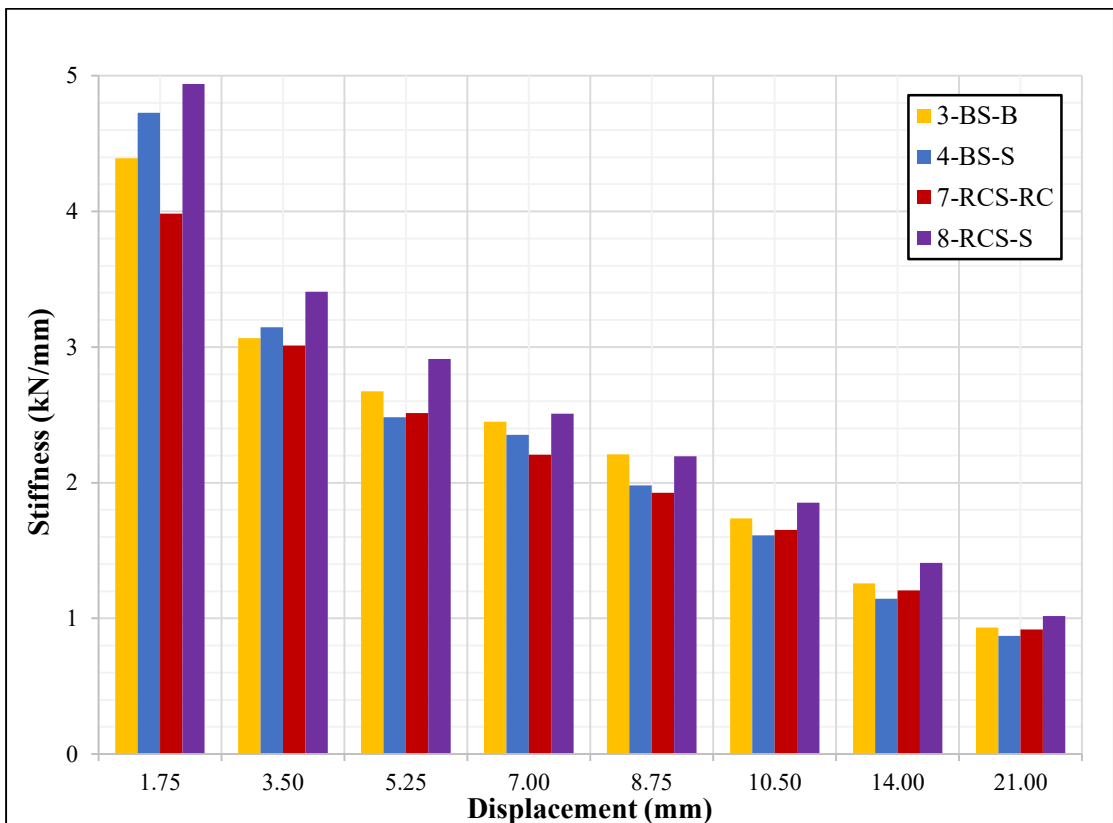
Figure 4.69: Stiffness degradations of 3-BS-B, 4-BS-S, 7-RCS-RC, and 8-RCS-S

4.10.4 Comparison of Displacement Ductilities

The displacement ductilities of 3-BS-B, 4-BS-S, 7-RCS-RC, and 8-RCS-S are listed in Table 4.9. For a better understanding, the ductility values are illustrated in Figure 4.70. It has been found that, the displacement ductilities of specimens cast with recycled aggregate concrete was slightly higher compared to those cast with brickbat aggregate concrete.

Table 4.9: Displacement ductilities of 3-BS-B, 4-BS-S, 7-RCS-RC, and 8-RCS-S

Specimen Designation	Yield Displacement (mm)	Ultimate Displacement (mm)	Displacement Ductility, μ
3-BS-B	7.36	15.9	2.16
4-BS-S	6.96	14.5	2.08
7-RCS-RC	7.91	17.7	2.24
8-RCS-S	7.67	18.0	2.35
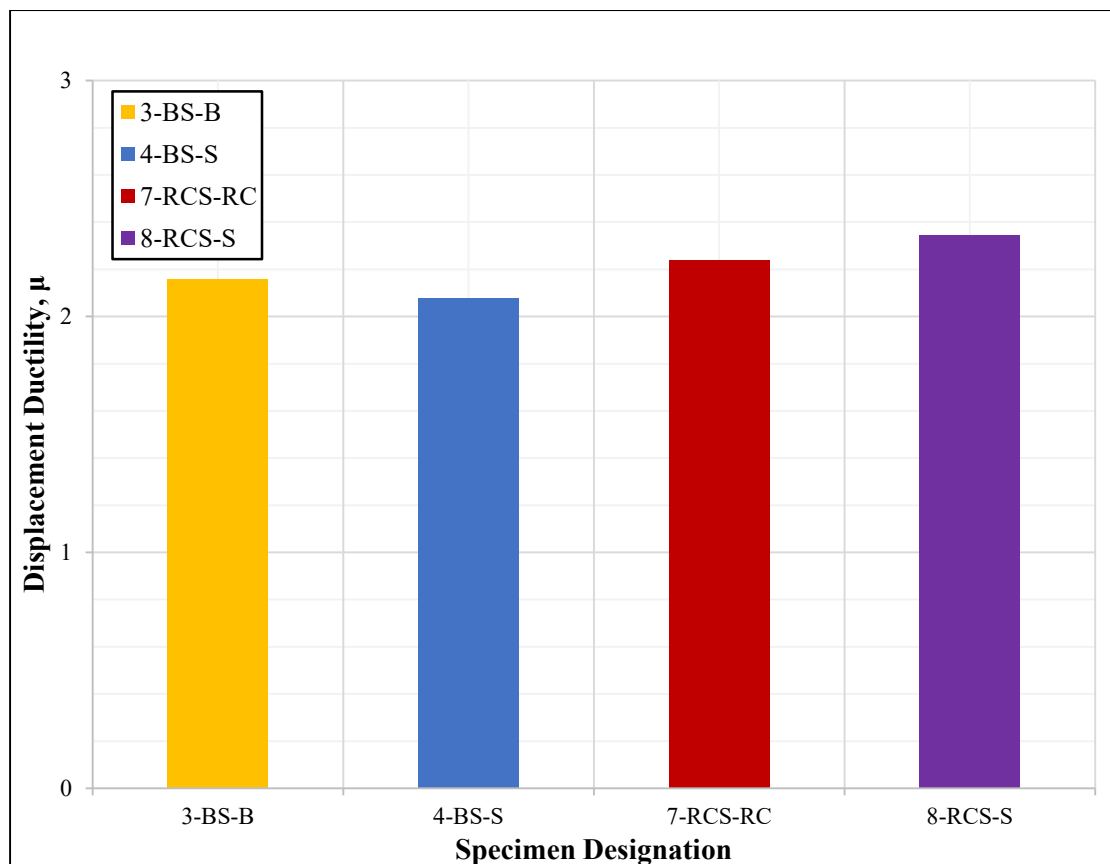
Figure 4.70: Displacement ductilities of 3-BS-B, 4-BS-S, 7-RCS-RC, and 8-RCS-S

4.10.5 Comparison of Energy Dissipation Capacities

The energy dissipation capacities of 3-BS-B, 4-BS-S, 7-RCS-RC, and 8-RCS-S are shown in Figure 4.71. It has been found that, the energy dissipation capacities of specimens cast with recycled aggregate concrete was much higher compared to that cast with brickbat aggregate concrete. Moreover, the energy dissipation capacity of specimen cast with stone chips aggregate concrete in joint region was much higher for joints cast with recycled aggregate concrete between 7-RCS-RC and 8-RCS-S.
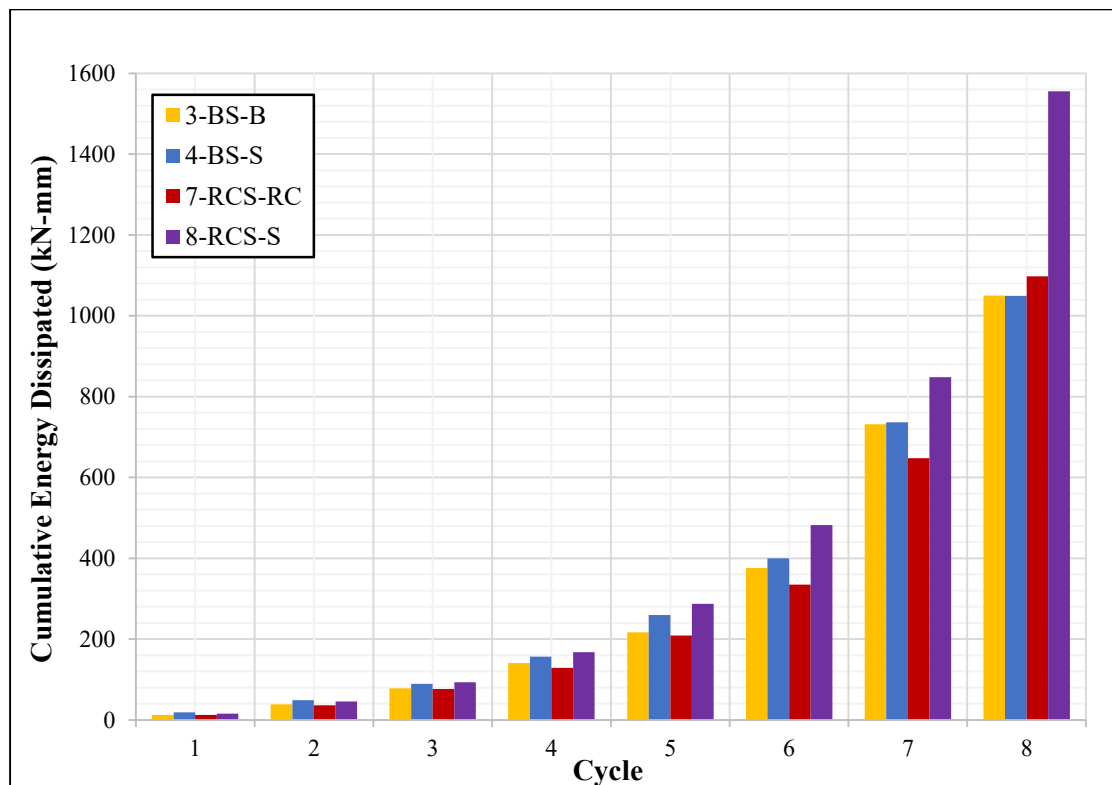
Figure 4.71: Energy dissipation capacities of specimens 3-BS-B, 4-BS-S, 7-RCS-RC, and 8-RCS-S

4.10.6 Summary of the Comparison

The summary of comparison on the tests performed on 3-BS-B, 4-BS-S, 7-RCS-RC, and 8-RCS-S is provided below:

i.   Although the cracking patterns have been found to be similar for all the specimens, the cracks formed faster and in smaller displacements for specimens cast with recycled aggregate concrete in beams compared to those cast with brickbat aggregate concrete. This suggests that adhesive force of recycled aggregate concrete is lesser than that of brickbat aggregate concrete.

ii. The failure envelope of the specimen 8-RCS-S have been found to be slightly better than that of the rest of the specimens. This is due to the fact that the bond performance of specimens made with stone chips aggregate concrete in joint region are superior to that made with recycled aggregate concrete (Xiao and Falkner 2007).

iii. The stiffness degraded exponentially which have been found to be similar in all the specimens.

iv. Ductility has been found to be 3.7% to 11.4% better for specimens made with recycled aggregate concrete instead of brickbat aggregate concrete. This is due to the fact that the tensile strength of recycled aggregate concrete is found to be higher than that of brickbat aggregate concrete (Saha 2019). Furthermore, the ductility of 8-RCS-S has been found to be 4.7% higher than 7-RCS-RC due to the fact that stone chips aggregate concrete shows 9% to 19% better bond performance with steel compared to recycled aggregate concrete (Butler et. al. 2011; Butler et. al. 2015).

v. The energy dissipation capacity has been found to be 4.3% to 32.5% higher for specimens made with recycled aggregate concrete compared to brickbat aggregate concrete. However, the energy dissipation capacity of 8-RCS-S has been found to be 29.4% higher than 7-RCS-RC due to the same reasons.

vi. The cracking characteristics, failure envelope, ductility, and energy dissipation capacity showed better results for 8-RCS-S than those for 7-RCS-RC. This suggests that, the bond strength between reinforcing steel and joint concrete mix plays a significant role in the overall seismic performance of the beam-column joint.

vii. The results lead to the conclusion that using recycled aggregate as a replacement of brickbat aggregate in concrete slightly enhances the performance of the beam-column joint in terms of hysteresis behavior, ductility, and energy dissipation capacity under cyclic excitation. However, recycled aggregate used in this study was aged just above 28 days and so the compressive strength of concrete, elasticity of concrete, and aggregate crushing value were better of recycled aggregate than those of brickbat aggregates. Thus, while choosing recycled aggregate as a replacement in framed structures, the physical and mechanical properties of concrete must be properly examined.

4.11 Summary

The reversed cyclic load test results of beam-column joints cast with different combinations of coarse aggregate concrete mixes have been described in this chapter. The test results have been presented for each specimen in terms of cracking characteristics, failure patterns, hysteresis behaviors, stiffness degradations, displacement ductilities, and energy dissipation capacities.

The results were later compared between specimens cast with uniform coarse aggregate concrete in all the frame components to those of the specimens cast with dissimilar coarse aggregate concrete. It has been observed that, using different concrete mixes in different components of the same frame weakens the performance of the beam-column joint under cyclic excitation even if the concrete mixes are of similar compressive strength and elasticity. Therefore, the use of dissimilar coarse aggregate concrete joints must be carefully analyzed and designed in terms of the seismic requirements of the structure before their use in different components of the same frame.

The results between dissimilar coarse aggregate concrete joint specimens cast with steel slag aggregate concrete in columns and those cast with stone chips aggregate concrete have been compared to determine the possibility of satisfactory replacement of coarse aggregates with steel slag. The results suggested that, using steel slag aggregate as a replacement of stone chips aggregate in concrete greatly enhances the performance of the beam-column joints sunder cyclic excitation. Thus, steel slag aggregate can be used as an excellent alternative choice of coarse aggregate in concrete used in framed structures.

Finally, the results between dissimilar coarse aggregate concrete joint specimens cast with recycled aggregate concrete in beams and those cast with brickbat aggregate concrete have been compared to determine the possibility of satisfactory replacement of coarse aggregates with recycled concrete. It has been found that, using recycled aggregate as a replacement of brickbat aggregate in concrete slightly enhances the performance of the beam-column joints under cyclic excitation. However, the physical and mechanical properties of recycled aggregate concrete must be properly examined before using it in framed structures.

CHAPTER 5
CONCLUSIONS AND RECOMMENDATIONS

5.1 Introduction

The objectives of the present research were to investigate the structural behavior of exterior beam-column joints made with dissimilar coarse aggregate concrete mixes in its different components of the frame as well as to evaluate the seismic performance of steel slag aggregate and recycled concrete aggregate as a replacement of conventional aggregates in concrete mixes. Eight specimens have been constructed and tested in the laboratory with a view to draw some conclusions and to recommend suitable choices of coarse aggregates that can be used in reinforced concrete frames subjected to seismic action.

Reversed cyclic load tests have been performed on the specimens in the laboratory in order to evaluate their performance qualitatively by observing the cracking and failure patterns as well as quantitatively by determining the load-deflection and moment-rotation hysteresis behaviors, stiffness degradations, displacement ductilities, and energy dissipation capacities. The conclusions of the research based on the experimental test results are presented in this chapter along with some suggestions for future work in this field.

5.2 Conclusions

The major findings of the present thesis are summarized below:

i.   The cracks in concrete appear faster in lower displacements and the number of cracks formed are higher for dissimilar coarse aggregate concrete beam-column joints compared to uniform coarse aggregate concrete joints due to the fact that the bond in uniform concrete mixes is higher which tends to increase the potential of concrete to remain uncracked under tension for longer periods.
The cracking characteristics have been found to be similar for dissimilar coarse aggregate concrete beam-column joints having the same concrete mix in the beam portions as flexural cracks have formed in all specimens which is mainly governed by the nature of concrete used in beam portion.

121

Although the cracking patterns have been found to be similar for all the dissimilar coarse aggregate concrete specimens, the cracks formed faster and in smaller displacements for specimens cast with recycled aggregate concrete in beams compared to those cast with brickbat aggregate concrete suggesting that the bond of recycled aggregate concrete is lesser than that of brickbat aggregate concrete.

ii. Brickbat aggregate concrete performed better in terms of cracking characteristics than stone chips aggregate concrete in spite of having similar compressive strength and elasticity of concrete. The failure envelopes, yield displacements, and ultimate displacements of brickbat aggregate concrete have been also found to be slightly better than that of stone chips aggregate concrete.

iii. The failure envelope of the specimen cast with steel slag aggregate concrete in joint portion have been found to be far better than that of the rest of the specimens due to the fact that the bond performance of specimens made with steel slag aggregates are superior to that made with stone aggregates.

The failure envelope of the specimen cast with stone chips aggregate concrete in the joint region have been also found to be slightly better than the specimen cast with recycled aggregate concrete in joint region due to the fact that the bond performance of specimens made with stone chips aggregate concrete in joint region are superior to that made with recycled aggregate concrete.

iv. The failure envelope, ductility, and energy dissipation capacity showed better results for 6-BSS-SS than those for 5-BSS-B and for 8-RCS-S than those for 7-RCS-RC. This suggests that, the bond strength between reinforcing steel and joint concrete mix plays a significant role in the overall seismic performance of the beam-column joint.

However, all the parameters between specimens 3-BS-B and 4-BS-S have been found to be almost same which suggests that the performance of beam-column joint is similar whether brickbat aggregate concrete or stone chips aggregate concrete is used in the joint region as there is no significant correlation between the bond strength of reinforcing steel with brickbat aggregate concrete and stone chips aggregate concrete.

v. The stiffness degraded exponentially which have been found to be similar in all the specimens. The stiffness degraded from 72.4% to 81.6% at the eighth cycle compared to the first cycle for the specimens.

vi. Ductility has been found to be 9.8% to 23.3% higher for uniform coarse aggregate concrete than those for dissimilar coarse aggregate concretes.

Ductility has been found to be almost same for specimens made with brickbat or stone chips aggregate concrete in joint region. However, the ductility has been found to be 34.6% higher for the specimen cast with steel slag aggregate concrete in the joint region compared to that cast with stone chips aggregate concrete as the ductility capacity of electric arc furnace steel slag aggregate specimens is superior to that of natural stone chips aggregate specimens although their flexural strengths are similar.

Ductility has been found to be 3.7% to 11.4% higher for specimens made with recycled aggregate concrete compared to brickbat aggregate concrete. Furthermore, the ductility of 8-RCS-S has been found to be 4.7% higher than 7-RCS-RC due to the fact that stone chips aggregate concrete shows 9% to 19% better bond performance with steel compared to recycled aggregate concrete.

vii. Energy dissipation capacity has been found to be 14.8% to 22.1% higher for uniform coarse aggregate concrete than those for dissimilar coarse aggregate concretes.

Energy dissipation capacity has been found to be 11.4% to 25.7% higher for specimens made with steel slag aggregate concrete compared to stone chips aggregate concrete as the bond performance of steel slag aggregate concrete is 8% to 20% higher than that of stone chips aggregate concrete.

Energy dissipation capacity has been found to be 4.3% to 32.5% higher for specimens made with recycled aggregate concrete compared to brickbat aggregate concrete. However, the energy dissipation capacity of 8-RCS-S has been found to be 29.4% higher than 7-RCS-RC.

viii. Using different concrete mixes in different components of the same frame weakens the performance of the joint under cyclic excitation even if the concrete mixes are of similar compressive strength and elasticity. Additionally, using steel slag aggregate as a replacement of stone chips aggregate in concrete greatly enhances the performance of the joint. Furthermore, using recycled aggregate as a replacement of brickbat aggregate in concrete slightly enhances the performance of the joint. Thus, steel slag aggregate and recycled aggregate can be used as excellent alternative choices of coarse aggregates in concrete used in reinforced concrete framed structures.

5.3   Recommendations for Future Studies

The focus of this study was to examine the structural performance of reinforced concrete beam-column joints made with different coarse aggregates in the concrete mix. However, there are scopes to conduct further research on structural behavior of joints under cyclic loading. Few of the possible fields where this research can be extended are listed below:

i.   A comprehensive study can be made by involving both experimental and finite element analysis.

ii.   The research can be conducted with strain gauges attached with the specimens which will provide more information about the stress strain behavior of the joint as well as reinforcements.

iii. Experiments have been carried out using quasi-static reversed cyclic loading applied with manually operated push-pull jack while the displacements were recorded using deflection dial gauges. Experiments can be done with dynamic actuators and LVDTs which will provide more realistic data.

iv.   The joints investigated in this study were designed in accordance with BNBC 2020 which does not allow the failure to occur in the joint region. As a result, failure occurred due to flexure near the beam-joint interface in the beam in all the specimens. However, joints not designed to fail in flexure can be studied as joint shear failure is another possible option for failure.

v.   Tests can be conducted on interior beam-column joints as only exterior joints have been studied in this thesis.

vi.   The suitability of two wastes, steel slag and recycled concrete aggregate, as a replacement of conventional coarse aggregates have been studied in this research. The use of more waste materials can be studied as recycling materials can preserve nature as well as help the environment.

Future researchers may extended the work in the abovementioned areas in order to address the existing gap in the present state of the art. The present study will provide a useful guidelines for the future researchers who may study the performance of reinforced concrete joints.

REFERENCES

ACI 318-11 (2011). *Building Code Requirements for Structural Concrete*. American Concrete Institute.

ACI 352R-76 (1976). *Recommendations for Design of Beam-Column Joints in Monolithic Reinforced Concrete Structures.* American Concrete Institute, 73, 375–393.

ACI 352R-02 (2002). *Recommendations for Design of Beam-Column Connections in Monolithic Reinforced Concrete Structures.* American Concrete Institute. Joint ACI-ASCE Committee 352.

ACI 374.1-05 (2014). *Acceptance Criteria for Moment Frames Based on Structural Testing and Commentary.* American Concrete Institute.

Ahmad, S., and Alghamdi, S. A. (2012). A Study on Effect of Coarse Aggregate Type on Concrete Performance. *Arabian Journal for Science and Engineering, 37(7),* 1777-1786.

Armstrong, T. (2013). An Overview of Global Cement Sector Trends. *International cement review.* XXX Technical Congress, FICAM-APCAC, Lima, Peru.

ASCE 31-03 (2003). *Seismic Evaluation of Existing Buildings.* American Society of Civil Engineers.

ASCE 41-17 (2017). *Seismic Evaluation and Retrofit of Existing Buildings.* American Society of Civil Engineers.

ASCE/SEI 7-10 (2010). *Minimum Design Loads for Buildings and Other Structures.* American Society of Civil Engineers.

Azimi, M., Campos, U. A., Matthews, J. C., Lu, H., Tehrani, F. M., Sun, S., and Alam, S. (2020). Experimental and Numerical Study of Cyclic Performance of Reinforced Concrete Exterior Connections with Rectangular-Spiral Reinforcement. *Journal of Structural Engineering, 146*(3), 04019219.

Bai, J. W., Center, M. A. E., and Hueste, M. B. (2003). Seismic retrofit for reinforced concrete building structures. *College Station: Mid-America Earthquake Center, CM-4,* Texas A&M University.

Berredjem, L., Arabi, N., and Molez, L. (2020). Mechanical and durability properties of concrete based on recycled coarse and fine aggregates produced from demolished concrete. *Construction and Building Materials, 246*, 118421.

Beshr, H., Almusallam, A., and Maslehuddin, M. (2003). Effect of coarse aggregate quality on the mechanical properties of high strength concrete. *Construction and Building Materials, 17(2)*, 97–103.

BNBC (2020). Bangladesh National Building Code. Ministry of Works, Bangladesh.

Bolt, B. A. (2021). Earthquake. *Encyclopedia Britannica.*
Retrieved from https://www.britannica.com/science/earthquake-geology

Britannica (2011). Earthquake-resistant structure. *Encyclopedia Britannica*, The Editors of Encyclopedia.
Retrieved from https://www.britannica.com/technology/earthquake-resistant-structure

Butler, L., West, J. S., and Tighe, S. L. (2011). The effect of recycled concrete aggregate properties on the bond strength between RCA concrete and steel reinforcement. *Cement and Concrete Research, 41(10)*, 1037–1049.

Butler, L. J., West, J. S., and Tighe, S. L. (2015). Bond of Reinforcement in Concrete Incorporating Recycled Concrete Aggregates. *Journal of Structural Engineering, 141(3)*.

Chalioris, C. E., Favvata, M. J., and Karayannis, C. G. (2008). Reinforced concrete beam-column joints with crossed inclined bars under cyclic deformations. *Earthquake Engineering and Structural Dynamics, 37(6)*, 881–897.

Cheung, P. C., Pauiay, T., Park, R. (1993). Behaviour of beam-column joints in seismically loaded RC frames. *The Structural Engineer, 71(8)*.

Chung, L., Park, H. S., and Roh, Y. S. (2004). Dynamic and Scale Effects on Reinforced Concrete Beam-Column Joint Structures. *Science and Engineering of Composite Materials, 11*(4), 267-282.

Choudhury, A. H., and Laskar, A. I. (2020). Effect of Hoop Reinforcement Yielding on the Cyclic Behavior of Beam-column Joint. *Journal of Earthquake Engineering.*

Cofer, A. (2015). Earthquake-resistant construction. *Encyclopedia Britannica*. Retrieved from https://www.britannica.com/technology/earthquake-resistant-construction

Cosgun, C., Turk, A. M., Mangir, A., Cosgun, T., and Kiymaz, G. (2019). Experimental behaviour and failure of beam-column joints with plain bars, low-strength concrete and different anchorage details. *Engineering Failure Analysis, 109*, 104247.

Dang, C., and Dinh, N. (2017). Experimental Study on Structural Performance of RC Exterior Beam-Column Joints Retrofitted by Steel Jacketing and Haunch Element under Cyclic Loading Simulating Earthquake Excitation. *Advances in Civil Engineering, 2017,* 9263460.

Elahi, T. E. (2021). Characteristics of Compressed Stabilized Earth Blocks Fabricated With Fly Ash and Steel Slag. *M.Sc. thesis*. Department of Civil Engineering, Bangladesh University of Engineering and Technology, Dhaka.

Eligehausen, R., Popov, E. P. and Bertero, V. V. (1983). Local Bond Stress-slip Relationships of Deformed Bars under Generalized Excitations. *Report UCB/EERC-83/19, Earthquake Engineering Research Center,* University of California.

FEMA P749-10 (2010). Earthquake-Resistant Design Concepts: An Introduction to the NEHRP Recommended Provisions Seismic Provisions. National Institute of Building Sciences, Building Seismic Safety Council, Washington, D. C.

FEMA P-751 (2012). 2009 NEHRP Recommended Seismic Provisions: Design Examples. National Institute of Building Sciences, Building Seismic Safety Council, Washington, D. C.

Genesio, G., Sharma, A., Eligehausen, R., Pampanin, S., Reddy, G. R., Vaze, K. K. (2010). Experimental Investigations on Seismic Retrofitting of Reinforced Concrete Beam-Column Joints. *Roorkee, India: 14th Symposium on Earthquake Engineering (14SEE), 17-19 Dec 2010.* (paper no. A007).

Ghobarah, A., and El-Amoury, T. (2005). Seismic Rehabilitation of Deficient Exterior Concrete Frame Joints. *Journal of Composites for Construction, 9(5)*, 408-416.

Giatec Scientific (2017). The History of Concrete. Retrieved from https://www.giatecscientific.com/education/the-history-of-concrete/

Gil-Martín, L. M., Rodríguez-Suesca, A. E., Fernández-Ruiz, M. A., and Hernández-Montes, E. (2019). Cyclic behavior of RC beam-column joints with epoxy resin and ground tire rubber as partial cement replacement. *Construction and Building Materials. 211*, 659-674.

Hamahara, M., Nishiyama, M., Okamoto, H., and Watanabe, F. (2007). Design for Shear of Prestressed Concrete Beam-Column Joint Cores. *Journal of Structural Engineering, 133*, 1520-1530.

Hoque, M. M., and Hossen, M. A. (2019). Sustainable Use of Steel Industry Slag (SIS) for Concrete Production. *Open Journal of Applied Sciences, 9(12)*, 841-850.

Hoque, M. M., Islam, M. N., Islam, M., and Kader, M. A. (2020). Bond behavior of reinforcing bars embedded in concrete made with crushed clay bricks as coarse aggregates. *Construction and Building Materials, 244*, 118364.

Hossain, M. K., Rashid, M. A., and Karim, M. R. (2015). Effect of Cement Content and Size of Coarse Aggregate on the Strength of Brick Aggregate Concrete. *DUET Journal, 2 (2)*.

Ichinose, T. (1991). Interaction between Bond at Beam Bars and Shear Reinforcement in RC Interior Joints. *Symposium Paper, American Concrete Institute, 123*, 379-400.

Indian Institute of Technology, Kanpur (2002). *Earthquake Tips,* Building Materials and Technology Promotion Council, New Delhi, India.

Jahan, M. K. E. (2016). Experimental investigation of an RC exterior beam column joint behavior strengthened with FRP. *M.Sc. thesis*. Department of Civil Engineering, Bangladesh University of Engineering and Technology, Dhaka.

Kalra, M., and Mehmood, G. (2018). A Review paper on the Effect of different types of coarse aggregate on Concrete. *IOP Conference Series: Materials Science and Engineering.* 431 082001.

Khan, M. I., Al-Osta, M. A., Ahmad, S., and Rahman, M. K. (2018). Seismic Behavior of Beam-Column Joints Strengthened With Ultra-High Performance Fiber Reinforced Concrete. *Composite Structures*, *200*, 103-119.

Khan, S. S., (2014). Experimental investigation on seismic performance of reinforced concrete beam-column joints with and without adequate ties at joint region. *M.Sc. thesis*. Department of Civil Engineering, Bangladesh University of Engineering and Technology, Dhaka.

Kibria, B. M. G., (2014). Experimental investigation on behavior of reinforced concrete (RC) interior beam column joints retrofitted with fiber reinforced polymers (FRP). *M.Sc. thesis*. Department of Civil Engineering, Bangladesh University of Engineering and Technology, Dhaka.

Kibria, B. M. G., Ahmed, F., Ahsan, R., and Ansary, M. A. (2020). Experimental investigation on behavior of reinforced concrete interior beam column joints retrofitted with fiber reinforced polymers. *Asian Journal of Civil Engineering, 21*, 157–171.

Kim, J., LaFave, J. M., and Song, J. (2007). A new statistical approach for joint shear strength determination of RC beam-column connections subjected to lateral earthquake loading. *Structural Engineering and Mechanics, 27(4),* 439-456.

Kim, S. W., Lee, Y. J., Jung, Y. J., Lee, J. Y., and Kim, K. H. (2014). Applicability of electric arc furnace oxidising slag aggregates for RC columns subjected to combined bending and axial loads. *Materials Research Innovations, 18(sup2)*, S2–793–S2–798.

Kim, S. W., Lee, Y. J., and Kim, K. H. (2012). Bond Behavior of RC Beams with Electric Arc Furnace Oxidizing Slag Aggregates. *Journal of Asian Architecture and Building Engineering, 11(2)*, 359–366.

Lee, J., Choi, T., Yuan, T., Yoon, Y., and Mitchell, D. (2019). Comparing Properties of Concrete Containing Electric Arc Furnace Slag and Granulated Blast Furnace Slag. *Materials*, 12, 1371 (2019).

Lee, Y. J., Kim, H. G., Kim, M. J., Kim, D. H., Kim, D. S., and Kim, K. H. (2020). Bond performance of reinforced concrete beams with electric arc furnace slag aggregates. Construction and Building Materials, 244, 118366.

Li, B., Lam, E. S., Wu, B., and Wang, Y. (2013). Experimental investigation on reinforced concrete interior beam-column joints rehabilitated by ferrocement jackets. Engineering Structures, 56, 897-909.

Lima, C., Martinelli, E., and Faella, C. (2012). Capacity models for shear strength of exterior joints in RC frames: state-of-the-art and synoptic examination. *Bulletin of Earthquake Engineering, 10*, 967-983.

Mady, M., El-Ragaby, A., and El-Salakawy, E. F. (2011). Experimental Investigation on the Seismic Performance of Beam-Column Joints Reinforced with GFRP Bars. *Journal of Earthquake Engineering, 15*(1), 77-98.

Majumder, S., and Saha, S. (2020). Experimental and numerical investigation on cyclic behaviour of RC beam column joints reinforced with geogrid material. *Materials Today: Proceedings.*

Meyer, C. (2009). The greening of the concrete industry. *Cement & Concrete Composites, 31(8)*, 601-605.

Mohammed, T. U., Hasan, P., Islam, B. K. M. A., Hasnat, A., and Sharkia, S. (2012). Investigation of Differente Cement Brands Commonly Used in Bangladesh. *Third International Conference on Construction in Developing Countries (ICCIDC–III),* July 4-6, 2012. Bangkok, Thailand.

Mohammed, T. U., Mahmood, A. H., Chowdhury, I. M., Humayun, A. M., and Ahmed, T. (2016). Sustainability of Construction Materials in Bangladesh. *Fourth International Conference on Sustainable Construction Materials and Technologies.* Las Vegas, USA, August 7-11, 2016.

Mukherjee, A., and Joshi, M. (2005). FRPC reinforced concrete beam-column joints under cyclic excitation. *Composite Structures*, *70*, 185-199.

Nilson, A. H., Darwin, D., and Dolan, C. W. (2010). *Design of Concrete Structures,* 14th Edition, McGraw-Hill Companies, Inc.

Ogunbayo, B. F., Ajao, A. M., Ogundipe, K. E., Joshua, O., Durotoye, T. O., and Bamigboye, G. (2018). Study of aggregate dormancy and its effects on the properties of aggregates and concrete. *Cogent Engineering, 5(1)*.

Özturan, T., and Çeçen, C. (1997). Effect of coarse aggregate type on mechanical properties of concretes with different strengths. *Cement and Concrete Research, 27(2)*, 165–170.

Pampanin, S., Calvi, G. M., Moratti, M. (2002). Seismic Behavior of R.C. Beam-Column Joints Designed for Gravity Only. *London: 12th European Conference on Earthquake Engineering, Sep 2002.* 726. Elsevier Science Ltd.

Park, R. (1988). Ductility Evaluation from Laboratory and Analytical Testing. *Proceedings of Ninth World Conference on Earthquake Engineering, Vol. VIII,* Aug 1988, Tokyo-Kyoto, Japan.

Paulay, T., and Priestley, M. J. N. (1992). *Seismic Design of Reinforced Concrete and Masonry Buildings.* John Wiley & Sons, Inc.

Prota, A., Nanni, A., Manfredi, G., and Cosenza, E. (2004). Selective Upgrade of Underdesigned Reinforced Concrete Beam-Column Joints Using Carbon Fiber-Reinforced Polymers. *Structural Journal, 101(5),* 699–707.

Rahman, M. M., Jadhav, S. M., and Shahrooz, B. M. (2018). Seismic performance of reinforce concrete buildings designed according to codes in Bangladesh, India and U.S. *Engineering Structures, 160*, 111–120.

Realfonzo, R., Napoli, A., and Pinilla, J. G. R. (2014). Cyclic behavior of RC beam-column joints strengthened with FRP systems. *Construction and Building Materials, 54,* 282-297.

Rezaul, R. M., Atahar, R., Tasnim, T. B., Kurny, A. S. W., Momtaz, R., and Gulshan, F. (2017). Reuse of Induction Furnace Steel Slag as a Replacement of Coarse Aggregate in Construction. *International Conference on Mechanical Engineering and Renewable Energy 2017 (ICMERE 2017), 18 – 20 December, 2017*, Chittagong, Bangladesh.

Saha, P., and Meesaraganda, L. V. (2019). Experimental investigation of reinforced SCC beam-column joint with rectangular spiral reinforcement under cyclic loading. *Construction and Building Materials, 201,* 171-185.

Saha, A. S., (2019). Mechanical properties of concrete using stone, brick chips and recycled concrete as aggregate. *M.Sc. thesis*. Department of Civil Engineering, Bangladesh University of Engineering and Technology, Dhaka.

Saiada, F. F., (2014). Experimental investigation on performance of beam column frames with column kickers. *M.Sc. thesis*. Department of Civil Engineering, Bangladesh University of Engineering and Technology, Dhaka.

Saravanan, M., Goswami, R., and Palani, G. S. (2021). Energy dissipative beam-column connection for earthquake resistant moment frames. *Journal of Constructional Steel Research, 176, 106428*.

Sasmal, S., and Ramanjaneyulu, K. (2012). Evaluation of Strength Hierarchy of Beam-Column Joints of Existing RC Structures under Seismic Type Loading. *Journal of Earthquake Engineering, 16*(6), 897-915.

Shen, X., Li, B., Chen, Y., and Tizani, W. (2021). Seismic performance of reinforced concrete interior beam-column joints with novel reinforcement detail. *Engineering Structures, 227,* 111408.

Siddique, A. F. A. (2018). Seismic Performance Evaluation of Concrete Bridges. *B.Sc. thesis*. Department of Civil Engineering, Bangladesh University of Engineering and Technology, Dhaka.

Siddique, A. F. A., Hossain, T. R. (2020). Seismic Behavior of Concrete Bridge Piers of Different Dimensions. *5th International Conference on Civil Engineering for Sustainable Development*, Khulna University of Engineering and Technology, Khulna.

Siddique, A. F. A., Hossain, T. R. (2020). Seismic Performance Evaluation of Bridge Piers Resting on Different Soil Classes. *IABSE-JSCE Joint Conference on Advances in Bridge Engineering-IV*, Dhaka, Bangladesh.

Syed, Z. I., Mohamed, O. A., Murad, K., and Kewalramani, M. (2017). Performance of Earthquake-resistant RCC Frame Structures under Blast Explosions. *Procedia Engineering, 180,* 82–90.

Takagi, J., and Wada, A. (2018). Recent earthquakes and the need for a new philosophy for earthquake-resistant design. *Soil Dynamics and Earthquake Engineering*.

Uddin, M. T. (2013). Sustainable Development of Concrete Construction Works in Bangladesh: Key Issues. *Third International Conference on Sustainable Construction Materials and Technologies.*

Uma, S. R. and Prasad, A. M. (2006) Seismic behavior of beam-column joints in RC moment resisting frames: A review. *Indian Concrete Journal, 80(1),* 33-42.

Uma, S. R. and Prasad, A. M. Seismic Behavior of Beam Column Joints in Reinforced Concrete Moment Resisting Frames. *Document No. IITK-GSDMA-EQ31-V1.0,* IITK-GSDMA Project on Building Codes.

Wight, J. K., and Macgregor, J. G. (2012). *Reinforced Concrete Mechanics and Design.* 6th Edition. Pearson Education, Inc., Upper Saddle River, New Jersey 07458.

Wu, K. R., Chen, B., Yao, W., and Zhang, D. (2001). Effect of coarse aggregate type on mechanical properties of high-performance concrete. *Cement and Concrete Research, 31(10)*, 1421–1425.

Xiao, J., and Falkner, H. (2007). Bond behaviour between recycled aggregate concrete and steel rebars. *Construction and Building Materials, 21(2)*, 395–401.

Zhanga, Z., Ding, R., Nie, X., and Fan, J. (2020). Seismic performance of a novel interior precast concrete beam-column joint using ultra-high performance concrete. *Engineering Structures, 222,* 111145.

Zhou, C., and Chen, Z. (2017). Mechanical properties of recycled concrete made with different types of coarse aggregate. *Construction and Building Materials, 134*, 497–506.

APPENDIX A1: Sieve analysis of aggregates

Table A1.1: Sieve analysis of sand

Sieve Designation	Sieve Size	Material Retained	Percent of Material Retained	Cumulative % Retained	Percent Finer	Fineness Modulus
	mm	gm	%	%	%	
No. 4	4.75	0	0	0	100	
No. 8	2.36	26	5	5	95	
No. 16	1.18	102	20	25	75	
No. 30	0.6	229	46	71	29	**2.92**
No. 50	0.3	108	22	93	7	
No. 100	0.15	25	5	98	2	
	Pan	8	2			
	Total	498	100			

Table A1.2: Sieve analysis of stone chips

Sieve Designation	Sieve Size	Material Retained	Percent of Material Retained	Cumulative % Retained	Percent Finer	Fineness Modulus
	mm	gm	%	%	%	
3/4"	19	0	0	0	100	
3/8"	9.5	113	5	5	95	
No. 4	4.75	1808	85	90	10	
No. 8	2.36	217	10	100	0	
No. 16	1.18	0	0	100	0	
No. 30	0.6	0	0	100	0	**5.95**
No. 50	0.3	0	0	100	0	
No. 100	0.15	0	0	100	0	
	Pan	0	0			
	Total	2138	100			

Table A1.3: Sieve analysis of brickbats

Sieve Designation	Sieve Size	Material Retained	Percent of Material Retained	Cumulative % Retained	Percent Finer	Fineness Modulus
	mm	gm	%	%	%	
3/4"	19	0	0	0	100	
3/8"	9.5	138	7	7	93	
No. 4	4.75	1705	86.5	93.5	7	
No. 8	2.36	128	6.5	100	0	
No. 16	1.18	0	0	100	0	
No. 30	0.6	0	0	100	0	**6.01**
No. 50	0.3	0	0	100	0	
No. 100	0.15	0	0	100	0	
	Pan	0	0			
	Total	1971	100			

Table A1.4: Sieve analysis of steel slags

Sieve Designation	Sieve Size	Material Retained	Percent of Material Retained	Cumulative % Retained	Percent Finer	Fineness Modulus
	mm	gm	%	%	%	
3/4"	19	0	0	0	100	
3/8"	9.5	91	4.6	4.6	95	
No. 4	4.75	1821	92.1	96.7	3	
No. 8	2.36	63	3.2	99.9	0	
No. 16	1.18	2	0.1	100	0	**6.01**
No. 30	0.6	0	0	100	0	
No. 50	0.3	0	0	100	0	
No. 100	0.15	0	0	100	0	
	Pan	0	0			
	Total	1977	100			

Table A1.5: Sieve analysis of recycled concrete

Sieve Designation	Sieve Size	Material Retained	Percent of Material Retained	Cumulative % Retained	Percent Finer	Fineness Modulus
	mm	gm	%	%	%	
3/4"	19	0	0	0	100	
3/8"	9.5	28	1.4	1.4	99	
No. 4	4.75	1702	85.2	86.6	13	
No. 8	2.36	260	13	99.6	0	
No. 16	1.18	6	0.3	99.9	0	**5.88**
No. 30	0.6	1	0.1	100	0	
No. 50	0.3	0	0	100	0	
No. 100	0.15	0	0	100	0	
	Pan	0	0			
	Total	1997	100			

APPENDIX A2: Load versus deflection graphs for steel reinforcements
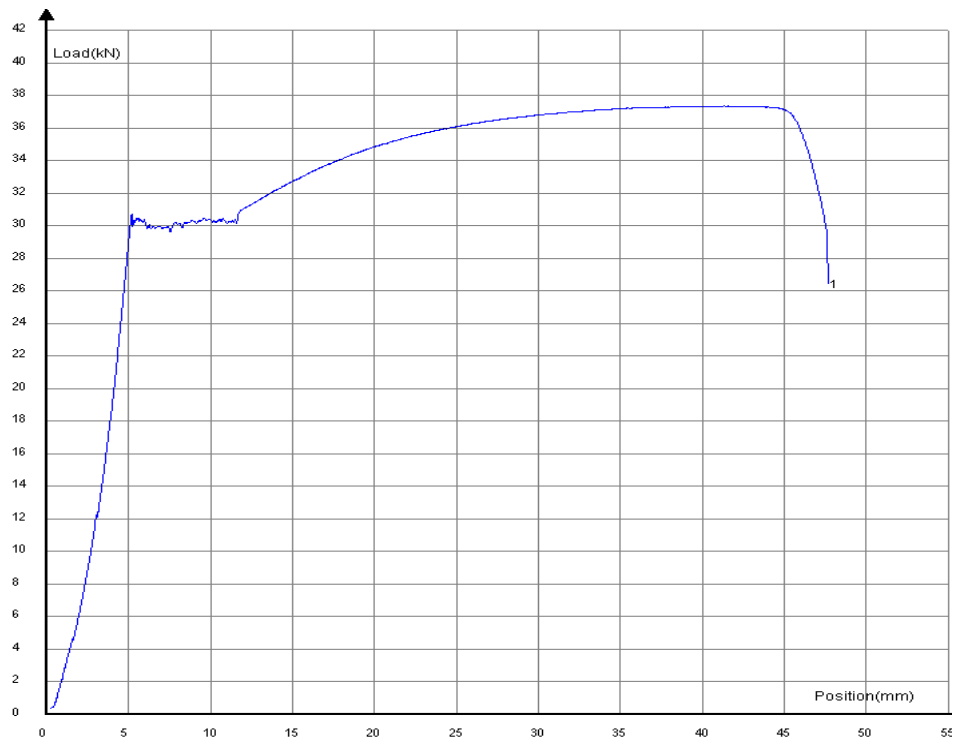
Figure A2.1: Load versus deflection graph for 8 mm bars (sl. no. 1)
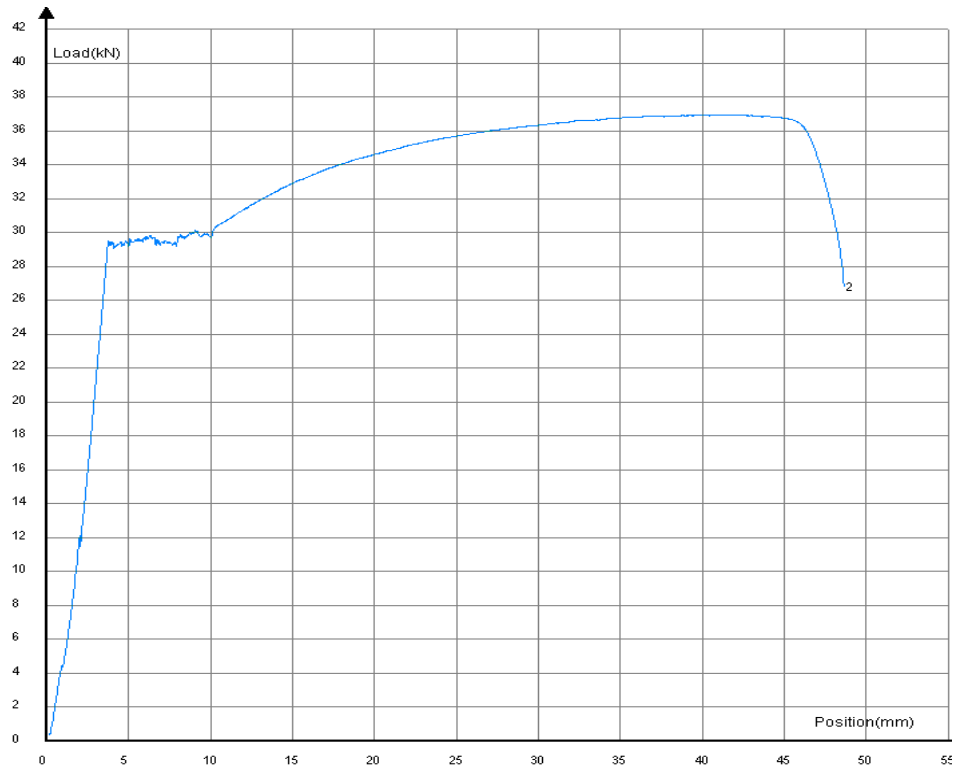
Figure A2.2: Load versus deflection graph for 8 mm bars (sl. no. 2)
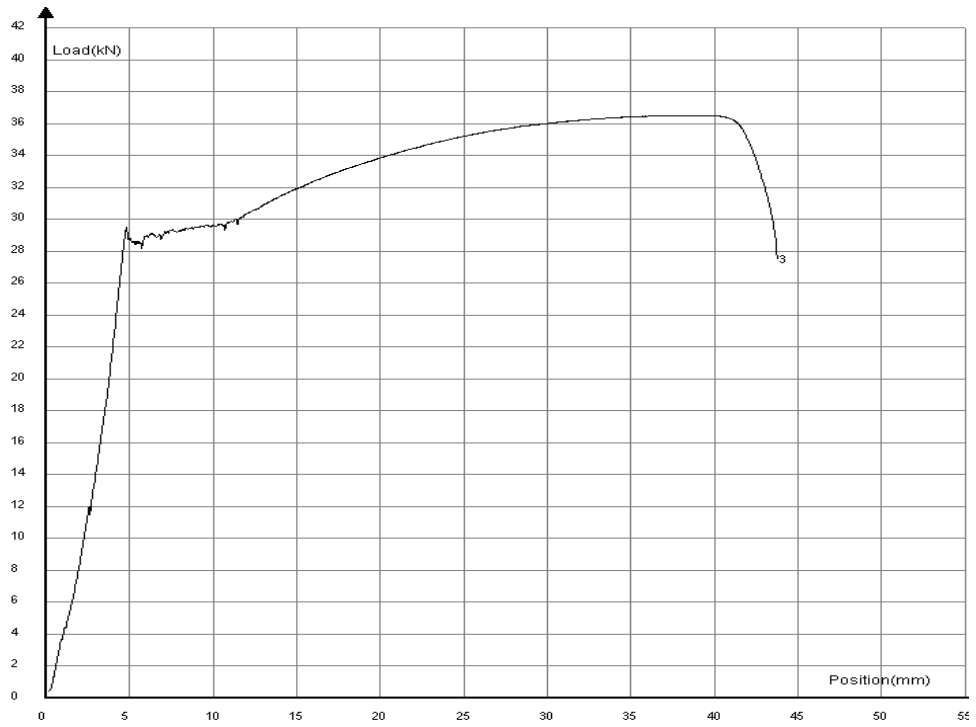
Figure A2.3: Load versus deflection graph for 8 mm bars (sl. no. 3)
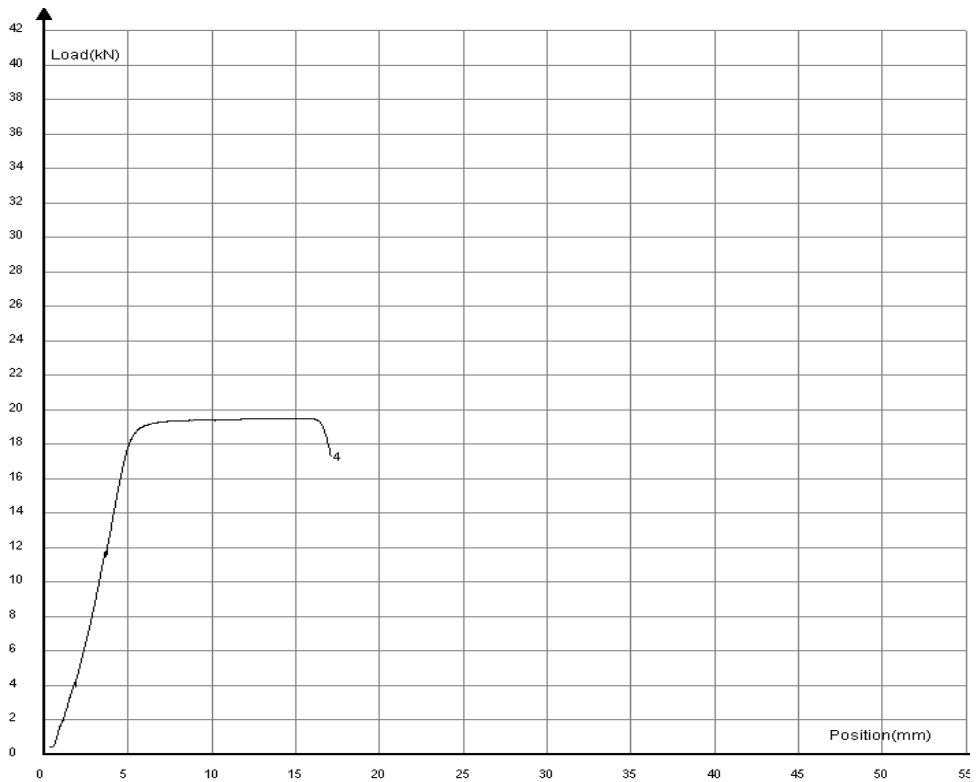
Figure A2.4: Load versus deflection graph for 6 mm bars (sl. no. 1)

137
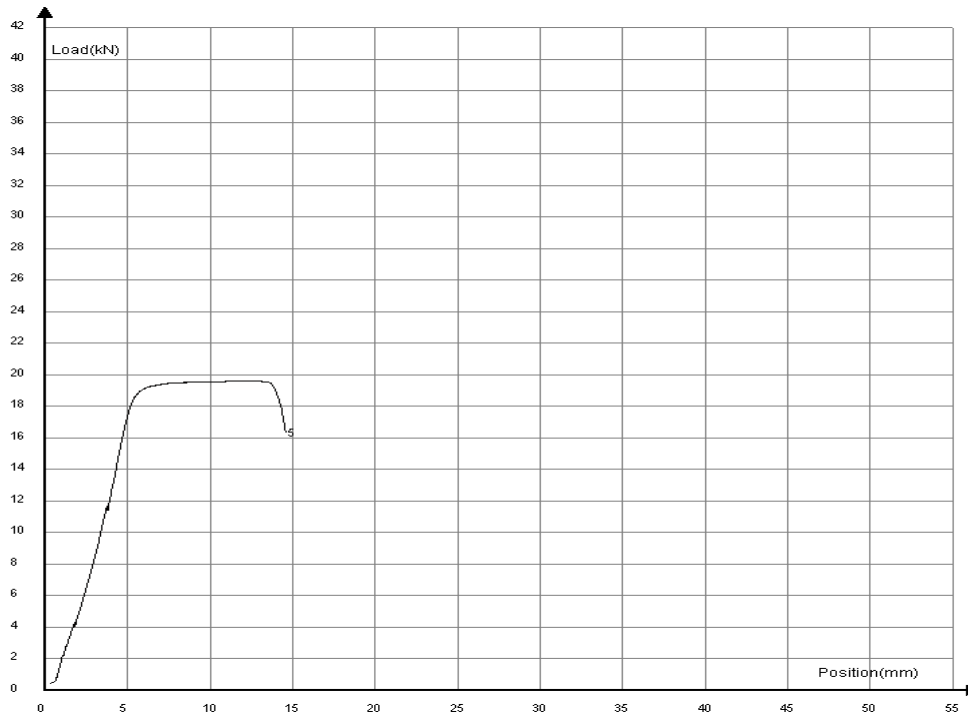
Figure A2.5: Load versus deflection graph for 6 mm bars (sl. no. 2)
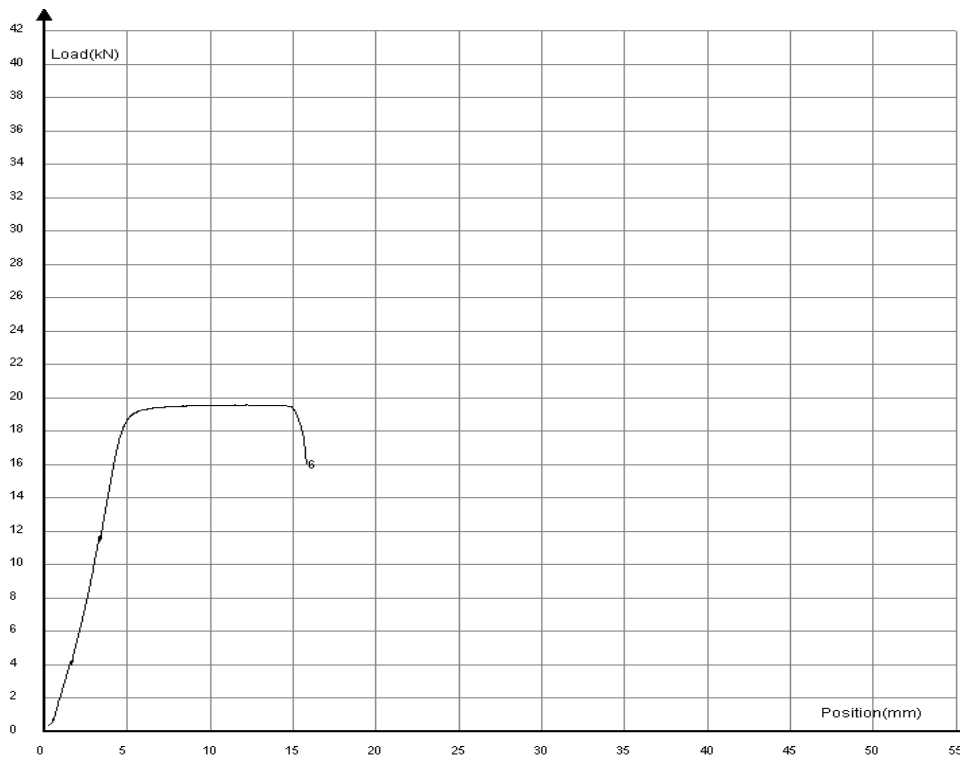
Figure A2.6: Load versus deflection graph for 6 mm bars (sl. no. 3)

APPENDIX A3: Stress versus strain graphs for concrete
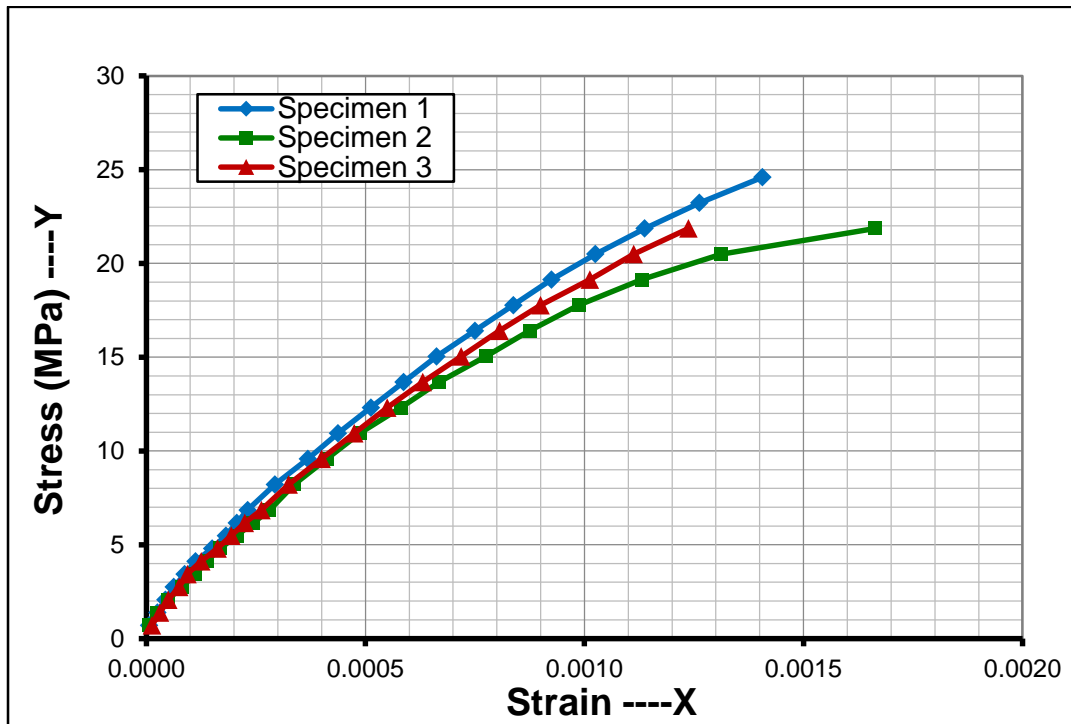
Figure A3.1: Stress versus strain graph for stone chips aggregate concrete
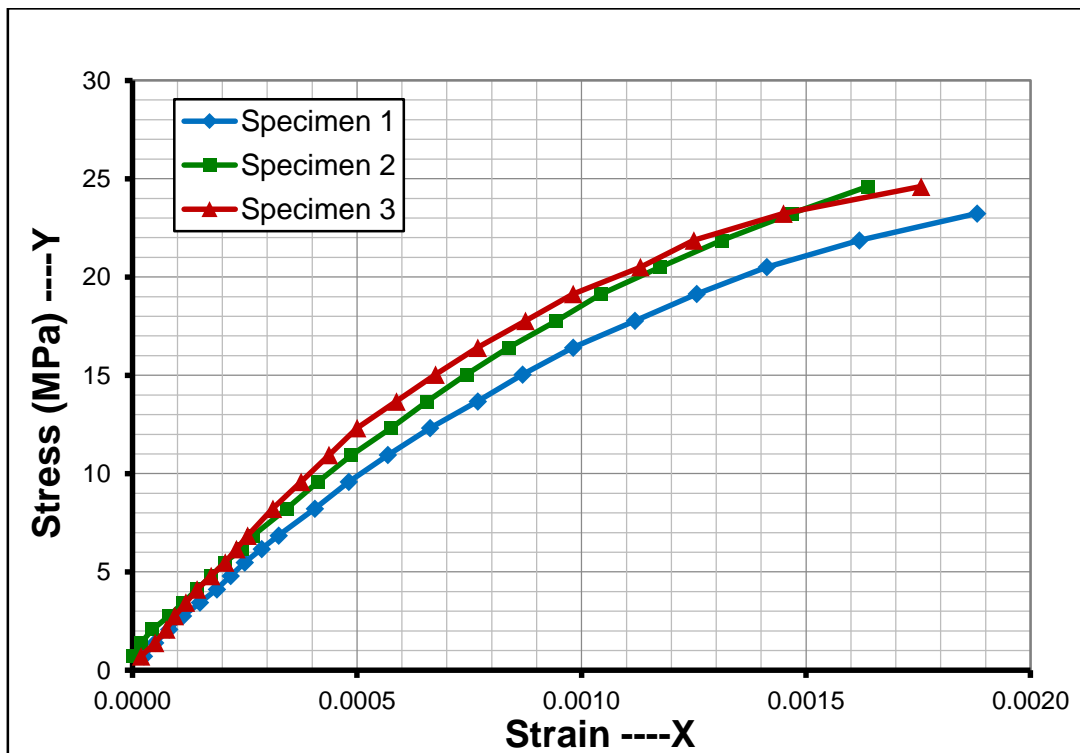
Figure A3.2: Stress versus strain graph for brickbat aggregate concrete
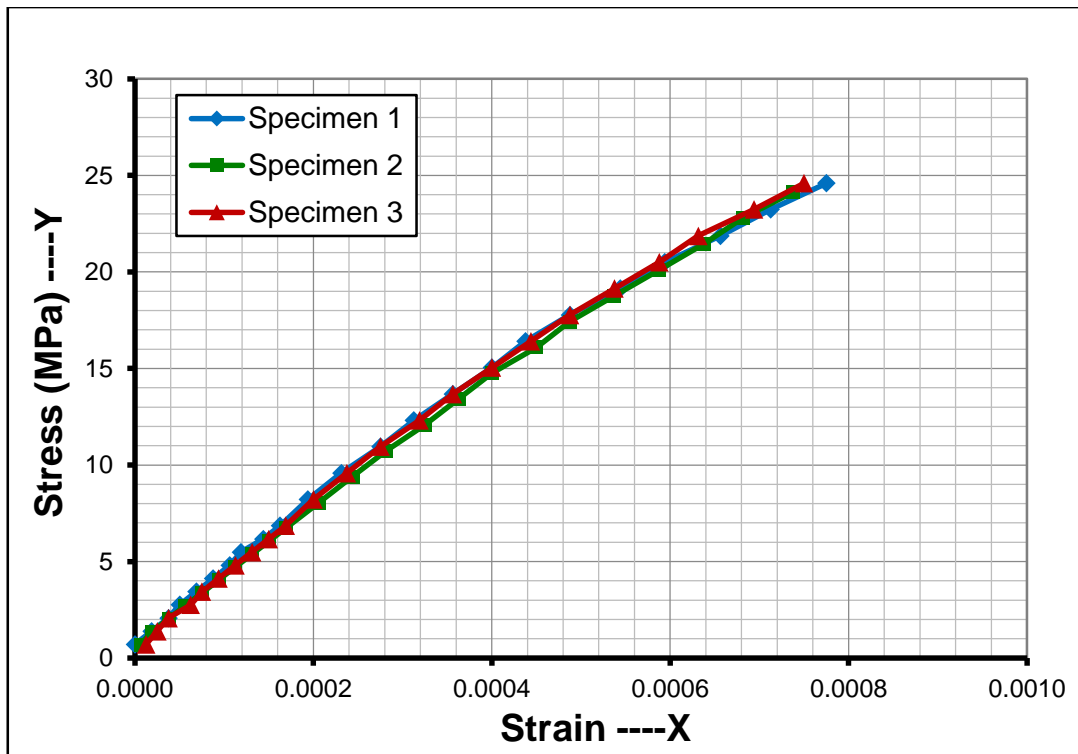
Figure A3.3: Stress versus strain graph for steel slag aggregate concrete
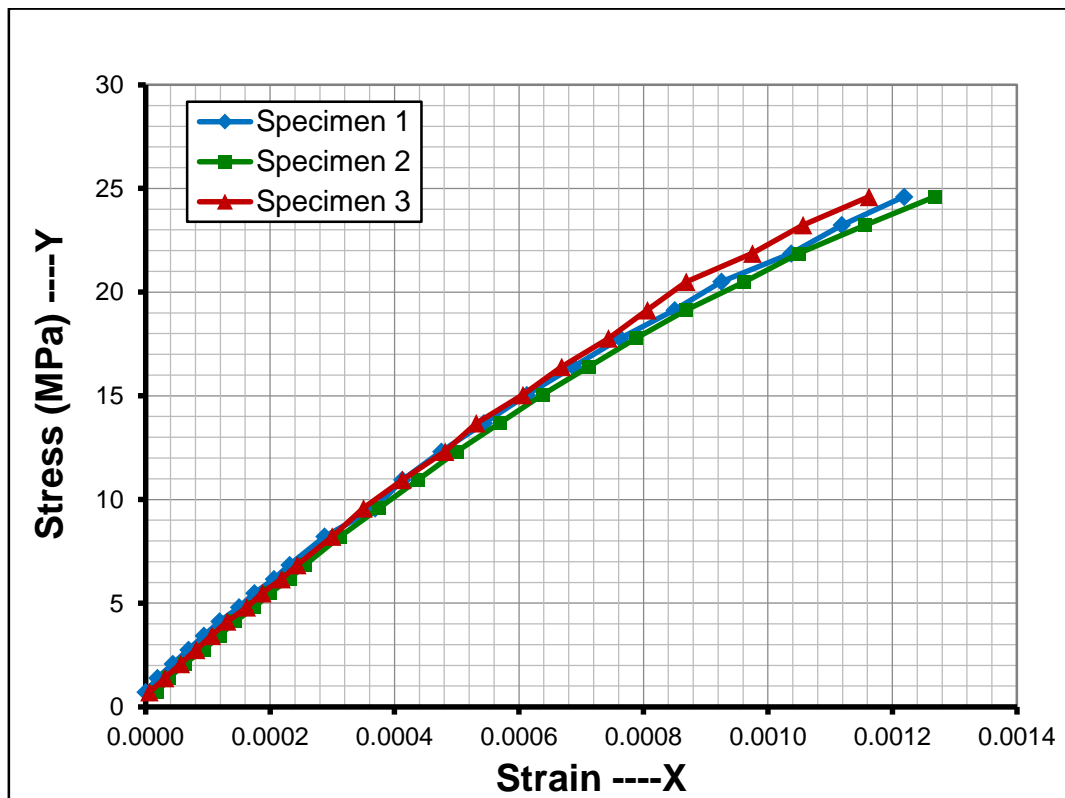
Figure A3.4: Stress versus strain graph for recycle concrete aggregate concrete

APPENDIX B: Design of beam-column joints

Table B1: Yield moment capacity of columns

Specimen	f_c' (MPa)	f_y (MPa)	b (mm)	d (mm)	A_s (mm^2)	a=$A_s f_y$/ 0.85f_c'b (mm)	Applied load at length (mm)	Yield Moment, M $A_s f_y$(d-a/2) (kN-m)	Lateral yield load capacity of beam (kN)
1-SS-C1	27.4	602.5	120	135	99.2	21.4	700	7.43	10.6
2-BB-C2	28.3	602.5	120	135	99.2	20.7	700	7.45	10.7
3-BS-B	27.4	602.5	120	135	99.2	21.4	700	7.43	10.6
4-BS-S	27.4	602.5	120	135	99.2	21.4	700	7.43	10.6
5-BSS-B	36.3	602.5	120	135	99.2	16.2	700	7.59	10.8
6-BSS-SS	36.3	602.5	120	135	99.2	16.2	700	7.59	10.8
7-RCS-RC	27.4	602.5	120	135	99.2	21.4	700	7.43	10.6
8-RCS-S	27.4	602.5	120	135	99.2	21.4	700	7.43	10.6

Table B2: Yield moment capacity of beams

Specimen	f_c' (MPa)	f_y (MPa)	b (mm)	d (mm)	A_s (mm^2)	a=$A_s f_y$/ 0.85f_c'b (mm)	Applied load at length (mm)	Yield Moment, M $A_s f_y$(d-a/2) (kN-m)	Lateral yield load capacity of beam (kN)
1-SS-C1	27.4	654.5	120	135	85.7	20.1	700	7.01	10.0
2-BB-C2	28.3	654.5	120	135	85.7	19.4	700	7.03	10.0
3-BS-B	28.3	654.5	120	135	85.7	19.4	700	7.03	10.0
4-BS-S	28.3	654.5	120	135	85.7	19.4	700	7.03	10.0
5-BSS-B	28.3	654.5	120	135	85.7	19.4	700	7.03	10.0
6-BSS-SS	28.3	654.5	120	135	85.7	19.4	700	7.03	10.0
7-RCS-RC	32	654.5	120	135	85.7	17.2	700	7.09	10.1
8-RCS-S	32	654.5	120	135	85.7	17.2	700	7.09	10.1

Table B3: Joint shear demands and capacities

Specimen	f_c' (MPa)	f_c' (psi)	f_y (MPa)	l_c (mm)	A_j (mm²)	A_s (mm²)	$T_{pr} = \alpha A_s f_y$ (kN)	$M_{pr}=A_s f_y$ (d-a/2) (kN-m)	Joint Shear Demand $V_{jh}=T_{pr} - M_{pr}/l_c$ (kN)	Joint Shear Capacity $\phi V_n = \varphi \gamma \sqrt{f_c'} A_j$ (lb)	Joint Shear Capacity ϕV_n (kN)
1-SS-C1	27.4	3980	654.5	1400	18000	85.7	70.1	7.01	65.1	19802	88.1
2-BB-C2	28.3	4100	654.5	1400	18000	85.7	70.1	7.03	65.1	20098	89.4
3-BS-B	28.3	4100	654.5	1400	18000	85.7	70.1	7.03	65.1	20098	89.4
4-BS-S	27.4	3980	654.5	1400	18000	85.7	70.1	7.03	65.1	19802	88.1
5-BSS-B	28.3	4100	654.5	1400	18000	85.7	70.1	7.03	65.1	20098	89.4
6-BSS-SS	36.3	5270	654.5	1400	18000	85.7	70.1	7.03	65.1	22786	101.4
7-RCS-RC	32	4640	654.5	1400	18000	85.7	70.1	7.09	65.1	21380	95.1
8-RCS-S	27.4	3980	654.5	1400	18000	85.7	70.1	7.09	65.1	19802	88.1

APPENDIX C: Peak load versus deflection data for all specimens

Table C1: Peak load versus deflection data for 1-SS-C1

Cycle	Peak Load (Forward Cycle) (kN)	Displacement (Forward Cycle) (mm)	Peak Load (Reverse Cycle) (kN)	Displacement (Reverse Cycle) (mm)
1	4.41	1.77	-11.39	-1.75
2	7.11	3.56	-14.47	-3.52
3	9.42	5.28	-17.55	-4.96
4	11.74	7.10	-19.10	-6.98
5	13.28	8.75	-20.25	-8.75
6	13.28	10.01	-20.64	-10.67
7	12.89	13.97	-18.33	-14.20
8	11.74	16.77	-16.01	-16.33

Table C2: Peak load versus deflection data for 2-BB-C2

Cycle	Peak Load (Forward Cycle) (kN)	Displacement (Forward Cycle) (mm)	Peak Load (Reverse Cycle) (kN)	Displacement (Reverse Cycle) (mm)
1	4.80	1.68	-10.62	-1.81
2	7.88	3.44	-13.70	-3.49
3	10.97	5.29	-16.78	-5.25
4	14.05	7.5	-19.87	-7.48
5	14.82	8.55	-20.64	-8.78
6	15.98	10.56	-20.64	-10.54
7	16.36	14.01	-20.64	-14.08
8	14.82	16.84	-19.87	-17.07

Table C3: Peak load versus deflection data for 3-BS-B

Cycle	Peak Load (Forward Cycle) (kN)	Displacement (Forward Cycle) (mm)	Peak Load (Reverse Cycle) (kN)	Displacement (Reverse Cycle) (mm)
1	4.41	1.76	-11.00	-1.75
2	7.11	3.52	-14.47	-3.52
3	10.19	5.19	-17.55	-5.19
4	12.51	6.82	-21.41	-7.02
5	12.51	7.23	-22.95	-8.82
6	14.82	10.33	-21.41	-10.52
7	15.20	14.03	-20.64	-14.46
8	14.43	17.31	-11.39	-10.38

Table C4: Peak load versus deflection data for 4-BS-S

Cycle	Peak Load (Forward Cycle) (kN)	Displacement (Forward Cycle) (mm)	Peak Load (Reverse Cycle) (kN)	Displacement (Reverse Cycle) (mm)
1	4.80	1.97	-12.93	-1.78
2	6.34	3.51	-15.24	-3.35
3	8.65	5.26	-17.55	-5.3
4	10.58	7	-22.18	-6.92
5	12.51	8.75	-22.18	-8.76
6	12.51	10.53	-20.64	-10.02
7	12.51	14.02	-19.10	-13.6
8	10.97	15.33	-12.93	-12.1

Table C5: Peak load versus deflection data for 5-BSS-B

Cycle	Peak Load (Forward Cycle) (kN)	Displacement (Forward Cycle) (mm)	Peak Load (Reverse Cycle) (kN)	Displacement (Reverse Cycle) (mm)
1	4.80	1.7	-10.62	-1.77
2	7.11	3.51	-14.47	-3.5
3	10.19	5.28	-17.55	-5.09
4	12.51	7.01	-19.87	-6.88
5	14.05	8.85	-21.41	-8.76
6	14.82	10.52	-21.41	-10.45
7	15.59	14.02	-20.64	-13.97
8	14.05	15.71	-13.70	-12.78

Table C6: Peak load versus deflection data for 6-BSS-SS

Cycle	Peak Load (Forward Cycle) (kN)	Displacement (Forward Cycle) (mm)	Peak Load (Reverse Cycle) (kN)	Displacement (Reverse Cycle) (mm)
1	4.80	1.8	-11.39	-1.75
2	7.88	3.24	-15.24	-3.45
3	12.12	5.31	-17.55	-5.07
4	14.82	7	-21.02	-7
5	15.98	8.76	-21.41	-8.74
6	16.36	10.54	-21.41	-10.58
7	16.75	13.94	-20.64	-14.08
8	7.88	20.28	-7.53	-20.39

Table C7: Peak load versus deflection data for 7-RCS-RC

Cycle	Peak Load (Forward Cycle) (kN)	Displacement (Forward Cycle) (mm)	Peak Load (Reverse Cycle) (kN)	Displacement (Reverse Cycle) (mm)
1	4.41	1.79	-9.85	-1.79
2	7.11	3.53	-14.09	-3.51
3	9.42	5.28	-17.17	-5.3
4	10.97	7.03	-19.87	-6.94
5	12.51	8.9	-21.41	-8.72
6	13.28	10.47	-21.41	-10.54
7	13.66	13.96	-20.64	-14.49
8	14.82	18.99	-12.93	-11.23

Table C8: Peak load versus deflection data for 8-RCS-S

Cycle	Peak Load (Forward Cycle) (kN)	Displacement (Forward Cycle) (mm)	Peak Load (Reverse Cycle) (kN)	Displacement (Reverse Cycle) (mm)
1	4.92	1.93	-13.16	-1.73
2	7.28	3.5	-16.30	-3.42
3	9.64	5	-20.23	-5.26
4	12.78	7.04	-22.59	-7.06
5	15.14	8.76	-23.38	-8.78
6	16.71	10.71	-22.59	-10.49
7	17.89	14.13	-21.80	-14.02
8	16.32	17.02	-20.23	-18.95

APPENDIX D: Peak moment versus rotation data for all specimens

Table D1: Peak moment versus rotation data for 1-SS-C1

Cycle	Peak Moment (Forward Cycle) (kN-mm)	Beam-Joint Rotation (Forward Cycle) (degree)	Column-Joint Rotation (Forward Cycle) (degree)	Peak Moment (Reverse Cycle) (kN-mm)	Beam-Joint Rotation (Reverse Cycle) (degree)	Column-Joint Rotation (Reverse Cycle) (degree)
1	3090	0.15	0.00	-7972	-0.10	0.05
2	4978	0.20	-0.01	-10130	-0.18	-0.06
3	6597	0.27	0.01	-12288	-0.28	-0.08
4	8215	0.40	0.03	-13367	-0.35	-0.11
5	9295	0.48	0.06	-14177	-0.56	-0.11
6	9295	0.71	0.07	-14446	-0.81	-0.15
7	9025	1.09	0.14	-12828	-1.27	-0.08
8	8215	1.67	0.18	-11209	-1.47	-0.11

Table D2: Peak moment versus rotation data for 2-BB-C2

Cycle	Peak Moment (Forward Cycle) (kN-mm)	Beam-Joint Rotation (Forward Cycle) (degree)	Column-Joint Rotation (Forward Cycle) (degree)	Peak Moment (Reverse Cycle) (kN-mm)	Beam-Joint Rotation (Reverse Cycle) (degree)	Column-Joint Rotation (Reverse Cycle) (degree)
1	3359	0.11	0.02	-7432	-0.09	0.02
2	5518	0.19	0.06	-9590	-0.16	0.05
3	7676	0.28	0.10	-11749	-0.28	0.05
4	9834	0.41	0.15	-13907	-0.46	0.05
5	10374	0.42	0.17	-14446	-0.59	0.05
6	11183	0.53	0.21	-14446	-0.76	0.05
7	11453	0.88	0.26	-14446	-1.18	0.05
8	10374	1.21	0.34	-13907	-1.60	0.13

Table D3: Peak moment versus rotation data for 3-BS-B

Cycle	Peak Moment (Forward Cycle) (kN-mm)	Beam-Joint Rotation (Forward Cycle) (degree)	Column-Joint Rotation (Forward Cycle) (degree)	Peak Moment (Reverse Cycle) (kN-mm)	Beam-Joint Rotation (Reverse Cycle) (degree)	Column-Joint Rotation (Reverse Cycle) (degree)
1	3090	0.11	0.04	-7702	-0.11	0.01
2	4978	0.18	0.08	-10130	-0.24	0.01
3	7136	0.25	0.14	-12288	-0.36	0.00
4	8755	0.32	0.19	-14986	-0.50	-0.03
5	8755	0.32	0.23	-16065	-0.65	-0.04
6	10374	0.57	0.29	-14986	-0.85	-0.01
7	10643	0.98	0.34	-14446	-1.49	0.03
8	10104	1.92	0.28	-7972	-1.34	0.18

Table D4: Peak moment versus rotation data for 4-BS-S

Cycle	Peak Moment (Forward Cycle) (kN-mm)	Beam-Joint Rotation (Forward Cycle) (degree)	Column-Joint Rotation (Forward Cycle) (degree)	Peak Moment (Reverse Cycle) (kN-mm)	Beam-Joint Rotation (Reverse Cycle) (degree)	Column-Joint Rotation (Reverse Cycle) (degree)
1	3359	0.11	0.01	-9051	-0.10	-0.02
2	4438	0.18	0.02	-10669	-0.19	-0.01
3	6057	0.24	0.04	-12288	-0.29	0.04
4	7406	0.34	0.08	-15526	-0.43	-0.01
5	8755	0.46	0.11	-15526	-0.63	0.01
6	8755	0.66	0.15	-14446	-0.86	0.02
7	8755	1.08	0.17	-13367	-1.55	0.06
8	7676	1.79	0.16	-9051	-1.24	0.12

Table D5: Peak moment versus rotation data for 5-BSS-B

Cycle	Peak Moment (Forward Cycle) (kN-mm)	Beam-Joint Rotation (Forward Cycle) (degree)	Column-Joint Rotation (Forward Cycle) (degree)	Peak Moment (Reverse Cycle) (kN-mm)	Beam-Joint Rotation (Reverse Cycle) (degree)	Column-Joint Rotation (Reverse Cycle) (degree)
1	3359	0.10	0.03	-7432	-0.10	-0.01
2	4978	0.19	0.06	-10130	-0.18	0.02
3	7136	0.31	0.09	-12288	-0.27	0.04
4	8755	0.43	0.14	-13907	-0.36	0.05
5	9834	0.57	0.18	-14986	-0.50	0.06
6	10374	0.73	0.23	-14986	-0.76	0.08
7	10913	1.10	0.28	-14446	-1.07	0.18
8	9834	1.58	0.33	-9590	-0.86	0.13

Table D6: Peak moment versus rotation data for 6-BSS-SS

Cycle	Peak Moment (Forward Cycle) (kN-mm)	Beam-Joint Rotation (Forward Cycle) (degree)	Column-Joint Rotation (Forward Cycle) (degree)	Peak Moment (Reverse Cycle) (kN-mm)	Beam-Joint Rotation (Reverse Cycle) (degree)	Column-Joint Rotation (Reverse Cycle) (degree)
1	3359	0.10	0.04	-7972	-0.08	-0.03
2	5518	0.17	0.07	-10669	-0.14	-0.05
3	8485	0.27	0.13	-12288	-0.23	-0.04
4	10374	0.33	0.21	-14716	-0.33	-0.05
5	11183	0.41	0.28	-14986	-0.49	-0.02
6	11453	0.54	0.31	-14986	-0.64	0.00
7	11723	0.87	0.34	-14446	-1.23	0.02
8	5518	1.58	0.32	-5274	-1.32	0.02

Table D7: Peak moment versus rotation data for 7-RCS-RC

Cycle	Peak Moment (Forward Cycle) (kN-mm)	Beam-Joint Rotation (Forward Cycle) (degree)	Column-Joint Rotation (Forward Cycle) (degree)	Peak Moment (Reverse Cycle) (kN-mm)	Beam-Joint Rotation (Reverse Cycle) (degree)	Column-Joint Rotation (Reverse Cycle) (degree)
1	3090	0.11	0.05	-6892	-0.11	0.01
2	4978	0.16	0.08	-9860	-0.18	0.02
3	6597	0.27	0.11	-12018	-0.31	0.02
4	7676	0.40	0.15	-13907	-0.43	0.02
5	8755	0.53	0.18	-14986	-0.57	0.02
6	9295	0.67	0.21	-14986	-0.76	0.03
7	9564	1.04	0.26	-14446	-1.32	0.12
8	10374	1.88	0.36	-9050	-0.48	0.22

Table D8: Peak moment versus rotation data for 8-RCS-S

Cycle	Peak Moment (Forward Cycle) (kN-mm)	Beam-Joint Rotation (Forward Cycle) (degree)	Column-Joint Rotation (Forward Cycle) (degree)	Peak Moment (Reverse Cycle) (kN-mm)	Beam-Joint Rotation (Reverse Cycle) (degree)	Column-Joint Rotation (Reverse Cycle) (degree)
1	3444	0.11	0.07	-9210	-0.08	-0.06
2	5095	0.20	0.10	-11411	-0.16	-0.08
3	6746	0.31	0.13	-14162	-0.27	-0.11
4	8946	0.47	0.18	-15813	-0.36	-0.13
5	10597	0.60	0.24	-16363	-0.44	-0.14
6	11697	0.81	0.31	-15813	-0.57	-0.12
7	12523	1.05	0.37	-15262	-0.87	-0.10
8	11422	1.21	0.36	-14162	-1.24	0.14

APPENDIX E: Equivalence of non-homogenous equations in SI-metric, MKS-metric, and U.S. customary units

Reference	SI-metric stress in MPa	MKS-metric stress in kgf/cm²	U.S. customary unit stress in psi
General	1 MPa	10 kgf/cm²	142.2 psi
	$\sqrt{f_c'}$ in MPa	$3.18\sqrt{f_c'}$ in kgf/cm²	$12\sqrt{f_c'}$ in psi
	$0.313\sqrt{f_c'}$ in MPa	$\sqrt{f_c'}$ in kgf/cm²	$3.77\sqrt{f_c'}$ in psi
	$0.083\sqrt{f_c'}$ in MPa	$0.27\sqrt{f_c'}$ in kgf/cm²	$\sqrt{f_c'}$ in psi
Equation 2.1	$l_{dh} = \dfrac{f_y d_b}{5.4\lambda\sqrt{f_c'}}$	$l_{dh} = \dfrac{f_y d_b}{17.2\lambda\sqrt{f_c'}}$	$l_{dh} = \dfrac{f_y d_b}{65\lambda\sqrt{f_c'}}$
Equation 2.7	$V_n = \dfrac{1}{12}\gamma\sqrt{f_c'}A_j$	$V_n = \dfrac{4}{15}\gamma\sqrt{f_c'}A_j$	$V_n = \gamma\sqrt{f_c'}A_j$